

AMPLIFYING SINGLE-GATE MESFET  
PHASE SHIFTERS AT X-BAND

by

DAVID HILLARY EVANS

A Thesis submitted for the  
Degree of Doctor of Philosophy  
at the  
University of Kent at Canterbury

- 1983 -



D50149/84

F 104252

ACKNOWLEDGEMENTS

The author would like to thank Dr. R.J. Collier of the University of Kent for his help and encouragement during the course of this research, and the UK Science and Engineering Research Council for providing financial support for himself. Also, thanks to Dr. B.H. Newton and Philips Research Laboratories, Redhill, for useful suggestions and assistance during this CASE project. Finally, a word of thanks to Miss D. Paine for her careful typing and preparation of this thesis.

ABSTRACT

The thesis will describe 0/180 degree digital switched-path phase shifters that exhibit insertion gains of approximately 3 dB at 9.5 GHz. The microwave switching and amplification in each phase shifter is performed with a pair of Plessey GAT4 single-gate MESFET devices. The basis for this microwave switch is a matched amplifier which when its device is pinched-off displays an insertion loss of about 17 dB down on the amplifier's peak gain of 6 dB. A characteristic feature of this switch is its large terminal mismatches when in its off state. Use has been made of these to recover part of the 3 dB division (or recombination) loss inherent in the type of switched path phase shifter used in this work. The paths that are being switched are the outputs of phase splitting networks and power dividers. A divider has been developed for use with these switches and utilises the broadband coupling properties of slotline to microstrip transitions. This phase shifter has a bandwidth of 1.4 GHz which is determined mainly by the network matching of the two devices. The phase error is less than 6 degrees in this bandwidth and phase transition times of less than 1 nS have been determined by spectrum analysis.

Contents

	<u>Page No.</u>
<u>ACKNOWLEDGEMENTS</u>	(i)
<u>ABSTRACT</u>	(ii)
<u>CHAPTER 1 - INTRODUCTION</u>	
1.1 Introduction	1
1.2 Review of MESFET Phase Shifters	2
1.3 Contents of this Work	5
1.4 References	7
<u>CHAPTER 2 - THEORY AND DESIGN : THE SINGLE GATE MESFET AS AN AMPLIFYING MICROWAVE SWITCH</u>	
2.1 Introduction	9
2.2 The MESFET Device	10
2.3 Device Mounting	11
2.4 Device Measurement	14
2.5 Device Scattering Parameters and a Lumped Element Model	18
2.6 The MESFET Amplifier and Switch	26
2.6.1 Two Port Theory	26
2.6.2 Matching Component Design	29
2.6.3 Amplifier Response	32
2.6.4 Optimum Switching Device Performance	34
2.7 Two-Way MESFET Switches	37
2.7.1 Three Port Theory	40
2.7.2 Two-Way Switch Design	43
2.8 Switching Performance, Limits and Device Control	51
2.9 Conclusion	55
2.10 References	56

CHAPTER 3 - POWER DIVIDING AND PHASE SHIFTING NETWORKS

3.1	Introduction	59
3.2	General Form of the Complete Phase Shifter	59
3.3	Constant Time Delay Type Phase Shift Network	60
3.4	Power Dividers: The Termination Problem	63
3.5	The Wilkinson Power Divider	65
3.6	The Uncompensated Wilkinson Power Divider	67
3.7	The Tee Power Divider	73
3.8	Schiffman Type Phase Shift Networks	79
3.9	A Bandpass Phase Shift Circuit (Stub Circuit)	84
3.10	Hybrid Power Dividers	86
3.11	The Slotline to Microstrip Power Divider	93
3.12	Conclusion	100
3.13	References	101

CHAPTER 4 - THEORY AND DESIGN OF THE COMPLETE PHASE SHIFTER

4.1	Introduction	104
4.2	A Constraint on the Angle of Phase Shift	104
4.3	Bandwidth: The Effect of Long Reference Lines	107
4.4	The Effect of the Scattering Parameter $S_{21}$	111
4.5	Phase Shifters Having Angles of 45 and 22.5 Degrees	118
4.6	Parallel Type Phase Shifters	121
4.7	Switching Behaviour and Measurement	129
4.8	Conclusion	138
4.9	References	139

CHAPTER 5 - MEASUREMENTS AND RESULTS OF PHASE SHIFTER COMPONENTS

5.1	Introduction	141
5.2	Substrate and Transitions	142
5.3	Device Scattering Parameter and Gain Compression Measurements	146
5.4	Amplifier Performance (MESFET Switch)	154
5.5	Transmission Bandwidth of Power Dividers with a Mismatched Output	158
5.6	The Dispersive Phase Shift Networks	160
5.7	Performance of Slotline-Type Power Divider	166
5.8	Conclusion	171
5.9	References	173

CHAPTER 6 - RESULTS OF THE COMPLETE PHASE SHIFTER MEASUREMENTS

6.1	Introduction	175
6.2	A Phase Shifter Using the Schiffman Network	175
6.3	A Phase Shifter Using the Stub Type Network	180
6.4	Phase Shifters Using the Slotline-Type Power Divider	185
6.5	Switching Speed and Spectrum Observations	191
6.6	Signal Handling	194
6.7	Conclusion	195
6.8	References	196

CHAPTER 7 - CONCLUSION

7.1	Summary of Results	197
7.2	Comparison with Other Phase Shifters	201
7.3	Future Work	201
7.4	References	205

CHAPTER 1INTRODUCTION1.1 INTRODUCTION

There are many areas where electrically adjustable microwave devices find applications. Typical components using such devices are switches, attenuators and variable gain amplifiers and phase shifters. Traditionally, these functions have been performed by PIN diodes. However, the requirements of modern systems have exemplified the limitation<sup>1</sup> of PIN diodes and alternatives are being sought.

The GaAs MESFET has been commercially available since 1971. It has found considerable use as an amplifier, notably low noise designs up to 18 GHz<sup>2</sup>, multioctave wide band amplifiers<sup>3</sup> and power devices yielding several watts in X-band<sup>4</sup>. However, it is only in recent years that its potential as a control device has been realised<sup>5,6</sup>.

One application where the advantages of MESFET control devices may be useful is in phase shifters. These are circuits that cause a known shift in the phase of a microwave signal without any accompanying change in its amplitude. There are two principle uses of phase shifter, firstly as phase modulators in communications systems and secondly, phase shifters for phased-array radar systems. In both instances the required phase shift is invariably a digital one, ie. 0 to 180 degrees or 0 to 90 degrees etc.

In communications systems the trend is to move to faster data rates to take advantage of the greater channel capacity of microwave frequencies. Fast switching devices and modulators are therefore

required. For phased-arrays, several bits of digital phase shift are needed with the consequent increase in loss and control complexity. Also, many identical circuits are required for a complete array.

Though the PIN device can be made to switch fast, it usually requires complicated control signals to achieve this. Also, it has an inherent insertion loss which can become significant if many devices are being used.

The MESFET device offers advantages here in that it can, as an amplifier, provide an insertion gain and its amplifying mechanism ensures that it will switch quickly. Its switching control is simply a change of voltage level with very little current. The MESFET device as an amplifier also needs a drain current but gain is not obtained without some cost and it is worth noting that this current is comparable to that typically required to drive PIN diodes. A further point in favour of the GaAs MESFET is its ability to be integrated into monolithic circuits. A considerable advantage exists for phased-array systems when the fruits of this technology become commercially available.

Some work has already been reported on the subject of MESFET phase shifters and a review will now be given to allow an idea of what is feasible and possible further work.

## 1.2 REVIEW OF MESFET PHASE SHIFTERS

The first known proposals for the use of MESFET devices for microwave switching in a phase shifter were by Cuccia and Matthews<sup>7</sup> in 1977. They suggested using a pair of dual-gate MESFET switches<sup>5</sup> in a parallel common drain common source arrangement. Signals with the required phase shift are applied to the device's first gates and complementary control voltages to the second gates. No results were given though it is suggested that the 100 pS transition time of the

dual-gate MESFETs should allow 2 Gbits/S data rates.

In 1978 Dobratz et. al.<sup>8</sup> reported the use of single-gate devices as reflective terminations for coupled line hybrids and circulator type 0/180 degree phase modulators. The device drain to source connection provided the switchable impedance with control applied to its gate. 2 Gbits/S data rate was this time measured for a thin film circuit at 6 GHz centre frequency. A J-band modulator using a waveguide circulator with the device mounted in a waveguide to microstrip transition gave 2 GHz bandwidth,  $\pm 5$  degrees phase accuracy and  $\pm 0.5$  dB amplitude balance.

A dual-gate MESFET PSK modulator was reported by Tsai et. al.<sup>9</sup> and displayed 3 dB gain over a 400 MHz bandwidth centred at 11.7 GHz. Two devices were used in conjunction with two compensated Wilkinson power dividers/combiners and a 180 degree delay.

Departing from digital phase shifts Fithian<sup>10</sup> has constructed a complex weighting circuit for the frequency range 7 to 8 GHz. This utilised four dual-gate MESFET devices operating as variable gain amplifiers/attenuators. Each device was driven by a quadrature signal from hybrids and the device outputs combined with an inphase circuit. By suitably adjusting each device's gain or loss a continuously variable 360 degrees of phase shift is obtained with an overall insertion loss of less than 6.4 dB. More recently<sup>11</sup> using a similar four device arrangement, a continuously variable 360 degree phase shifter approached 0 dB overall insertion loss. A further circuit<sup>12</sup> used only three dual-gate devices driven with 0, 120 and 240 degree signals. This displayed a minimum insertion loss of 6 dB.

A further variation on the use of dual-gate devices as phase shifters is the variation in the transmission phase between their gates and drain when their gate voltages are varied in suitable proportion. Phase shifts of over 50 degrees<sup>13,14</sup> with an associated insertion gain

are obtainable if the device's gates have the appropriate terminations.

Considering the useage of single-gate devices in phase shifter then invariably they are used as switched impedance, their source to drain connection being used for this. Pengelly<sup>6</sup> has shown how six such devices can be used in a third order high-pass/low-pass phase shift type network to give 180 degrees of shift over a 20% bandwidth. A monolithic four bit phase shifter<sup>14</sup> using single-gate devices required two devices per bit in a loaded line configuration for 22.5 and 45 degrees shifts and three devices per bit for 90 and 180 degrees in a switched path structure. Operating from 8.5 to 10.5 GHz it exhibited about 5 dB insertion loss. It is interesting to note that Naster<sup>15</sup> has compared the single-gate MESFET as controlled impedance with the PIN diode and suggests that the PIN is approximately 4 times better as a switch. Though this may be so, it is the MESFET's ability to be integrated into a monolithic circuit that is causing the current interest in its development.

A further dual-gate MESFET 0/180 degree phase shifter has been reported by Vorhaus et. al.<sup>16</sup>. This used two devices with a common input gate, a 180 degree delay at one of their drains and a compensated Wilkinson combiner at the circuits output. The circuit was monolithic and gave 3 dBs of gain across a 10% bandwidth in X-band. Other phase shifts could be achieved with this circuit by using the correct delay.

The conclusion drawn from this review is that only the dual-gate device has been used as a switch with an insertion gain and when the single-gate device is employed, it is as a switchable impedance with an inherent insertion loss. A possible reason for this is that use is being made of the MESFET's three terminal structure (the dual-gate has four) compared with the PIN diode two terminals. This means that the microwave signals and the control signals are inherently separate

without the need to combine them with suitable filters as is the case for the PIN diode. A point to note about the amplifying MESFET phase shifters is that they are switched path types (because the device is a transmission amplifier). This is no problem since any type of phase shift can be produced with these circuits.

It can also be concluded from this review that there is no fundamental reason why an amplifying single-gate MESFET device cannot be used as a switch with most of the benefits that accrue to the GaAs MESFET. The only difference is that both the microwave input and control have to be applied to the same device terminal. This should not present a problem since this is an inherent feature of the PIN diode and much work has been done on the necessary bias circuits. There is, therefore, scope for work in this area to add to the knowledge about the GaAs MESFET as a control device.

### 1.3 CONTENTS OF THIS WORK

Chapter 2 will consider the matched single-gate MESFET amplifier as the basis for a microwave switch. Use will be made of its lumped element equivalent model to assess its performance when it is in its off state and highlight any special features that it may have. A two-way switch suitable for use in a phase shifter will be developed along with the necessary three port theory. Considerable use will be made of scattering parameters to present overall circuit performance though computation and analysis are performed with current, voltage and cascade parameters.

The passive components such as power dividers and phase shift networks that are required to complete the phase shifter are considered

in Chapter 3. The distinction will be made between time delay and constant phase types, though this work concentrates on the latter. The effect of the MESFET switch on these components will be taken into account, especially with respect to the various power dividers that are discussed. Dispersive type phase shift networks will be investigated and a broadband phase splitting power divider for 0/180 degree phase shifts developed.

These various components are brought together in Chapter 4 and their effect on each other in respect of the complete phase shifter's performance analysed. Most of the discussion will be about 0/180 degree phase shifters but a method will be present<sup>ed</sup> whereby any shift can be caused using a pair of these circuits. It was shown in the review that the MESFET device is a fast switch. One technique for measuring this performance is spectrum analysis. The effect of finite switching times, amplitude imbalance and phase error on a phase modulated carrier are determined for use as a means of estimating the complete phase shifters switching speed.

Chapter 5 concentrates on the measured results of both the devices and component. The ability of the single-gate MESFET to perform microwave switching is demonstrated by measurement. Effects observed in the complete phase shifters performance can be accounted for by noting the behaviour of the components in isolation. Finally, Chapter 6 presents the performance of various experimental phase shifters that have been constructed, demonstrating that only two single-gate MESFET devices plus passive components are required for a 0/180 degree phase shifter that exhibits an insertion gain in X-band with a switching time of less than 1 nS.

1.4 REFERENCES

- 1 R.V. Garver, Microwave Semiconductor Control Devices, IEEE Trans. MTT27, May 1979, pp. 523-529.
- 2 S.R. Hennies, A 7-18 GHz Amplifier Using GaAs FETs, IEEE International Solid-State Circuits Conference, 1978, pp. 124-125.
- 3 K.B. Niclas, W.T. Wilser, R.B. Gold and W.R. Hitchens, The Matched Feedback Amplifier: Ultrawide-Band Microwave Amplification with GaAs MESFETs, IEEE Trans. MTT28, April 1980, pp. 285-294.
- 4 H.Q. Tserng, H.M. Mackey and S.R. Nelson, 2W, 8-12 GHz GaAs FET Amplifier, Electronics Letters, 14 August 1980, Vol. 16, pp. 680-681.
- 5 C.A. Liechti, Performance of Dual-Gate GaAs MESFETs as Gain-Controlled Low-Noise Amplifiers and High-Speed Modulators, IEEE Trans. MIT23, June 1975, pp. 461-469.
- 6 R.S. Pengelly, GaAs Monolithic Microwave Circuits for Phased-Array Applications, IEE Proc., Vol. 127, Part F, No. 4, August 1980, pp. 301-311.
- 7 C.L. Cuccia and E.W. Matthews, PSK and QPSK Modulators for Gigabit Data Rates, IEEE MTT Symposium 1977, pp. 208-211.
- 8 B.E. Dobratz, N.J. Ho, G.L. Lee and H.T. Suyematsu, Gigabit Rate GaAs FET RF Phase Modulators, IEEE International Solid-State Circuits Conference, 1978, pp. 76-77.
- 9 W.C. Tsai, T.L. Tsai and S.F. Paik, PSK Modulator Using Dual-Gate FETs, IEEE International Solid-State Circuits Conference, 1979, pp. 164-165.

- 10 M.J. Fithian, Two Microwave Complex Weighting Circuits, IEEE MIT Symposium, 1980, pp. 126-128.
- 11 M. Kumar, R.J. Menna and Ho-Chung Huang, Broadband Dual-Gate FET Continuously Variable Phase Shifter, IEEE MIT Symposium, 1981, pp. 431-433.
- 12 Y. Gazit and H.C. Johnson, A Continuously Variable Ku-Band Phase/Amplitude Control Module, IEEE MIT Symposium, 1981, pp. 436-438.
- 13 C. Tsironis and P. Harrop, Dual Gate GaAs MESFET Phase Shifter with Gain at 12 GHz, Electronics Letters, 3 July 1980, Vol. 16, pp. 553-554.
- 14 Y. Ayasli, A. Platzker, J.L. Vorhaus and L.D. Reynolds, A Monolithic X-Band Four-Bit Phase Shifter, IEEE MIT Symposium, 1982, pp. 486-488.
- 15 R.J. Naster, MMIC Technology for Microwave Radar and Communications Systems, Microwave Journal, February 1983, pp. 109-113.
- 16 J.L. Vorhaus, R.A. Pucel and Y. Tajima, Monolithic Dual-Gate GaAs FET Digital Phase Shifter, IEEE Trans. MIT30, July 1982, pp. 982-991.

CHAPTER 2THEORY AND DESIGN : THE SINGLE GATE MESFET AS AN  
AMPLIFYING MICROWAVE SWITCH2.1 INTRODUCTION

This chapter will introduce the single gate MESFET and show how it can be used as an amplifying microwave switch. The switch will be developed as a narrow band amplifier, consideration being given to maximum gain, bandwidth and circuit topology. The design will centre on the device's scattering parameters as given by its manufacturer. A lumped element model is developed from these parameters and an attempt is made to predict the variation of this model and the resultant scattering parameters of the device as it is pinched-off. The development of a two-way switch suitable for use in a phase shifter will be presented. Device bias and a switching control circuit will be discussed. It will be shown that this circuit, the device bias circuit and associated d.c. breaks impose a greater constraint on switching speed than the device itself does.

Following in Chapter 3, the passive components that are required for the construction of phase shifters will be considered. Of specific interest are various power dividers and phase shifting networks. The two-way switch of this chapter and the various components of Chapter 3 are brought together in Chapter 4 where their interaction and the complete phase shifter's behaviour will be assessed.

## 2.2 THE MESFET DEVICE

The principle requirements of the device chosen for this work is that it should give a reasonable gain at 10 GHz. This frequency was chosen since it allows the construction of compact microstrip circuits, the standard one inch square substrate with a dielectric constant of ten is approximately two wavelengths wide. Measurements are easily performed, though for the devices, data is invariably published by their manufacturers. There are many commercially available GaAs MESFETs supplied by a host of manufacturers<sup>1</sup>, many of which meet the above requirement. The device selected for this work was the Plessey GAT4 single gate device. This device is readily available in both packaged and chip forms, the latter being preferred for this work. Apart from the necessity of having to wire bond the chip devices, the mounting requirements in terms of substrate and support are simpler than for packaged devices. Also the chips are better electrically, their parasitics being smaller with the consequent advantages in bandwidth and gain.

The GAT4 is a small signal low noise recessed gate device having gate dimensions of<sup>2</sup> length,  $L_g = 1.0 \mu\text{m}$  and width,  $W = 300 \mu\text{m}$ . The device's active channel layer is buffered from the semi-insulating substrate and results<sup>3</sup> in a reduced noise figure and a more linear drain current,  $I_{DS}$  versus gate to source voltage  $V_{GS}$  characteristic which in turn gives a sustained transconductance,  $g_M$  value down to low drain currents. Though the device's noise performance is of no importance in this work, the presence of the buffer layer **may** cause an increase **in** device gain both at zero gate source voltage (drain current,  $I_{DS} = I_{DSS}$ ) and for decreasing values of drain current .

gate width is made up from two 150  $\mu\text{m}$  metalisations. This reduces the parasitics, both resistive and inductive associated with the gate **and** allows the use of a wide gate to achieve a high value of trans-conductance. The manufacturer has obtained<sup>4</sup> an 8 dB power gain from this device at a frequency of 10 GHz.

### 2.3 DEVICE MOUNTING

A device mounting configuration has been employed that is comparable to that used by the manufacturer to characterise the device at microwave frequencies<sup>5</sup>. The reasons for this are two-fold, the mount allows a good device to ground bond connections<sup>6</sup> resulting in low (and consistent) parasitics and the manufacturer's published scattering parameters can be taken as reasonably correct for a like mounted device enabling their use in amplifier design.

The mount used by the manufacturer is their chip on disc (COD) arrangement. The pertinent features of this are as follows. The device's surface is raised through a hole in substrate to be level with its microstrip conductors. This keeps the device to microstrip bond wires as short as possible. The disc is soldered or glued (conductive) to the microstrip's ground plane to achieve good device grounding (and heat dissipation). The diameter of the disc is 1.0 mm and this determines the spacing of the two microstrips at the device.

In this work the disc has been replaced by a ridge on the substrate's supporting block. Either side of the ridge are the two microstrip substrates, one for the device's input circuitry (gate) and another for the output (drain), the device being placed on the ridge between the substrates. This method is shown in Figure 2.1. The substrate <sup>is</sup> glued with conductive epoxy to the block to ensure good

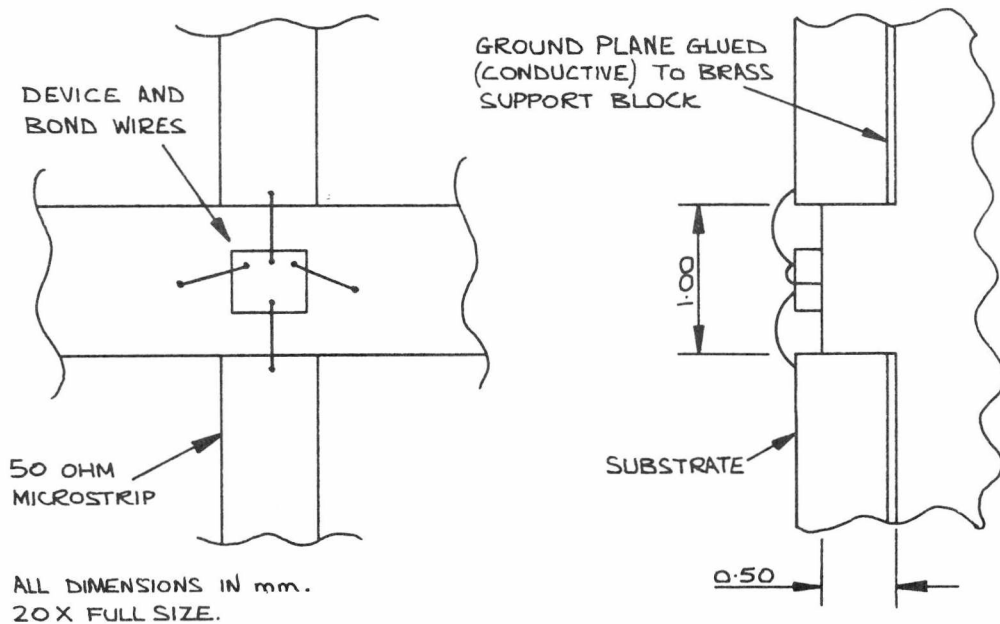


Figure 2.1 : Device and substrate mounting on support block. The assembled block and etched substrate are gold plated before device mounting.

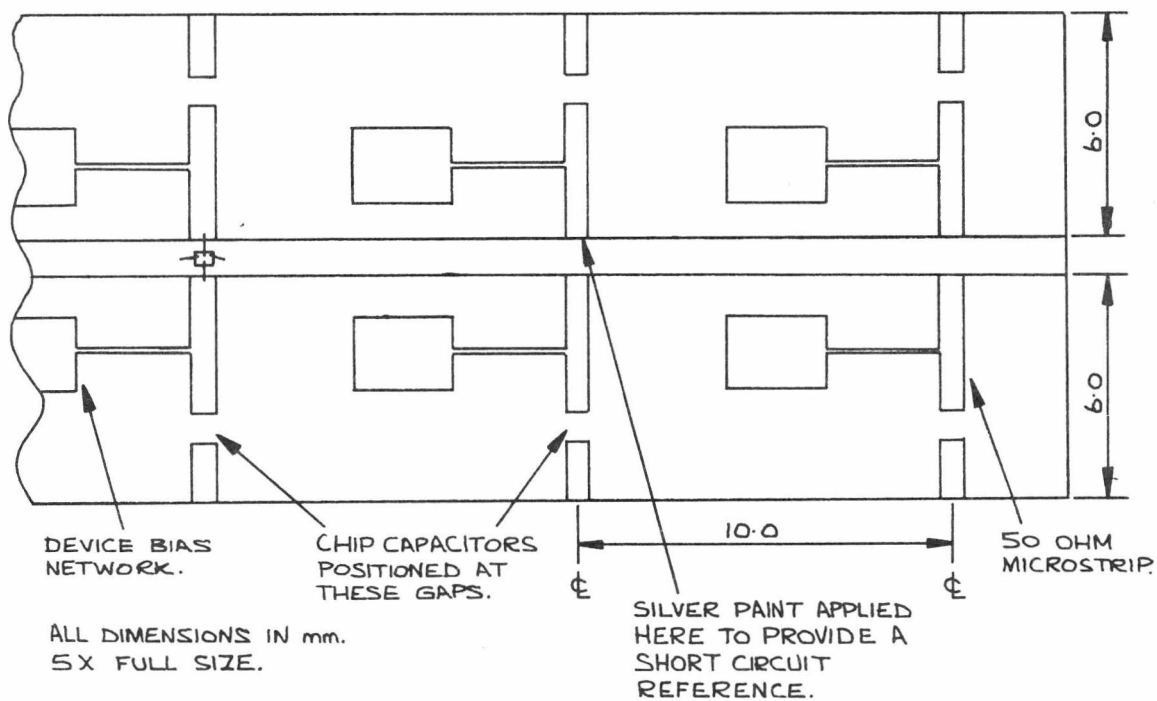


Figure 2.2 : A plan of device measurement jig showing the microstrip layout.

electrical contact and mechanical rigidity between substrates and device. The device is glued to the ridge according to the manufacturers instructions and bonded to the ridge and microstrip with 25  $\mu\text{m}$  gold wire also shown in Figure 2.1. The block also supports the coaxial SMA to microstrip transitions.

This mounting is thought to be electrically comparable to the manufacturer's in that as near as identical lengths of bond wire have been used and that the fringing capacitances from the ends of the microstrips to the ground (the ridge or the disc) are near equal. These fringing capacitances need to be considered since their effect is known<sup>5</sup> to be included in the device's published scattering parameters. It is worth noting however that this capacitance is very small, an estimate from a curve of Matthaei et. al.<sup>7</sup> gives it as 0.004 pF and a second from an equation by Howe<sup>8</sup> as 0.0036 pF.

This mounting method is thought to be slightly advantageous in that the device mount and substrate support are fabricated in one process. In a phase shifter circuit where two devices may be used, they can be mounted adjacent on the same ridge. Also the substrate does not need to have a 1 mm hole drilled or punched through it, plain rectangular substrates being adequate. The two separate substrates required precludes direct microstrip connections between the input and output circuitry but this is not needed in this work and so does not present a problem.

For this work the 3Ms Epsilam 10 substrate material has been used. Though the attenuation for 50 ohm microstrip lines at 10 GHz is about 0.15 dB/cm, a factor of four worse than that of alumina<sup>9,10</sup>, low loss is not really needed and the Epsilam 10 is easier to handle and process. It is not fragile and is easily cut to any desired size. The substrate dielectric is copper clad and so conventional printed circuit board construction techniques can be used. However, because of the finer

structure of microstrip circuits, reasonably accurate circuit masks must be made; a ten-to-one photographic reduction process being used to achieve this. Device bonding requires the circuitry to be gold plated. This is done after the etched substrates have been glued to the supporting block and so reducing oxidation of this and so allowing good transition contact to be preserved.

#### 2.4 DEVICE MEASUREMENT

In the last section it was stated that the intention was to use the manufacturer's device data for amplifier design purposes. However, it is clearly useful to attempt to measure the device's scattering parameters to obtain an idea of their values in the mount discussed previously. Also the device's parameters when pinched-off need to be known if its usefulness as a microwave switch is to be assessed. This data is not readily available. Methods of determining these scattering parameters will now be considered.

The devices d.c. parameters are easily measured, requiring a voltmeter and an ammeter plus a fixed five volt supply for the drain bias and a variable supply, zero to about three volt negative for gate bias. The parameters of interest are the variation of drain current,  $I_{DS}$ , with gate voltage,  $V_{GS}$ , the gradient of which is the transconductance,  $g_M$ . The point at which  $V_{GS}$  takes  $I_{DS}$  to zero, the pinch-off voltage,  $V_p$ , allows the most negative voltage that needs to be applied to the device to be fixed. Since  $g_M$  is the gradient of  $I_{DS}$  with respect to  $V_{GS}$ , causing  $I_{DS}$  to go to zero makes  $g_M$  zero also. This, therefore, indicates that the device may be used as a switchable amplifier having a gain proportional to  $g_M$ , control being effected by the gate bias voltage. These measurements are done with 50 ohm terminations on the device to avoid instability.

The scattering parameter measurements were performed using a Hewlett Packard 8410 manual network analyser. This equipment was calibrated (phase reference plane and unit magnitude) by using open circuited (or short circuited) microstrip lines of equal length and adjacent to those leading to the device. All lines are 50 ohms and the reference lines have identical d.c. breaks (chip capacitors) and d.c. bias network to those used on the lines leading to the device for its biasing (and when being used as a switch). The lengths of line between device and the microstrip to SMA coaxial transitions are kept as short as practicable to keep losses and the resultant errors to a minimum. A diagram of this measurement circuit is shown in Figure 2.2. Transmission calibration was done with a length of 50 ohm through line.

Such an arrangement unfortunately allows the introduction of inaccuracies into the measurements from many sources. Contributing sources are the lengths of microstrip, the presence of the d.c. break and bias network, the transition<sup>11</sup> and the SMA to APC7 adaptor and those errors within the network analyser. Methods by which their effect can be compensated for are error correction of the network analyser and de-embedding of the device from the effect of the circuitry between it and the network analyser. Both of these are best accomplished by use of an automatic network analyser whose controlling computer can readily accumulate the calibration data and process the measurements. It is however worth considering the de-embedding technique by which the greater errors of the microstrip and transition may be deducted from that measured at the input of the network analyser to improve the device parameters accuracy.

The de-embedding method described by Bauer and Penfield<sup>12</sup> is as follows. If  $E$  are the two port cascade parameters of the embedding network (which cannot be measured directly) and  $S$  its output termina-

tion (the device) which is subject to error caused by E and M is the measured data at the input of the embedding network, then

$$[M] = [E][S]$$

and hence,

$$[S] = [E]^{-1}[M]$$

(2.1)

The output termination of S being neglected to demonstrate the method; hence taking S as a one port then,

$$M = E_{11} + \frac{E_{12}E_{21}}{1-E_{22}} \frac{S}{S} \quad (2.2)$$

which when rearranged gives,

$$M/S = E_{22} M - (E_{11}E_{22} - E_{12}E_{21}) + E_{11}/S \quad (2.3)$$

By substituting the device with three known values of termination S and measuring M, three simultaneous equations can be formed using equation (2.3).  $E_{11}$ ,  $E_{22}$  and the product  $E_{12}E_{21}$  can hence be found, **this being** sufficient to characterising the embedding network and take its inverse.

It is known<sup>13</sup> that the accuracy of this de-embedding process is good if the calibrating terminations lie in regions of the Smith chart near to that which is to be measured. The device presents mainly capacitive terminations which lie on the lower half-plane of the Smith chart. Possible calibrating terminations are therefore open and short circuited lengths of microstrip and capacitive types.

Since it is the off biased device's parameters that are of most interest and that the on biased device's parameters are actually known from its data sheet, the device itself could be used to calibrate its embedding network. The device provides two terminations in the form of its input and output reflection coefficients and these probably lie in the same region of the Smith chart as its off biased parameters. Unfortunately, a discussion with the manufacturer<sup>5</sup> revealed that the device's scattering parameters could be noticeably different to the published data, spreads of up to 10% for devices from the same GaAs slice and up to 20% between devices from different slices were suggested. Hence, the devices parameters are too uncertain to be used for calibration.

Since the devices are subject to these tolerances when biased on they probably exhibit a comparable spread in their biased off parameters. This being the case, many devices would have to be measured to obtain satisfactory means values for these parameters. This is a time consuming exercise when performed with a manual network analyser and is expensive in terms of devices, it being difficult to reuse chip devices once they have been glued and bonded into a mount. The situation is therefore to accept the manufacturer's parameters and use them for amplifier design and attempt to measure the device's biased off parameters using the open circuited (or short circuited) lines to calibrate the network analyser and also perform de-embedding if the terminations available give sensible results. This is probably adequate since with the amplifier and switch designs presented later, the biased on device parameters tend to be dominant, the biased off parameters giving mainly an indication of switch performance in the attenuating state though the phases of the input and output reflection coefficients will be seen to be

significant in two-way switch and phase shifter design. An attempt will be made in the following section to predict these biased off parameters from knowledge of the device's equivalent circuit with elements that are gate voltage dependent.

### 2.5 DEVICE SCATTERING PARAMETERS AND A LUMPED ELEMENT MODEL

A lumped element model that has successfully been used to model MESFET devices has been given by Vendelin and Omori<sup>14</sup>. To this model drain and gate parasitic series resistances have been added since they are known in some instances<sup>2,15</sup> to be non-zero. This model is shown in Figure 2.3. Analysis is performed first determining the two port Y parameters of the basic device as denoted in Figure 2.3. These are then converted to Z parameters and the effect of the source elements  $L_s$  and  $R_s$  are added. The resultant two port is converted to cascade parameters (ABCD) and the gate and drain elements cascaded onto these. Finally, the overall cascade parameters are converted to scattering parameters for comparison with the manufacturer's data.

The following error function<sup>14</sup> is used to describe the model fit between the calculated and manufacturer's data:

$$EF = \frac{1}{N} \sum_{F_\ell}^{F_h} \sum_{i=1}^2 \sum_{j=1}^2 (W_{ij} |S_{ij_c} - S_{ij_m}|^2) \quad (2.4)$$

where  $N$  is the number of frequency steps summed from the lowest  $F_\ell$  to the highest frequency  $F_h$ .  $S_{ij_c}$  are the calculated scattering parameters and  $S_{ij_m}$  are those as given by the manufacturer.  $W_{ij}$  are weighting factors which are assigned values given by,

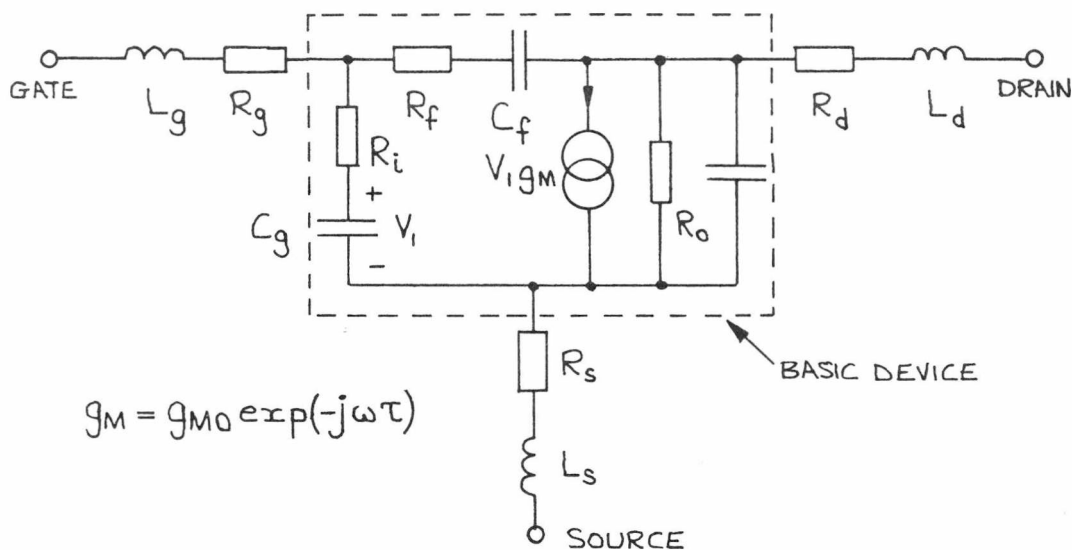


Figure 2.3 : Lumped element model of the MESFET device whose component values are fitted to the Plessey GAT4 data.

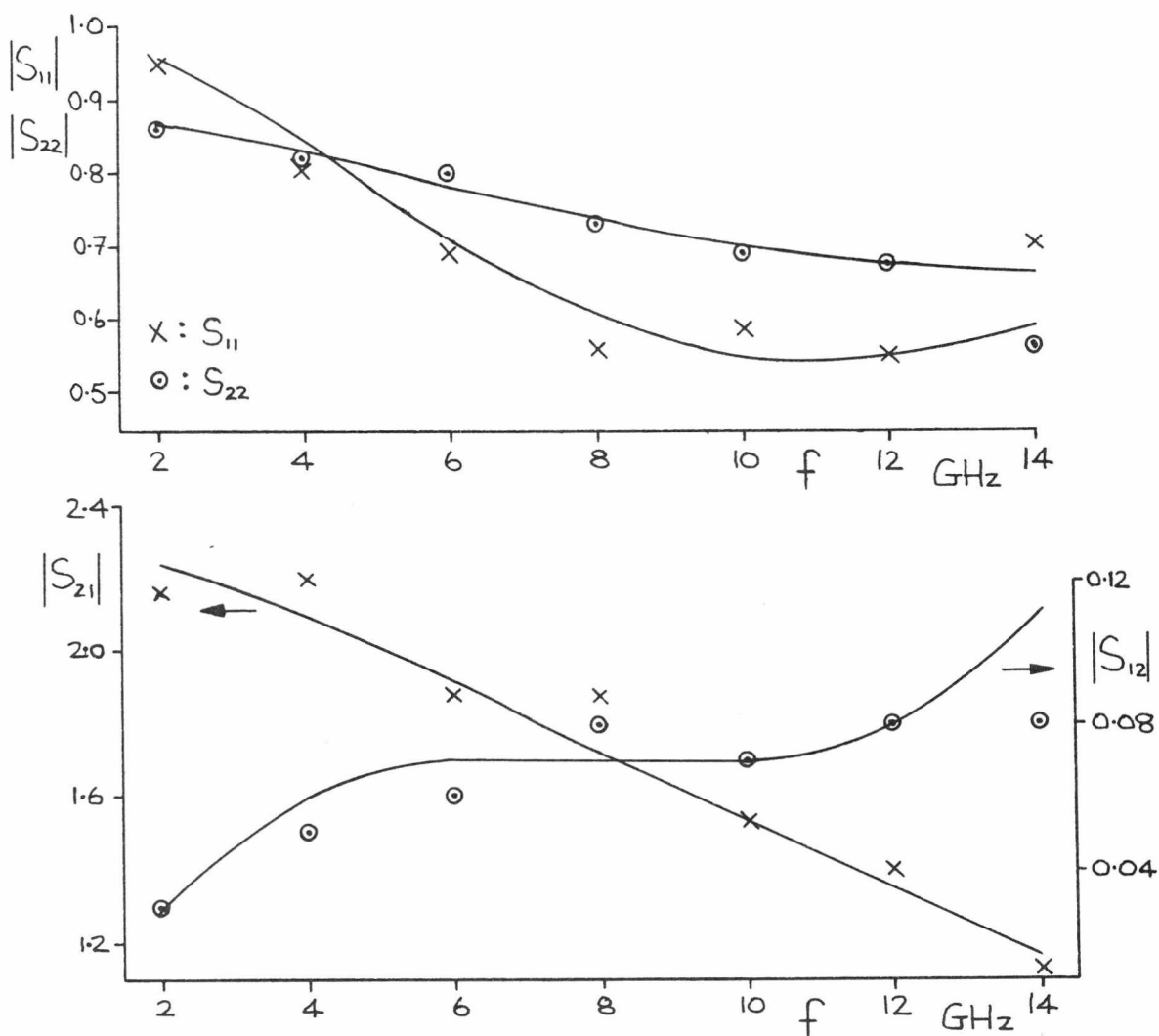


Figure 2.4 : S parameter magnitudes which have been derived from the lumped element model. Continuous curves are for the model and discrete points are Plessey data.

$$W_{ij} = \frac{1}{|S_{ij_m}|} \quad (2.5)$$

so as to give equal weight to all four parameters, the values of  $S_{ij_m}$  are taken as the 10 GHz values, this being the principle frequency of interest. A quasi-Newton optimisation routine has been used to minimise the error function by operating on the component values of the model. This routine is available on the University of Kent's EMAS computing system and is called directly by a Fortran program that has been written by the author to perform this analysis and fitting.

To reduce the number of variables that the computer has to adjust,  $g_{MO}$  is taken as 0.025 A/V as given in the device's data sheet. The delay,  $\tau$ , can be calculated from<sup>14</sup>,

$$\tau = L_g/V_s \quad (2.6)$$

where  $V_s$  is the scattering limited velocity of electrons under the gate and is  $2 \times 10^5$  m/s. Hence,  $\tau$  is 5 pS for the GAT4 device. Twelve component values remain to be optimised by the computer to provide a fit from 2 to 12 GHz in 1 GHz steps.

The first runnings of this program returned values for  $R_g$  and  $R_f$  that were tending to zero and hence their values are taken as zero and eliminated from the model. Also a value of  $L_g$  was returned that was near equal to  $L_d$ , hence their values are taken as equal in the model. Nine components now remain to be optimised and have been given values as shown in Table 2.1.

Fitted values:	$C_d = 0.139$ pF	$L_d = 0.406$ nH	$R_d = 1.23$ $\Omega$
	$C_f = 0.028$ pF	$L_g = L_d$	$R_i = 12.9$ $\Omega$
	$C_g = 0.368$ pF	$L_s = 0.09$ nH	$R_o = 800$ $\Omega$
			$R_s = 0.89$ $\Omega$
Fixed values:	$g_{MO} = 0.025$ A/V	$R_g = 0$	
	$\tau = 5$ pS	$R_f = 0$	

Table 2.1 : Component values for lumped element model of Plessey GAT4 device, fit from 2 to 12 GHz.

Some of the component values are similar to what would be expected from physical considerations of the device. The gate and drain inductances,  $L_g$  and  $L_d$ , are mainly caused by the bond wires and since a fine wire has an inductance of about 0.8 nH/mm, the values of  $L_g$  and  $L_d = 0.406$  nH are reasonable. The sum of  $R_s$  and  $R_d$  approximately equals a value of 2.5 ohms given by Slaymaker et. al.<sup>6</sup> for the GAT4 spreading resistances. Sze<sup>16</sup> gives the capacitance of a metal semiconductor junction as approximately

$$C = \sqrt{\frac{q \epsilon_s N_D}{2(V_{bi} - V_{GS})}} \text{ F/m}^2 \quad (2.7)$$

If  $q = 1.6 \times 10^{-19}$  J,  $\epsilon_s^{(16)} = 10.9 \epsilon_o$ ,  $N_D^{(2)} = 1.4 \times 10^{23} \text{ m}^{-3}$  and  $V_{bi}^{(16)} = 0.8 \text{ v}$  then  $C_g = 0.35$  pF for a  $1.0 \times 300$   $\mu\text{m}$  gate area with  $V_{GS} = 0 \text{ v}$ .

The calculated scattering parameters of this model are shown in Figures 2.4 and 2.5. A good agreement can be seen between these and those of the actual GAT4 device especially in the 8 to 12 GHz region

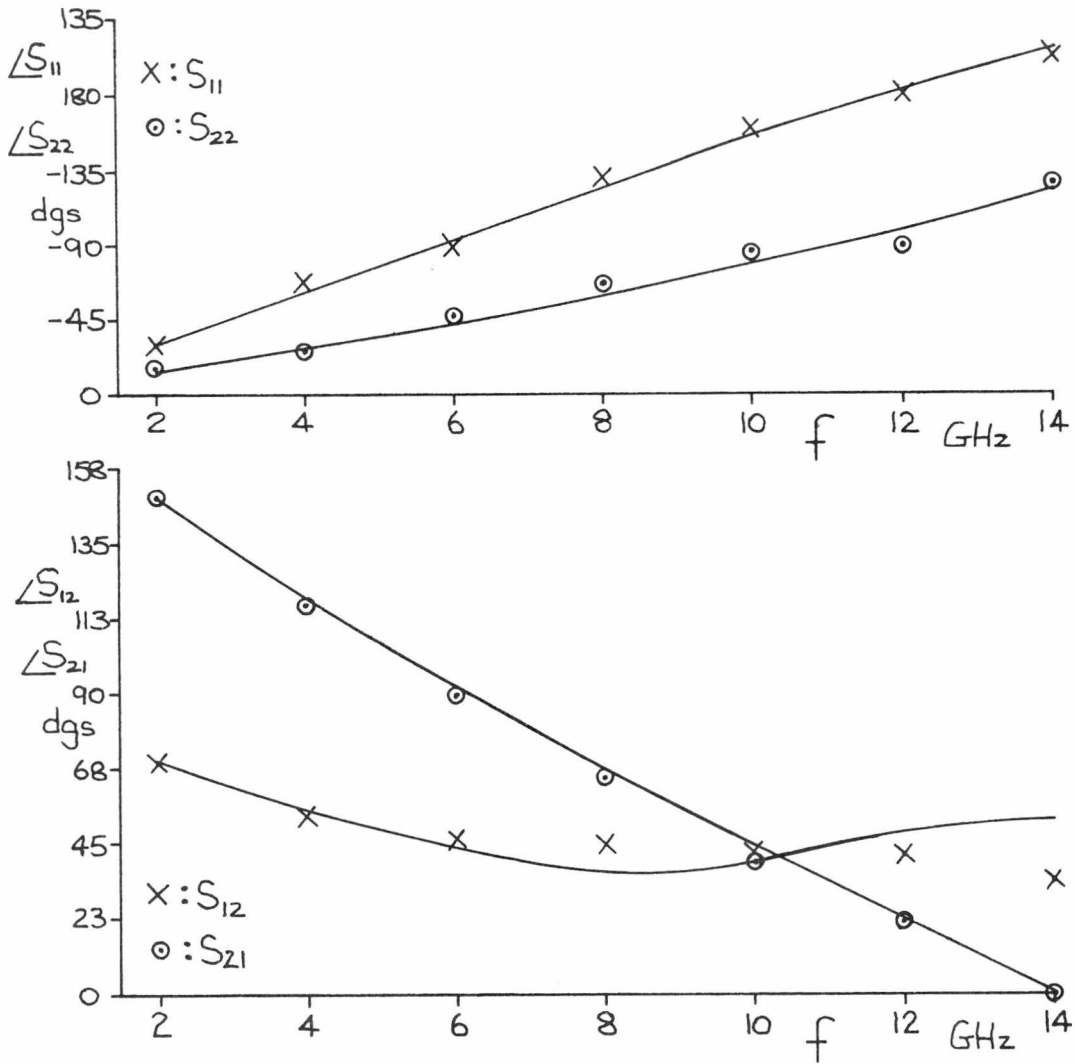


Figure 2.5 : S parameter arguments which have been derived from the lumped element model. Continuous curves are for the model and discrete points are Plessey data.

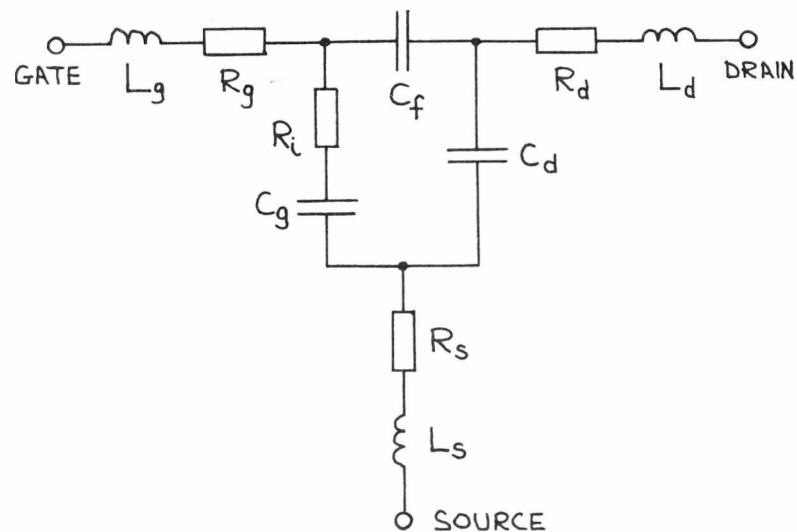


Figure 2.6 : Lumped element model of pinched-off MESFET device.

which is of most interest in this work. The fitting was not extended to above 12 GHz because of the abrupt jumps in the actual devices parameters. These might degrade the fit below 12 GHz and are hence neglected.

Having deduced a lumped element model for the device when it is biased on consideration can now be given to a model for it in the pinched-off condition. It must be noted that it is still the small signal scattering parameters that are of interest. The large signal that causes a change in the device parameters is the steady gate to source voltage ( $V_{GS}$ ), principally as it is taken to a negative value,  $V_p$ , to cause device pinch off. The drain to source bias voltage ( $V_{DS}$ ) is held constant at +5v. The continuous variation of the scattering parameters as  $V_{GS}$  is taken from 0v to  $V_p$  is now important in terms of switch behaviour but device model fitting at the minimum noise figure bias can give an estimate of how the model components vary with  $V_{GS}$ .

The first element of the model that is known to vary is  $g_M$ . This was shown in section 2.4 to go to zero at pinch-off and hence the model becomes purely passive. Similarly,  $R_O$  tends to a considerably higher value at pinch-off and is taken as infinite. These two variations are confirmed by output non-linearity measurements of Minasian<sup>17</sup> which have shown that the values of  $g_M$  and  $R_O$  remain steady at their zero  $V_{GS}$  values for decreasing  $V_{GS}$  and then change abruptly as pinch-off is approached.

Equation (2.7) can be written so that  $C_g$  can be estimated at pinch off

$$C_g = \frac{C_{go}}{\sqrt{0.8 - V_{GS}}} \text{ F} \quad (2.8)$$

If  $C_{go}$  is chosen so as to give the value of  $C_g$  at  $V_{GS} = 0v$  that was given in the fitted model, then  $C_g = 0.169$  pF for  $V_p = -3.0v$ .  $C_d$  and  $R_i$  are

thought<sup>17</sup> to be constant for changes in  $V_{GS}$ . Also the inductances  $L_d$ ,  $L_g$  and  $L_s$  and the spreading resistances do not change with device bias.

The final component of the model that needs to be given a value is  $C_f$ . Further measurements by Minasian<sup>18</sup> give  $C_f$  as slowly varying function with gate to drain voltage ( $V_{GS} + V_{DS}$ ) and having a negative gradient. Hence, as  $V_{GS}$  is taken negative to pinch-off,  $C_f$  should be seen to decrease slightly. Further measurements and model fitting performed by Willing et. al.<sup>19</sup> indicate the converse, an increasing  $C_f$  as  $V_{GS}$  is taken negative. This dependence appears to be strong,  $C_f$  increasing several times from  $V_{GS} = 0v$  to  $V_p$ . The data given by Willing et. al. is more specific in that it separates the effect on  $C_f$  of  $V_{GS}$  and  $V_{DS}$ . Their device model is more comprehensive, being similar to the one used here rather than the much simplified one used by Minasian.  $C_f$  is therefore thought to increase as the device is pinched-off but not in exactly what relationship.

The proposed pinched-off MESFET model is shown in Figure 2.6. As just discussed, the component values are as for the biased on model except  $C_g = 0.169$  pF and  $C_f$  which will be taken as 0.028 pF and 0.056 pF to obtain an idea of its effect on the device parameters. The same two port analysis is used to determine the overall scattering parameters of this model as that of the previous. The passive nature of the pinched-off device results in a  $S_{12}$  equal to  $S_{21}$ . The parameters are shown in Figure 2.7. As can be seen the value of the capacitance  $C_f$  has a strong effect on the parameter  $S_{21}$  especially its magnitude. Its effect on  $S_{11}$  or  $S_{22}$  is small, being a slight change in the magnitude and phase of  $S_{22}$  at higher frequencies and similarly  $S_{11}$  but less so.

Considering these parameters in the wider context of using the device as a switch then the large change in  $|S_{21}|$  of about 20 dB indicates that the device may offer potential in this area. Unfortunately

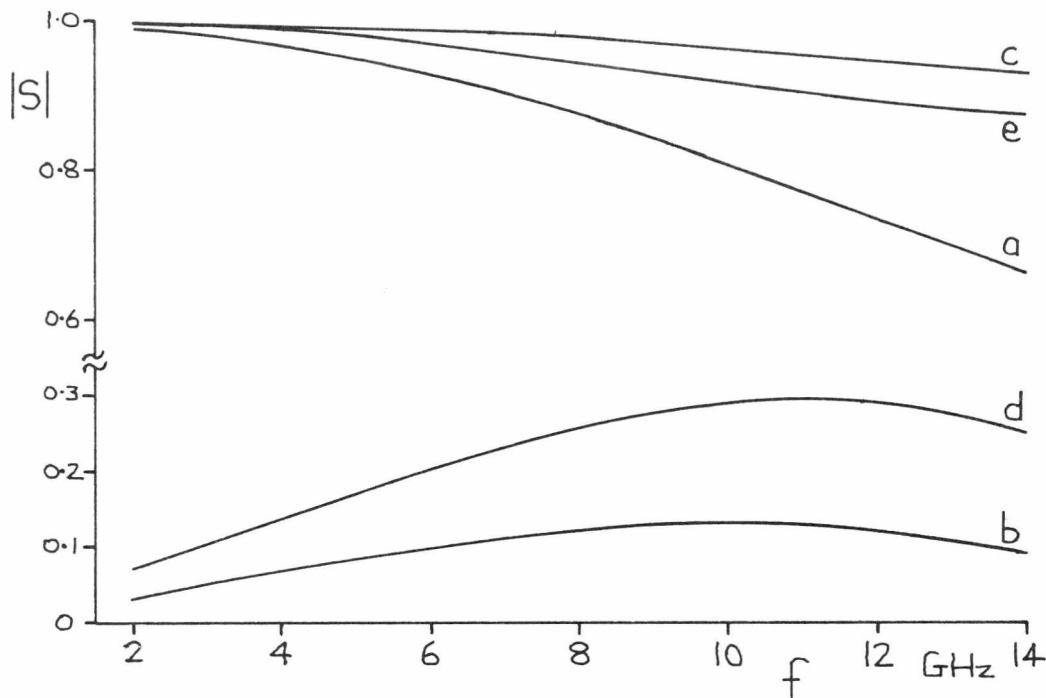


Figure 2.7a : Scattering parameter magnitudes for device lumped element model in pinched-off condition. Key is given in Figure 2.7b below.

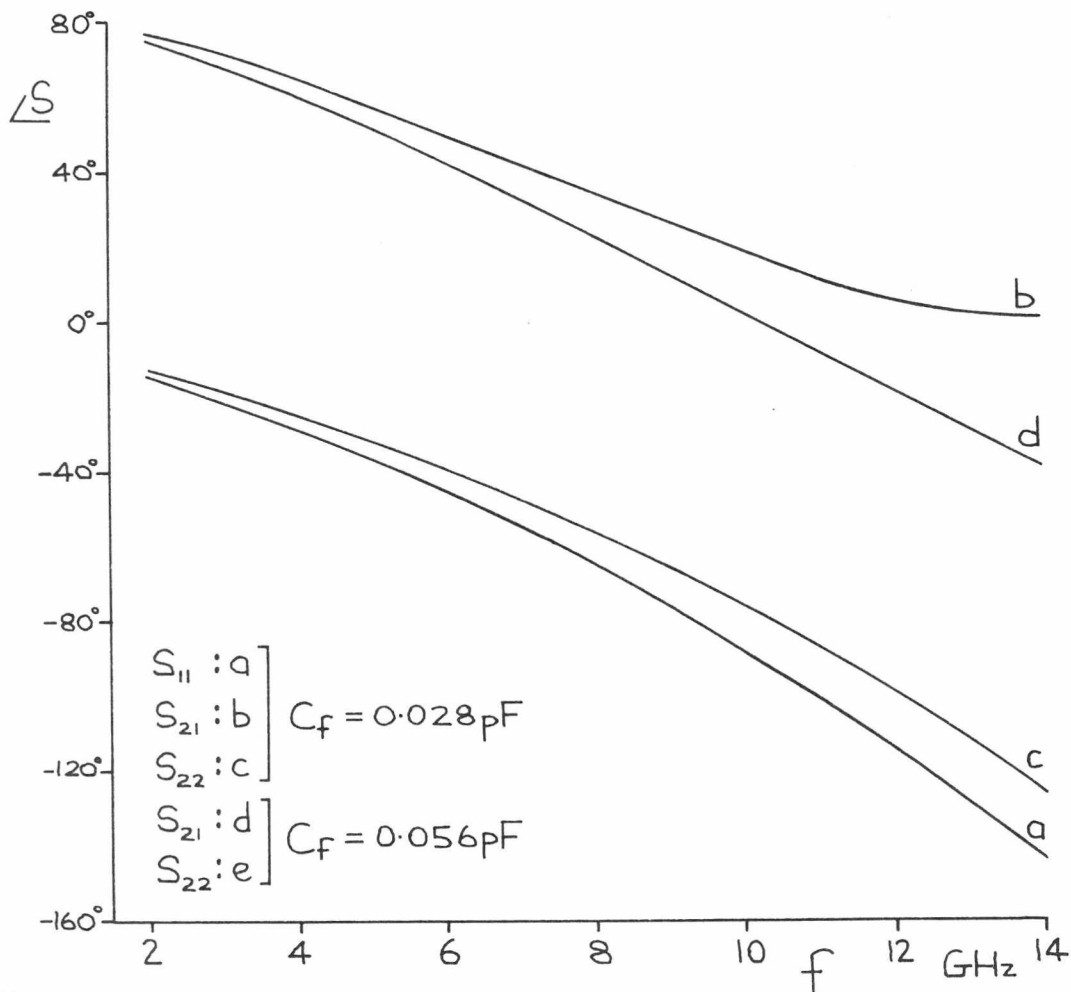


Figure 2.7b : Scattering parameter arguments for device lumped element model in pinched-off condition. Note:  $S_{12} = S_{21}$ .

the magnitude of  $S_{21}$  reaches a maxima at 10 GHz. Ideally this should be as small as possible to give a good insertion loss in the pinched-off condition. The change in  $S_{11}$  and  $S_{22}$  from biased on to pinched-off means that if the device is matched as an amplifier, when turned off a mismatch will be observed at its input and output.

The pinched-off model though far from complete does give an indication of the expected parameters and behaviour of the device. To obtain a more exact model either a fit to the measured pinched-off needs to be done or a better understanding of how the components vary with bias obtained so that their pinched-off values can be more accurately predicted. The feedback capacitance  $C_f$  appears to have a significant effect on the device's transmission parameters being also the component whose value is subject to the greatest uncertainty.

## 2.6 THE MESFET AMPLIFIER AND SWITCH

### 2.6.1 Two Port Theory

At 10 GHz the GAT4 MESFET device has the following scattering parameters<sup>4</sup>,

$$[S] = \begin{bmatrix} 0.59 \angle -157^\circ & 0.07 \angle 41^\circ \\ 1.54 \angle 40^\circ & 0.69 \angle -77^\circ \end{bmatrix} \quad (2.9)$$

Its forward gain,  $S_{21}$ , is only 3.75 dB and it exhibits large mismatches at its input and output. If matching is applied then this gain can be improved by 1.86 dB ( $1/(1-|S_{11}|^2)$ ) and 2.81 dB ( $1/(1-|S_{22}|^2)$ ) resulting in an overall gain of 8.4 dB. This gain is described as the maximum unilateral gain since it assumes  $S_{12}$  to be zero and is given<sup>20</sup> by,

$$G_{u,\max} = |S_{21}|^2 \cdot \frac{1}{1 - |S_{11}|^2} \cdot \frac{1}{1 - |S_{22}|^2} \quad (2.10)$$

To achieve this conjugate matching must be applied to the device such that if  $\Gamma_s$  is the reflection coefficient presented to the device's input and  $\Gamma_\ell$  to its output, then

$$\left. \begin{aligned} \Gamma_s &= S_{11}^* \\ \Gamma_\ell &= S_{22}^* \end{aligned} \right\} \quad (2.11)$$

However, it will be noted that for this device  $S_{12}$  is not zero. Presenting  $\Gamma_s$  and  $\Gamma_\ell$  to the device will cause  $S_{11}$  and  $S_{22}$  to change to new values given by,

$$\Gamma_i = S_{11} + \frac{S_{12} S_{21} \Gamma_\ell}{1 - S_{22} \Gamma_\ell} \quad (2.12a)$$

$$\Gamma_o = S_{22} + \frac{S_{12} S_{21} \Gamma_s}{1 - S_{11} \Gamma_s} \quad (2.12b)$$

Hence, conjugate matching does not give a perfect match when  $S_{12}$  is non-zero. The correct terminations are therefore  $\Gamma_o^*$  and  $\Gamma_i^*$ . Since  $\Gamma_i^*$  depends on  $\Gamma_\ell$  which equals  $\Gamma_o^*$  and  $\Gamma_o$  in turn depends on  $\Gamma_s$  which equals  $\Gamma_i^*$ , equations (2.12a) and (2.12b) must be solved iteratively until  $\Gamma_i$  and  $\Gamma_o$  settle to static values. Alternatively, Ha<sup>20</sup> gives equations whereby  $\Gamma_\ell$  and  $\Gamma_s$  may be determined from the four scattering parameters. The iterative solution of equations (2.12a) and (2.12b) with the parameters (2.9) gives,

$$\left. \begin{aligned} \Gamma_s &= 0.767 \angle 165^\circ \\ \Gamma_\ell &= 0.822 \angle 82^\circ \end{aligned} \right\} \quad (2.13)$$

The overall gain that now includes the effect of  $S_{12}$  is described as the maximum transducer gain and is given by<sup>20</sup>,

$$G_T = \frac{|S_{21}|^2(1-|\Gamma_S|^2)(1-|\Gamma_\ell|^2)}{|(1-S_{11}\Gamma_S)(1-S_{22}\Gamma_\ell) - S_{12}S_{21}\Gamma_S\Gamma_\ell|^2} \quad (2.14)$$

Solution of equation (2.14) with (2.13) and (2.9) gives  $G_T = 9.9$  dB.

Since the device's input and output reflection coefficients,  $\Gamma_i$  and  $\Gamma_o$ , are dependent on its terminations,  $\Gamma_S$  and  $\Gamma_\ell$ , there could be a situation whereby for given scattering parameters (S), certain terminations could give rise to values of  $|\Gamma_i|$  and  $|\Gamma_o|$  that are greater than unity even though  $|\Gamma_S|$  and  $|\Gamma_\ell|$  are less than unity. If this situation arises then instability could occur. The scattering parameters, S, can be checked to see if this is likely to occur by calculating the magnitude of Rollett's stability factor which is given by<sup>20</sup>,

$$K = \frac{1-|S_{11}|^2 - |S_{22}|^2 + |S_{11}S_{22} - S_{12}S_{21}|^2}{2|S_{12}S_{21}|} \quad (2.15)$$

If this is greater than unity then unconditional stability exists such that for either  $|\Gamma_S|$  or  $|\Gamma_\ell| \leq 1$  then  $|\Gamma_i|$  and  $|\Gamma_o| \leq 1$  else if K is less than or equal to unity then conditional stability occurs.

If the parameters (2.9) are tested then  $K = 1.35$ , hence unconditional stability. If the GAT4 MESFET's parameters at other frequencies are tested, then at 8 GHz,  $K = 0.987$  and similarly at 7 GHz and below  $K < 1.0$  and so the device is conditionally stable below 8 GHz. At all frequencies above 8 GHz the device is unconditionally stable. If the moduli of equations (2.12a) and (2.12b) are equated to unity a boundary can be found such that values of  $\Gamma_\ell$  or  $\Gamma_S$  lying on one side of

this cause  $|\Gamma_i|$  or  $|\Gamma_o|$  to be greater than unity and less than unity when  $\Gamma_\ell$  or  $\Gamma_s$  are on the other side. This boundary is circular such that its radius is given by<sup>20</sup>,

$$r_s = \left| \frac{S_{12}S_{21}}{|\Delta|^2 - |S_{11}|^2} \right| \quad (2.16)$$

and its centre in relation to the centre of the Smith chart given by,

$$C_s = \frac{S_{22}^* - S_{11}^*}{|\Delta|^2 - |S_{11}|^2} \quad (2.17)$$

where  $\Delta = S_{11}S_{22} - S_{12}S_{21}$ . For  $r_\ell$  and  $C_\ell$  interchange  $S_{11}$  with  $S_{22}$  in equations (2.16) and (2.17). These loci have been determined for GAT4 devices and are shown in Figure 2.8. The unstable regions are on the inside of the circles. The output load termination is seen to be more critical than the input. Clearly, the matching networks must not present these inductive terminations to the device at 8 GHz and below.

### 2.6.2 Matching Component Design

Simple narrow band matching will be used in this work. The matching components will consist of the minimum of two elements at both the device's input and output. A rough estimate of the bandwidth that can be obtained can be found by noting the device's input and output Q factors. Referring to the lumped element model shown in Figure 2.3 then the input and output  $Q_s$  will be defined as:

$$\left. \begin{aligned} Q_i &= 1/2 \pi f C_g R_i \\ Q_o &= 2\pi f C_d R_o \end{aligned} \right\} \quad (2.18)$$

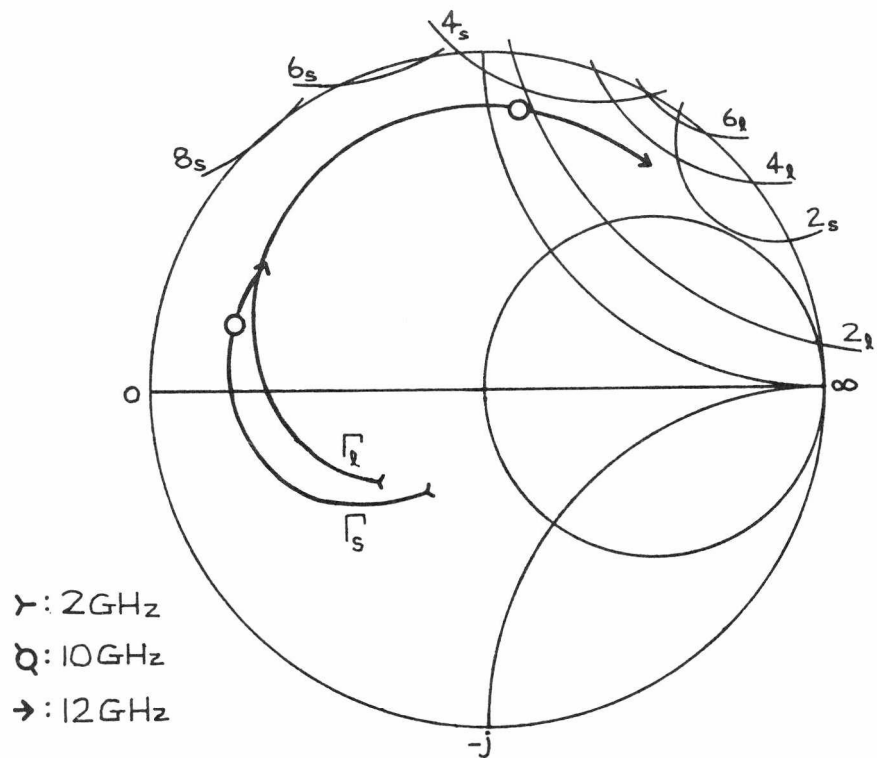


Figure 2.8 : Stability circles of the GAT4 MESFET device and the terminations presented by its matching circuitry. The unstable regions are on the concave side of the arcs. The figures associated with these indicate their frequency in GHz and whether they are for the source (s) or the load (l).

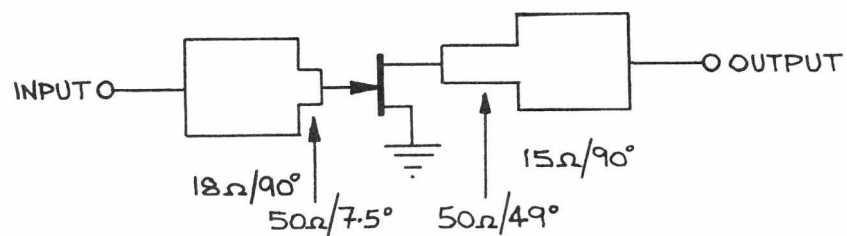


Figure 2.9 : The GAT4 MESFET device with distributed matching components for 10 GHz centre frequency. The electrical lengths are at 10 GHz centre frequency.

If these are evaluated for a 10 GHz centre frequency ( $f$ ) then  $Q_i = 3.3$  and  $Q_o = 7.0$ . The device's drain circuitry hence imposes a greater limit on device bandwidth at this frequency  $Q_o$  indicated that the amplifier will have a 3 dB bandwidth of approximately 1.4 GHz. The 6 dB/octave decrease<sup>20</sup> in  $G_T$  with frequency will have little effect on the amplifier's gain at this bandwidth since at 11 GHz the GAT4's scattering parameters give a value of  $G_T = 8.6$  dB and hence contributes only a 1.3 dB reduction in gain. The simple two element matching will result in matching responses that are good at one specific frequency and degrade sharply away from this frequency, hence giving rise to the sharp reduction in gain away from the centre frequency.

The terminations  $\Gamma_s$  and  $\Gamma_\ell$  can be synthesised by splitting them into their moduli and arguments. The moduli can be synthesised by using a quarter-wave transformer and the arguments by lengths of 50 ohm line. The resistance associated with  $|\Gamma|$  is given by:

$$R = Z_o \left( \frac{1 + |\Gamma|}{1 - |\Gamma|} \right) \quad (2.19)$$

where  $Z_o = 50$  ohms. If the quarter-wave transformer impedances,  $Z_q$ , are determined for  $\Gamma_\ell$  and  $\Gamma_s$  (equations (2.13)), then these are found to be greater than  $Z_o$ . Also the lengths of 50 ohm line required to transform  $Z$  which lies on the 1 to  $\infty$  axis of the Smith chart is given by  $180 - \arg(\Gamma)/2$ . This is arrived at by noting that the addition of a 50 ohm line to an impedance causes a clockwise rotation around the Smith chart (and at a constant radius from the centre). The 50 ohm lines are therefore greater than 90 degrees in lengths and unnecessarily long. If the quarter-wave lines transform  $|\Gamma|$  to an impedance less than  $Z_o$  (0 to 1 axis of the Smith chart) then the 50 ohm lines needed can be less than 90 degrees and their electrical lengths are given by,

$$\theta_M = 90 - \arg(\Gamma)/2 \quad (2.20)$$

Equation (2.19) can be rearranged and combined with the quarter-wave equation to give,

$$Z_q = Z_o \sqrt{\frac{1-|\Gamma|}{1+|\Gamma|}} \quad (2.21)$$

Solution of equations (2.20) and (2.21) with the terminations (2.9) gives a MESFET matching circuit whose topology is shown in Figure 2.9. If these matching circuits are checked to see what terminations they present to the device especially at 8 GHz and below then fortunately they are well away from the problematic region of the Smith chart as is shown Figure 2.8.

### 2.6.3 Amplifier Response

The calculated frequency responses of this amplifier are shown in Figure 2.10. As can be seen the forward gain exhibits a 3 dB bandwidth of 1.4 GHz, coincidentally equal to that predicted by the device's output Q factor ( $Q_o$  equation (2.18)). The dips in the input and output return losses do not occur at 10 GHz as designed since the data (scattering parameters) used to generate these curves required interpolating between the 1 GHz intervals of the available parameters. This was done by a least squares fit to the 8 to 12 GHz parameters and this consequently introduced differences between these parameters and the original data at the 1 GHz interval points, ie. 10 GHz. Such shifts in these dips are easily caused by either errors in the device's parameters just discussed or by errors in the topology of the matching circuitry. This is not important because the behaviour away from the centre frequency

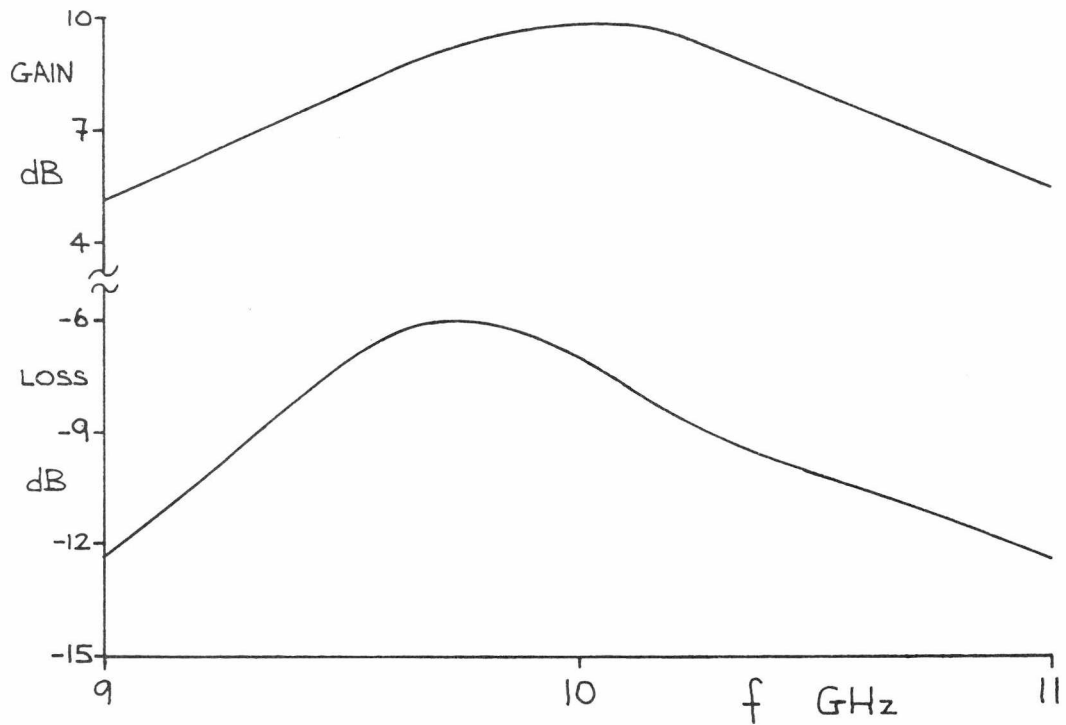


Figure 2.10a : The forward transmission gain/loss of the MESFET amplifier/switch.

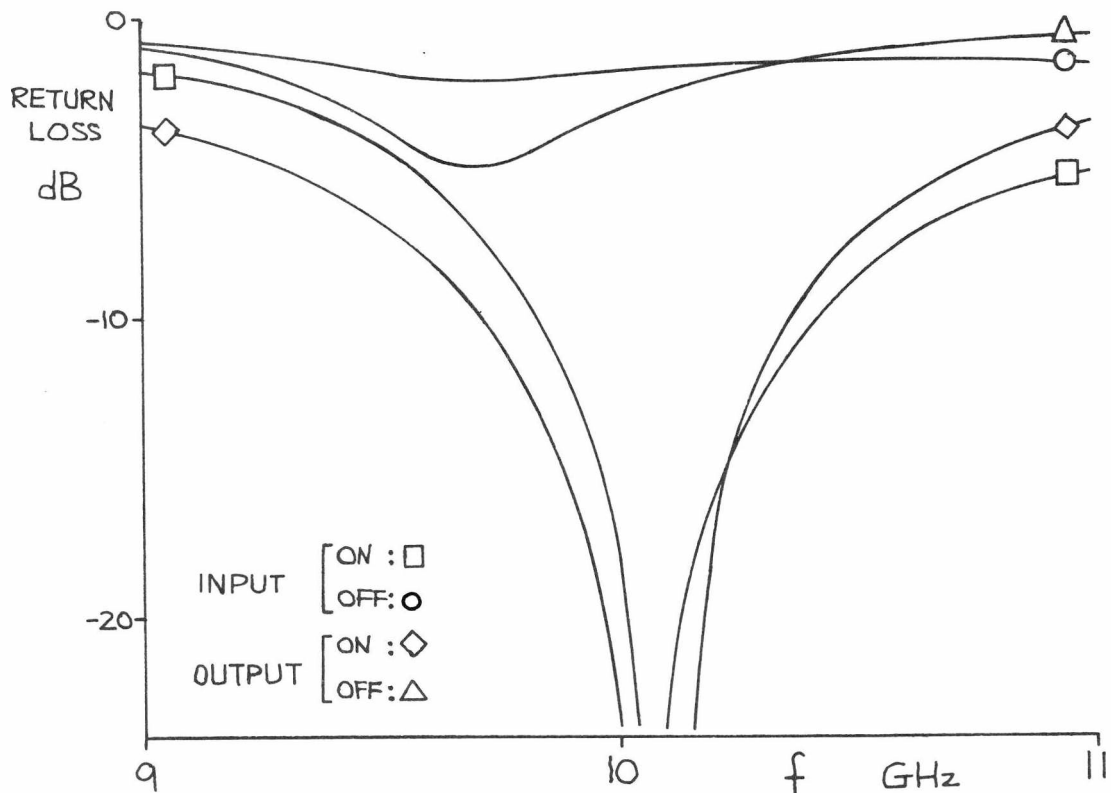


Figure 2.10b : Return losses of the MESFET amplifier/switch for both its on and off states.

is little affected by shifts in the dips.

Also shown in Figure 2.10 is the response of the amplifier with the MESFET pinched-off, ie. the amplifier used as a switch. The scattering parameter data for these responses was obtained from the lumped element model of the device with  $C_f = 0.056$  pF. (These parameters are shown in Figure 2.7). As can be seen, the amplifier's forward gain becomes an attenuation such that the amplifier gives a 16.8 dB on to off ratio at 10 GHz when used as a switch. The input and output return losses are seen to be highly reflective, a property which will be shown to be of use in the design of the phase shifters. The d.c. breaks and bias feeds associated with this circuit will be discussed in a latter section when the switching behaviour of this switch is considered.

A microwave switch can, therefore, be made by taking a MESFET amplifier which gives a gain when its device is normally biased and an insertion loss when the device's bias is adjusted to cause pinch-off. This control can be effected by applying a voltage to the device's gate. If this is zero volts then the device will be turned on and the switch will behave as a matched amplifier. If the voltage is taken negative to typically -3v, the device will be pinched-off and the switch will give an attenuation being also mismatched.

#### 2.6.4 Optimum Switching Device Performance

It is worth considering at this point the specific features of a device suitable for use as a microwave switch and ways by which a device's structure may be optimised to achieve good performance for this function. The GAT4 device like most other commercially available devices have had their geometry optimised for low noise small signal

conditions (power devices apart) and probably do not give good switch performance especially in relation to their pinched-off characteristics. The properties of a device suitable for use as a switch can be listed as follows:

- I. A stable forward gain of a few dBs at the frequency of interest ( $G_T > 1$  and possibly  $S_{21} > 1$  with  $K > 1$ ).
- II. Reflection coefficient magnitudes which are low so as to facilitate simple and broadband matching ( $|S_{11}|$  and  $|S_{22}| \rightarrow 0$ ).
- III. A very small value of gain (high insertion loss) when pinched-off to give a high on to off ratio. ( $S_{21} \rightarrow 0$  and in turn  $G_T \rightarrow 0$ ).
- IV. Either reflection coefficients that are invariant with the change in gate bias from device fully on (0v) to pinch-off so that the switch is always matched or,
- V. Reflection coefficients that change appreciably, possibly to unity in magnitude when the device is pinched-off so that the switch is highly reflective when off.
- VI. Good signal handling.

Points I and III are satisfied by the dual-gate MESFET device and also to some extent point IV, its reflection coefficients changing slightly with device bias. However, in respect of points V and VI the advantage is with the single-gate device. For dual and single-gate devices with having the same gate geometry then the single-gate has a 3 dB higher signal handling ability when measured in terms of 1 dB gain

compression<sup>4,21</sup>. In comparing the two types of device, if a reasonable match is required at all bias conditions, then the dual-gate must be used noting also its good on to off ratio. In this work the single-gate device is being investigated. It appears to have limited on to off ratio and exhibits large mismatches when biased off. The large mismatches might be put to good use but an improvement in its on to off ratio would be desirable.

In the lumped element model it was seen that the internal feedback capacitance ( $C_f$ ) seemed to have a significant effect on the off biased device's insertion loss. If  $C_f$  could be reduced then the loss would be increased resulting in a larger on to off ratio. Possible methods of achieving this are a larger gate to drain spacing to reduce the inter-electrode capacitance and increase the terminal voltages to reduce the depletion capacitances<sup>16</sup>. This is only possible if terminal spacing is increased and possibly reduce the doping density to reduce the likelihood of voltage breakdown. The consequent reduction in gain could be tolerated since this is more than adequate at present.

It might be possible to select a device that offered better off biased performance than the GAT4. Vendelin<sup>14</sup> gives a list of the lumped element component values of several MESFET devices. A Nippon Electric Co. device which coincidentally has the same gate dimensions as the GAT4 is given as having a  $C_f$  of 0.004 pF (c.f. GAT4 :  $C_f = 0.014$  pF). Notwithstanding the change in  $C_f$  with device bias, this could be an indication of better device behaviour when pinched-off.

Since the gate capacitance,  $C_g$ , is highly dependent on gate to source voltage,  $V_{GS}$  (equation 2.7) then by making this more negative a greater decrease in  $C_g$  can be effected which in turn should change the device's input reflection coefficient ( $S_{11}$ ) more and increase the coefficient's magnitude. It is not possible to reduce  $V_{GS}$  much below -3v because the GAT4's voltage breakdown limit is being reached. This

is given as <sup>4</sup> 10v and being, in this case, the total gate to drain voltage which is 5v + 3v at pinch-off, a margin of 2v allowed for safety. It is obviously possible to reduce  $V_{DS}$  to allow an increase in  $V_{GS}$  at pinch-off since the increase in  $V_{DS}$  will change the device's scattering parameters and reduce its signal handling ability drastically. Alternatively, if the device's geometry can be changed, then for an increase in  $V_{GS}$  to have its maximum effect an increase in channel thickness under the gate may be required to allow for a greater depletion width<sup>16</sup>. At present, the GAT4 has<sup>2</sup> a channel thickness of approximately 0.35  $\mu\text{m}$  and hence an increase is feasible keeping in mind its gate length of 1  $\mu\text{m}$ .

Considering the device's output reflection coefficient,  $S_{22}$ , then the feedback capacitance,  $C_f$ , seems to have some effect on this (see Figure 2.7) such that a small value of  $C_f$  causes  $S_{22}$ 's magnitude to become larger when the device is pinched-off. Also, it is thought that reducing the drain capacitance,  $C_d$ , would further cause the magnitude of  $S_{22}$  to tend to unity. The physical changes required to improve  $S_{22}$  are consistent with those to reduce  $|S_{21}|$  and increase  $|S_{11}|$  as just discussed.

## 2.7 TWO-WAY MESFET SWITCHES

Having demonstrated the potential of the single-gate MESFET device as a microwave switch that can give a gain, circuits will now be developed using this device which can be used in the construction of a phase shifter. An important feature of the MESFET amplifier is its unilateral nature. In phase shifter circuits the MESFET amplifier can therefore only be used with transmission type phase shift networks<sup>22</sup> such as the switched path types. This is not an important constraint

since it only precludes the reflection type phase shifter and allows the choice of the three switched path types. Though these networks could use the simple MESFET switch so far described, a more effective and economic switch would be one that could switch specifically between two circuits. Figure 2.11 shows a general switched path circuit and its associated two-way switches. Because of the unilateral nature of the MESFET switch, the two-way switch at the input is different to that at the output in that it behaves as a selective dividing circuit whereas the one at the output is a selective combiner being able to select one of two signals.

It would appear at first that both of these types of two-way MESFET switch needs to be developed. However, only one two-way switch need be used to effectively switch between the two paths, the justification for which will be discussed in the following chapters. In this work, the design will concentrate on the output combining type two-way switch. This choice is based on d.c. bias and control considerations.

To construct a two-way switch, two devices are required, one that is biased on and another that is pinched-off. The d.c. conditions applied to the two devices are such that the +5v drain bias does not change when they are switched, only the drain currents and when one gate voltage is zero the other is at  $V_p$ . It is therefore possible to connect their drains together so that they can share a common bias, the common drain connection being also the combining signal junction. The two devices' gates are separate to allow the complementary control voltages to be applied and the two differing signals from each half of the switched path length network are also applied to the gates.

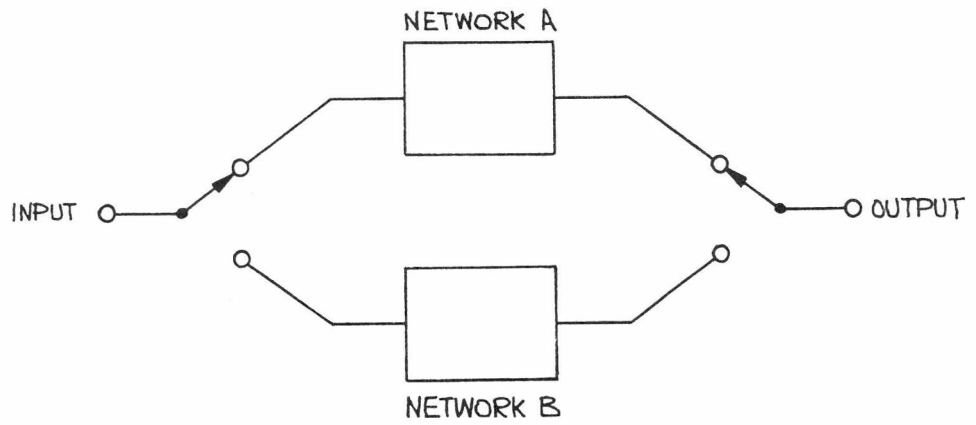


Figure 2.11 : General form of a switched path circuit showing the two-way switches.

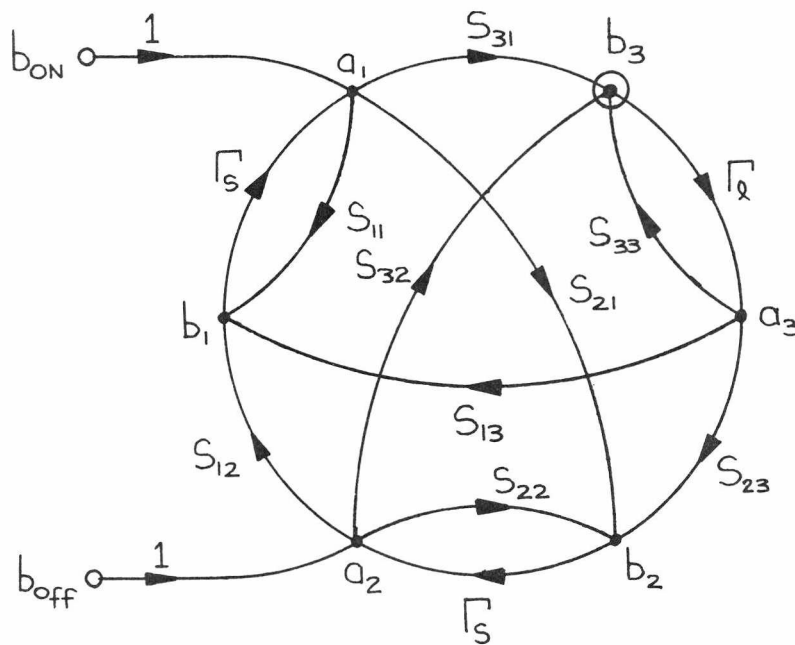


Figure 2.12 : Three port flow diagram showing the nine scattering parameters and the three terminations.

### 2.7.1 Three Port Theory

The three port scattering parameters (S) of the device pair are determined by converting<sup>23</sup> the scattering parameters of each device to admittance parameters (Y) and then combining both sets according to:

$$[Y] = \begin{bmatrix} Y_{a11} & 0 & Y_{a12} \\ 0 & Y_{b11} & Y_{b12} \\ Y_{a21} & Y_{b21} & Y_{a22} + Y_{b22} \end{bmatrix} \quad (2.22)$$

where Y are the three port parameters of the device pair and  $Y_a$  and  $Y_b$  are the two port parameters for each device. The three port parameters [Y] are converted back to scattering parameters by first reducing them to those of a two port by terminating the third port with  $Y_o$ . Hence if,

$$[i] = [Y][v] \quad (2.23)$$

and,

$$i_3 = -Y_o v_3 \quad (2.24)$$

then from (2.23)

$$v_3 = -\frac{Y_{31} v_1}{Y_o + Y_{33}} - \frac{Y_{32} v_2}{Y_o + Y_{33}}$$

Substituting (2.25) into (2.23) then,

$$\left. \begin{aligned} i_1 &= \left( Y_{11} - \frac{Y_{13} Y_{31}}{Y_o + Y_{33}} \right) v_1 + \left( Y_{12} - \frac{Y_{13} Y_{32}}{Y_o + Y_{33}} \right) v_2 \\ i_2 &= \left( Y_{21} - \frac{Y_{31} Y_{23}}{Y_o + Y_{33}} \right) v_1 + \left( Y_{22} - \frac{Y_{23} Y_{32}}{Y_o + Y_{33}} \right) v_2 \end{aligned} \right\} \quad (2.26)$$

The four Y parameters of (2.26) can easily be converted<sup>23</sup> to scattering parameters and this process can be repeated to obtain all nine three port scattering parameters by terminating ports one and two with  $Y_0$  in turn.

Matching is applied to this three port such that the device that is biased on is matched at its input (gate). To preserve the symmetry of the two-way switch, identical matching components are placed at both device inputs. The common output junction is also matched. The required matching terminations for this three port can be obtained as follows. Let  $\Gamma_s$  be the terminations applied to both inputs and  $\Gamma_\ell$  be that applied at the common output. Let port 1 be the on device input, 2 the off device input and 3 the common output. If,

$$[b] = [S] \times [a] \quad (2.27)$$

and since  $a_2 = \Gamma_s b_2$ , substituting this into (2.27) gives,

$$a_2 = \frac{S_{21}\Gamma_s a_1}{1-S_{22}\Gamma_s} + \frac{S_{23}\Gamma_s a_3}{1-S_{22}\Gamma_s} \quad (2.28)$$

Substituting (2.28) into (2.27) gives,

$$b_1 = \left( S_{11} + \frac{S_{12}S_{21}\Gamma_s}{1-S_{22}\Gamma_s} \right) a_1 + \left( S_{13} + \frac{S_{23}S_{12}\Gamma_s}{1-S_{22}\Gamma_s} \right) a_3 \quad (2.29a)$$

$$b_3 = \left( S_{31} + \frac{S_{21}S_{32}\Gamma_s}{1-S_{22}\Gamma_s} \right) a_1 + \left( S_{33} + \frac{S_{23}S_{32}\Gamma_s}{1-S_{22}\Gamma_s} \right) a_3 \quad (2.29b)$$

Now since  $a_3 = \Gamma_\ell b_3$ , equation (2.29b) becomes,

$$b_3 \left( 1 - \Gamma_\ell \left( S_{33} + \frac{S_{23}S_{32}\Gamma_s}{1-S_{22}\Gamma_s} \right) \right) = \left( S_{31} + \frac{S_{21}S_{32}\Gamma_s}{1-S_{22}\Gamma_s} \right) a_1 \quad (2.30)$$

Substituting (2.30) into (2.29a) and (2.29b) and letting  $\Gamma_i = b_1/a_1$ , this being the on biased device's input reflection coefficient and let  $\Gamma_o = b_3/a_3$ , the output reflection coefficient then,

$$\Gamma_i = S_{11} + \frac{S_{12}S_{21}\Gamma_s}{1-S_{22}\Gamma_s} + \frac{\left( S_{13} + \frac{S_{12}S_{23}\Gamma_s}{1-S_{22}\Gamma_s} \right) \left( S_{31} + \frac{S_{21}S_{32}\Gamma_s}{1-S_{22}\Gamma_s} \Gamma_\ell \right)}{1 - \left( S_{33} + \frac{S_{23}S_{32}\Gamma_s}{1-S_{22}\Gamma_s} \right) \Gamma_\ell} \quad (2.31a)$$

$$\Gamma_o = S_{33} + \frac{S_{23}S_{32}\Gamma_s}{1-S_{22}\Gamma_s} + \frac{\left( S_{13} + \frac{S_{12}S_{23}\Gamma_s}{1-S_{22}\Gamma_s} \right) \left( S_{31} + \frac{S_{21}S_{32}\Gamma_s}{1-S_{22}\Gamma_s} \Gamma_s \right)}{1 - \left( S_{11} + \frac{S_{12}S_{21}\Gamma_s}{1-S_{22}\Gamma_s} \right) \Gamma_s} \quad (2.31b)$$

Hence, applying conjugate matching,  $\Gamma_s$  becomes  $\Gamma_i^*$  and  $\Gamma_\ell$  becomes  $\Gamma_o^*$ . These two equations can be solved iteratively until  $\Gamma_s$  and  $\Gamma_\ell$  settle to unchanging values with each calculation.

The gain of this three port can be calculated by using Mason's non-touching loop rule<sup>24</sup>. Referring to the three port flow diagram as shown in Figure 2.12, then the gains of interest are that from port one to three, the on biased device's gain (switch on gain) and that from port two to three, the off biased device's loss (switch insertion loss). Applying Mason's rule then,

$$\frac{b_3}{b_{on}} = \frac{S_{31}(1 - S_{22}\Gamma_s) + S_{21}\Gamma_s S_{32}}{1 - \Sigma(1) + \Sigma(2) - \Sigma(3)} \quad (2.32)$$

and,

$$\frac{b_3}{b_{\text{off}}} = \frac{S_{32}(1 - S_{11}\Gamma_s) + S_{12}\Gamma_s S_{31}}{1 - \Sigma(1) + \Sigma(2) - \Sigma(3)} \quad (2.33)$$

where,

$$\begin{aligned} \Sigma(1) = & S_{11}\Gamma_s + S_{22}\Gamma_s + S_{33}\Gamma_\ell + S_{13}S_{31}\Gamma_\ell\Gamma_s + S_{12}S_{21}\Gamma_\ell\Gamma_s \\ & + S_{23}S_{32}\Gamma_\ell\Gamma_s + S_{12}S_{23}S_{31}\Gamma_s^2\Gamma_\ell \end{aligned}$$

$$\Sigma(2) = S_{11}S_{22}\Gamma_s^2 + S_{11}S_{33}\Gamma_\ell\Gamma_s + S_{22}S_{33}\Gamma_\ell\Gamma_s$$

$$\Sigma(3) = S_{11}S_{22}S_{33}\Gamma_s^2\Gamma_\ell$$

Since it is the overall transducer power gain which is of interest then,

$$G_T = \frac{|b_3|^2}{|b_{\text{in}}|^2} (1 - |\Gamma_\ell|^2)(1 - |\Gamma_s|^2) \quad (2.34)$$

where  $b_{\text{in}}$  is either  $b_{\text{on}}$  or  $b_{\text{off}}$  for either the switch on or off gain.

### 2.7.2 Two-Way Switch Design

Returning now to the two device switch, then a practical difficulty is seen to occur when an attempt is made to physically connect the device drains together. The presence of the source bonding dictates that the devices are kept at least 2 mm apart. The drain bond wires hence become unacceptably long, both physically and electrically. The two drains must, therefore, be brought together with lengths of 50 ohm line. The question now arises as to what

effect these line lengths have on its performance. Of specific interest is switch gain, on to off ratio and the magnitude of the matching terminations. These can be calculated by using the above equations, the effect of the 50 ohm lines being added to the two devices' parameters before they are converted to Y parameters for combining.

The device scattering parameters used for this analysis are again the interpolated Plessey parameters for the on biased device so as to remain consistent with frequency response analyses. In the case of the off biased device, the scattering parameter data is from actual measurements done on a device. This data is more realistic than that generated by the proposed lumped element model. These measurements will be discussed in a latter chapter. The scattering parameter data use in the development of the two-way switch is given in Table 2.2.

Parameter	Device biased on	Device biased off
$S_{11}$	$0.57 \angle -156$	$0.77 \angle -70$
$S_{12}$	$0.07 \angle 41$	$0.37 \angle 33$
$S_{21}$	$1.55 \angle 42$	$0.37 \angle 27$
$S_{22}$	$0.70 \angle -74$	$0.78 \angle -45$

Table 2.2 : Device scattering parameters at 10 GHz that are used in the design of the two-way MESFET switch.

The performance of the two-way switch with devices joined by lengths of 50 ohm line is shown in Figures 2.13 and 2.14. In the region 0.1 to 0.2 wavelengths, this being the closest the two devices can be physically placed together, the gain and required matching

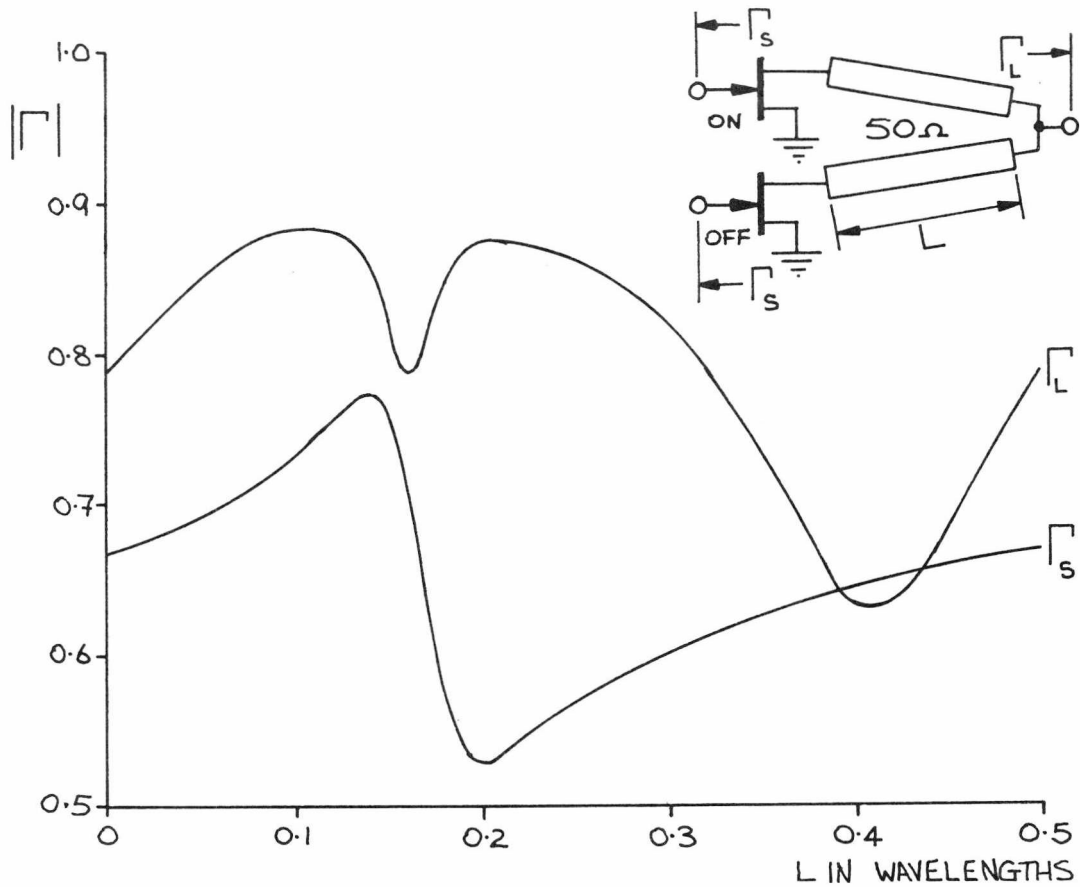


Figure 2.13 : Termination magnitudes required to match the two-way MESFET switch shown inset above as a function of the drain combining line length.

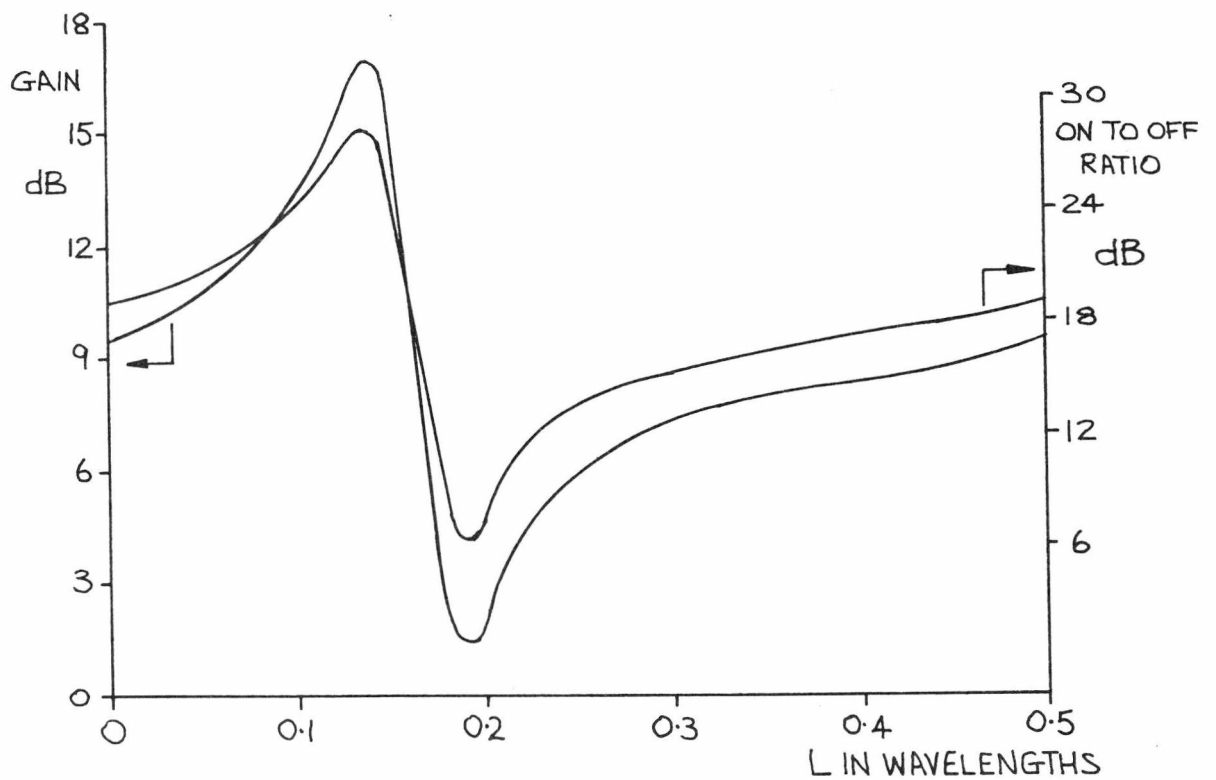


Figure 2.14 : Two-way MESFET switch (as inset in Figure 2.13) gain and on to off ratio as a function of the drain combining line length.

terminations are seen to fluctuate greatly. This is thought to be caused in part by the off biased devices  $S_{22}$  return to the common junction with an argument of 180 degrees (short circuit). If, however, the lines are increased to 0.4 wavelengths, the sensitivity of the gain and  $|\Gamma_s|$  to changes in line length drops to a minimum. Also the magnitude of the required  $\Gamma_\ell$  drops to a minimum. Matching can be achieved with a length of 50 ohm line and a quarter-wave transformer, the values for which can be determined using equations (2.20) and (2.21).

In view of the length of the lines spacing the devices and junction an attempt was made to see if by changing the impedance of part of these 50 ohm lines a match could be obtained at the common junction. This would eliminate the need for the matching components after the common output junction. If the MESFET amplifier shown in Figure 2.9 is recalled then the total electrical length of the output matching components is about 0.4 wavelengths. This indicates that if the last 0.25 wavelengths of the spacing lines where they join have their impedances changed, a match may be obtainable at the common junction. The topology of this circuit is shown in Figure 2.15.

The object of the design procedure is to make  $|\Gamma_\ell| = 0$  (or  $Z_{out} = 50$  ohms) by use of  $\theta_\ell$  and  $Z_\ell$ . Graphical analysis of this output matching circuit (using a Smith chart) has shown that the effect of  $\theta_\ell$  is to change the arguments of the device output reflection coefficients ( $\Gamma_{on}$  and  $\Gamma_{off}$ ) so that when they are transformed by  $Z_q$ , the imaginary parts of their associated admittance cancel at the output junction. The effect of  $Z_q$  is to transform the device output reflection so that when their associated admittances are combined they equal 50 ohms, both effects resulting in a  $|\Gamma_o| = 0$ . Analysis of this combining circuit has yielded a transcendental solution and the situation is further complicated by the non-unilateral nature of the devices. Hence, an iterative solution using a computer must be used.

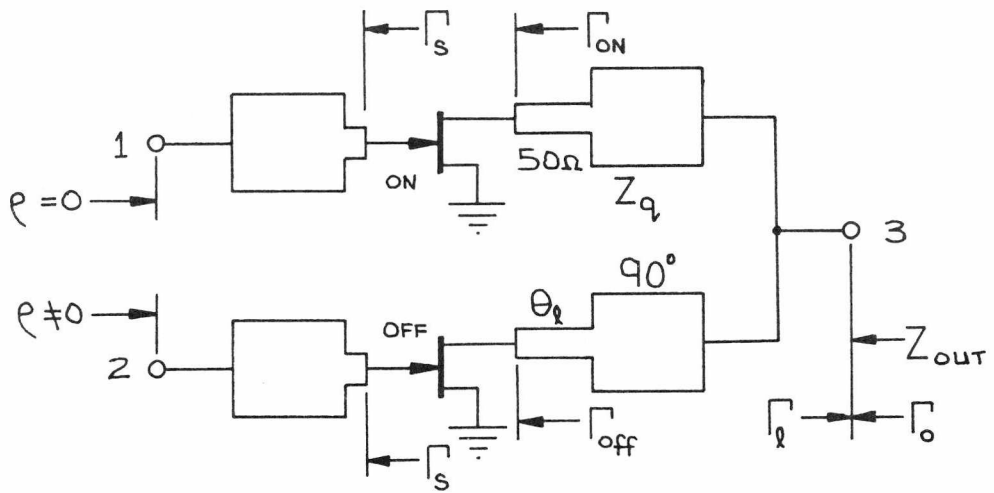


Figure 2.15 : Two-way MESFET switch topology of the circuit with output matching components placed between devices and combining junction.

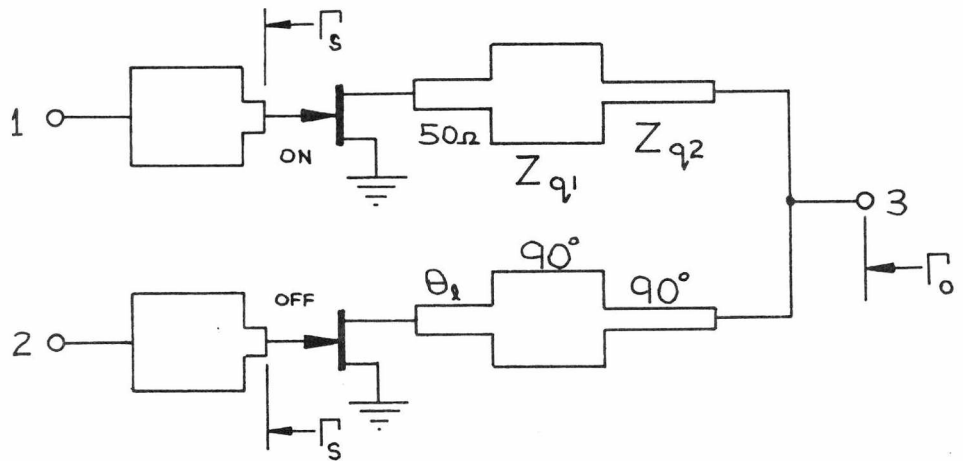


Figure 2.16 : Two-way MESFET switch with modified output matching topology consisting of double quarter-wave transformer sections.

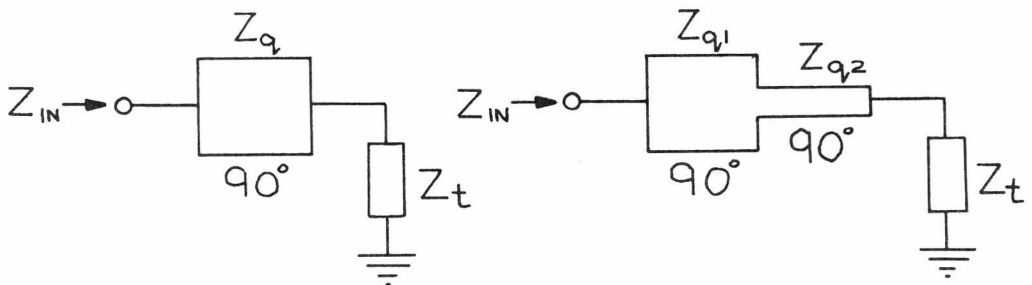


Figure 2.17 : Impedances associated with the switch output matching circuits.

The procedure is to evaluate  $\Gamma_s$  and  $\Gamma_\ell$  using equations (2.31a) and (2.31b) and then test for  $Z_{\text{out}} = 50$  ohms. If the imaginary part of  $Z_{\text{out}}$  is not zero  $\theta_\ell$  is adjusted and if the real part not equal to 50 ohms then  $Z_q$  is adjusted and then re-evaluated continuing like so until  $|\Gamma_o|$  becomes near zero.

For the device parameters given in Table 2.2,  $\theta_\ell$  has been determined to be 0.16 wavelengths,  $Z_q = 23.8$  ohms and  $\Gamma_s = 0.64 \angle 161$  degrees giving an on biased device gain (matched) of 7.7 dB and an on to off ratio of 17.7 dB. Note that the same procedure can be used to design a two-way MESFET switch which is common at its input (device gate side) rather than output. The switch, however, gives a 6.1 dB gain and an on to off ratio of only 11.8 dB.

A final variation of this two-way switch is the replacement of the output quarter-wave transformer by a cascade pair of transformers as is shown in Figure 2.16. The significance of this design will become apparent when the complete phase shifter behaviour is discussed in Chapter 4. Referring to Figure 2.17 then for the single quarter-wave section, its impedance is given by

$$Z_q = \sqrt{Z_{\text{in}} Z_t} \quad (2.35)$$

However, for the cascade pair, only the ratio of their impedances is given explicitly

$$\frac{Z_{q1}}{Z_{q2}} = \sqrt{\frac{Z_{\text{in}}}{Z_t}} \quad (2.36)$$

Hence, since  $Z_{\text{in}}$  and  $Z_t$  are not known for the switch circuit (Figure 2.15),  $Z_{q1}$  and  $Z_{q2}$  cannot be evaluated from (2.35) and (2.36), knowing

only  $Z_{q1}$ . However, if  $Z_{q2}$  is fixed,  $Z_{q1}$  can be varied to obtain a match by using the procedure used for the previous switch.  $Z_{q2}$  can be chosen by making a calculated guess for  $Z_t \approx 100$  ohms which from equations (2.35) and (2.36) gives  $Z_{q2} = 4Z_{q1}$ . Hence, to keep both impedances in the practical range for microstrip  $Z_{q2}$  is chosen as 70.7 ohms. Use of the iterative procedure gives  $Z_{q1} = 24.5$  ohms and  $\theta_\ell = 0.16$  wavelengths with  $\Gamma_s = 0.712 \angle 173$  degrees. The on biased device gain becomes 8.0 dB and the on to off ratio is 19.5 dB, a slight improvement.

The frequency responses of these two switches are shown in Figure 2.18 and 2.19. Considering first the two-way switch with the single quarter-wave section then its performance is comparable to the amplifier of Figure 2.9. Its 3 dB bandwidth is the same, being 1.4 GHz and likewise its output return loss is the same though fortunately the input return loss of the two-way switch is better. In the case of the second two-way switch with the cascade pair of output matching transformers, its gain response is seen to suffer a sharp drop at 10.5 GHz. This is thought to be caused by the off biased device's output mismatch returning to the combining junction with a phase of 180 degrees (short circuit). This effect has been seen previously when the behaviour of the first two-way switch was discussed. A satisfactory gain response can still be obtained, centred at 9.6 GHz with a slightly reduced and asymmetric bandwidth of 1.25 GHz. No significant change in return losses occurred with the addition of the second quarter-wave output matching section. Note that the pair of 70.7 ohms quarter-wave lines effectively form an uncompensated Wilkinson combiner.

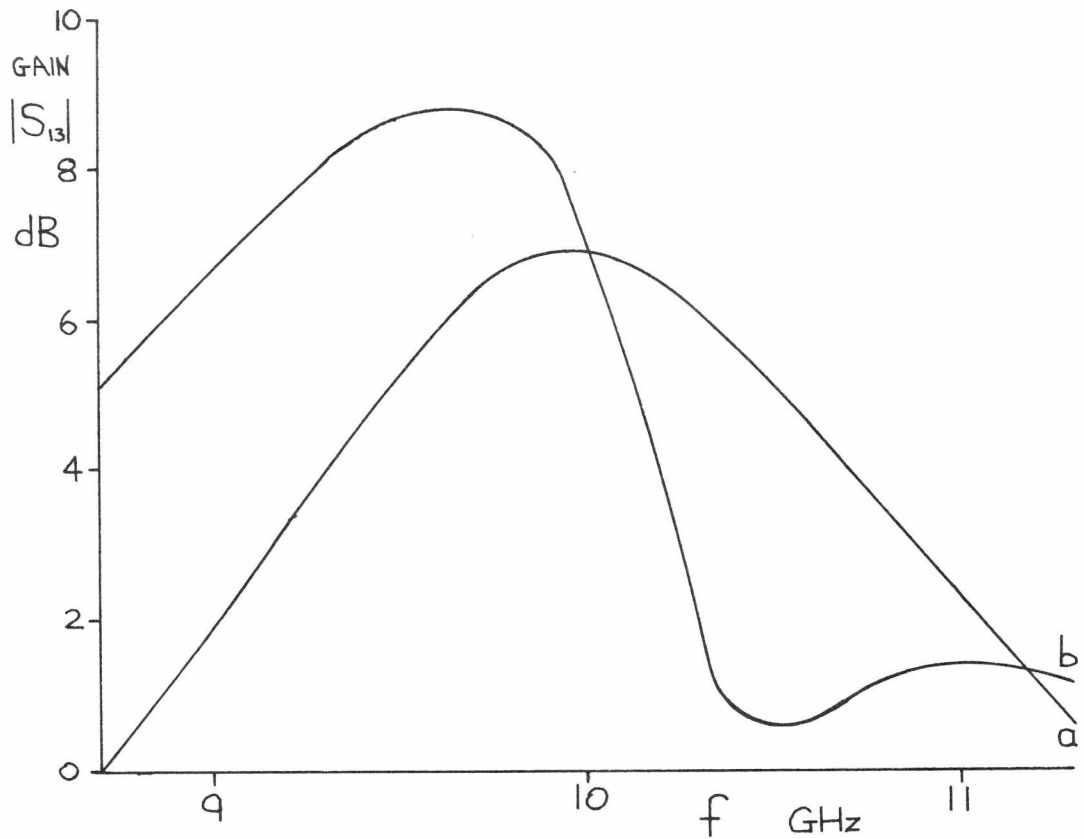


Figure 2.18 : Forward gain responses of the two-way MESFET switches.  
 a : switch with single quarter-wave output match and  
 b : double.

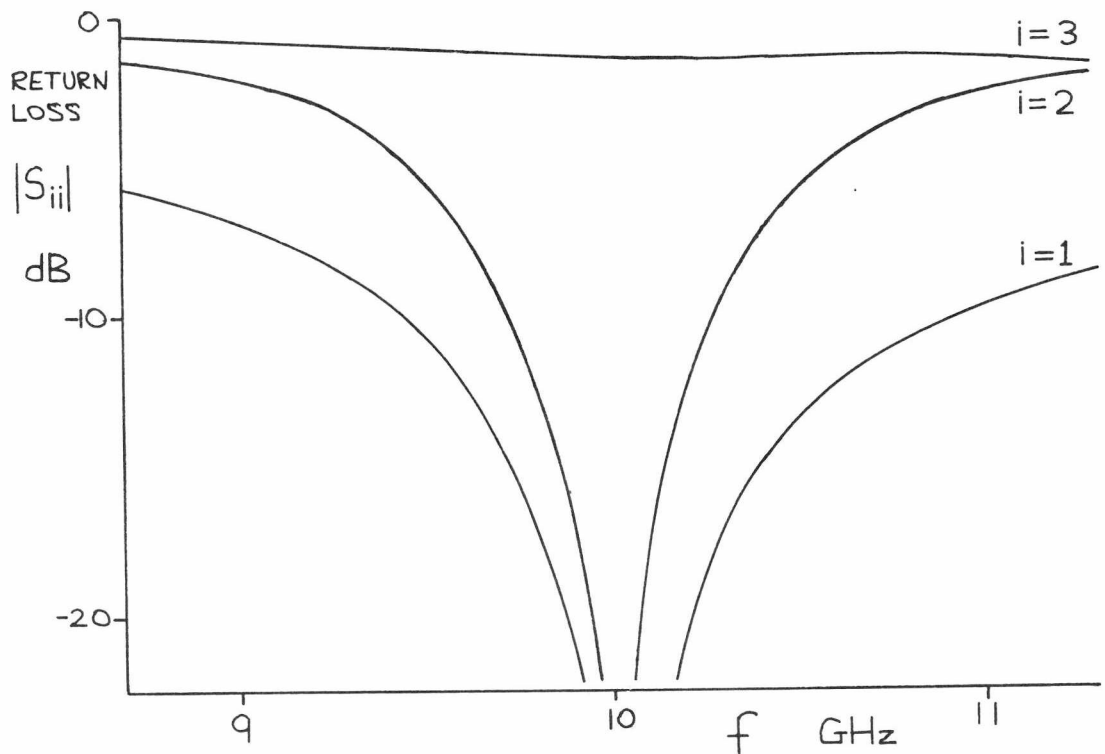


Figure 2.19 : Return losses of the two-way MESFET switch with the single quarter-wave output matching section.

## 2.8 SWITCHING PERFORMANCE, LIMITS AND DEVICE CONTROL

The MESFET device when switched, is inherent a fast device. A measure of this can be obtained by noting the device's cut-off frequency,  $f_T$ , which is given by<sup>25</sup>

$$f_T = g_M / 2\pi C_g \quad (2.37)$$

If this is evaluated for the GAT4 device using the lumped element model values for  $g_M$  and  $C_g$  then  $f_T = 11.4$  GHz. This indicates that switching times of under 100 pS are possible. This has been confirmed in digital measurement by Van Tuy1 and Liechti<sup>25</sup> who observed 50 pS rise time and microwave switching measurements by Liechti<sup>26</sup> who obtained a 70 pS response time. Both of these were with 1  $\mu\text{m}$  gate length devices though the latter was a dual-gate.

In a microwave control situation using a single-gate device both microwave and control (modulation) have to be applied together to the device's gate. To keep these two signals separate at their sources they must be applied via filters. For the modulation, a low pass filter and the microwave signal a high pass (or band pass) such that the low pass's 3 dB cut-off corresponds to the 3 dB cut-off of the high pass. An optimum is obtained when this cut-off occurs at half the carrier frequency. Garver<sup>22</sup> has shown that this sets a limit to the maximum switching speed of

$$T_{\min} = 1.24/f_o \text{ (s)} \quad (2.38)$$

Hence, for a 10 GHz centre frequency a 124 pS limit exists. Note that this applies only to unbalanced structures such as the MESFET switch.

The low pass filters used to apply bias and modulation to the device are shown in Figure 2.20. Considering the capacitors  $C_i$  and  $C_o$  then these are serving as d.c. breaks. Since the device's drain voltage does not change with switching, the voltage across  $C_o$  is constant and the charging or discharging of this component does not need to be considered.  $C_o$  can be made large so as not to disturb the microwave output. In the case of  $C_i$ , however, the voltage on the gate side of this component must rise and fall with the control voltage on the MESFET device's gate. To obtain an estimate of the effect of  $C_i$  on the device switching speed the gate drive circuit must be considered.

The gate voltage requirements are -3v to pinch the device and 0v to bias it on. Also, it would be convenient to be able to adjust the device on bias to a slightly negative value to trim the switch's gain. For the two-way MESFET switch a complementary device drive is further required. This can be accomplished by using a differential amplifier as shown in Figure 2.21. The variable resistors allow the devices to be trimmed. The drive can be from a TTL logic source or any other that can give 0v to +2v or more of output. The circuit should be fast because of its non-saturating switching behaviour.

This drive circuit, however, can only give a limited output current to charge the capacitances associated with the gate circuitry. The gate itself takes a negligible current at low frequencies. A simple estimate of the switching behaviour of the drive circuit can be obtained by reducing it to an equivalent shown in Figure 2.22. The current generated represents the output of transistor in the pair, R the resistive load on the transistor of interest and C the parallel capacitance of all those on the gate circuit such as  $C_g$  itself,  $C_o$  and any plate capacitance of the microstrip to its ground plane. Solution for  $V_g$  as a function of time gives,



$$V_g = iR(1 - \exp(-t/RC)) - 3 \quad (2.39a)$$

for C charging, ie.  $V_g$  rising from -3 to 0v and

$$V_g = iR \exp(-t/RC) - 3 \quad (2.39b)$$

for C discharging, ie.  $V_g$  falling from 0 to -3v. Note that the product  $iR$  is 3v since this determines the devices on state bias of 0v. Taking a value of  $R = 150$  ohms (hence,  $i = 20$  mA),  $C = 10$  pF of which 2 pF is due to the device and microstrip and the remainder the input capacitor  $C_o$  then the following rise and fall times occur as given in Table 2.3

$V_g$ (v)	$t_r$ (nS)	$t_f$ (nS)
0	-	0
-0.4	3.0	0.21
-0.7	2.2	0.4
-1.0	1.65	0.61
-2.0	0.61	1.65
-3.0	0	-

Table 2.3 : Device control voltage as a function of time just after switching.

Switching times of the order of nanoseconds are therefore likely to be observed with this drive circuit. An increase in speed can be obtained by reducing C or the R to i ratio. C is probably approaching its lower limit just below 10 pF since its reactance is becoming significant.

## 2.9 CONCLUSION

The ability of the single-gate MESFET device to perform microwave switching and give an associated gain appears to be feasible. The proposed switch is a narrow band MESFET amplifier that gives an on gain of better than 7 dB in a 1.4 GHz bandwidth with a switch on to off ratio of about 17 dB. This switch though matched when on exhibits large mismatches when off. This switch idea has been extended to give a two-way MESFET switch suitable for use in the design of a phase shifter. It appears that the switching speed of the MESFET switch is restricted more by its drive circuitry than any fundamental switching limit. Consideration has been given to device mounting, its scattering parameters and their measurement. A scattering parameter fit to a lumped element model allowed an estimate of the device's off biased parameters to be obtained.

2.10 REFERENCES

- 1 EDN, Vol. 25, 20 June 1980, pp. 159.
- 2 Private Communication with Plessey Optoelectronics and Microwave Ltd., July 1983.
- 3 R.S. Butlin, D. Parker, A.J. Waller and J.A. Turner, Improvements in Low Noise Gallium Arsenide FETs for X-Band Applications, 6th European Microwave Conference, 1976, pp. 606-610.
- 4 Plessey GAT4 Data Sheet, Publication No. PS1872, Issue 2-1177.
- 5 Private Communication with Plessey Optoelectronics and Microwave Ltd., December 1981.
- 6 N.A. Slaymaker, R.A. Soares and J.A. Turner, GaAs MESFET Small-Signal X-Band Amplifiers, IEEE Trans. MTT24, June 1976, pp. 329-337.
- 7 G.L. Matthaii, L. Young and E.M.T. Jones, Microwave Filters etc., McGraw-Hill, 1964, p. 190.
- 8 H. Howe, Stripline Design, Artech, p. 35.
- 9 3M Epsilam 10 Data Sheet.
- 10 I.J. Bahl and D.K. Trivedi, A Designer's Guide to Microstrip Line, Microwaves, May 1977, pp. 174-182.
- 11 J.S. Wight, O.P. Jain, W.J. Chudobaik and V. Makios, Equivalent Circuits of Microstrip Impedances and Launchers, IEEE Trans. MTT22, January 1974, pp. 48-52.
- 12 R.F. Bauer and P. Penfield, De-Embedding and Unterminating, IEEE Trans. MTT22, March 1974, pp. 282-288.
- 13 L.A. Glasser, An Analysis of Microwave De-Embedding Errors, IEEE Trans. MTT26, May 1978, pp. 379-380.

- 14 G.D. Vendelin and M. Omori, Try CAD for Accurate GaAs MESFET Models, *Microwaves*, June 1975, pp. 58-70.
- 15 R.H. Dawson, Equivalent Circuit of the Schottky-Barrier Field-Effect Transistors at Microwave Frequencies, *IEEE Trans. MTT23*, June 1975, pp. 499-501.
- 16 S.M. Sze, *Physics of Semiconductor Design*, Wiley, 1969, pp. 20, 371 and 397.
- 17 R.A. Minasian, Modelling the MESFET Output Nonlinearity, *Electronics Letters*, Vol. 15, 16 August 1979, pp. 515-516.
- 18 R.A. Minasian, Large Signal GaAs MESFET Model and Distortion Analysis, *Electronics Letters*, Vol. 14, 16 March 1978, pp. 183-185.
- 19 H.A. Willing, C. Rauscher and P. de Santis, A Technique for Predicting Large-Signal Performance of a GaAs MESFET, *IEEE Trans. MTT26*, December 1978, pp. 1017-1023.
- 20 Tri T. Ha, *Solid-State Microwave Amplifier Design*, Wiley, 1981, pp. 34-40 and p. 67.
- 21 Plessey DUGAT 10/000 Data Sheet, Publication No. PS4781, Issue 2-179.
- 22 R.V. Garver, *Microwave Diode Control Devices*, Artech, 1976, pp. 63-65 and p. 236.
- 23 R.W. Beatty and D.M. Kerns, Relationship Between Different Kinds of Network Parameters, *Proc. IEEE*, Vol. 52, January 1964, p. 84.
- 24 S Parameter Design, Hewlett Packard Application Note 154, May 1973, p. 11 (Mason's Rule)
- 25 R.L. Van Tuy1 and C.A. Liechti, High-Speed Integrated Logic with

GaAs MESFET's, IEEE J. Solid-State Circuits, SC9, October 1974, pp. 269-276.

- 26 C.A. Liechti, Performance of Dual-Gate GaAs MESFET's as Gain-Controlled Low-Noise Amplifiers and High-Speed Modulators, IEEE Trans. MTT23, June 1975, pp. 461-469.

CHAPTER 3POWER DIVIDING AND PHASE SHIFTING NETWORKS3.1 INTRODUCTION

This chapter will concern itself with circuits that can be used to cause phase shifts. Of specific interest are circuits that can be used with the FET switches as described in Chapter 2. The general form of the overall phase shifter circuit used will be introduced and the distinction between time delay and constant phase types stated. The type of circuit required is that which gives a required phase difference between a pair of output ports, the outputs being of equal amplitude. A further requirement is that, in some circumstances, a constant amplitude and phase difference is needed over a wide bandwidth. The behaviour of various power dividing circuits used in conjunction with these phase shifting networks is considered. In particular, a power divider that produces an inherent broadband antiphase power division will also be described.

3.2 GENERAL FORM OF THE COMPLETE PHASE SHIFTER

In Chapter 2 it was shown how a single gate MESFET device could be used as an amplifying microwave switch. This idea was extended to give a two-way switch which could route and amplify one of a pair of input signals to a common output. The two-way switch with the common output was preferred since the devices can share a common drain bias

network. If two equal amplitude signals,  $V_{\text{exp}}(-j\omega t + \phi_1)$  and  $V_{\text{exp}}(-j\omega t + \phi_2)$ , are applied to the two-way switch's inputs, the phase between these two signals differing by the required phase shift,  $\Delta\phi = \phi_1 - \phi_2$ , one signal with its associated phase will be amplified by the device that is biased on and the other attenuated by the device which is biased off. Switching of the two devices biases will cause the other signal to be amplified and the first to be attenuated. The phase difference  $\Delta\phi$  will therefore be imposed on the transmitted signal appearing at the two-way switch's output.

The pair of signals can be generated by a 3 dB power divider such as either the Wilkinson<sup>1</sup>, a tee junction<sup>2</sup> or the hybrid ring<sup>3</sup>. Briefly, each can give equal amplitude signals with the same phase ( $\phi_1 = \phi_2$ ) except for the hybrid ring whose outputs are in antiphase ( $\phi_2 = \phi_1 + \pi$ ). The performance and merits of each of these in relation to the present application will be discussed in greater detail in the following sections.

Phase shifting elements can be placed at the outputs of these dividers to produce the required phase difference. A simple circuit element that is able to give a phase shift is a length of transmission line. Its electrical length  $\beta\ell$  is designed such as to give the required phase difference between the two outputs. For example, if a Wilkinson divider is used, whose outputs are in phase, then  $\Delta\phi = \beta\ell$ . The line's impedance can be 50 ohms so as to be matched. This arrangement is shown in Figure 3.1.

### 3.3 CONSTANT TIME DELAY TYPE PHASE SHIFT NETWORK

It must be noted that though the divider and 50 ohm line can be designed to give the desired phase difference  $\Delta\phi$  at a design centre

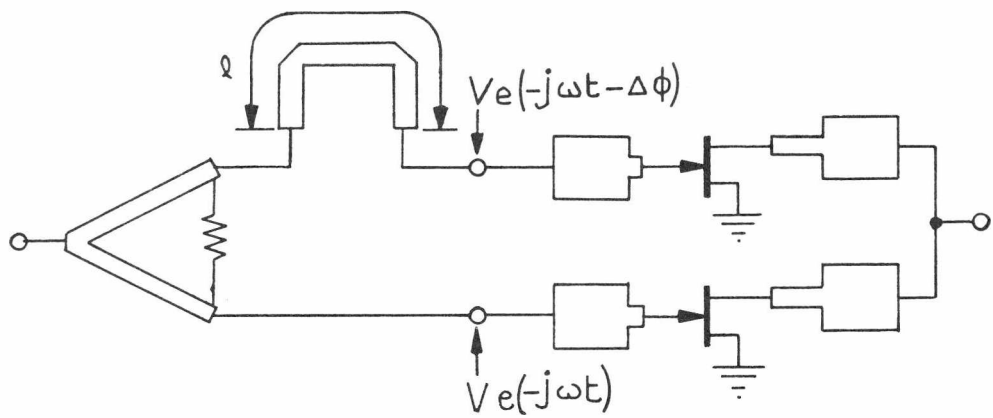


Figure 3.1 : General form of a constant time delay type digital phase shifter.

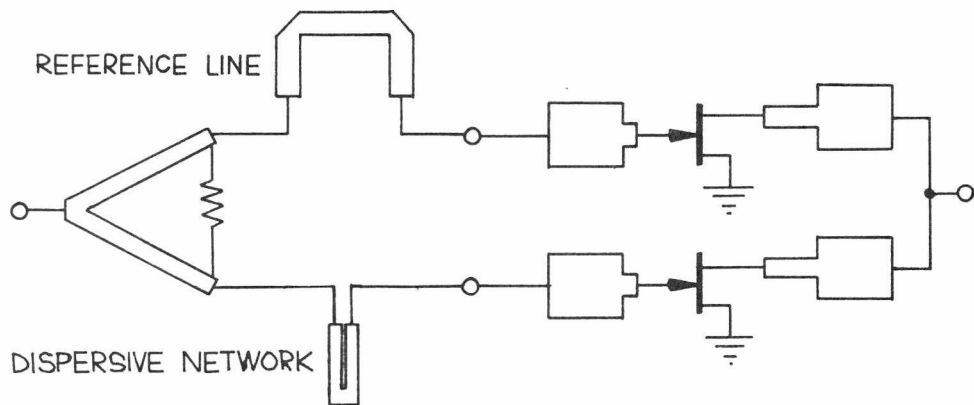


Figure 3.2 : General form of constant phase versus frequency type digital phase shifter.

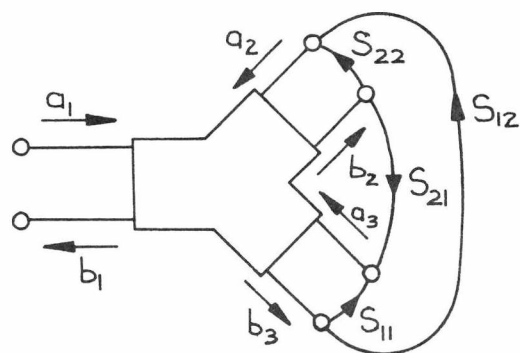


Figure 3.3 : An arbitrary power divider with its terminations as found in a phase shifter.

frequency  $f_0$ ,  $\Delta\phi$  is frequency dependant when generated by a length of non-dispersive transmission line. The phase shift  $\Delta\phi = \beta\ell = kf$ , where  $k = 18$  degrees/GHz for a half wavelength line giving 180 degrees phase shift at 10 GHz. Though this phase deviation may be tolerable in a narrow bandwidth, the large phase error further away from the centre frequency may cause a degradation in a PSK system's performance<sup>4</sup> if such a phase shifter is used as the modulator.

The transmission line type phase shifting network is, however, of interest due to its time delaying properties. Since the propagation time delay along the phase shifting line is given by  $t_d = \ell/v_p$  and since  $v_p$ , the phase velocity, is independent of frequency on a non-dispersive transmission line, this type of phase shifting network is referred to as constant time delay. From the definition  $\Delta\phi = kf$ , the relationship  $t_d = k/2\pi$  can be obtained. An application where such time delay networks are of use is pulsed and frequency agile phased array radar systems<sup>5</sup>. It is important in these systems that the electronic beam pointing angle of the antenna array is independent of frequency otherwise the beam will be spread by the spectrum of a pulse or its direction and polar diagram changed as the operating frequency is varied. These effects are caused by changes in the electrical spacing of the array's radiating elements as the operating frequency is changed. This can be compensated by use of time delay type phase shifters in the array's electronic beam pointing circuitry.

The constant time delay networks in the form of lengths of 50 ohm transmission line have been used in this present research but only for design modelling purposes to allow the development of the MESFET phase shifter concept. A length of 50 ohm line is clearly easy to model and is comparable to the constant phase shift type at one frequency. The phase shifters constructed during this work have used either networks exhibiting dispersive behaviour or a Balun type circuit to give a near constant phase

difference and 3 dB power division over a desired bandwidth. They are more complicated in structure than the time delay circuits and in the case of the dispersive networks require a reference line to compare their transmission phase as shown in Figure 3.2. The theory of two dispersive circuits, the Schiffman<sup>6</sup> coupled line and a band pass filter<sup>7</sup> and the Balun circuit using both microstrip and slotline are described later in this chapter.

#### 3.4 POWER DIVIDERS: THE TERMINATION PROBLEM

It will be recalled from section 3.4 earlier in this chapter that the general form of the complete MESFET phase shifter (Figures 3.1 or 3.2) requires a power dividing circuit at its input. It may be also recalled from Chapter 2, section 2.7 that the two-way switch has one input which is matched to 50 ohms when its associated device is biased on and a second input that is mismatched because of the off biased MESFET. This mismatch will be transmitted to the input power divider either directly or via a phase shift network or through a network reference line. To minimise insertion losses in these networks each should be matched to 50 ohms and possess all-pass properties in the desired bandwidth of interest about the centre frequency. Such all-pass networks will therefore transmit the mismatch to the divider's outputs with its magnitude unchanged. The phase of the mismatch however will be delayed and hence changed according to which network it passes through. The phase delay of these networks will at present be ignored and considered again in the following chapter when the complete behaviour of the MESFET phase shifter is discussed. Only the magnitude and phase of the mismatch, as presented to the divider's outputs, are of importance in the following analyses.

The analysis is to determine how the mismatch on the second divider output affects the transmission to the matched first output and its effect on the dividers input match. This mismatch is denoted by the parameter  $S_{22}$  in keeping with the definitions used in Chapter 2 for the two-way switch. The dividers first output is matched as given by  $S_{11} = 0$ . The parameter representing transmission from the matched output to the mismatched one (via the two-way switch)  $S_{21}$  is included in this analysis. For the devices and circuitry used in the two-way switch,  $S_{21}$  is comparable in magnitude to  $S_{22}$  and hence its effect may be significant. The parameter  $S_{12}$  representing transmission in the reverse direction to  $S_{21}$  is small, typically less than -30 dB in magnitude and can consequently eventually be neglected. The dividers input match is denoted by the scattering parameter  $R$  and the transmission scattering parameter to the matched output is  $T$ . The above parameters in relation to a typical power divider are shown in Figure 3.3.

The basic analysis is performed at one frequency, the most important feature of this analysis being to determine a divider's behaviour for a specific termination at a given centre frequency. If the variation of  $R$  and  $T$  with frequency is to be considered, then the variation of the mismatch with frequency needs to be known. This is determined firstly by the off biased device and is then transformed by the gate matching circuitry of the two-way switch and further phase delayed by the phase shifting networks. Since the mismatch from the off biased device is a function of frequency and also the phase delay through the phase shift networks, the mismatch presented to the divider's outputs has a strong frequency dependence. The phase delay is dependant on which phase shift network is used, this at present being undecided and so the mismatch variation with frequency will be ignored and reconsidered when discussing the specific forms of complete phase

shifters. The mismatch at the divider,  $S_{22}$ , and the term  $S_{21}$  will therefore be assumed constant with frequency for the purposes of the present analysis of the input power divider.

### 3.5 THE WILKINSON POWER DIVIDER

The first power divider to be considered is the Wilkinson<sup>1</sup> N-way power divider. In this work a two-way equal power split is required and this divider serves this purpose well. Its structure is simple consisting of a pair of quarter-wave transformers and a compensating resistor. The output ports are in phase and its input VSWR is less than 1.44:1 in an octave of bandwidth<sup>8</sup>, this bandwidth being well in excess of that of the MESFET switches. It is possible to remove the resistor without affecting the input match and power division, its purpose is to improve the output ports matching and their isolation. Since only the power division and input match is of importance in the phase shifter, the uncompensated version was also investigated. The starting point of the following analysis is the dividers scattering parameters<sup>9</sup> with all ports normalised to  $Z_0$ .

The compensated Wilkinson divider with  $\sqrt{2}Z_0$  quarter-wave lines and a 100 ohm resistor ( $2Z_0$ ) will be considered first. Its scattering matrix is<sup>9</sup>

$$[\mathbf{w}] = \frac{1}{\sqrt{2}} \begin{bmatrix} 0 & -j & -j \\ -j & 0 & 0 \\ -j & 0 & 0 \end{bmatrix} \quad (3.1)$$

If,

$$[\mathbf{b}] = [\mathbf{W}] \times [\mathbf{a}]$$

where,

$$\left. \begin{aligned} a_1 &= \text{input signal} \\ a_2 &= S_{22}b_2 + S_{21}b_3 \\ a_3 &= S_{12}b_2 + S_{11}b_3 \end{aligned} \right\} \quad (3.2)$$

then, 
$$b_1 = -j(S_{22}b_2 + S_{21}b_3)/\sqrt{2} - j(S_{12}b_2 + S_{11}b_3)/\sqrt{2} \quad (3.3)$$

$$b_2 = -j a_1/\sqrt{2} \quad (3.4)$$

$$b_3 = -j a_1 \sqrt{2} \quad (3.5)$$

Rearranging (3.2) and substituting (3.3) and (3.4) into this equation:

$$b_1 = -(S_{22} + S_{12} + S_{21} + S_{11})a_1/2$$

$$\therefore R = b_1/a_1 = -(S_{22} + S_{12} + S_{21} + S_{11})/2 \quad (3.6)$$

and from (3.4)

$$T = b_3/a_1 = -j/\sqrt{2} \quad (3.7)$$

The performance of the compensated Wilkinson power divider can be summarised as follows:

- I. T, the power division, is -3 dB and is independent of the terminations  $S_{22}$  etc.
- II. R, the divider's input mismatch is determined by  $S_{22}$  and the terms  $S_{21}$ ,  $S_{12}$  and  $S_{11}$ .
- III.  $|R|$  is 6 dB better than  $|(S_{22} + S_{21} + S_{12} + S_{11})|$ .
- IV. The argument of  $(S_{22} + S_{21} + S_{12} + S_{11})$  has no effect on  $|R|$ .
- V. Interchanging  $S_{22}$  with  $S_{11}$  and  $S_{21}$  with  $S_{12}$  has no effect on R or T. This is equivalent to switching of the two-way switch.

Therefore if the phase shifter is to have an overall net gain, the two-way switch must have a gain of greater than 3 dB to overcome the inherent 3 dB power division loss of this divider. A net gain could be expected since the two-way switch was shown to exhibit gains of typically greater than 6 dB.

Recalling that the two-way switch has a mismatch of about -2 dB ( $|S_{22}|$ ), this results in a mismatch at the dividers input ( $|R|$ ) of -8 dB. Since  $R$  does not change when the two-way switch is toggled, it may be possible to add matching elements at the divider's input to improve this figure. This is however dependant on the interchanging of the terms  $S_{22}$  and  $S_{11}$  at the divider's outputs. The phase shift networks will cause phase shifts of their arguments and this may impose constraints on the overall phase shifter. This effect will be investigated in the following chapter.

### 3.6 THE UNCOMPENSATED WILKINSON POWER DIVIDER

This divider consists only of a pair of  $\sqrt{2}Z_0$  quarter-wave lines. A match is obtained at the input port but the isolation between the output ports and their match to  $Z_0$  has deteriorated due to the omission of the resistor. This divider's scattering matrix is<sup>9</sup>:

$$[\mathbf{V}] = \begin{bmatrix} 0 & -j/\sqrt{2} & -j/\sqrt{2} \\ -j/\sqrt{2} & 1/2 & -1/2 \\ -j/\sqrt{2} & -1/2 & 1/2 \end{bmatrix} \quad (3.8)$$

The input waves  $a_i$  are the same as for the compensated Wilkinson divider and are as given by equations (3.2).

Therefore,

$$b_1 = -j(S_{22}b_2 + S_{21}b_3)/\sqrt{2} - j(S_{12}b_2 + S_{11}b_3)/\sqrt{2} \quad (3.9)$$

$$b_2 = -j a_1/\sqrt{2} + S_{22}b_2/2 + S_{21}b_3/2 - S_{12}b_2/2 - S_{11}b_3/2 \quad (3.10)$$

$$b_3 = -j a_1/\sqrt{2} - S_{22}b_2/2 - S_{21}b_3/2 + S_{12}b_2/2 + S_{11}b_3/2 \quad (3.11)$$

Rearranging (3.10) and (3.11),

$$b_2 = \frac{-j a_1\sqrt{2}}{2-S_{22}+S_{12}} + \frac{(S_{21}-S_{11})b_3}{2-S_{22}+S_{12}} \quad (3.12)$$

$$b_3 = \frac{-j a_1/\sqrt{2}}{2-S_{11}+S_{21}} + \frac{(S_{12}-S_{22})b_2}{2-S_{11}+S_{21}} \quad (3.13)$$

Substituting (3.12) into (3.13),

$$T = \frac{b_3}{a_1} = -j\sqrt{2} \left[ \frac{1-(S_{22}-S_{12})}{2-(S_{22}+S_{11}) + (S_{21}+S_{12})} \right] \quad (3.14)$$

Substituting (3.13) into (3.12),

$$\frac{b_2}{a_1} = -j\sqrt{2} \left[ \frac{1-(S_{11}-S_{21})}{2-(S_{22}+S_{11}) + (S_{21}+S_{12})} \right] \quad (3.15)$$

Substituting (3.14) and (3.15) into (3.9),

$$R = \frac{b_1}{a_1} = \frac{-(S_{22}+S_{11}+S_{21}+S_{12}) + 2(S_{11}S_{22}-S_{12}S_{21})}{2-(S_{22}+S_{11}) + (S_{21}+S_{12})} \quad (3.16)$$

The performance of the uncompensated Wilkinson power divider can be summarised as follows:

- I.  $T$ , the transmission, is dependant in a complex manner on the magnitudes and arguments of the terminations  $S_{22}$  etc.
- II.  $R$ , the dividers input mismatch, is dependant in a complex manner on the magnitudes and arguments of the terminations  $S_{22}$  etc.
- III. If  $S_{22}$  etc. are made equal to zero then  $|R| = 0$ , ie. matched.
- IV. If  $S_{22}$  etc. are made equal to zero then  $|T| = -3$  dB, ie. equal power division. Both this and III can be expected from the scattering matrix (3.8).
- V. Interchanging  $S_{22}$  with  $S_{11}$  and  $S_{21}$  with  $S_{12}$  has no effect on  $R$ .

Therefore both  $|R|$  and  $|T|$  are dependant on the terminations of this divider. If  $S_{11}$ ,  $S_{12}$  and  $S_{21}$  are set equal to zero then this can be seen more clearly. The moduli of equations (3.14) and (3.16) become:

$$|T| = \sqrt{2} \left| \frac{1-S_{22}}{2-S_{22}} \right| \quad (3.17)$$

$$|R| = \left| \frac{S_{22}}{2-S_{22}} \right| \quad (3.18)$$

If the magnitude of  $S_{22}$  is held constant and its phase varied,  $|T|$  and  $|R|$  go through maxima and minima as the argument of  $S_{22}$  goes through 0 and 180 degrees. Values of  $|T|$  and  $|R|$  using equations (3.17) and (3.18) are plotted against the argument of  $S_{22}$  for various values of

$|S_{22}|$  in Figures 3.4 and 3.5. Values of  $|T|$  and  $|R|$  for the compensated Wilkinson divider are also shown. If for a given value of  $|S_{22}|$  its argument can be adjusted an improvement in  $|T|$  and  $|R|$  can be obtained in comparison to the compensated Wilkinson divider. Figures 3.4 and 3.5 indicate that the optimum angle for the argument of  $S_{22}$  is 180 degrees. This is reasonable since this mismatch will be transformed by the quarter-wave lines of the divider to an effective open circuit at the divider's junction. Any argument of  $S_{22}$  other than 180 degrees will cause the transformed mismatch to tend to a short circuit with the resultant reduction in  $|T|$  and increase in  $|R|$ .

It is possible to adjust the argument of  $S_{22}$  by inserting equal lengths of 50 ohm compensating lines between the divider's outputs and the phase shifting networks. The equality preserves the symmetry of the power divider and also does not contribute to the differential phase of the phase shift networks. Knowing that 180 degrees is the optimum for the phase of  $S_{22}$  (from Figures 3.4 and 3.5) and that a length of line delays the phase of a terminating mismatch by twice the line's length the relationship,

$$\theta = (\pi + \arg(S_{22}))/2 \quad (3.19)$$

can be inferred for the phase compensating line's electrical length. The optimum performance can therefore be obtained from the uncompensated Wilkinson divider for any given value of  $S_{22}$  (or  $S_{21}$  etc.). Its performance is better than that of the compensated Wilkinson under these conditions.

Having established the optimum value for the phase of  $S_{22}$  some consideration can be given to the variation of  $|R|$  and  $|T|$  with  $|S_{22}|$ . Of specific interest are their behaviour as  $|S_{22}|$  approaches unity, this

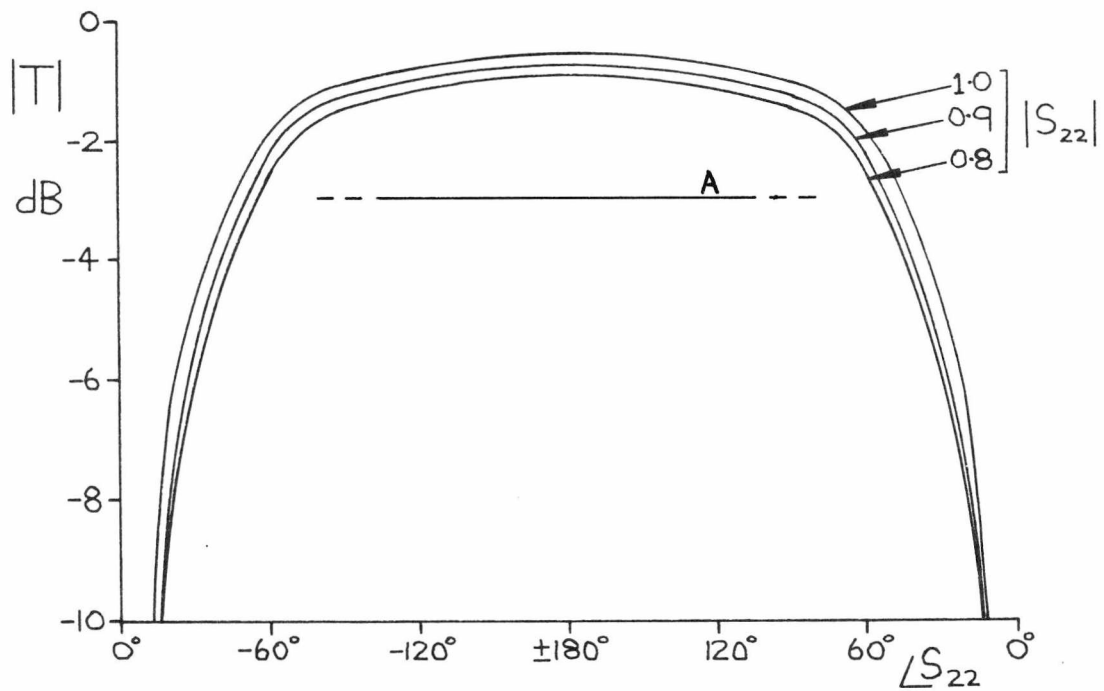


Figure 3.4 : Transmission loss from the input to one output of an uncompensated Wilkinson divider having its second output mismatched with  $S_{22}$ . **A, compensated divider, all  $|S_{22}|$ .**

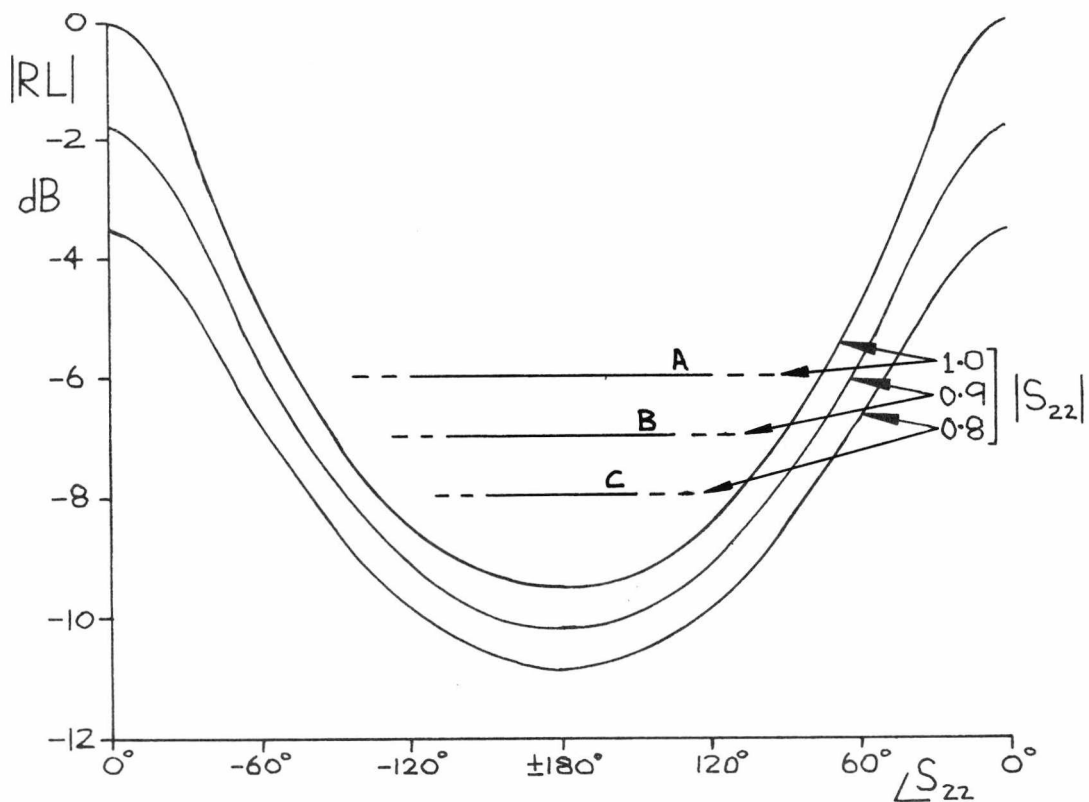


Figure 3.5 : Input return loss of an uncompensated Wilkinson divider having one of its outputs mismatched with  $S_{22}$ . **A, B and C, compensated divider.**

being the typical magnitude of reflections from the MESFET switches. Referring to Figures 3.4 and 3.5, it can be seen that as  $|S_{22}|$  tends to 1.0,  $|T|$  tends to a maximum of 0.94 (-0.51 dB) and  $|R|$  also to a maximum of 0.33 (-9.54 dB).

Two conclusions can be drawn from this. Firstly, if the transmission,  $|T|$ , is to be optimised the  $|S_{22}|$  needs to be unity or approaching it. In respect to the phase shifter circuit, if the two-way switch is to have a mismatch at its off biased input port, then it is better that this mismatch be perfect, ie.  $|S_{22}| = 1$ . Secondly, as  $|S_{22}|$  tends to unity,  $|R|$  degrades to a value of -9.54 dB. If the circuit of the uncompensated Wilkinson is considered then the quarter-wave line to the mismatched port can be neglected. It can be replaced by an open circuit at the input junction since for  $S_{22} = -1$ , the quarter-wave line transforms this to +1 at the junction. The remaining quarter-wave line to the matched output port transforms this match to  $2Z_0$  at the divider's input junction. Hence,  $2Z_0$  in parallel with an open circuit causes a mismatch of 1/3 (-9.54 dB) at the divider's input. Also, since  $|T|^2 = 1 - |R|^2$  for the lossless two port, the poor value of  $|R|$  degrades  $|T|$ .

An improvement in this situation is possible by replacing the  $\sqrt{2}Z_0$  quarter-wave lines of the Wilkinson by lines of impedance  $Z_0$ . The effect of  $S_{22}$  at the divider's junction will be unaltered, ie. an open circuit at this point. At the matched output port though, the terminating impedance  $Z_0$  will be transformed by the  $Z_0$  line to a match at the divider's input. Hence,  $|R| = 0$  and  $|T| = 1.0$ , when  $|S_{22}|$  is unity. The divider now consists of a junction of three 50 ohm lines. This is the tee divider and is analysed by reduction of its scattering matrix in the following section.

### 3.7 THE TEE POWER DIVIDER

This simple divider consists of a "y" junction of three 50 ohm lines. There are no lengths of transmission line associated with this divider and its bandwidth is very wide, extending upwards from d.c. Its properties are, however, limited at higher frequency by discontinuity effects<sup>2,10</sup>. The variation of the tee's scattering parameters from low frequencies to 10 GHz is small so these effects can be ignored. The tee's scattering matrix is:

$$[\mathbf{N}] = \frac{1}{3} \begin{bmatrix} -1 & 2 & 2 \\ 2 & -1 & 2 \\ 2 & 2 & -1 \end{bmatrix} \quad (3.20)$$

Again, the input waves  $a_i$  are the same as for the compensated Wilkinson divider as given by equations (3.2). The scattering matrix can be reduced to the equations:

$$b_1 = -a_1/3 + 2(S_{22}b_2 + S_{21}b_3)/3 + 2(S_{12}b_2 + S_{11}b_3)/3 \quad (3.21)$$

$$b_2 = 2a_1/3 - (S_{22}b_2 + S_{21}b_3)/3 + 2(S_{12}b_2 + S_{11}b_3)/3 \quad (3.22)$$

$$b_3 = 2a_1/3 + 2(S_{22}b_2 + S_{21}b_3)/3 - (S_{12}b_2 + S_{11}b_3)/3 \quad (3.23)$$

Rearranging (3.22) and (3.23),

$$b_2 = \frac{2a_1}{3+S_{22}-2S_{12}} - \frac{(S_{21}-2S_{11})b_3}{3+S_{22}-2S_{12}} \quad (3.24)$$

$$b_3 = \frac{2a_1}{3+S_{11}-2S_{21}} - \frac{(S_{21}-2S_{22})b_2}{3+S_{11}-2S_{21}} \quad (3.25)$$

Substituting (3.24) into (3.25),

$$T = \frac{b_3}{a_1} = \left[ \frac{2(1+S_{22}-S_{12})}{3+(S_{22}-2S_{21})+(S_{11}-2S_{12})-S_{11}S_{22}+S_{12}S_{21}} \right] \quad (3.26)$$

Substituting (3.25) into (3.24),

$$\frac{b_2}{a_1} = \left[ \frac{2(1+S_{11}-S_{21})}{3+(S_{22}-2S_{21})+(S_{11}-2S_{12})-S_{11}S_{22}+S_{12}S_{21}} \right] \quad (3.27)$$

Substitute (3.26) and (3.27) into (3.21),

$$R = \frac{b_1}{a_1} = \left[ \frac{S_{22}+2S_{21}+S_{11}+2S_{12}+3S_{11}S_{22}-3S_{12}S_{21}-1}{3+(S_{22}-2S_{21})+(S_{11}-2S_{12})-S_{11}S_{22}+S_{12}S_{21}} \right] \quad (3.28)$$

The performance of the tee power divider can be summarised as follows:

- I. T, the transmission to the matched output port, is dependant in a complex manner on the magnitudes and arguments of the terminations  $S_{22}$  etc.
- II. R, the divider's input mismatch, is dependant in a complex manner on the magnitudes and arguments of the terminations  $S_{22}$  etc.
- III. Setting  $S_{22} = 1$  and the remaining terminations  $S_{11}$  etc. to zero gives  $|R| = 0$  and  $|T| = 1$ .
- IV. Interchanging  $S_{22}$  with  $S_{11}$  and  $S_{21}$  with  $S_{12}$  has no effect on R.

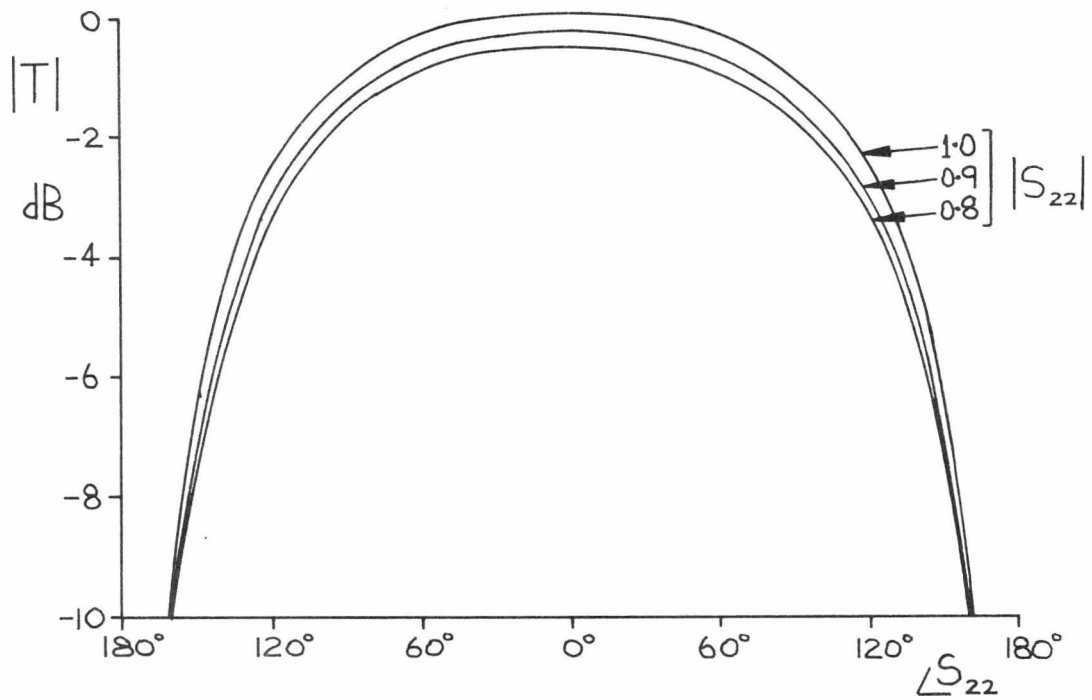


Figure 3.6 : Transmission loss from the input to one output of a tee divider having its second output mismatched with  $S_{22}$ .

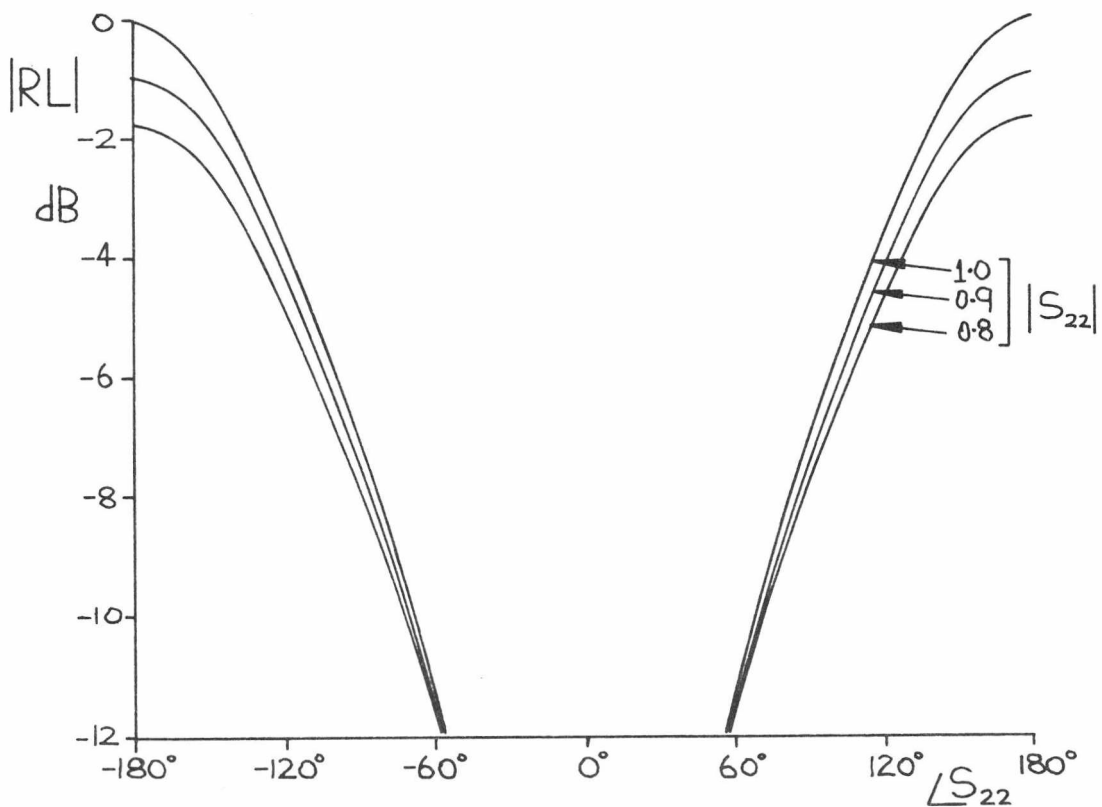


Figure 3.7 : Input return loss of a tee divider having one of its outputs mismatched with  $S_{22}$ .

Hence, again both  $|R|$  and  $|T|$  are dependant on the divider's terminations. This can be seen more clearly if the terminations  $S_{11}$ ,  $S_{12}$  and  $S_{21}$  are set equal to zero. The moduli of equations (3.26) and (3.28) therefore become,

$$|T| = 2 \left| \frac{S_{22}+1}{S_{22}+3} \right| \quad (3.29)$$

$$|R| = \left| \frac{S_{22}-1}{S_{22}+3} \right| \quad (3.30)$$

These moduli are plotted against the argument of  $S_{22}$  in Figures 3.6 and 3.7 for various fixed values of  $|S_{22}|$ . As with the uncompensated Wilkinson divider the maxima and minima of  $|R|$  and  $|T|$  are periodic with the argument of  $S_{22}$ . For this divider though they are both shifted by 180 degrees since the tee does not possess the quarter-wave lines that the Wilkinson has. Hence, again the mismatch needs to be returned to the divider's junction with a phase of 0 degrees, ie. like that of an open circuit. For a given  $S_{22}$  with an arbitrary phase, this can be achieved by lengths of 50 ohm compensating line whose length can be determined from

$$\theta = \arg(S_{22})/2 \quad (3.31)$$

Having established the optimum phase angle of  $S_{22}$ , the variation of  $|T|$  and  $|R|$  with  $|S_{22}|$  needs to be considered. These values from equations (3.29) and (3.30) are plotted in Figures 3.8 and 3.9 respectively. Also shown are  $|T|$  and  $|R|$  for the two Wilkinson power dividers from equations (3.7), (3.18), (3.6) and (3.17). As expected the tee exhibits an improvement in both  $|T|$  and  $|R|$  for  $|S_{22}| = 1$ . This

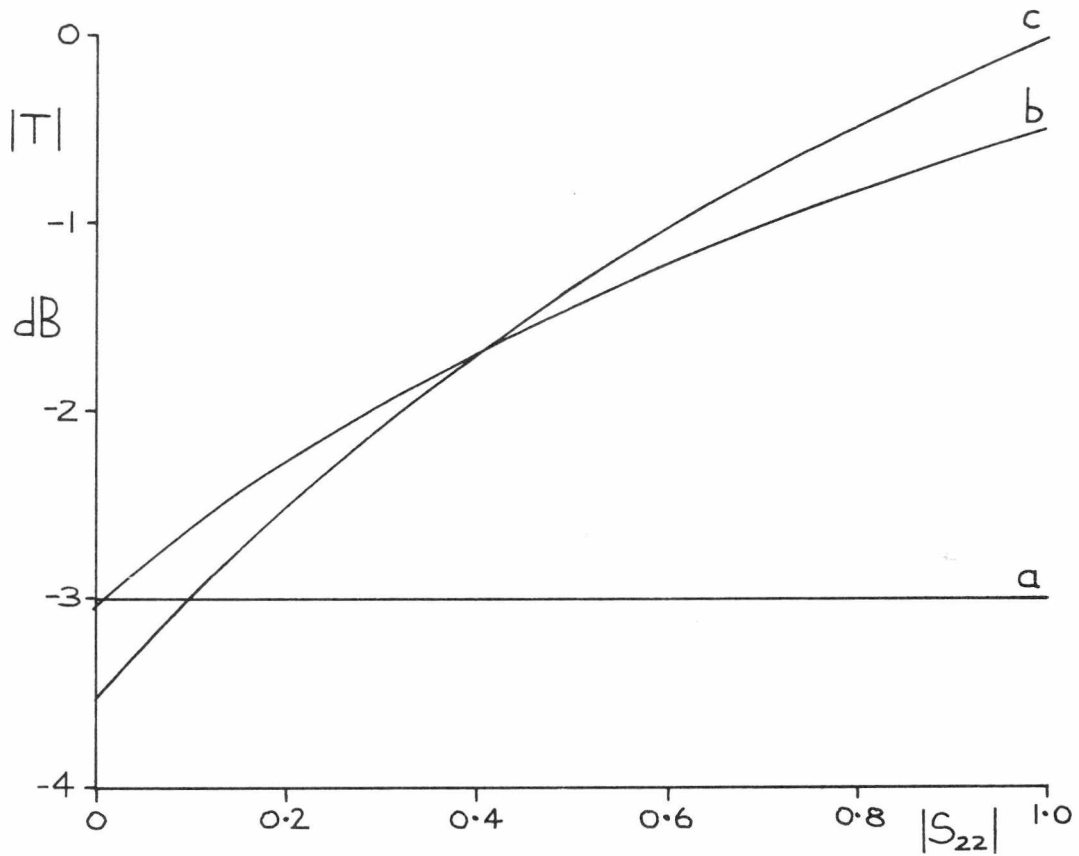


Figure 3.8 : Transmission from input to an output for various dividers with their second output terminated with  $S_{22}$  having an optimum phase. a: Compensated Wilkinson. b: Uncompensated Wilkinson. c: Tee.

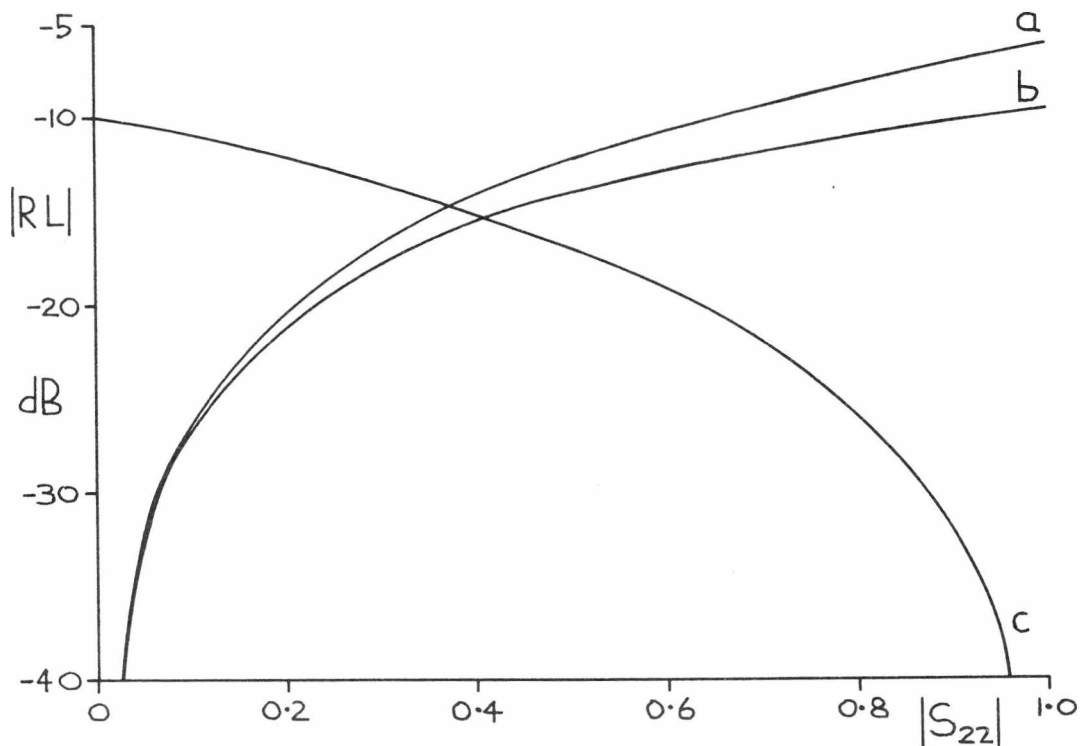


Figure 3.9 : Input return loss of various dividers with one matched output and the second terminated with  $S_{22}$  having an optimum phase. a: Compensated Wilkinson. b: Uncompensated Wilkinson. c: Tee.

advantage remains until  $|S_{22}|$  reduces to  $\sqrt{2}-1$  when the behaviour of the tee and uncompensated Wilkinson become equal. Below this the advantage is with the uncompensated Wilkinson. (The value of  $|S_{22}| = \sqrt{2}-1$  is obtained by equating equations (3.18) and (3.30) or (3.17) and (3.29) and noting that the tee requires  $S_{22}$  equal to the negative of that required by the Wilkinson. Also, the argument of R for the uncompensated Wilkinson is 0 degrees and that for the tee is 180 degrees and this must be taken into account. Solving for  $S_{22}$  yields a quadratic whose solutions are  $\pm\sqrt{2}-1$ ; hence,  $|S_{22}| = \sqrt{2}-1$ ).

The most important region of the curves in Figures 3.8 and 3.9 are however for  $S_{22} = 0.7$  and  $0.9$ , this being the typical range of mismatches produced by the MESFET switch. Taking a nominal value of  $S_{22} = 0.8$ , the tee gives a 0.35 dB advantage in  $|T|$  and a 14.6 dB improvement in  $|R|$  compared to the Wilkinson.

The bandwidth of these effects is determined by the variation of the phase of  $S_{22}$  with frequency. The lower this variation the broader the effect. The source of  $S_{22}$ , the off biased MESFET has a reasonably constant reflection phase but the switch's matching network, the phase shift networks and the compensating lines introduce a frequency dependence. A slight advantage is expected from the tee. Given a typical value of  $S_{22} = 0.9 \angle 150$  for the MESFET switch, then the compensating line's length for the tee is a quarter-wave shorter than that for the Wilkinson (from equations (3.19) and (3.31)). It is possible though that the phase shifter's bandwidth would be dominated more by the bandpass response of the MESFET switches.

Two types of phase shift network that can be used in conjunction with these dividers will now be discussed. These are the Schiffman or 'C' section coupled lines and a bandpass filter circuit.

### 3.8 SCHIFFMAN TYPE PHASE SHIFT NETWORKS

The basis for this phase shift network is a pair of coupled strip transmission lines<sup>11</sup>. If this four port is reduced to a two port by joining the two lines together at one end and applying the condition<sup>11</sup> that

$$Z_o = \sqrt{Z_{oo} \cdot Z_{oe}} \quad (3.32)$$

an all pass response is obtained.  $Z_{oo}$  and  $Z_{oe}$  are the odd and even mode impedances respectively of the coupled lines. The transmission phase of such a network is given<sup>11</sup> by

$$\cos \phi = \frac{(Z_{oe}/Z_{oo}) - \tan^2 \beta \ell}{(Z_{oe}/Z_{oo}) + \tan^2 \beta \ell} \quad (3.33)$$

Schiffman<sup>6</sup> noted that since  $Z_{oo}$  and  $Z_{oe}$  are independent, the product  $Z_{oo}Z_{oe}$  and the ratio  $Z_{oe}/Z_{oo}$  can be adjusted separately. Hence, the all pass condition (3.32) ensures a match at all frequencies and the ratio  $Z_{oe}/Z_{oo}$  and  $\ell$  in equation (3.33) can be set to give the desired phase response.

This phase response exhibits a dispersive behaviour. By comparing this with the transmission phase of a suitable length of matched transmission line a constant phase difference can be obtained. Since the Schiffman network has a transmission phase  $\phi$  of 180 degrees at its centre frequency, the reference lines length can be given by

$$\phi_R = 180 + \Delta\phi \text{ degrees} \quad (3.34)$$

where  $\Delta\phi$  is the differential phase between the Schiffman and reference lines. Choosing  $Z_{oe}/Z_{oo} = 2.73$  and comparing the Schiffman network with

a  $3\lambda/4$  reference line, a 90 degree phase difference can be obtained with an error of  $\pm 2.8$  degrees in a octave bandwidth<sup>12</sup>.

Two problems are known to exist in the design of Schiffman networks. One relates to the construction of coupled microstrip lines with large values of  $Z_{oe}/Z_{oo}$  and the other to differences in the mode phase velocities. Considering the first of these, a Schiffman network giving 180 degrees phase difference requires  $Z_{oe}/Z_{oo} = 7.18$ <sup>12</sup>. This degree of coupling is difficult to realise with microstrip. This value though gives an octave of phase shifter bandwidth. A lower value for  $Z_{oe}/Z_{oo}$  for a given phase difference can be found as follows. If the gradient of  $\phi$  with respect to  $\beta\lambda$  is derived from equation (3.33), the differential (3.35) is obtained

$$\frac{d\phi}{d\beta\lambda} = \frac{2\sqrt{Z_{oe}/Z_{oo}}}{Z_{oe}/Z_{oo} \cos^2 \beta\lambda + \sin^2 \beta\lambda} \quad (3.35)$$

If  $\beta\lambda$  is set to  $\pi/2$  (centre frequency value) and equation (3.35) equated to the gradient of the reference line (from equation (3.34)), the ratio  $Z_{oe}/Z_{oo}$  can be found for a given phase difference,  $\Delta\phi$ , hence

$$\frac{Z_{oe}}{Z_{oo}} = \left( \frac{\Delta\phi}{180} + 1 \right)^2 \quad (3.36)$$

Table 3.1 lists values of  $Z_{oe}/Z_{oo}$  on the reference line's length for commonly required values of  $\Delta\phi$ .

$\Delta\phi$ (degrees)	$Z_{oe}/Z_{oo}$	$\phi_R$ (degrees)
180	4	360
90	2.25	270
60	1.778	225
45	1.5625	202.5
22.5	1.2656	191.2

Table 3.1 : Schiffman network parameters

It can be seen that for a 180 degree Schiffman, a value of 4.0 is required. It is just possible to reduce this more but the bandwidth decreases rapidly and phase error rises. Again, this is difficult to realise especially if copper clad type substrates are used (3M's Epsilam 10). The use of two cascaded 90 degree Schiffman networks is more practicable or even a cascade of three 60 degree networks which would relax the requirement on  $Z_{oe}/Z_{oo}$  even further. Such cascades though require ever increasing lengths of reference line. Two 90 degree Schiffmans require 540 degrees of reference line and the three 60's require 720 degrees. The possible effect on complete phase shifter bandwidth as a result of long lengths of line between input divider and MESFET switch was noted in the previous section [3.7]. This effect will be considered in detail in the following chapter.

Consider now the second problem that occurs with Schiffman networks. Despite ensuring that the equality of equation (3.32) is correct a poor input return loss occurs. For a pair of lines with  $Z_{oe}/Z_{oo} = 2.73$  on a substrate having a relative dielectric constant of 10, the even mode electrical length ( $\beta_e \ell$ ) is 5.2 degrees longer and the odd mode ( $\beta_o \ell$ ) 5.2 degrees shorter<sup>12</sup> than the quarter wavelength centre frequency value of 90 degrees. Reducing the value of  $Z_{oe}/Z_{oo}$

reduces this phase difference<sup>13</sup> though the amount is not significant. Starting with a  $Z$  parameter model<sup>14</sup> of the coupled lines and converting these to cascade and scattering parameters the input return loss has been calculated for  $Z_{oe}/Z_{oo} = 2.73$ . This is shown in Figure 3.10. Using two such Schiffman networks in cascade to give a 180 degree phase shift network, the poor return loss is degraded further as shown in Figure 3.10.

A solution that can be applied to the two cascaded Schiffman networks is to space them a quarter of a wavelength apart, the reference line being extended by the same amount to preserve the 180 degree phase difference. The quarter-wave line of 50 ohms impedance acts as an impedance inverter<sup>15</sup> and effectively causes a resonance between the equivalent mismatch elements of the two Schiffmans. The calculated return loss of this arrangement is shown in Figure 3.10. As can be seen a good return loss can be obtained. However, the effect is narrow band and also the phase error becomes severe about the centre frequency as is shown in Figure 3.11.

Schiek and Kohler<sup>12</sup> and also Ho<sup>13</sup> have shown how the differences in the odd and even mode phase velocities and their effect on the Schiffman can be compensated by use of stepped design. One eighth of a wavelength of the coupled lines has one value of  $Z_{oe}/Z_{oo}$  and  $Z_{oe} \times Z_{oo}$  and the remaining eighth wavelength another pair of values. Schiek and Kohler's method attempts to bring the pole of the odd mode input impedance nearer in frequency to the zero of the even mode whereas Ho's technique deliberately causes a mismatch between the two eighth wavelength sections. Both result in an improvement in the input return loss, the first claiming better than 28 dB across an octave and the second better than 23 dB. Ho has also taken into account the short length of line that joins the coupled lines. Both give designs that are suitable for

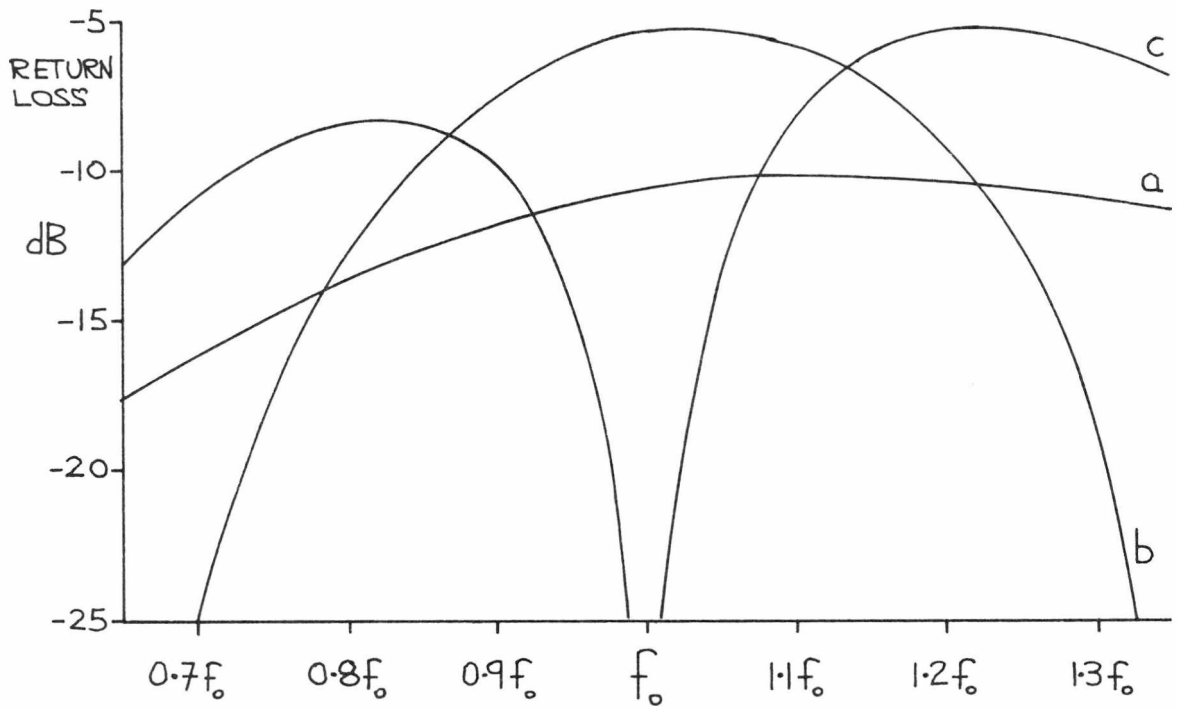


Figure 3.10 : Return loss of Schiffman coupled lines having  $\theta_e \neq \theta_o$ .  
 a: Single coupled line. b: Cascaded pair. c: Cascaded pair spaced by a quarter-wave 50 ohm line.

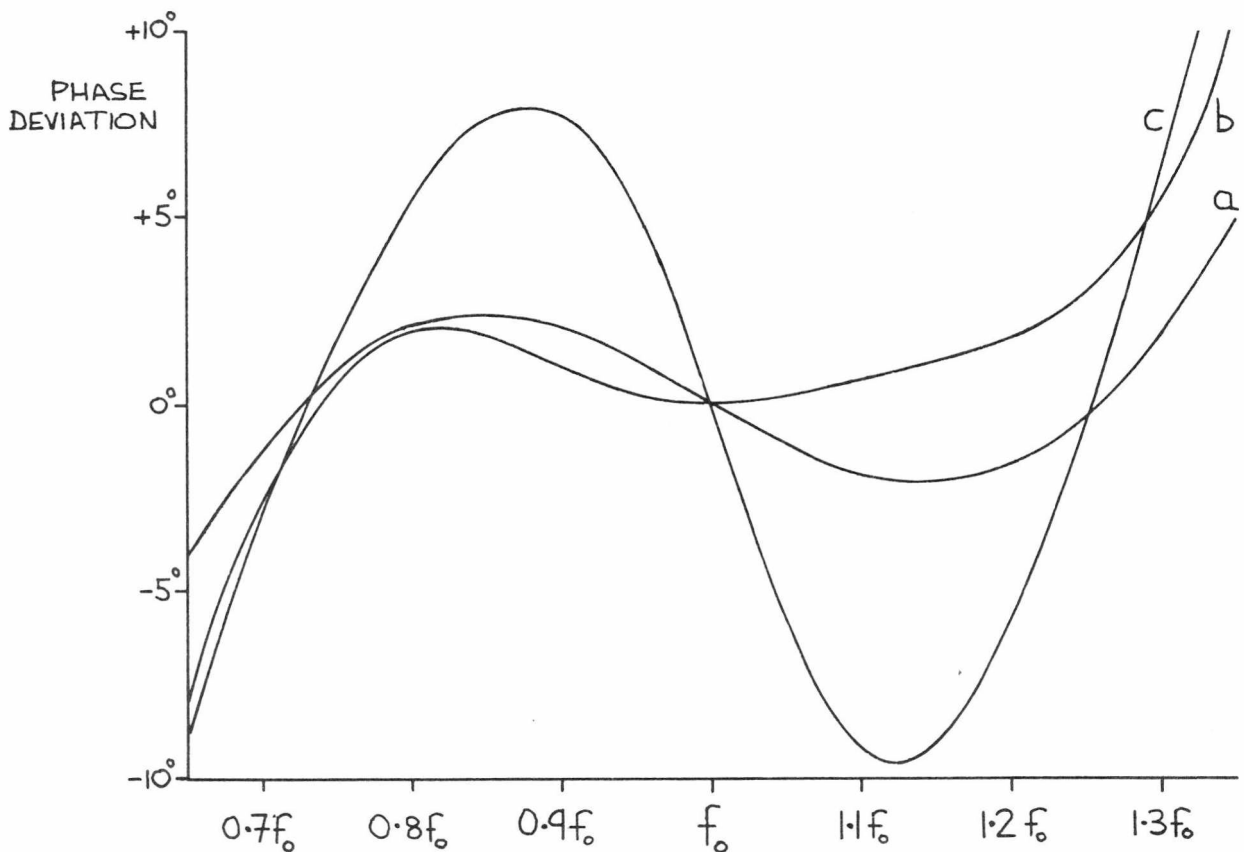


Figure 3.11 : Phase deviation from the ideal for Schiffman coupled lines having  $\theta_e \neq \theta_o$ . a: Single coupled line (90 degrees). b: Cascaded pair (180 degrees). c: Cascaded pair spaced with a quarter-wave line (180 degrees).

use with the two-way switch in a phase shifter circuit. As a consequence their theory has not been investigated in great detail.

### 3.9 A BANDPASS PHASE SHIFT CIRCUIT (STUB CIRCUIT)

A network has been described by Wilds<sup>7</sup> that exhibits a dispersive phase versus frequency behaviour. The network consists of a half wavelength line shunted at one point by an open circuit and a short circuited pair of eighth wavelength stubs. It can be made to give a near constant differential phase over a given bandwidth. The network's transmission phase is compared to a reference line whose length, like that of the Schiffman, is given by equation (3.34). This network though has an important difference in that both its transmission phase and input match are bandpass in response. The line and stub impedance are adjusted relative to each other and to  $Z_0$  to obtain the desired return loss and phase accuracy for a given bandwidth<sup>16</sup>.

Wilds gives curves of phase shift versus stub and line impedances for an octave bandwidth. A limit of about 135 degrees is shown for a single section phase shifter since the line and stub impedances become impracticably small. A 180 degree network would therefore consist of two 90 degree networks. Both line and stubs require impedances of 30.7 ohms and a 90 degree network would give less than 2 degrees phase error and better than 23 dB return loss in an octave bandwidth.

This phase shift circuit has the advantage that it is simpler to design than the Schiffman network. Also, it does not require coupled lines, needing only lengths of transmission line and is hence easier to construct on microstrip. However, at higher frequencies junction discontinuities effects<sup>2,17</sup> where the stubs join the main line may be present. To avoid this problem a computer model was used to investigate

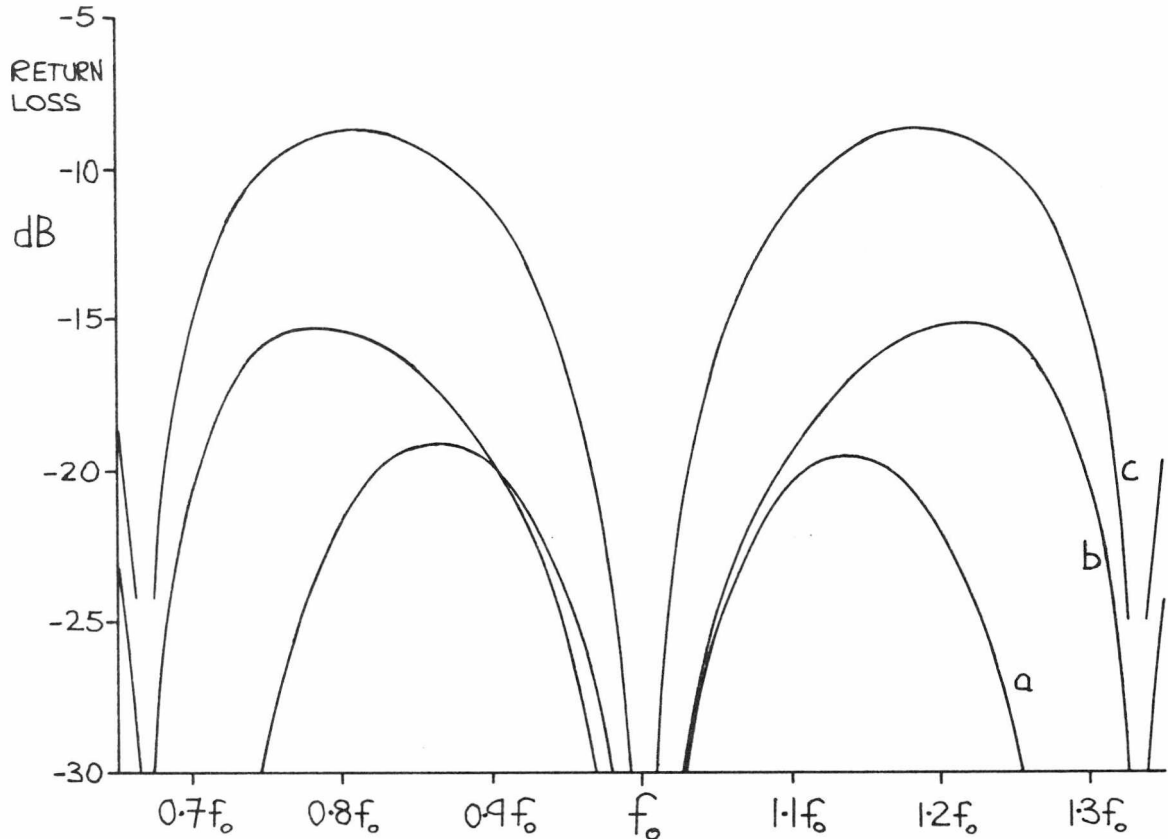


Figure 3.12 : Return loss of a cascaded pair of stub type phase shifters having  $Z_\ell = Z_S$ . a:  $Z_\ell = 30.7$  ohms. b:  $Z_\ell = 40.0$  ohms. c:  $Z_\ell = 50.0$  ohms.

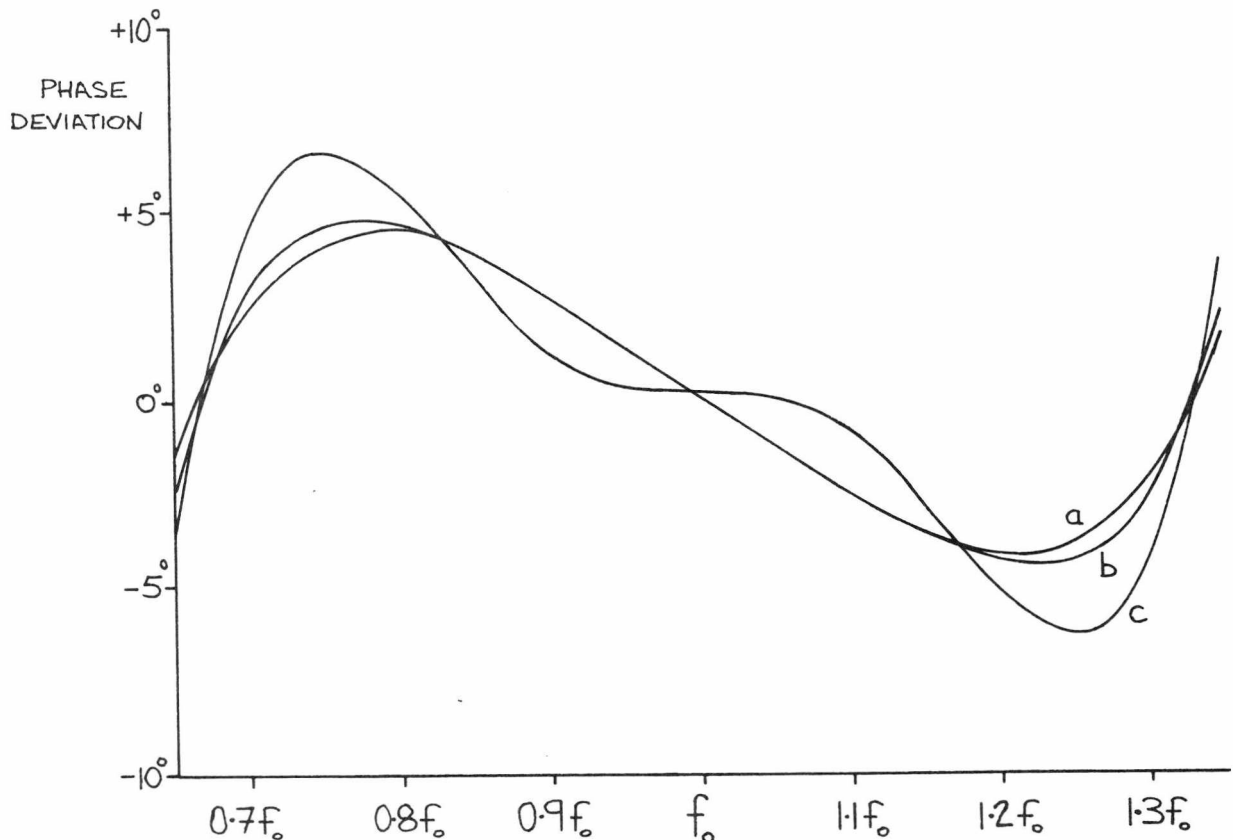


Figure 3.13 : Phase deviation from 180 degrees differential phase shift for a cascaded pair of stub type phase shifters having  $Z_\ell = Z_S$ . a:  $Z_\ell = 30.7$  ohms. b:  $Z_\ell = 40.0$  ohms. c:  $Z_\ell = 50.0$  ohms.

the behaviour of this circuit in relation to its line and stub impedances. Wilds gives an equation that relates the phase shift to the ratio  $Z_\ell/Z_S$  where  $Z_\ell$  and  $Z_S$  are the line and stub impedances respectively. For a 90 degree phase shift  $Z_\ell/Z_S$  needs to be unity. Hence it appears that a value of  $Z_\ell = Z_S$  other than 30.7 ohms can be used to achieve 90 degree phase shifts. Figures 3.12 and 3.13 confirm this by showing the performance of two cascaded stub networks for several values of  $Z_\ell = Z_S$ . The effect of increasing  $Z_\ell$  (and  $Z_S$ ) is to cause an increase in the return loss with a slight degradation of the phase error. Figures 3.14 and 3.15 show the behaviour of the same network with values of  $Z_\ell$  not equal to  $Z_S$  about a nominal value of  $Z_\ell = Z_S = 40$  ohms. With  $Z_\ell$  greater than  $Z_S$  the return loss degrades and the phase error improves with respect to the  $Z_\ell = Z_S$  values and for  $Z_\ell$  less than  $Z_S$  the converse occurs. Note that the bandwidth for all these variations remains near an octave.

Hence, it can be concluded that some scope exists for increasing the circuit impedances providing either an increase in return loss or phase error can be tolerated. Problems with discontinuity effects at the junction of wide lines can therefore be reduced.

### 3.10 HYBRID POWER DIVIDERS

An alternative to using the power dividers as described in sections 3.5, 3.6 and 3.7 with the phase shift networks of sections 3.8 and 3.9 is to use networks that give the power division with an associated phase split. The interest in such networks arises from the deficiencies of the previous circuits such as coupled line fabrication problems, discontinuity effects and possible bandwidth restrictions caused by long reference lines. A class of networks that possess a power dividing and

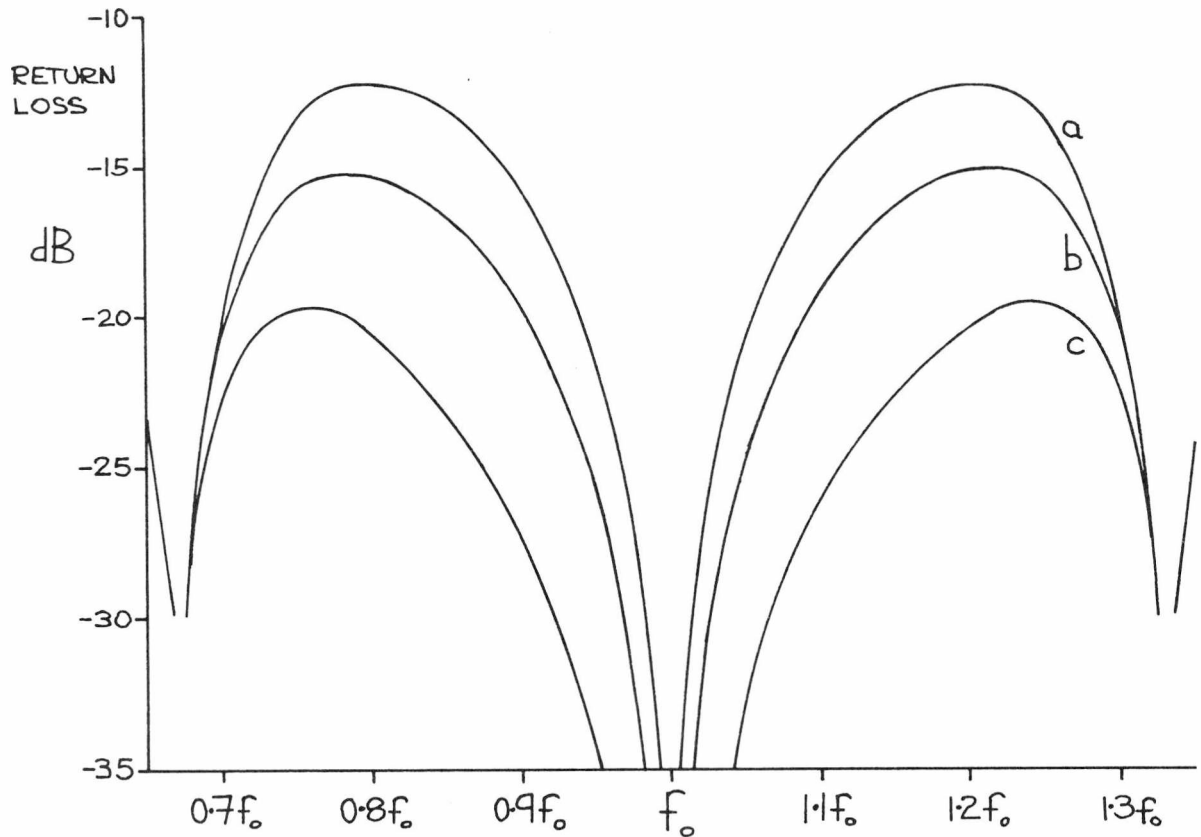


Figure 3.14 : Return loss of a cascaded pair of stub type phase shifters.  
 a:  $Z_L = 42$  ohms and  $Z_S = 38$  ohms. b:  $Z_L = Z_S = 40.0$  ohms.  
 c:  $Z_L = 38$  ohms and  $Z_S = 42$  ohms.

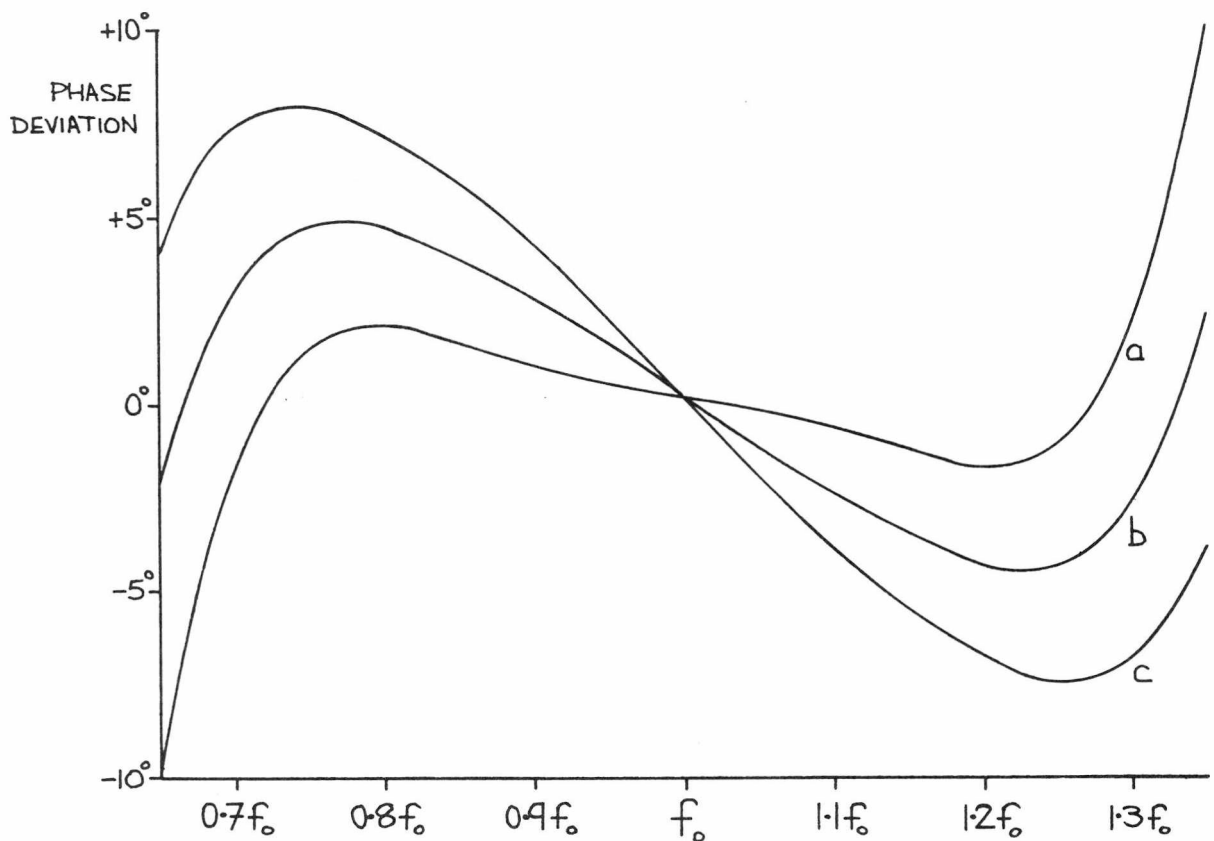


Figure 3.14 : Phase deviation from 180 degrees differential phase shift for a cascaded pair of stub type phase shifters. a:  $Z_L = 42$  ohms and  $Z_S = 38$  ohms. b:  $Z_L = Z_S = 40$  ohms. c:  $Z_L = 38$  ohms and  $Z_S = 42$  ohms.

phase splitting ability are the hybrids. They are typically four port networks and have the property of directionality in that power reflected from the dividing port's identical terminations will emerge from the fourth port rather than the first from which it originally entered. This property is of no significance in the design of the phase shifters considered in this work but it does allow the hybrid's behaviour to be modified to give better power division properties.

Three hybrids are suitable for construction using microstrip, the TEM coupled line or Lange type<sup>18</sup>, the branch line<sup>19</sup>, and the rat race<sup>3</sup>. The first two will be discussed briefly and the third in greater depth. In all three cases, it is the 3 dB or equal power splitting versions of these that is of interest, each being able to give any ratio of power division by design.

The first two, the coupled line and the branch line are considered together since their power splitting outputs are in quadrature, ie.  $\phi_2 = \phi_1 + \pi/2$ . As a consequence of this, if the terminations at the two output ports are interchanged (toggling of the two-way switch) the phase of the mismatch returning to the input port will change phase by 180 degrees. It will therefore be impossible to improve the match at the hybrid's input (recall section 3.5). This can be overcome by delaying one of the output ports by 90 degrees. The outputs can then be made either in phase or with 180 degrees difference. This though defeats the object of using hybrids since a phase shifting network is required to achieve the desired performance.

From practical considerations the coupled line hybrid requires the fabrication of narrow gaps and strips to get the tight coupling for 3 dB division and so may be difficult to construct using copper clad substrates. The branch line hybrid requires lines of  $Z_0/\sqrt{2}$  ohms impedance and the tee junction with the two  $Z_0$  lines may suffer discontinuity problems<sup>20,21</sup>. The coupled line and branch line hybrids are

therefore rejected.

The third hybrid considered, the rat race, has a pair of output ports that are in antiphase for a given input port. This hybrid hence does not need extra phase shifting circuitry and so conforms to the requirement. For 3 dB power division the rat race's ring has an impedance of  $\sqrt{2}Z_0$  ohms. Its structure, port numbering and terminations are shown in Figure 3.16. The rat race's scattering matrix is<sup>3</sup>

$$[\mathbf{P}] = \frac{1}{\sqrt{2}} \begin{bmatrix} 0 & +j & -j & 0 \\ +j & 0 & 0 & -j \\ -j & 0 & 0 & -j \\ 0 & -j & -j & 0 \end{bmatrix} \quad (3.37)$$

If,

$$[b] = [\mathbf{P}] \times [a]$$

where,

$$\left. \begin{aligned} a_1 &= \text{input} \\ a_2 &= S_{22}b_2 + S_{21}b_3 \\ a_3 &= S_{12}b_2 + S_{11}b_3 \\ a_4 &= U b_4 \end{aligned} \right\} \quad (3.38)$$

U being a termination whose value is specified latter, then

$$b_1 = \frac{j(S_{22}-S_{12})b_2}{\sqrt{2}} + \frac{j(S_{21}-S_{11})b_3}{\sqrt{2}} \quad (3.39)$$

$$b_2 = \frac{j a_1}{\sqrt{2}} - \frac{j U b_4}{\sqrt{2}} \quad (3.40)$$

$$b_3 = -\frac{j a_1}{\sqrt{2}} - \frac{j U b_4}{\sqrt{2}} \quad (3.41)$$

$$b_4 = -\frac{j(S_{22}+S_{12})b_2}{\sqrt{2}} - \frac{j(S_{11}+S_{21})b_3}{\sqrt{2}} \quad (3.42)$$

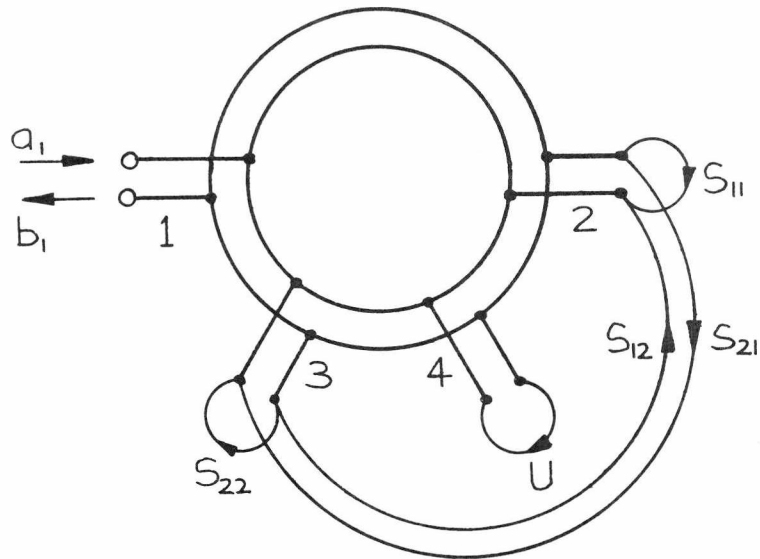


Figure 3.16 : The rate race directional ring with the termination presented to its three output ports.

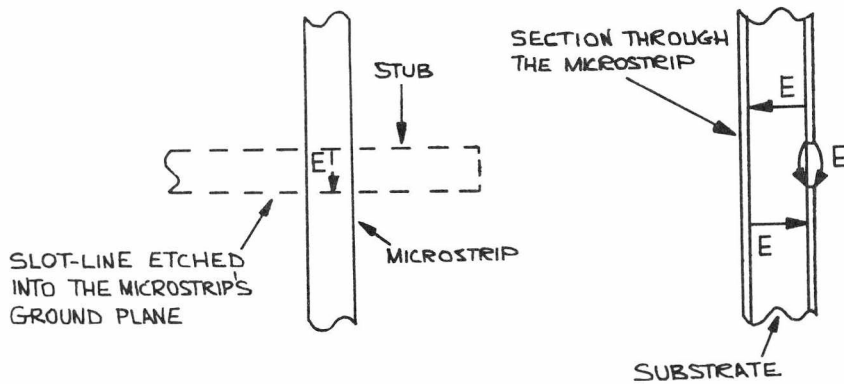


Figure 3.17a : The slotline to microstrip transition showing the electric field ( $E$ ) in the vicinity slot to microstrip crossing.

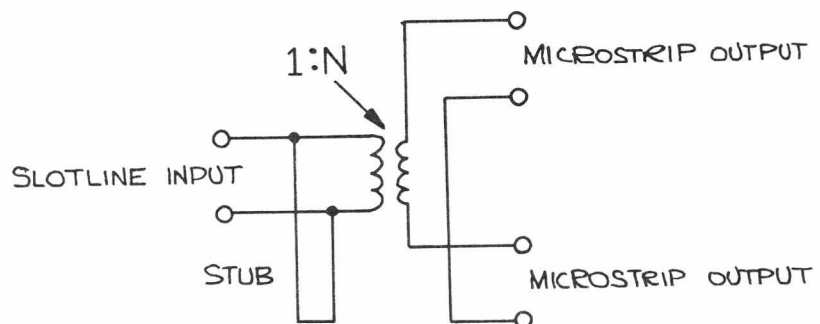


Figure 3.17b : The electrical equivalent circuit of slotline to microstrip transition.

Note that the input waves  $a_1$ ,  $a_2$  and  $a_3$  are the same as those for the Wilkinson and tee with the addition of  $a_4$ . Letting  $S_1 = S_{11} + S_{21}$  and  $S_2 = S_{22} + S_{12}$  and substituting equation (3.42) into equation (3.41)

$$b_3 = \frac{-j a_1}{\sqrt{2}} - \frac{U S_1 b_2}{2} - \frac{U S_2 b_3}{2}$$

$$b_3 = \frac{-j a_1 \sqrt{2} - U S_1 b_2}{2 + U S_2} \quad (3.43)$$

Substitute equation (3.42) into equation (3.40)

$$b_2 = \frac{j a_1}{\sqrt{2}} - \frac{U S_1 b_2}{2} - U S_2 b_3$$

$$b_2 = \frac{j a_1 \sqrt{2} - U S_2 b_3}{2 + U S_1} \quad (3.44)$$

Substitute equation (3.44) into equation (3.43)

$$\frac{b_3}{a_1} = T_2 = \frac{-j\sqrt{2}(1 + U S_1)}{2 + U(S_1 + S_2)}$$

$$T_2 = \frac{-j\sqrt{2}(1 + U(S_{11} + S_{21}))}{2 + U(S_{11} + S_{12} + S_{21} + S_{22})} \quad (3.45)$$

Substitute equation (3.43) into equation (3.44)

$$\frac{b_2}{a_1} = T = \frac{j\sqrt{2}(1 + U S_2)}{2 + U(S_1 + S_2)}$$

$$T = \frac{j\sqrt{2}(1 + U(S_{22} + S_{12}))}{2 + U(S_{11} + S_{12} + S_{21} + S_{22})} \quad (3.46)$$

Substitute equations (3.45) and (3.46) into equation (3.39)

$$\frac{b_1}{a_1} = R = \frac{-S_{22}(1 + U S_1) + S_{12}(1 + U S_1) + S_{21}(1 + U S_2) - S_{11}(1 + U S)}{2 + U(S_1 + S_2)}$$

$$R = \frac{-S_{22} + S_{12} + S_{21} - S_{11}}{2 + U(S_{11} + S_{12} + S_{21} + S_{22})} \quad (3.47)$$

Hence it can be seen from equations (3.45) and (3.46) for  $T$  and  $T_2$  that the two outputs are in antiphase. Interchanging  $S_{11}$  with  $S_{22}$  and  $S_{12}$  with  $S_{21}$  has no effect on  $R$ . If the termination  $U$  is zero then equations (3.46) and (3.47) for  $T$  and  $R$  become equal to those for the compensated Wilkinson, ie. a 3 dB power division loss occurs and the mismatch,  $S_{22}$ , is only improved by 6 dB,  $|T|$  and  $|R|$  being independent of the argument of  $S_{22}$ . If the modulus of  $U$  is made equal to unity the  $|T|$  and  $|R|$  become dependant and their values can be improved by choice of  $S_{22}$ .

From the denominator of equations (3.46) and (3.47) it can be seen that  $U$  must be the complex conjugate of  $(S_{22} + S_{21} + S_{12} + S_{11})$  to maximise  $|T|$  and minimise  $|R|$ . Specifically, if  $U = -1$ , then the moduli of equations (3.46) and (3.47) become equivalent to (3.17) and (3.18), the equations for  $|T|$  and  $|R|$  for the uncompensated Wilkinson. The optimisation of the dividers performance can therefore be done by the adjustment of the termination  $U$  rather than by using lengths of phase compensating line as is required for the Wilkinson and tee dividers.

Though the rat race appears to have the advantage over the Wilkinson and tee, the phase split and power division are known<sup>22</sup> to be frequency dependant. The phase is seen to vary linearly, having 6

degrees error in 180 degrees for a 10% change in frequency. The amplitude imbalance reaches 0.4 dBs at this point. Though this is considerably better than a half wavelength line it is worse than that which can be obtained from dispersive type networks. Apart from simplicity this hybrid offers no benefit. The hybrid power dividers are therefore of no significant use in this current phase shifter work.

### 3.11 THE SLOTLINE TO MICROSTRIP POWER DIVIDER

In an attempt to find a simple method of producing a broadband power divider with a phase split, consideration has been given to alternative stripline technologies. One problem that limits the ability of microstrip circuitry to give broadband antiphase signals is that a series type junction does not exist in this technology. Consider the common microstrip junction, the tee junction, all three lines at the common point are in parallel and hence in phase. An alternative such as slotline<sup>23</sup> effectively has the three arms of a tee junction in series and so splits the phase of signals departing from the junction point. Further to this, de Ronde<sup>24</sup> has shown how the coupling properties from slotline to microstrip offer the means of introducing a series type junction into microstrip. It is this latter junction which is of interest in this work, the divider being designed to have a microstrip input and output so as to be compatible with the MESFET switches.

The phase splitting coupling using slotline and microstrip consists of a continuous microstrip placed perpendicular across a slot, the slot being formed in the microstrip's ground plane. The slot is terminated on one side of the microstrip in either an open circuit or a short circuit stub. A model proposed by Knorr<sup>25</sup> for this transition

represents the coupling by a transformer. The associated slotline stub is modelled as being in parallel with the transformer. A phase splitting transition and its equivalent circuit are shown in Figure 3.17. The symmetry of the microstrip about the slot indicates that an equal power division and a good phase split should occur. The turns ratio of the coupling transformer is known<sup>25</sup> to be dependant on the substrate's dielectric constant, the width and effective dielectric constant of the slotline, and frequency. Evaluation of Knorr's equations has shown this to be a slowly varying function with frequency (1:0.87 at 8 GHz to 1:0.82 at 12 GHz for a 70 ohm line) and since the transition is of a lumped nature a broadband behaviour is possible.

The phase splitting transition must be preceded by a microstrip to slotline transition where the microstrip on one side of the slot is terminated in an open circuit stub. The complete power dividing circuit has a microstrip input coupled by slotline to a pair of microstrip outputs. The two outputs, nominally 50 ohms are in series and need to be matched to the 50 ohm input. This can be done by the slotline whose length is made a quarter of a wavelength between the two microstrips. Referring to the circuit of this power divider as shown in Figure 3.18, it can be seen that the slotline's impedance,  $Z_{SL}$ , is given by:

$$Z_{SL} = \frac{\sqrt{5000}}{N^2} \quad (3.48)$$

All three stubs are assumed to be a quarter wavelength also. The scattering parameters of this circuit are as follows:

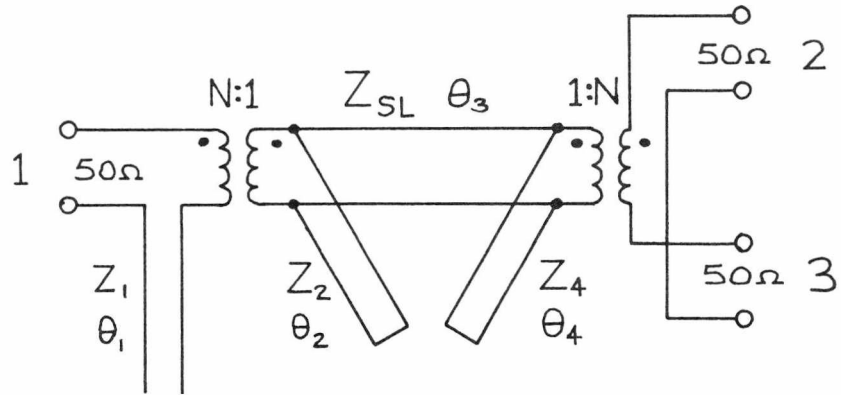


Figure 3.18 : Electrical topology of the slot-line type power divider. The electrical lengths,  $\theta$ , are nominally 90 degrees at the centre frequency unless stated otherwise.

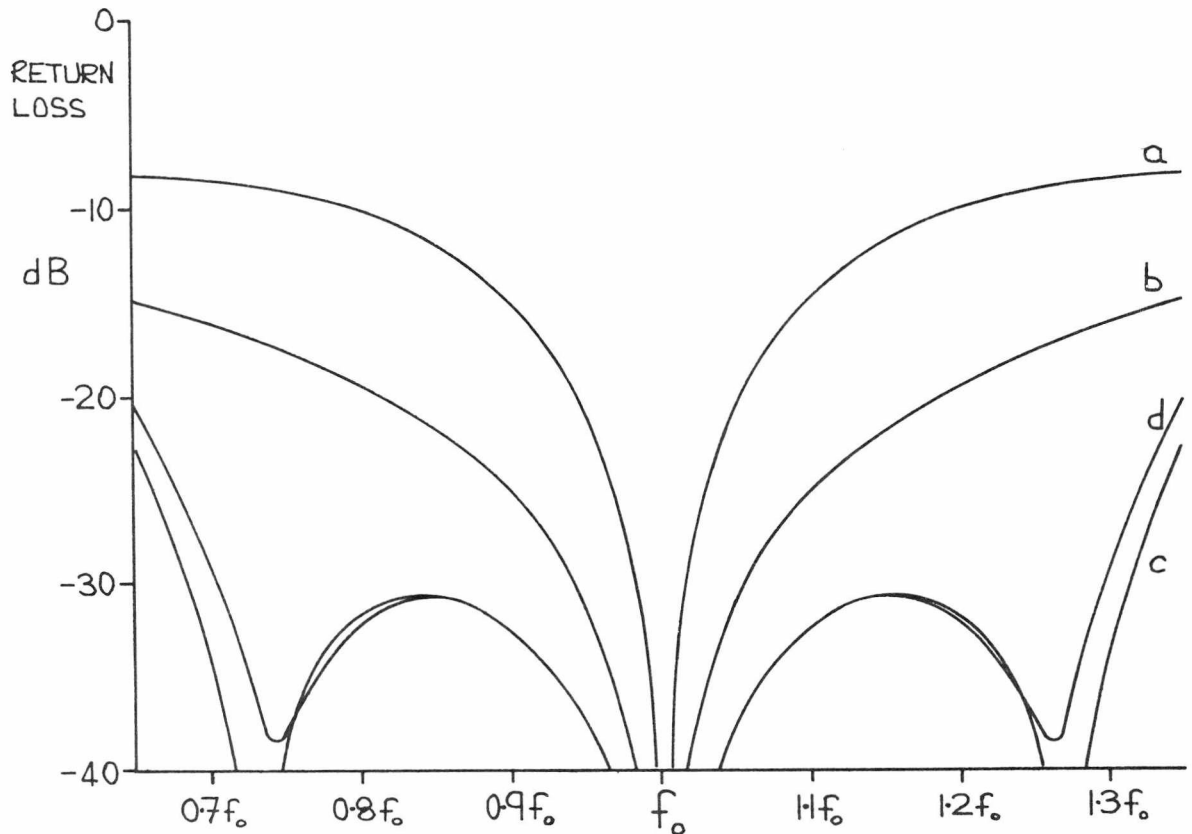


Figure 3.19 : Input return loss of the slot-line type power divider.  
 a:  $Z_1 = 50$  ohms,  $Z_2 = Z_{SL} = Z_4 = 70.7$  ohms and  $N = 1$ .  
 b:  $Z_{SL} = 70.7$  ohms,  $N = 1$  and no stub. c: Ideal third order response. d:  $Z_1 = Z_2 = 50.0$  ohms,  $Z_{SL} = 95.6$  ohms,  $N = 0.86$  and no  $Z_4$  stub.

$$\begin{aligned}
 S_{11} &= \frac{Z_{SL}^2 N^4 - 5000}{Z_{SL}^2 N^4 + 5000} \\
 S_{22} = S_{33} &= \frac{Z_{SL}^2 N^4}{Z_{SL}^2 N^4 + 5000} \\
 S_{23} = S_{32} &= \frac{2500}{Z_{SL}^2 N^4 + 2500} \\
 S_{21} = -S_{31} &= \frac{-j 50}{Z_{SL} N^2} \\
 S_{12} = -S_{13} &= \frac{-j 75 Z_{SL} N^2}{Z_{SL}^2 N^4 + 2500}
 \end{aligned}
 \tag{3.49a}$$

For  $S_{11}$  to be zero,  $Z_{SL}$  is given by equation (3.48) and the divider's scattering matrix becomes:

$$[S] = \begin{bmatrix} 0 & -j/\sqrt{2} & j/\sqrt{2} \\ -j/\sqrt{2} & 1/2 & 1/2 \\ j/\sqrt{2} & 1/2 & 1/2 \end{bmatrix}
 \tag{3.49b}$$

It will be noticed that this scattering matrix is similar to that for the uncompensated Wilkinson as given by (3.8). Applying terminations to this divider as given by equations (3.2) the scattering matrix can be reduced by using the same procedure as that used for the previous three port circuit that have been discussed to give the following:

$$\frac{b_3}{a_1} = T = \frac{-j\sqrt{2}(S_{22} + S_{12} - 1)}{S_{22} + S_{21} + S_{12} + S_{11} - 2}
 \tag{3.50}$$

$$\frac{b_2}{a_1} = T_2 = \frac{j\sqrt{2}(S_{21}+S_{11}-1)}{S_{22}+S_{21}+S_{12}+S_{11}-2} \quad (3.51)$$

$$\frac{b_1}{a_1} = R = \frac{S_{22}+S_{11}-S_{21}-S_{12}}{S_{22}+S_{21}+S_{12}+S_{11}-2} \quad (3.52)$$

It can be seen that by interchanging  $S_{22}$  with  $S_{11}$  and  $S_{12}$  with  $S_{21}$ , the input mismatch  $R$  is unchanged. If the terms  $S_{11}$ ,  $S_{12}$  and  $S_{21}$  are made zero, the moduli of equations (3.50) and (3.52) become:

$$|T| = \sqrt{2} \left| \frac{(S_{22}-1)}{(S_{22}-2)} \right| \quad (3.53)$$

$$|R| = \left| \frac{S_{22}}{S_{22}-2} \right| \quad (3.54)$$

As expected, these moduli are equivalent to those for the uncompensated Wilkinson as given by equations (3.17) and (3.18). Despite the similarity of the slotline type divider to the uncompensated Wilkinson, the series nature of the output junction requires the mismatch  $S_{22}$  to be a short circuit at this point. However, since the dividing junction is actually at the output of the divider (unlike the Wilkinson which is spaced by quarter-wave lines), the argument of  $S_{22}$  again needs to be 180 degrees for maximum  $|T|$  and minimum  $|R|$ . The performance of the slotline type divider in terms of the variation of  $|T|$  and  $|R|$  with the phase of  $S_{22}$  and its modulus is the same as that given for the uncompensated Wilkinson in Figures 3.4, 3.5, 3.8 and 3.9. The length of the phase compensating line is given by equation (3.19).

The frequency dependant behaviour of this circuit will be determined by the input reflection coefficient,  $S_{11}$ . The power division

and phase split are invariant with frequency in the model used.  $S_{11}$  is limited by the ability of the quarter-wave length of slotline to match the two series 50 ohm outputs to the 50 ohm input. The bandwidth would be that of a single section transformer matching a 2:1 impedance ratio but the presence of the three stubs degrades this. The input return loss of the slotline divider with the stubs and that of a quarter-wave transformer are shown in Figure 3.19. The slotline divider's stubs are assumed to be extensions of the quarter-wave line and hence have 70.7 ohms impedance and likewise the microstrip stub is 50 ohms (the coupling transformer's turns ratio is at present taken as 1:1).

These stubs despite their degradation of the divider's performance can be used to improve it. Cloete<sup>26</sup> in discussing the behaviour of the Marchand balun gives an equivalent circuit for this balun that is comparable to the slotline divider's in Figure 3.18. The balun analysis indicates that by removing the slotline stub from the dividers output, the two remaining stubs inconjunction with the quarter-wave line can be made to give the circuit a third order Tchebycheff response. This is done by making all three elements commensurate and by suitable choice of their impedances the third order response can be obtained for a chosen bandwidth. Cloete gives values for a decade of bandwidth,  $Z_1 = 17.5$  ohms,  $Z_2 = 215$  ohms and  $Z_{SL} = 70.7$  ohms. This bandwidth is unnecessarily wide for use with the two-way MESFET switch and also the element impedances are impractical for construction in microstrip and slotline. Laughlin<sup>27</sup> concentrates his balun design on an octave bandwidth and for a third order response the values of  $Z_1 = 46.2$  ohms,  $Z_2 = 39$  ohms and  $Z_{SL} = 70.7$  ohms are required. The input return loss for the slotline divider using these values is shown in Figure 3.19 and can be seen to be better than 30 dB in nearly the full octave of bandwidth.

So far  $N$  has been taken as being unity. Using the curves of

Mariani et al<sup>28</sup> the slotline dimensions for  $Z_{SL} = 70.7$  ohms can be obtained. Using these dimensions to evaluate  $N$  by using Knorr's<sup>25</sup> equations, it is found that  $N$  is 0.841. Using equation (3.48) a value of  $Z_{SL} = 100$  ohms is needed to obtain a match, this value of  $Z_{SL}$  requiring different slotline dimensions. By repeating the evaluation of  $N$  and  $Z_{SL}$  successively several times, they settle to values of 0.86 and 95.6 ohms respectively. Using these two values in the two stub model, the third order response deteriorates though the return loss is still better than that of the single quarter-wave transformer from  $0.7 f_0$  to  $1.3 f_0$ . In the interests of practicality both stubs were raised in impedance to 50 ohms. The microstrip is now a continuation of the 50 ohm input line and the 50 ohm slotline stub more easily realised on a copper clad substrate. This improves the return loss, the slotline power dividing circuit giving a theoretical figure of better than 30 dB from  $0.71 f_0$  to  $1.29 f_0$  as shown in Figure 3.19.

The slotline power dividing circuit is therefore capable of giving a broadband phase splitting power division. Its performance appears to be limited only by its input return loss. Its structure is relatively simple though it does require fabrication onto both sides of a substrate. Its design and construction are simpler than microstrip baluns<sup>27</sup> in that the balun cavity is not required making construction simpler and that balun junction effects are possibly avoided by use of the quarter-wave microstrip spacing which could result in improved performance. A magic-tee proposed by Aikawa and Ogawa<sup>29</sup> has a similar structure to the slotline divider but their circuit uses coupled slotlines (coplanar lines) to perform the quarter-wave coupling. The physical dimensions of these lines would prove difficult to construct using copper clad substrates. Their circuit also requires through hole connections with their accompanying construction and electrical problems.

The behaviour of the slotline power divider is like that of the uncompensated Wilkinson divider when the mismatched terminations of the MESFET switch are applied to its outputs. Hence, the divider's 3 dB power division loss and input mismatch as caused by the MESFET switch can be improved by suitable choice of mismatch.

### 3.12 CONCLUSION

This chapter has concerned itself with various ways of producing constant amplitude differential phase shifts. This has involved discussion about various types of power dividing circuits, both in-phase and otherwise and circuits that exhibit a near constant differential phase versus frequency behaviour. The in-phase power dividers require the use of phase shift circuits to achieve the desired differential phase shift. These phase shift circuits were shown to present design problems both inherent in their electrical behaviour and from a constructional point of view. Ways of overcoming these have been discussed.

Alternative power dividers that give a power division and phase split have been considered. The hybrid type power dividers were rejected since they either suffered the same problems as the phase shift circuits or failed to give satisfactory performance. A final power dividing circuit that was investigated uses the coupling properties of slotline to microstrip. A power divider using this coupling has been proposed that appears theoretically to give a good power and phase split over a near octave bandwidth.

The effect of the MESFET switches inherent mismatch on these circuits has been evaluated. It has been shown that the mismatch can be put to good use since the inherent 3 dB power division loss of the dividers can be improved by suitably adjusting the phase of the mismatch.

3.13 REFERENCES

- 1 E.J. Wilkinson, A N-Way Hybrid Power Divider, IRE Trans. MIT8, January 1960, pp. 116-118.
- 2 A.G. Franco and A.A. Oliver, Symmetric Strip Transmission Line Tee Junctions, IRE Trans. MIT10, March 1962, pp. 118-124.
- 3 C.Y. Pon, Hybrid-Ring Directional Coupler for Arbitrary Power Divisions, IRE Trans. MIT9, November 1961, pp. 529-535.
- 4 H. Yamamoto, K. Morita and S. Komaki, QPSK System Error Rate Performance, Review of the Electrical Communications Laboratories, Vol. 25, No. 5-6, May-June 1977, pp. 515-526.
- 5 J.F. White, Semiconductor Control, Artech House, 1977, pp. 395-399.
- 6 B.M. Schiffman, A New Class of Broad-Band Microwave 90-Degree Phase Shifters, IRE Trans. MIT6, April 1958, pp. 232-237.
- 7 R.B. Wilds, Try  $\lambda/8$  Stubs for Fast Fixed Phase Shifts, Microwaves, December 1979, pp. 67-68.
- 8 S.B. Cohn, A Class of Broadband Three Port TEM-Mode Hybrids, IEEE Trans. MIT16, No. 2, February 1968, pp. 110-116.
- 9 R.J. Collier, Lecture Notes on Microstrip Circuits, University of Kent, October 1981.
- 10 W. Menzel, Frequency Dependant Transmission Properties of Microstrip Y-Junctions and  $120^\circ$  Bends, IEE, Microwaves, Optics and Acoustics, March 1978, Vol. 2, No. 2, pp. 55-59.
- 11 E.M.T. Jones and J.T. Bolljahn, Coupled-Strip Transmission Line Filters and Directional Couplers, IRE Trans. MIT4, April 1956, pp. 75-81.



- 12 B. Schiek and J. Kohler, A Method for Broad-Band Matching of Microstrip Differential Phase Shifters, IEEE Trans. MTT25, No. 8, August 1977, pp. 666-671.
- 13 C.Y. Ho, Microstrip Phase Shifter Provides Improved Match, Microwaves, October 1979, pp. 44-48.
- 14 D. Kajfez, Raise Coupler Directivity with Lumped Compensation, Microwaves, March 1978, pp. 64-70.
- 15 G.L. Matthai, L. Young and E.M.T. Jones, Microwave Filters etc., McGraw-Hill, pp. 144.
- 16 J.K. Hunton, New Differential Phase Shift Networks Combining All-Pass and Band-Pass Elements, IEEE Symposium on Microwave Theory and Techniques, 1981, pp. 223-225.
- 17 E.O. Hammerstad, Equation for Microstrip Circuit Design, 5th European Microwave Conference, Hamburg, 1975, pp. 268-272.
- 18 J. Lange, Interdigitated Stripline Quadrature Hybrid, IEEE Trans. MTT17, December 1969, pp. 1150-1151.
- 19 R. Levy, Advances in Microwaves, Vol. 1, Academic Press, 1966, pp. 164-209, edited by L. Young.
- 20 W.H. Leighton and A.G. Milnes, Junction Reactance and Dimensional Tolerance Effects on X-Band 3 dB Directional Couplers, IEEE Trans. MTT19, No. 10, October 1971, pp. 818-824.
- 21 R.W. Vogel, Effects of the T-Junction Discontinuity on the Design of Microstrip Directional Couplers, IEEE Trans. MTT21, March 1973, pp. 145-146.
- 22 V.J. Albanese and W.P. Peyser, An Analysis of a Broad-Band Coaxial Hybrid Ring, IRE Trans. MTT6, October 1958, pp. 369-373.

- 23 S.B. Cohn, Slotline on a Dielectric Substrate, IEEE Trans. MTT17, No. 10, October 1969, pp. 768-778.
- 24 F.C. de Ronde, A New Class of Microstrip Directional Couplers, IEEE Symposium on Microwave Theory and Techniques, 1970, pp. 184-189.
- 25 J.B. Knott, Slot-Line Transitions, IEEE Trans. MTT22, May 1974, pp. 548-553.
- 26 J.H. Cloete, Exact Design of the Marchand Balun, Microwave Journal, May 1980, pp. 99-102.
- 27 G.J. Laughlin, A New Impedance-Matched Wide-Band Balun and Magic Tee, IEE Trans. MTT24, No. 3, March 1976, pp. 135-141.
- 28 E.A. Mariani et al, Slot Line Characteristics, IEEE Trans. MTT17, No. 12, December 1969, pp. 1091-1096.
- 29 M. Aikawa and H. Ogawa, A New MIC Magic-T Using Coupled Slot Lines, IEEE Trans. MTT28, No. 6, June 1980, pp. 523-527.

CHAPTER 4THEORY AND DESIGN OF THE COMPLETE PHASE SHIFTER4.1 INTRODUCTION

Chapters 2 and 3 have shown how the various components of the phase shifters may be designed. Chapter 3 also briefly introduced the overall form of the phase shifter. This will now be investigated further. The benefits and limitations of several phase shift circuits and dividers when used in association with the MESFET switch will be presented. These circuits will concentrate on 0/180 degree phase shifters but proposals will be given for phase shifters exhibiting smaller angles and having a parallel type structure. The effect of phase shifter switching is considered and spectrum analysis of the phase modulated signal presented whereby switching speed, phase error and amplitude imbalance may be measured.

4.2 A CONSTRAINT ON THE ANGLE OF PHASE SHIFT

The overall form of the complete phase shifter was introduced in Chapter 3 (Figure 3.2). The two-way MESFET switch acts as a combining circuit, being able to switch between the outputs of a differential phase shift circuit. The phase shifting circuit can consist of either a phase splitting power divider (the slotline type divider) or dispersive type network (Schiffman) and a tee divider. The effect of these various components on the overall shifter will now be considered.

In the analyses of the various dividers in the previous chapter several points were noted in terms of divider performance and two are of specific importance now. The first is the improvement in the switches mismatch caused by the divider's scattering behaviour (and by suitably adjusting the mismatches phase) and the second point is that the mismatch eventually appearing at the divider's input does not change if the divider's output terminations are interchanged. The second point allows further matching, if required, at the divider's input. These points will now be shown to impose a constraint on the phase shift angles that the complete phase shifter can be made to exhibit.

To achieve the optimum behaviour at the phase shifters input it was assumed that the terminations (denoted by  $S_{22}$  etc.) could be switched in a symmetrical manner between the divider's outputs. This symmetry exists at the two-way MESFET switch's inputs, this being the source of the mismatch. Hence, by introducing equal lengths of phase compensating line at both of the divider's outputs, correct mismatch phase adjustment occurs for either two-way switch state. This symmetry though is upset by the introduction of the differential phase shift network whether it is a simple time delay line or a Schiffman type network and its reference line.

Consider a differential phase shift network so designed to produce a transmission phase difference defined as  $\Delta\phi = \phi_1 - \phi_2$ . The phase delay at the networks input of mismatch terminations placed at its output is twice the transmission phase delay<sup>1</sup> (the phase shift networks are assumed to be in their pass bands and so their  $S_{11}$  and  $S_{22}$  are zero and, being reciprocal,  $|S_{21}| = |S_{12}| = 1$ ). Hence, the differential phase of this input mismatch is given by,

$$2\Delta\phi = 2\phi_1 - 2\phi_2 \quad (4.1)$$

If the interchangability of the terminations at the divider is to be preserved then  $2\Delta\phi$  in equation (4.1) must equal either zero or a multiple of 360 degrees (full rotations around the Smith chart).

Therefore  $\Delta\phi$  is constrained to be either 0 or 180 degrees. The 0 degree solution for  $\Delta\phi$  is meaningless since it implies no phase shift when the shifter is switched. The phase shifter is hence limited to 180 degree phase shifts so as to ensure optimum divider performance with the consequent good gain and input match.

This constraint is not essential but the performance accompanying other phase shifts is poor. A phase shifter designed to give a 90 degree phase shift requires a  $\Delta\phi$  of 90 degrees which in turn causes the two mismatches at the divider to be 180 degrees apart (diametrically opposite on the Smith chart). If one state is optimised the other will be at its worst. If an attempt is made to make the complete circuit's response symmetrical by adjusting the mismatch phases to be  $\pm 90$  degrees from optimum (or the worst case) the return loss magnitudes at the divider's input become equal at 7 dB. This can be seen in Figures 3.5 and 3.7 of the previous chapter for  $S_{22} = 1 \angle \pm 90$  degrees. The phases of the return losses can be calculated by equation (3.16) (or (3.28)) and are found to be +63.4 and -63.4 degrees. It is hence difficult to improve on the return loss figure of 7 dB by introducing matching at the dividers input. The best case is therefore  $\Delta\phi = 180$  degrees and the worst is 90 degrees with decreasing amounts of degradation for the smaller angles of say 45 and 22.5 degrees. Note that as the phase shift angle decreases, the 0 degree solution of equation (4.1) is achieved.

The constraint also applies to the use of phase splitting power dividers such as hybrids. If a 90 degree hybrid is considered then the

electrical behaviour<sup>2</sup> that is responsible for the 90 degree phase split at its outputs will delay the mismatch of one by 180 degrees and the other by 360 degrees. The result is a 180 degree difference between the input return loss phases and hence a problem with matching. The slotline type power divider constrains the complete phase shifter to 180 degrees by virtue of its own phase split.

#### 4.3 BANDWIDTH: THE EFFECT OF LONG REFERENCE LINES

It was mentioned briefly in the previous chapter that the use of long reference lines (for the dispersive phase shift networks) may limit the bandwidth of a complete phase shifter circuit. This will now be investigated. The problem occurs because though the phase of the mismatch  $S_{22}$  can be corrected at one frequency, the frequency dependant phase delay of the phase shift networks destroys this optimum at other frequencies. Note that this is not the differential phase shift of the networks but rather their individual transmission phases. For simplicity the analysis will assume  $S_{22}$  to be constant with frequency and unity in magnitude. The terms  $S_{21}$ ,  $S_{12}$  and  $S_{11}$  will be taken as being zero. Phase compensating lines are placed at the inputs of the two-way MESFET switch to adjust the phase of  $S_{22}$  to be 0 degrees, the optimum for the tee divider. The reference line at the tee's output is therefore terminated in an open circuit. If it has a length  $\ell$ , a propagation constant  $\beta$  and an impedance of  $Z_0$ , the reflection coefficient presented to the tee divider is given by,

$$\rho = \frac{j + \tan \beta \ell}{j - \tan \beta \ell} \quad (4.2)$$

The term  $\rho$  can be substituted for  $S_{22}$  in equation (3.29) such that the transmission becomes,

$$|T| = \left| \frac{2j}{2j - \tan \beta \ell} \right| \quad (4.3)$$

The bandwidth will be defined as the point when  $|T|$  is reduced by 3 dB. Since  $|T|$  is unity at the centre frequency,  $|T| = 1/\sqrt{2}$  at the band edges and therefore,

$$\frac{|2j - \tan \beta \ell|}{\sqrt{2}} = 2$$

which reduces to,

$$\tan \beta \ell = \pm 2 \quad (4.4)$$

Replacing wavelength by frequency and noting that this defines the half bandwidth, the full 3 dB bandwidth is given by,

$$BW = \frac{v \tan^{-1} 2}{\pi \ell} \quad (4.5)$$

where  $v$  is the line's phase velocity.

The analysis can also be done for the uncompensated Wilkinson and gives the solution that  $\tan \beta \ell = \pm 3$  indicating a slightly wider bandwidth (about 13%). However, the Wilkinson's transmission  $|T|$  as given by equation 3.17 is inadequate for this purpose since the divider's scattering parameters are frequency dependant. This is not important since only the general effect of the long reference line is of interest and the tee divider serves to demonstrate this adequately.

For a 180 degree phase shifter using two 90 degree phase shift networks in cascade a 1.5 wavelength (540 degree) reference line is required (note that the two cascaded 90 degree networks are 1 wavelength long). Equation (4.5) is shown graphically in Figure 4.1. This indicates a bandwidth of approximately 2.3 GHz for a 10 GHz centre frequency and exceeds that of the two-way MESFET switch as discussed in Chapter 2. Two points however have to be considered since they both reduce this bandwidth. Firstly, the length of phase compensating line and the MESFET input matching circuit, both of which are frequency dependant, effectively add to the length of the reference line. Together they increase the line's length between the source of the mismatch (MESFET's gate) and the divider's junction to over 2 wavelengths and so reduce this bandwidth to about 1.7 GHz. Secondly, the 3 dB reduction in the divider's transmission corresponds to a return loss of 3 dB. This is very poor and so it may be advisable to define the bandwidth when  $|T|$  drops by say 0.5 dB or 1 dB at which points the input return loss is 9.6 dB and 7 dB respectively.

If  $|T|$  is redefined at the 0.5 dB and 1 dB bandwidth points and solving equation (4.3) with these values, a 45% and 28% reduction in bandwidth is observed respectively. These two curves are also shown in Figure 4.1. For the typical phase shifter with about 2 wavelengths of line a 0.5 dB bandwidth of 1 GHz is predicted for the reference line/mismatch effect. This is comparable with the bandwidth of the MESFET switch and hence it is expected that the differential phase shift networks may limit the phase shifters overall bandwidth. The length of these networks must be made as short as possible to maximise phase shifter bandwidth. The preference is therefore for two 90 degree networks rather than three 60 degree networks in cascade.

Further to bandwidth limitation, the asymmetric nature of the phase shift networks (the reference line is 1.5 wavelengths or 540

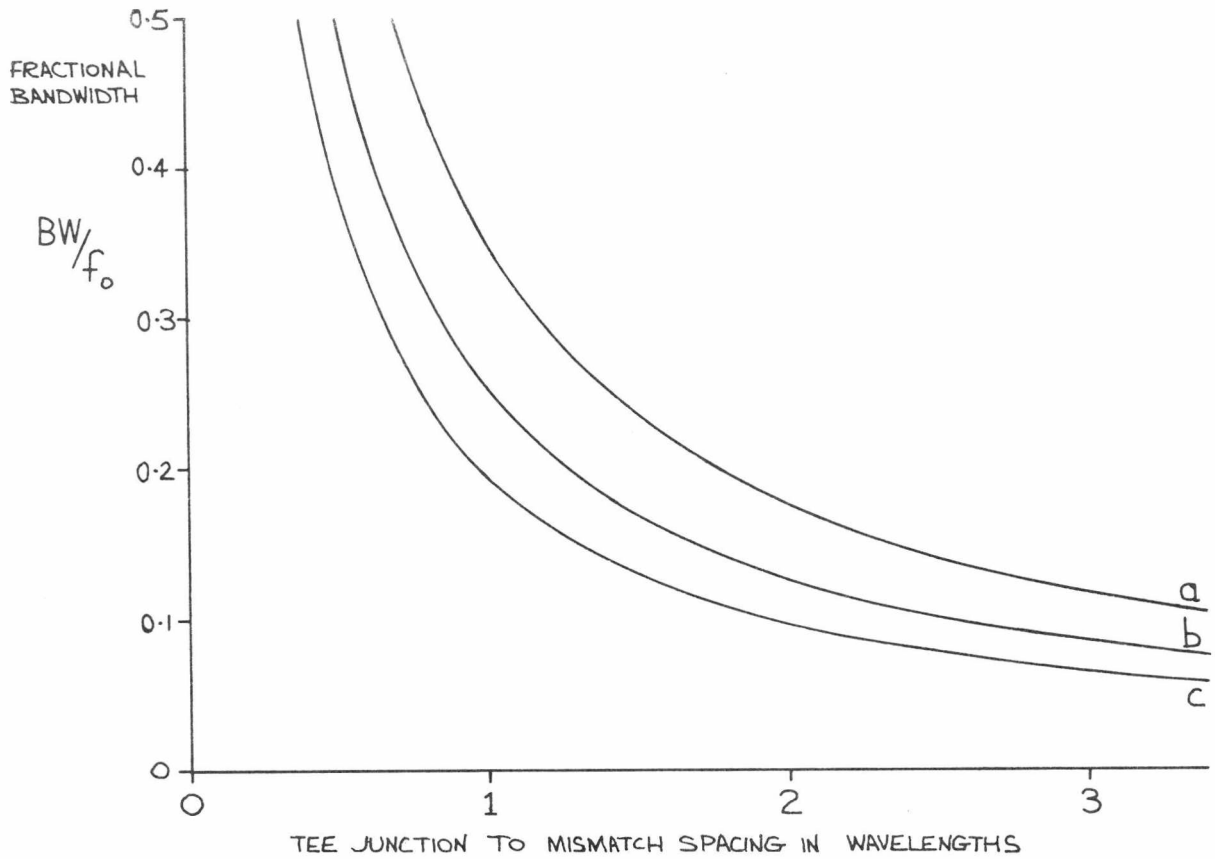


Figure 4.1 : Fractional bandwidth of the tee divider's transmission with a mismatch terminating its second output at the end of a length of line. a: 3 dB bandwidth. b: 1 dB. c: 0.5 dB.

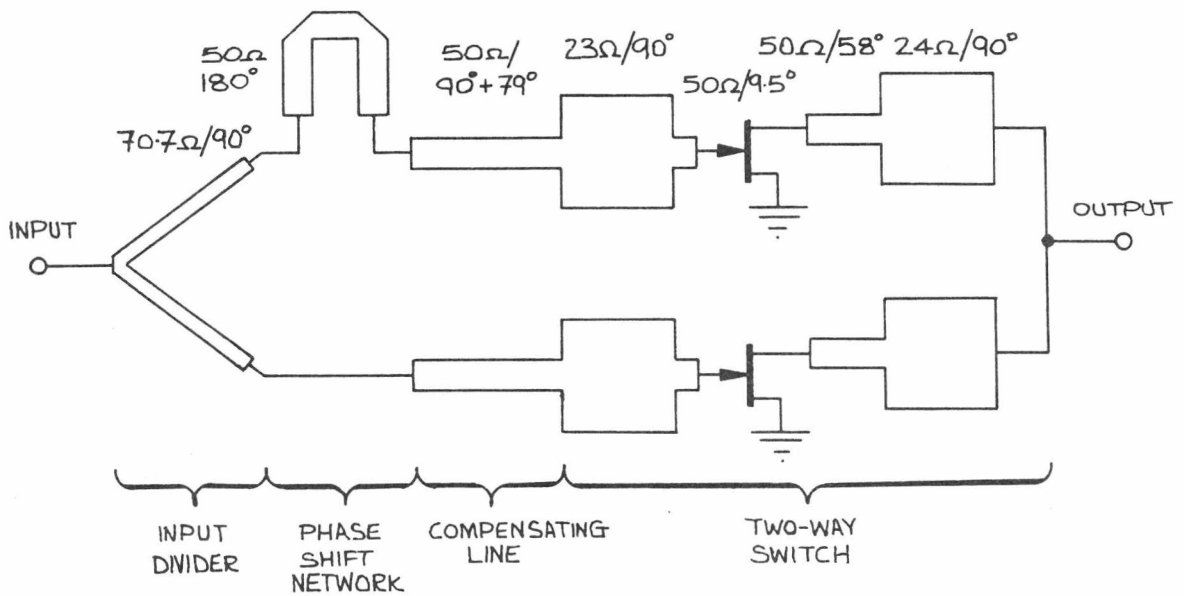


Figure 4.2 : Topology of phase shifter showing the various components in relation to the two-way MESFET switch.

degrees long whereas the dispersive network is 1 wavelength or 360 degrees) asymmetry may occur between the two states of the phase shifter. The phase state associated with the reference line will have a narrower gain bandwidth response than the phase state caused by the dispersive network. Though the gains can be balanced at one frequency, the differences in responses will introduce amplitude modulation on to the phase modulated signal with the resultant degradation<sup>3</sup>. Phase splitting power dividers such as the slotline type can overcome this problem by virtue of their symmetrical outputs.

The limitations on the complete phase shifter of bandwidth and phase shift that have just been discussed arise because of the effect of the mismatch parameter  $S_{22}$  on the input divider. The analyses of Chapter 3 also included the parameter  $S_{21}$  since it was noted in Chapter 2 that its magnitude was comparable to  $S_{22}$ . Its effect on the complete phase shifter will now be discussed.

#### 4.4 THE EFFECT OF THE SCATTERING PARAMETER $S_{21}$

Consider a complete phase shifter design such as that shown in Figure 4.2. Though lengths of phase compensating line have been used to adjust the phase of  $S_{22}$  to be 180 degrees at the input divider, computer modelling of this circuit predicts poor input and output return losses of 3.2 dB and 6.6 dB respectively (10 GHz centre frequency). The input return loss is about 7 dB worst than expected. Also the gain of this phase shifter is high. The forward gain parameters for the two-way MESFET switch are  $S_{31} = 2.22 \angle 164$  degrees and  $S_{32} = 0.29 \angle 160$  degrees and should effectively subtract once one is delayed by the half wavelength line. A phase shifter gain of less than 6 dB would therefore be expected but the computer model predicts 8.1 dB.

To explain these effects the parameter  $S_{21}$  must be taken into account. It has a value of  $0.64 \angle -30$  degrees and compares to a  $S_{22}$  value of  $0.85 \angle 158$  degrees. If the phase delay of the half wavelength is added to these two parameters,  $S_{22}$  is delayed by either 0 or 360 degrees depending on the phase state and  $S_{21}$  by 180 degrees irrespective of this. They are now nearly in phase and will combine to give an apparent mismatch magnitude of greater than unity. The result of this is a poorer input return loss as indicated by equations (3.16) and (3.28) and an increase in phase shifter gain caused by an increase in the divider's transmission modulus as given by equations (3.14) and (3.26). The transmission modulus becomes greater than unity when the combined mismatch becomes more than 1.0 when using the tee divider and more than  $\sqrt{2}$  with the uncompensated Wilkinson.

The increase in overall phase shifter gain may be desirable but the very poor return losses are not. It should be noted that the loop phase is 728 degrees, being the sum of the argument of  $S_{21}$  plus the delay of two phase compensating lines, the half wavelength phase shift line and the 180 delay between the Wilkinson's outputs. Though the loop gain is well below unity (approximately  $S_{21} = 0.64$  multiplied by the Wilkinson's  $S_{23} = 0.5$ ), the condition is best avoided.

Inspection of equations (3.16) and (3.28) shows that if  $S_{22}$  is adjusted to have a 0 degree argument at the divider's junction, then the argument of  $S_{21}$  must be 180 degrees. The adjustment of  $\arg(S_{22})$  to be 0 degrees is preferred since its magnitude is greater than that of  $S_{21}$  (minimises R) and since the numerators of equations (3.14) and (3.26) contain only the  $S_{22}$  term, T is maximised. Tables 4.1 and 4.2 demonstrate this by showing the effect on R and T of various values of  $S_{21}$  and  $S_{22}$ .

$S_{22}$	$S_{21}$	R	T
0.8	0.8	-0.8	0.14
0.8	-0.8	0.0	0.71 *
-0.8	0.8	0.0	0.71 *
-0.8	-0.8	0.8	1.27
0.9	0.4	-0.87	0.09
0.9	-0.4	-0.71	0.2
-0.9	0.4	0.15	0.81 *
-0.9	-0.4	0.52	1.07

Table 4.1 : The effect of  $S_{22}$  and  $S_{21}$  on the transmission T and return loss R of an uncompensated Wilkinson. Asterisk denotes optimum condition.

$S_{22}$	$S_{21}$	R	T
0.8	0.8	0.64	1.64
0.8	-0.8	-0.33	0.67 *
-0.8	0.8	-0.33	0.67 *
-0.8	-0.8	-0.89	0.11
0.9	0.4	0.23	1.23
0.9	-0.4	-0.19	0.81 *
-0.9	0.4	-0.85	0.15
-0.9	-0.4	-0.93	0.07

Table 4.2 : The effect of  $S_{22}$  and  $S_{21}$  on the transmission T and return loss R of a tee divider.

If equations (3.50) and (3.52) for the slotline type divider are considered then the converse appears to be required for optimum, i.e.  $\arg(S_{21}) = \arg(S_{22})$ . However, this is consistent with the requirement of two previous "in phase" power dividers since this divider does not need a phase shift network. The tee and Wilkinson require a network to give the 180 degree phase split and when this is added to these dividers, it effectively brings the required arguments together. Table 4.3 shows the behaviour of the slotline type divider's return loss and transmission for various values of  $S_{21}$  and  $S_{22}$ .

$S_{22}$	$S_{21}$	R	T
0.8	0.8	0.0	0.71 *
0.8	-0.8	-0.8	0.14
-0.8	0.8	0.8	1.27
-0.8	-0.8	0.0	0.71 *
0.9	0.4	-0.71	0.2
0.9	-0.4	-0.87	0.09
-0.9	0.4	0.52	1.07
-0.9	-0.4	0.15	0.81 *

Table 4.3 : The effect of  $S_{22}$  and  $S_{21}$  on the transmission T and return loss R of slotline type power divider.

The implication of this is that to obtain the optimum behaviour from any of these three dividers, the two-way MESFET switch must have either a  $S_{21}$  whose magnitude is considerably smaller than  $S_{22}$ 's or an argument which is similar. This can be achieved as follows:

- I. Reduce the forward gain of the MESFET device that is biased on so that  $|S_{21}|$  is reduced. This can easily be done by adjusting the device's bias to a more negative value. However, reduction of  $|S_{21}|$  by this method would result in a proportional decrease in the overall phase shifter's gain.
- II. Reduce the reverse gain of the MESFET device that is biased off so that  $|S_{21}|$  is reduced. Again this could be done by adjusting the device's bias such that the device is not fully pinched off. This is based on the observation that the  $|S_{12}|$  of the device used has a value of 0.3 when fully pinched off but decreases to 0.07 when biased on. Such an adjustment may be difficult to achieve since the device's forward gain would begin to increase with a consequent degradation of the two-way switches on to off ratio. Choosing another MESFET device with a better pinched off  $S_{21}$  might be simpler.
- III. Use a power divider and/or a combiner that has improved isolation between its output ports. The compensated Wilkinson would meet this requirement but the penalty would be reduced phase shifter gain (inherent 3 dB power division loss) and a poorer return loss (this divider performance is independent of the mismatch phase).
- IV. Adjust the phase of the two-way MESFET switch's  $S_{21}$  to be as near equal as possible to that of  $S_{22}$ . This can be done by adding a half wavelength of line into the output circuit of the two-way switch.  $S_{21}$  will therefore be delayed by

about 180 degrees and  $S_{22}$  virtually unaltered and so bring their phases together. The loop phase would also become an odd multiple of 180 degrees.

Of these, IV was deemed to be the most feasible.

To preserve the symmetry of the two-way switch equal lengths of line must be added to both MESFET output circuits. This is done by the inclusion of a pair of quarter wavelength lines. A two-way MESFET switch that meets this requirement was introduced in Chapter 2 consisting of a pair of matched MESFET amplifiers with their outputs combined with an uncompensated Wilkinson. Its relevant scattering parameters are  $S_{22} = 0.83 \angle 161$  degrees and  $S_{21} = 0.56 \angle -176$  degrees and so their angles are better placed to achieve a good behaviour from the input divider. A complete phase shifter using this circuit and the slotline type divider is shown in Figure 4.3 and its computed performance shown in Figure 4.4. As can be seen the return losses are a considerable improvement on those of the circuit shown in Figure 4.2. Note that they could be further improved (and shift the dips down in frequency to correspond to the gain peak) by the addition of matching components at the shifter's input and output. Both phase states have identical gain and return loss curves and the phase difference is constant at 180 degrees. Also shown in Figure 4.4 is the gain responses of a phase shifter using the stub type differential phase shifter network with an uncompensated Wilkinson divider and the two-way switch of Figure 4.3. Each phase state exhibits a different response, the average of these having a narrower bandwidth than the slotline type phase shifter. The bandwidth difference is not large indicating that the long reference line is only just beginning to have an effect, the overall bandwidth being determined mainly by the two-way switch and the MESFET's matching.

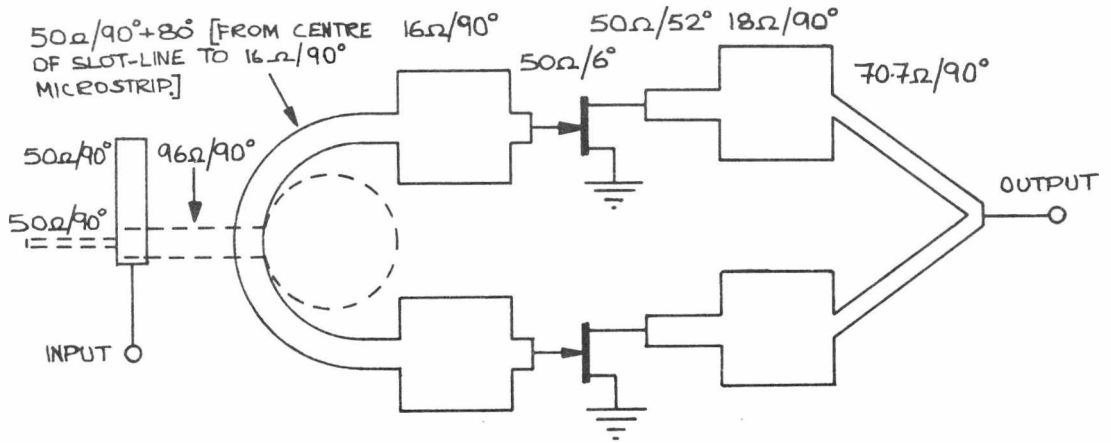


Figure 4.3 : Complete 0/180 degree phase shifter using the slot-line type power divider.

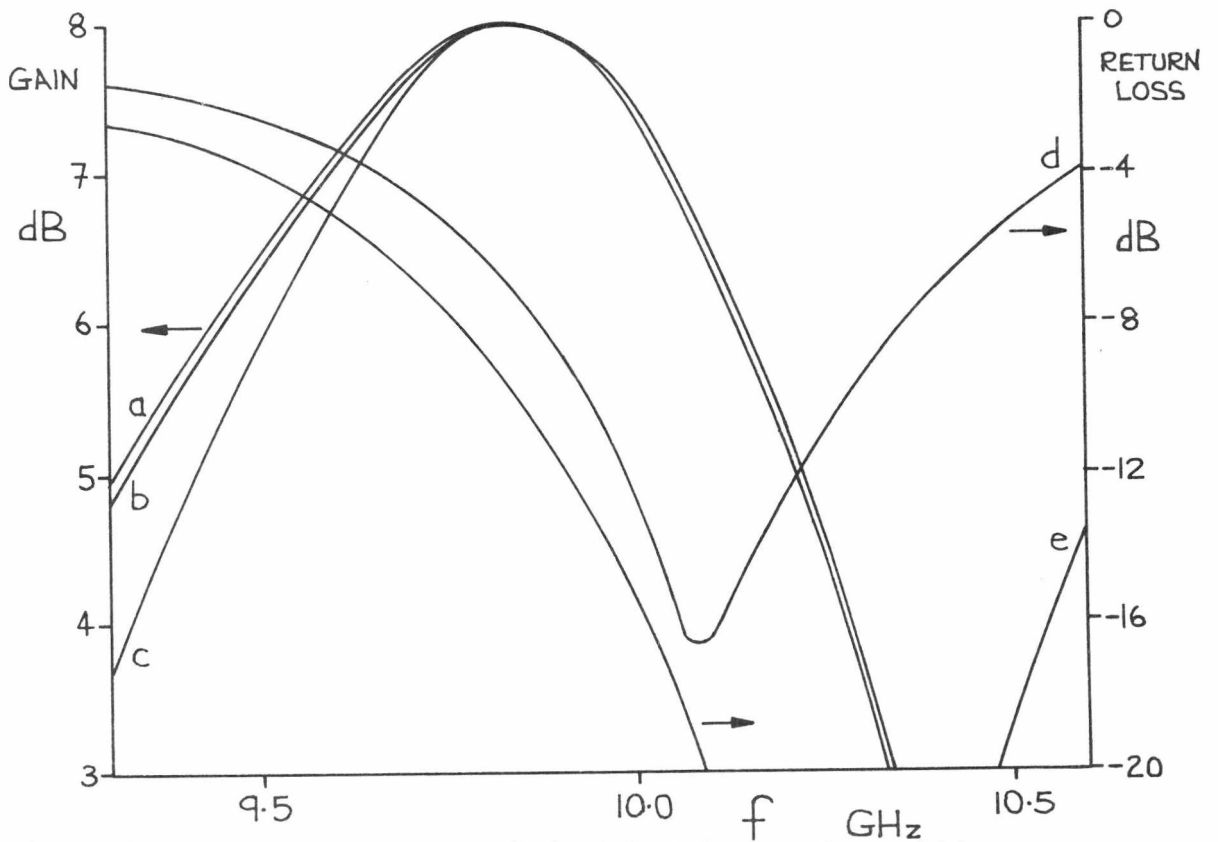


Figure 4.4 : Overall response of the 0/180 degree phase shifter.  
 a: Forward gain of slot-line type. b: Stub type. c: Stub type's reference line state. d and e: Input and output return losses respectively of slot-line type.

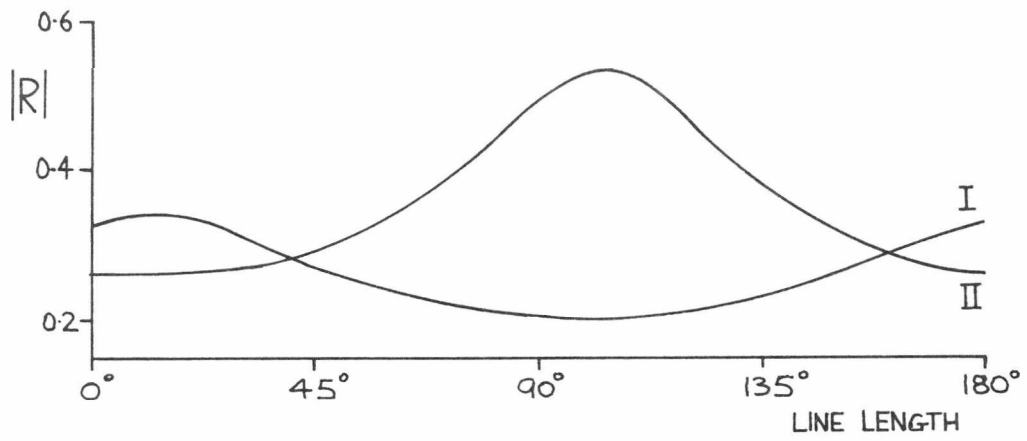
This and the previous two sections of this chapter have attempted to investigate the behaviour of a complete phase shifter once the various component parts have been brought together. A restriction on the overall bandwidth was shown to exist and taken with the 180 degree phase shift constraint lead to the conclusion that the use of the slotline type divider offers advantages.

#### 4.5 PHASE SHIFTERS HAVING ANGLES OF 45 AND 22.5 DEGREES

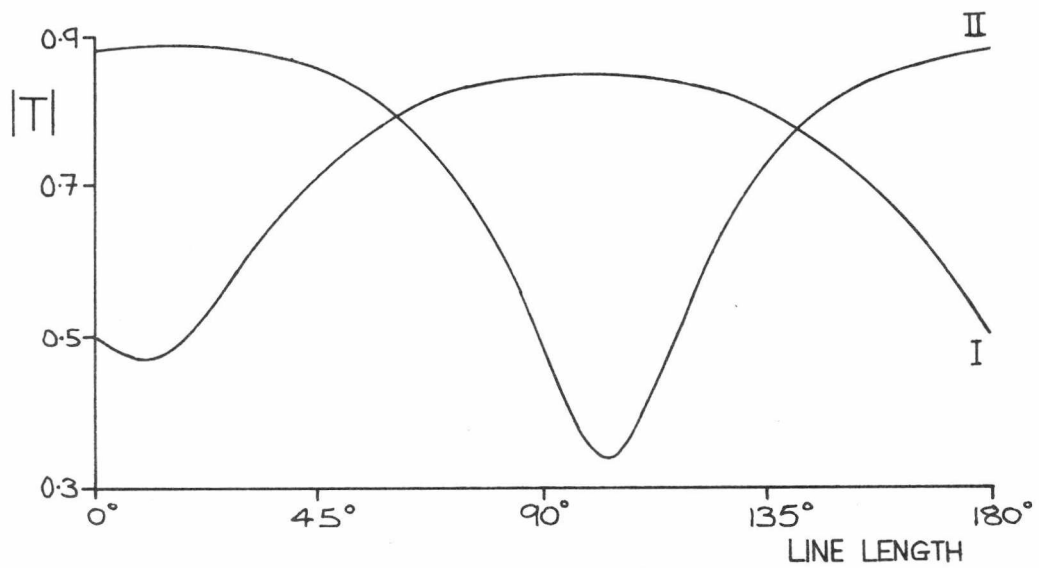
It was mentioned in section 4.2 that it might be possible to construct phase shifters having angles of 45 or 22.5 degrees providing a good input return loss is not essential. This possibility will now be discussed.

Consider the two-way MESFET switch as shown in Figure 4.2. The important parameters affecting the input divider's behaviour are  $S_{21}$  and  $S_{22}$  and they have values of  $0.64 \angle -30$  degrees and  $0.85 \angle 158$  degrees respectively. Add to these the delay of a 45 degree phase shift line and they become  $0.64 \angle -75$  degrees and  $0.85 \angle 158$  or  $0.85 \angle 68$  degrees depending on the phase state. The total mismatch returning to the input divider (uncompensated Wilkinson) is the sum of  $S_{21}$  and  $S_{22}$ . Hence the mismatches for each phase state become  $0.69 \angle -154$  degrees and  $0.51 \angle 19$  degrees noting that their magnitudes are different.

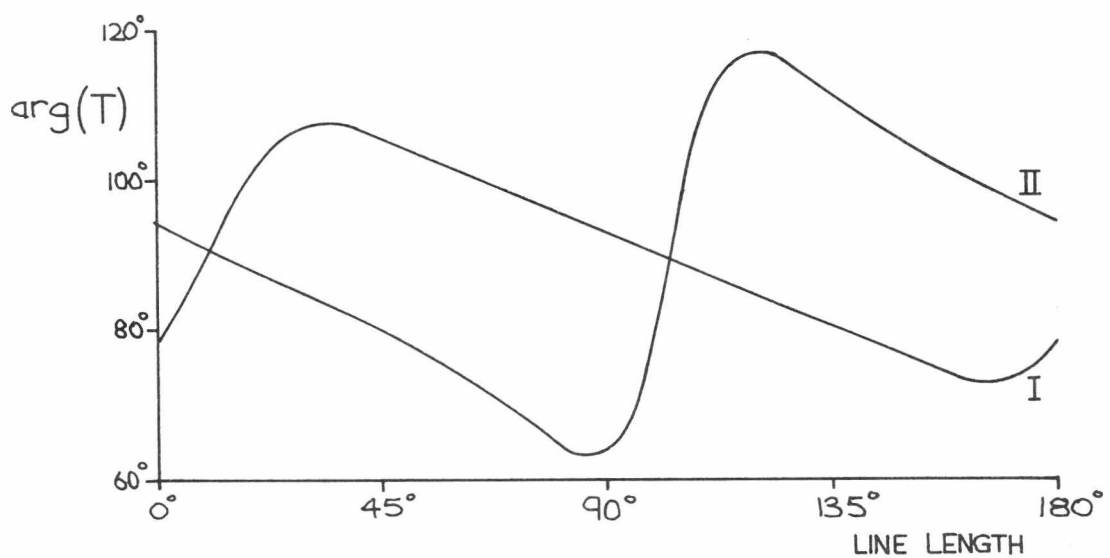
Though it is possible to add lengths of phase compensating lines so that the return loss magnitudes ( $|R|$ ) for each phase state are equal, the transmission magnitudes ( $|T|$ ) will be unequal. Figure 4.5 shows the variation of R and T for the uncompensated Wilkinson divider as the above pair of mismatches are delayed by a compensating line. For 40 degrees of line length,  $|R| = -11$  dB whilst the associated transmissions, T are  $-3.3$  dB  $\angle 106$  degrees and  $-1.2$  dB  $\angle 81$  degrees; hence 2.1 dB



(a)



(b)



(c)

Figure 4.5 : Transmission and return loss for an uncompensated Wilkinson divider in a 45 degree phase shifter as a function of the mismatch phase compensating line's length. a: Input return loss. b and c: Transmission to the two-way switch's matched (on state) input. I and II are for each phase state.

difference. If emphasis is put on equating the transmission magnitudes of each phase state, then at 62 degrees of line length,  $T = -1.9$  dB  $\angle$  100 degrees and  $-1.9$  dB  $\angle$  72 degrees with return losses of 12.8 dB and 9.4 dB. The larger return loss may be tolerable but observation of the two phases associated with T indicates a further problem when the delay of the 45 degree phase shift line is added to the latter value of T's argument it becomes 27 degrees. The phase difference presented to the inputs of the two-way MESFET switch is therefore 100-27 or 73 degrees. The mismatches are causing a phase error.

The arguments of the two transmissions, T, can be equated with 10 degrees of phase compensating line the return losses are again no worse than -9.4 dB but the magnitudes of T become -6.6 dB and -1.0 dB, a 5.5 dB difference. Such a magnitude error would be difficult to remove by device bias adjustment without seriously altering the device's parameters, this would in turn, probably introduce a further phase error.

These problems also arise when a 22.5 degree phase shifter is considered and likewise the two-way MESFET switch as shown in Figure 4.3 suffers the same limitations. The finite on to off ratio of these switches will also introduce a phase error, leakage through the off biased device will combine with that from the on biased device at the common output and introduce a phase offset. For a typical on to off ratio of 20 dB, a 45 degree phase shift will reduce by 7.5 degrees and that of a 22.5 degree phase shifter by 4.0 degrees. This effect is not noticed in a 180 degree shift since the two combining signals are always 180 degrees apart and cause only a slight reduction in phase shifter gain.

Having previously shown that it is not possible to construct a 90 degree phase shifter with the proposed two-way MESFET switch, the 45

and 22.5 degree shifts are now also eliminated. A method must therefore be found to use the viable 180 degree phase shift circuits in combination to produce these other angles.

#### 4.6 PARALLEL TYPE PHASE SHIFTERS

The conventional technique for designing a phase shifter having several bits is to use a cascade arrangement<sup>4</sup>. For example, a three bit phase shifter would consist of a 0 to 180 degrees phase shifter (0/180) followed by one giving 0 to 90 degrees and another giving 0 to 45 degrees. Hence to construct a multi-bit phase shifter by this method, individual phase shifters having angles from the largest (0/180 degrees) down to the smallest desired phase increment are required. It has been shown that though a 0/180 degree MESFET phase shifter is feasible, other phase angles are not. The cascade arrangement cannot therefore be used to employ the MESFET phase shifter so far described. An alternative topology must be used. One that is suitable is a parallel arrangement, the two bit circuit given by Bennett and Davey<sup>5</sup> requires two 0/180 degree phase shifters plus a constant 90 degree delay. It will be shown how this idea can be extended to give more than two bits of phase shift.

Consider the two bit parallel phase shifter as shown in Figure 4.6. The 0/180 degree phase shifters are assumed to be matched and have a gain (or loss) of  $G$  in the 0 degree state and  $-G$  in the 180 degree state. The 90 degree delay denoted by  $-j$  is a constant differential phase type as described in Chapter 3. The input divider and output combiner can be Wilkinson's. The overall gain of this phase shifter is given by:

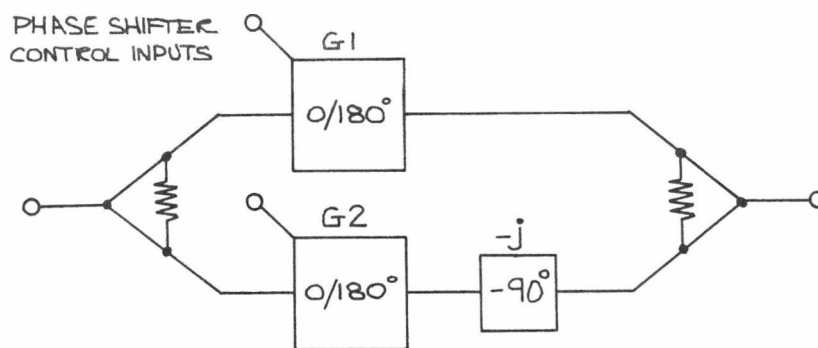


Figure 4.6 : A two-bit parallel phase shifter.

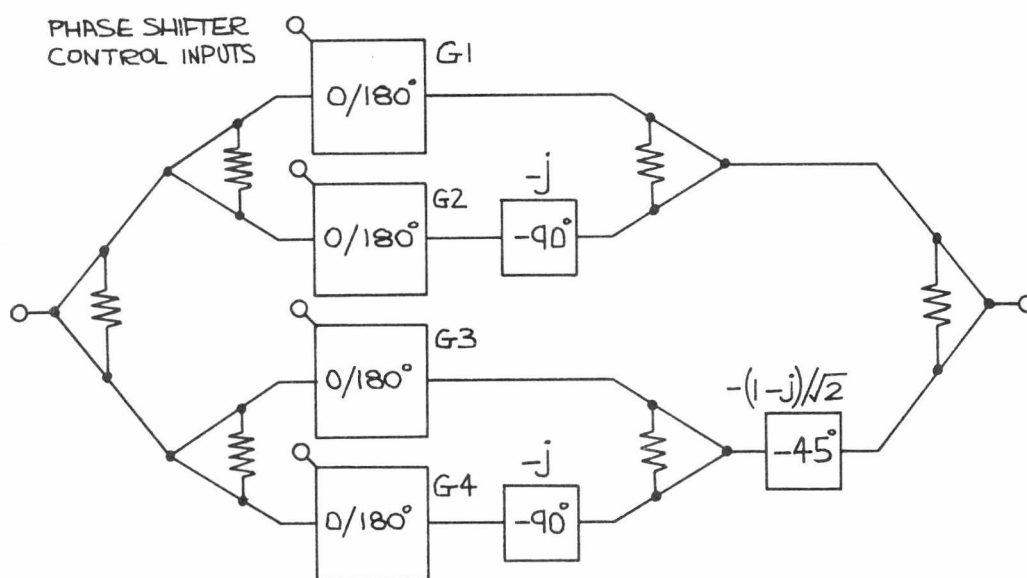


Figure 4.7 : A three-bit parallel phase shifter.

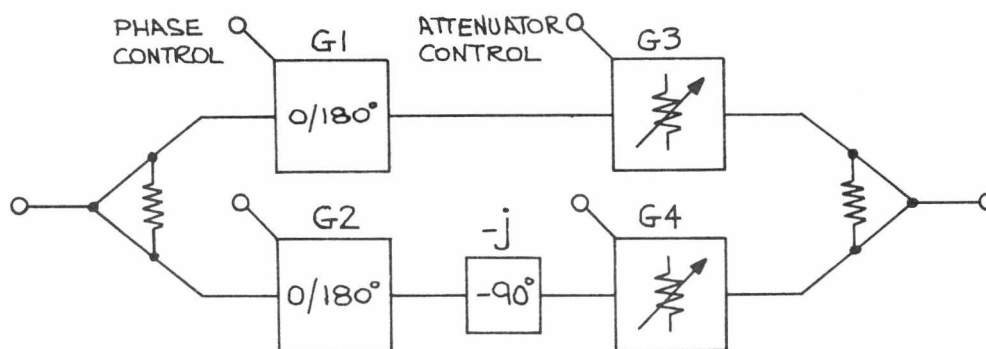


Figure 4.8 : A phase shifter capable of giving three or more bits of phase shift using a combination of digital phase and amplitude control.

$$G_T = \frac{G_1 - j G_2}{2} \quad (4.6)$$

This equation ignores the phase delay of the Wilkinson power dividers though the denominator arises because of the 3 dB division and recombination losses. If  $|G_1| = |G_2|$  the four equal amplitude phase states occur with 90 degree spacing and 45 degree offset from zero. Their magnitudes are given by the modulus of equation (4.6), hence  $|G_T| = G/\sqrt{2}$ , where  $G$  is the modulus of  $G_1$  or  $G_2$ . The two bit phase shifter's gain (or loss) is therefore 3 dB worse than that of the individual 0/180 degree phase shifters used in its construction.

This idea can be extended to give three bits of phase shift by use of two of the above two bit phase shifters and delaying one by 45 degrees. This circuit is shown in Figure 4.7. The gain in each 0/180 degree phase shifter is given by  $G_1, G_2, G_3$  and  $G_4$  and they are nominally equal again with a magnitude of  $G$ . The 45 degree delay is a constant differential phase shift circuit and has a transmission of  $(1-j)/\sqrt{2}$ . The overall gain of this phase shifter is given by

$$G_T = \frac{G_1 - j G_2 + (1 - j)(G_3 - j G_4)/\sqrt{2}}{4} \quad (4.7)$$

It will be noticed that the four 0/180 degree phase shifters allow  $2^4$  possible states. These divide into two sets of eight, both giving phase states at 45 degree intervals with a 22.5 degree offset from zero. The two sets however, have different magnitudes such that if the modulus of equation (4.7) is taken with  $G = G_1, G_2, G_3$  and  $G_4$  then

$$\left. \begin{aligned} |G_T| &= G \sqrt{\frac{2 + \sqrt{2}}{8}} \\ |G_T| &= 0.6533 G \end{aligned} \right\} \quad (4.8)$$

Taking the modulus of equation (4.7) again but with  $G = G_1, G_2$  and  $G_4$  and  $G_3 = -G$  then,

$$\left. \begin{aligned} |G_T| &= G \sqrt{\frac{2 - \sqrt{2}}{8}} \\ |G_T| &= 0.2706 G \end{aligned} \right\} \quad (4.9)$$

The desired eight states having the higher gain as given by equation (4.8) can be selected by suitable combinational logic driving the four 0/180 degree phase shifters.

If this parallel arrangement is further extended to give four bits, two of the above three bit circuits are required with one being delayed by 22.5 degrees. This four bit circuit has eight 0/180 degree phase shifters giving a total of  $2^8$  possible states. Analysis has shown that these divide into sixteen sets of sixteen like states. All of the sets have phase states spaced by 22.5 degrees as required. Of these eight sets have an offset of 11.25 degrees though with different overall gains, the highest being 0.641 G and the smallest 0.053 G. The eight remaining sets have dissimilar offsets ranging from 2 to 20.5 degrees and with a variety of gains no higher than 0.455 G.

It will be noticed that the number of 0/180 degree phase shifters and hence MESFET devices increases rapidly as the number of phase shifter bits is increased. Also, the overall phase shifter gain  $G_T$  decreases with increasing bit numbers. Table 4.4 shows a comparison of the parallel phase shifters just discussed with a cascade equivalent. It is assumed that each bit of the cascade phase shifter would require only two devices and that each bit has a gain (or loss) of G.

BITS		1	2	3	4
Smallest Phase Increment		180°	90°	45°	22.5°
No. of devices	} parallel cascade	2	4	8	16
		2	4	6	8
Overall gain	} parallel cascade	G	0.707 G	0.653 G	0.641 G
		G	G <sup>2</sup>	G <sup>3</sup>	G <sup>4</sup>
Power dividers	} parallel cascade	/	2	6	14
			0	0	0
Delay networks	} parallel cascade	/	1	3	7
			0	0	0

Table 4.4 : A comparison of the properties of parallel and cascade type multi-bit phase shifters. (Only dividers and delays that are needed for a multi-bit phase shifter are given).

It appears that the parallel arrangement is at a disadvantage. However, several points must be noted. Consider first the overall gain, it can be seen that this is tending to a limit for an increasing number of bits. From equations (4.6) and (4.7) the following equation can be inferred,

$$G_{T_N} = G_{T_{N-1}} \left( \frac{1 + \cos \phi_N + j \sin \phi_N}{2} \right) \quad (4.10)$$

where  $G_{T_N}$  is the overall gain of an N bit phase shifter whose smallest phase increment,  $\phi_N$  is given by  $180/2^{N-1}$  degrees. If this is solved iteratively for increasing N, a value of  $G_T = 0.63662 G$  is soon reached. Hence the overall gain is at worst 3.92 dB less than that of the individual 0/180 degree phase shifters. Recalling from Figure 4.4 that a gain of 8 dB is predicted for the 0/180 degree phase shifter, an overall gain of better than 4 dB is still achievable with the parallel arrangement. Most typical cascade phase shifters<sup>3</sup> employ PIN diodes and

as a consequence have an inherent loss such that the overall gain would be an increasing loss for increasing  $N$ .

If device numbers are considered then the parallel arrangement's requirement rises as the square of the number of bits whereas that of the cascade is directly proportional. However, some device economy can be gained in the parallel phase shifter by use of amplitude control<sup>5,6</sup> to effect phase shifts. Consider the phase shift circuit shown in Figure 4.8. Again the input signal is split equally to a pair of 0/180 degree phase shifters  $G_1$  and  $G_2$ , one of which is phase delayed by 90 degrees. However, before combining their output signals they are amplitude modulated by  $G_3$  and  $G_4$ , a pair of switchable attenuators (or amplifiers). The purpose of  $G_3$  and  $G_4$  is to cause a  $\pm 22.5$  degree phase shift in the combined signal. To do so the attenuation (or gain) introduced by  $G_3$  or  $G_4$  must change from unity to  $\tan(22.5 \text{ degrees})$ , i.e. 0.4142 or 7.7 dB. Hence, when one switch is at a 0 dB setting the other must be 7.7 dB different. The resultant phase shifter will exhibit phase increments of 45 degrees.

By using an amplifying MESFET switch as described in Chapter 2 further gain can be obtained from this phase shifter. The overall gain of the phase shifter shown in Figure 4.8 is,

$$G_T = \frac{G_1 G_3 - j G_2 G_4}{2} \quad (4.11)$$

Taking the condition where  $G_1 = G_2$  and  $G_4 = G_3 \tan(22.5)$  then equation (4.11) becomes,

$$G_T = G_1 G_3 (1 - j \tan(22.5)) / 2 \quad (4.12)$$

whose modulus is  $|G_T| = |G_1| |G_3| 0.5412$ . Hence the overall phase shifter gain is 5.33 dB lower than the combined gain of the 0/180 degree phase

shifter (8 dB) and that of the MESFET switch at its maximum (>8 dB).

To obtain four bits of phase shift,  $G_3$  and  $G_4$  need to be set to give offset phases of 0 and 45 degrees plus the 22.5 and 67.5 degrees already demonstrated. If the modulus of equation 4.12 is obtained for an arbitrary offset phase of  $\phi_0$ , then,

$$\left. \begin{aligned} |G_T| &= \frac{|G_1||G_3|}{2} \sqrt{1 + \tan^2 \phi_0} \\ \text{or, } |G_T| &= \frac{|G_1||G_4|}{2} \sqrt{1 + \cot^2 \phi_0} \end{aligned} \right\} \quad (4.13)$$

It will be noticed that if  $|G_T|$  is to remain constant for all offset angles, both  $G_3$  and  $G_4$  must be varied. Also when  $|G_T|$  is a minimum,  $\phi_0 = 0$  (or 90) degrees, at which point  $G_3 = \text{unity}$ . Gain contributions from the amplifying MESFET switch are at present being ignored. Equations (4.13) therefore become,

$$\left. \begin{aligned} |G_3| &= \frac{1}{\sqrt{1 + \tan^2 \phi_0}} \\ |G_4| &= \frac{1}{\sqrt{1 + \cot^2 \phi_0}} \end{aligned} \right\} \quad (4.14)$$

If equations (4.14) are solved for the zero degree offset then  $|G_3| = 1.0$  (0 dB) and  $|G_4| = 0.0$  ( $-\infty$  dB). Therefore the on to off ratio of the switchable attenuator needs to be very large. This is beyond the ability of the amplifying MESFET switch whose on to off ratio is about 20 dB. This difficulty can be overcome by introducing an 11.25 degree offset to all the phase states. The first four phase states and the required values of  $|G_3|$  and  $|G_4|$  are given in Table 4.5.

Phase state	$ G_3 $	$ G_4 $
11.25°	0.9808 (-0.17 dB)	0.1951 (-14.2 dB)
33.75°	0.8315 (-1.60 dB)	0.5556 (-5.11 dB)
56.25°	0.5556 (-5.11 dB)	0.8315 (-1.60 dB)
78.75°	0.1951 (-14.2 dB)	0.9808 (-0.17 dB)

Table 4.5 : Values of relative attenuation required to produce 22.5 degree phase increments for a four bit phase shifter.

Hence the maximum on to off ratio required of the MESFET switch is approximately 14 dB. The values of  $|G_3|$  and  $|G_4|$  will all increase in the same ratio when the gain of the MESFET switch is taken into account. It has been assumed that the transmission phases of  $G_3$  and  $G_4$  are equal. If these phases begin to differ at say the large values of attenuation (caused by the MESFET approaching pinch off) compensation could be applied by adjusting the attenuation of each switch.

A method has therefore been demonstrated which can effect digital phase shifts using only 0/180 degree phase shifters and various fixed components in a parallel structure. There is no limit to the number of phase states that this technique can be made to exhibit. However, the consequent complexity and rapidly increasing number of MESFET devices would begin to impose a constraint, possibly for four bits and more. This limitation can be overcome by amplitude controlling the quadrature signals of a parallel two bit shifter and so generating the smaller phase increments required for three and four bit circuits. The amplitude control is achieved by a pair of switched MESFET amplifiers which contribute to the overall gain of the complete phase shifter. This circuit requires only six devices, two pairs in each 0/180 degree phase shifter plus one in each of the switched MESFET amplifiers.

#### 4.7 SWITCHING BEHAVIOUR AND MEASUREMENT

There are several reasons why fast switching times are desirable of a digital phase shifter. Firstly, in a digital communications system where a phase shifter is being used as a phase modulator, slow switching times give rise to discrete spectral lines<sup>7</sup> in an otherwise continuous spectrum. These transmit no useful information and contribute to a degradation in the systems noise performance<sup>3</sup>. Secondly, if the phase shifter is being followed by a limiting amplifier, the reductions in signal amplitude during switching cause AM to PM conversion within the amplifier<sup>1</sup>. Also, this reduction in signal amplitude reduces the information available for receiver synchronisation<sup>8</sup>. As discussed in Chapter 2, the switching speed of the MESFET switch appears to be limited more by its drive circuitry rather than by device switching speed or bias filter considerations. The same applies to the two-way MESFET switch as used in the phase shifter.

Lastly, an effect though not being caused by slow switching is inherently present in some phase shifters and may manifest itself as the switching speed approaches its limits. Differences in the phase shift networks paths lengths cause amplitude variations and phase jitter<sup>9</sup>. The amplitude variations that may exist because of differing network losses may be balanced out by adjusting device gains by means of their biases. However, the differing delays of the dispersive network and its reference line give rise to jitter and amplitude variations just after switching.

Consider the phase shifter circuit as shown in Figure 4.2. The total electrical lengths of the lines from the device gates to the input junction are approximately 1 and 1.5 wavelengths. These have propagation delays of 100 and 150 pS. If the MESFET devices are switched, then depending on which device is now biased off, the

mismatch will take either 100 or 150 pS to reach the input junction and a total of 250 pS to reach the device that is biased on. During this period an amplitude variation will occur before the mismatch combines with the input wave at the device. This disruption is asymmetrical for each phase reversal because of the half wavelength difference (50 pS) in the phase shift circuit. This disruption time is shorter than the switching limitation of the drive circuitry and may not be seen. It is worth noting however that this time can be reduced and made symmetrical by using the slotline type phase shifter as shown in Figure 4.3. It is of a balanced nature and hence symmetrical during switching. The total line lengths between devices and the dividers junction are shorter than that of the previous circuit.

Having established the various factors affecting the switching behaviour consideration will now be given to its measurement. One method is the direct observation of the modulated carrier or the phase detected carrier. Observation of the carrier however becomes increasingly difficult as frequencies rise through the microwave region, 10 GHz being the typical limit for sampling oscilloscopes. If the modulated carrier is detected then only the modulations need to be handled by the oscilloscope. A balanced mixer can be used as a phase detector by comparing an equal amplitude carrier reference whose phase can be adjusted to maximise the mixer's output. Though the method allows direct measurement of the phase transitions and any switching transients that may be present, no information can readily be obtained about either the carrier rejection, AM or phase error. If, however, analysis of the modulated signal is performed in the frequency domain information about all of these can be gleaned from its spectrum. To do so the effect of these on the carrier must be determined.

The spectrum analysis can be split into two parts, those which can be classified firstly on amplitude effects such as AM and switching time and secondly phase error. The distinction is drawn because the first can be determined simply by using the convolution theorem but the second requires direct evaluation of the Fourier integral.

Let  $f_c(t)$  be the carrier as a function of time and  $f_m(t)$  be the modulation signal such that the phase reversals of the carrier (0 and 180 degrees) are accomplished by giving  $f_m(t)$  a positive or negative sign. The phase modulated carrier can be expressed as,

$$f(t) = f_c(t) f_m(t) \quad (4.15)$$

Noting that the Fourier transform of modulation can invariably be readily obtained, the transform of  $f(t)$  can be determined by using convolution such that<sup>10</sup>,

$$f(\omega) = f_c(\omega) * f_m(\omega) / \sqrt{2\pi} \quad (4.16)$$

where  $f(\omega)$  is the Fourier transform of  $f(t)$ , etc. Hence, the spectrum of the 0/180 degree phase modulated carrier is that of the modulation placed as a mirror image about the carrier frequency which is itself suppressed. For square-wave modulation having a period  $T$  ( $\omega = 2\pi/T$ ) then,

$$\left. \begin{aligned} f_m(t) &= -A \quad \text{for } t = -T/2 \text{ to } 0 \\ f_m(t) &= 1 \quad \text{for } t = 0 \text{ to } T/2 \end{aligned} \right\} \quad (4.17)$$

where  $A$  is the amplitude imbalance (AM) such that  $A$  lies between zero and unity. The Fourier coefficients are,

$$\begin{aligned}
 a_0 &= \frac{2}{T} \int_0^{T/2} dt - \frac{2}{T} \int_{-T/2}^0 A dt \\
 a_0 &= 1-A
 \end{aligned}
 \quad \left. \vphantom{\begin{aligned} a_0 &= \frac{2}{T} \int_0^{T/2} dt - \frac{2}{T} \int_{-T/2}^0 A dt \\ a_0 &= 1-A \end{aligned}} \right\} (4.18)$$

$$\begin{aligned}
 a_k &= \frac{2}{T} \int_0^{T/2} \text{Cos } k \omega t dt - \frac{2}{T} \int_{-T/2}^0 A \text{Cos } k \omega t dt \\
 a_k &= 0 \text{ for all } k
 \end{aligned}
 \quad \left. \vphantom{\begin{aligned} a_k &= \frac{2}{T} \int_0^{T/2} \text{Cos } k \omega t dt - \frac{2}{T} \int_{-T/2}^0 A \text{Cos } k \omega t dt \\ a_k &= 0 \text{ for all } k \end{aligned}} \right\} (4.19)$$

$$\begin{aligned}
 b_k &= \frac{2}{T} \int_0^{T/2} \text{Sin } k \omega t dt - \frac{2}{T} \int_{-T/2}^0 A \text{Sin } k \omega t dt \\
 b_k &= \frac{2(k+1)}{k\pi}, \quad k = 1, 3, 5, \text{ etc.}
 \end{aligned}
 \quad \left. \vphantom{\begin{aligned} b_k &= \frac{2}{T} \int_0^{T/2} \text{Sin } k \omega t dt - \frac{2}{T} \int_{-T/2}^0 A \text{Sin } k \omega t dt \\ b_k &= \frac{2(k+1)}{k\pi}, \quad k = 1, 3, 5, \text{ etc.} \end{aligned}} \right\} (4.20)$$

The constant  $1/\sqrt{2\pi}$  in the convolution (equation (4.16)) is unimportant since only relative magnitudes of the suppressed carrier given by  $a_0$  and the harmonic spectra  $b_1$  is important. The ratio between  $b_1, b_3, b_5$ , etc. are constant for all  $A$ . The carrier rejection,  $a_0 - b_1$  is shown plotted in Figure 4.9 against  $A$ , the amplitude imbalance.

If  $A$  is now made equal to unity and the square-wave modulation given finite rise and fall times the effect of switching times on the spectrum can be assessed. If  $f_m(t)$  is defined as follows,

$$\begin{aligned}
 f_m(t) &= -t/t_f & \text{for } t &= -T/2 - t_f \text{ to } -T/2 + t_f \\
 f_m(t) &= -1 & \text{for } t &= -T/2 + t_f \text{ to } -t_r \\
 f_m(t) &= t/t_r & \text{for } t &= -t_r \text{ to } t_r \\
 f_m(t) &= 1 & \text{for } t &= t_r \text{ to } T/2 - t_f
 \end{aligned}
 \quad \left. \vphantom{\begin{aligned} f_m(t) &= -t/t_f & \text{for } t &= -T/2 - t_f \text{ to } -T/2 + t_f \\ f_m(t) &= -1 & \text{for } t &= -T/2 + t_f \text{ to } -t_r \\ f_m(t) &= t/t_r & \text{for } t &= -t_r \text{ to } t_r \\ f_m(t) &= 1 & \text{for } t &= t_r \text{ to } T/2 - t_f \end{aligned}} \right\} (4.21)$$

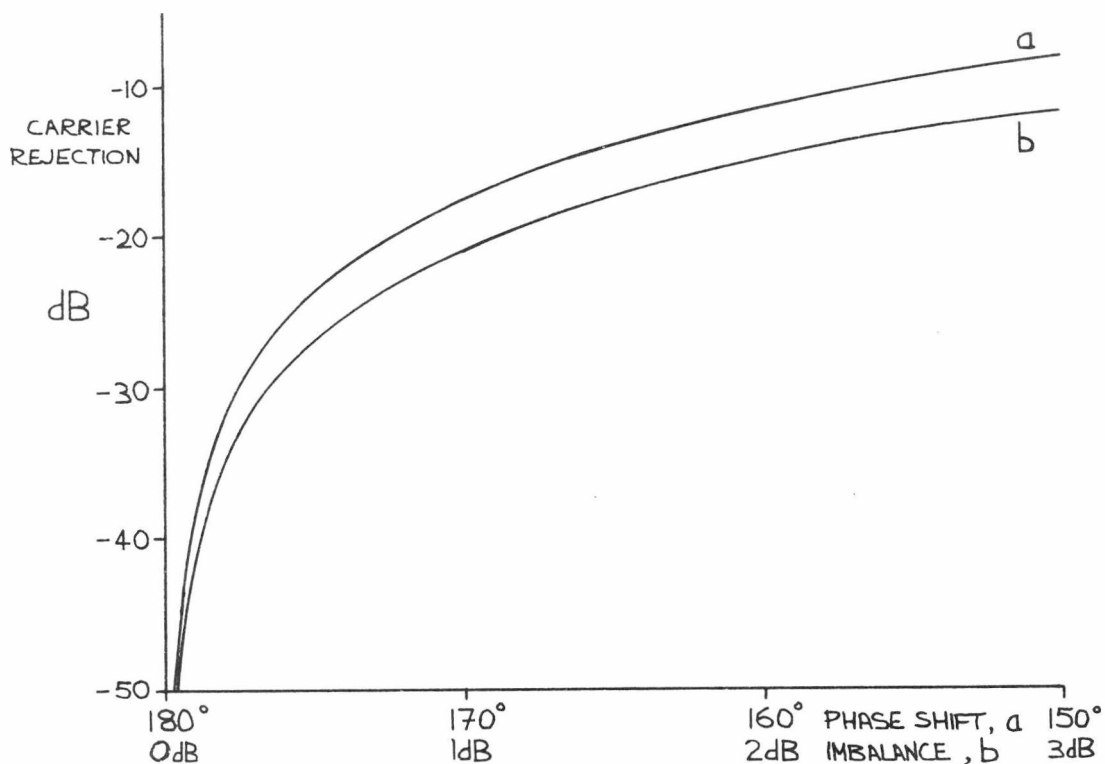


Figure 4.9 : Carrier rejection as a function of a: phase shift and b: amplitude imbalance for a binary phase modulated signal.

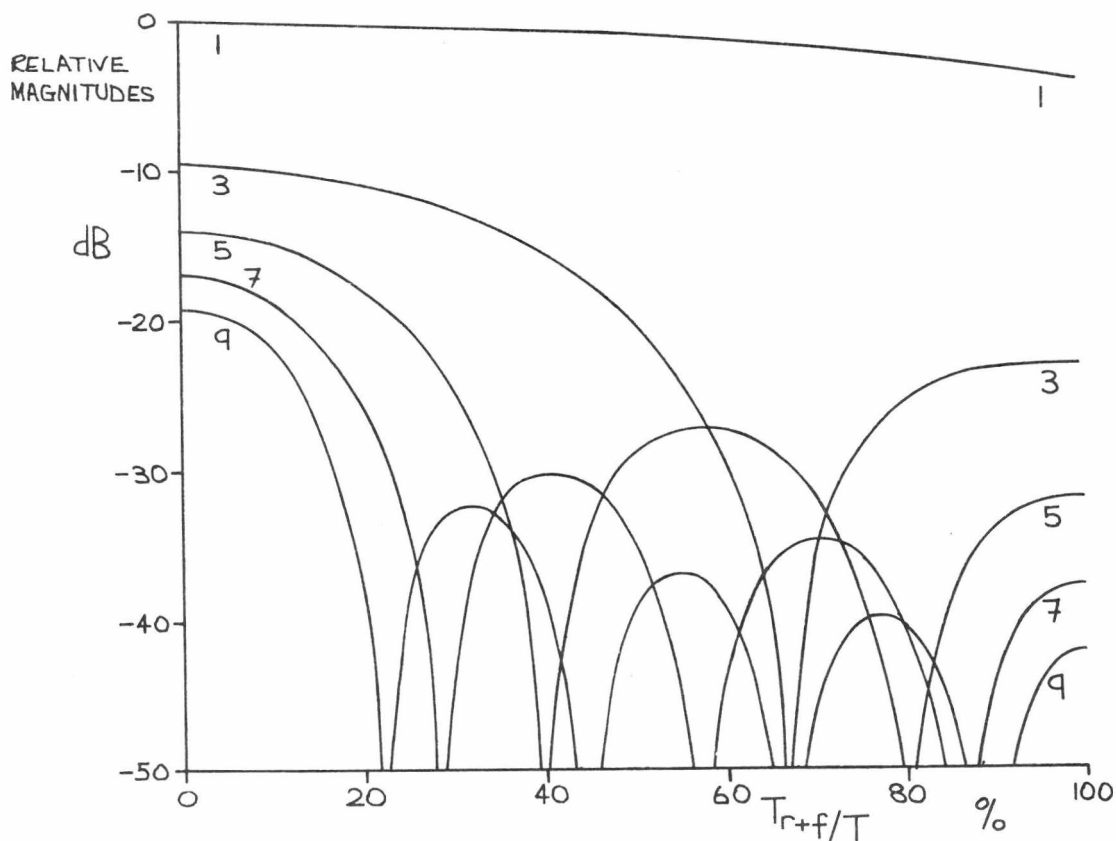


Figure 4.10 : Variation of the spectrum's component magnitudes (1st, 3rd, etc.) for a 0/180 degree phase modulated signal having finite transitions times  $T_r$  and  $T_f$ .  $T$  is the period of the modulation having equal mark to space ratio.

where  $2t_r$  and  $2t_f$  are the total rise and fall times respectively. Since  $A$  is unity  $a_0$  is zero and because  $f_m(t)$  is an odd function all the  $a_k$  are zero. Evaluation of the Fourier integral gives,

$$b_k = \frac{T \sin k \omega t_r}{t_r k^2 \pi^2} - \frac{T \sin k \omega t_f \cos k \pi}{t_f k^2 \pi^2} \quad k = 1, 2, 3, \text{ etc.} \quad (4.22)$$

Hence, the spectral magnitudes are functions of the rise and fall times. If  $t_r = t_f$  then only odd harmonics are present otherwise even terms appear. These magnitudes are plotted in Figure 4.10 for  $t_r = t_f$  against the total rise and fall time  $2t_r + 2t_f$  as a percentage of the period  $T$ . If  $t_f$  is not equal to  $t_r$  then the situation is complicated. Not only does the total rise and fall time affect the spectrum but also the ratio of  $t_r$  to  $t_f$ . It is difficult to give a complete picture of this but by fixing  $t_f$  at 20% of  $T$  and varying  $t_r$  the change in spectrum can be obtained as is shown in Figure 4.11. It is envisaged that in most instances the rise and fall time will be very near equal. Care must be taken to keep the modulating square-wave's mark to space ratio equal to avoid even harmonic contributions from this.

If the effect of phase error is now considered, the phase modulated signal must be expressed as,

$$\left. \begin{aligned} f(t) &= \sin(\omega_c t + \Delta\phi) & \text{for } t &= -T/2 \text{ to } 0 \\ f(t) &= \sin \omega_c t & \text{for } t &= 0 \text{ to } T/2 \end{aligned} \right\} \quad (4.23)$$

where  $\Delta\phi$  is the phase shift of the modulation, nominally 180 degrees but with an additional phase error and  $\omega_c = 2\pi/t_c$ , to being the carrier period. It is impossible to separate  $f(t)$  into a product of carrier and modulation, hence convolution cannot be used to obtain the spectrum,

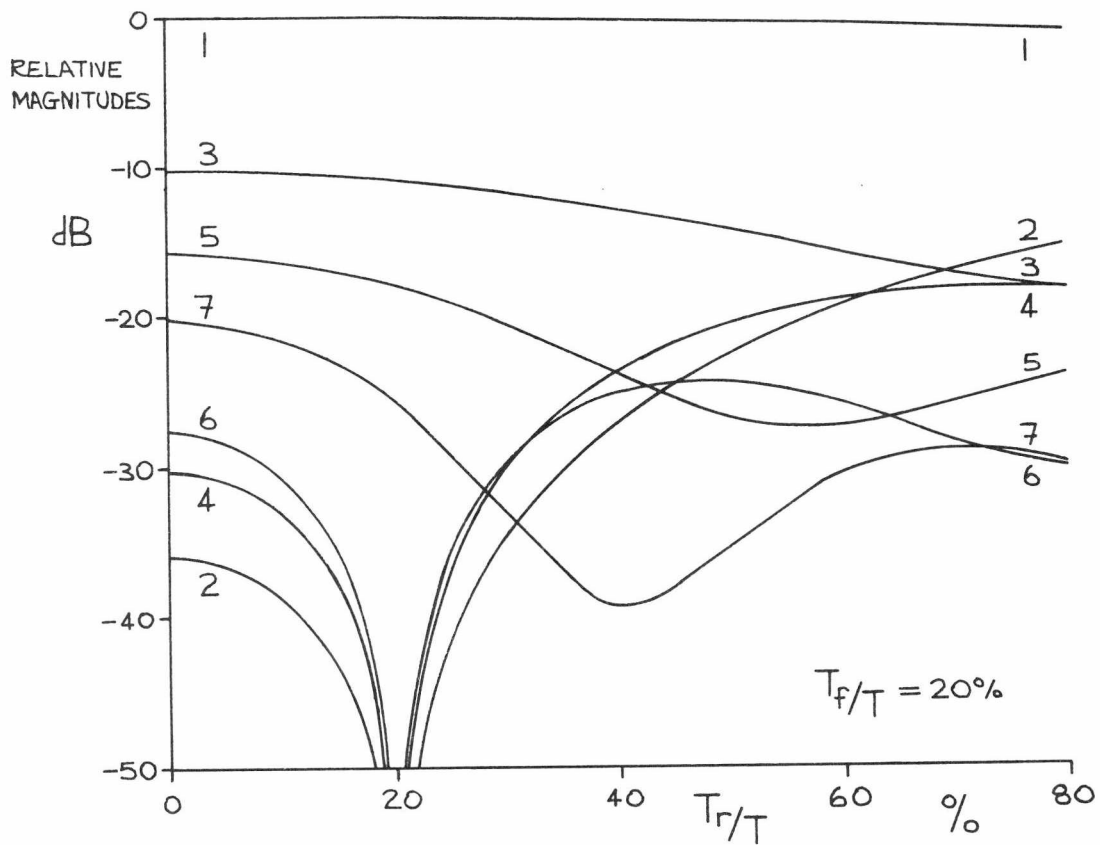


Figure 4.11 : Variation of the spectrum's component magnitudes (1st, 2nd, etc.) for a 0/180 degree phase modulated signal having finite transition that are different between each phase state.

rather Fourier analysis has to be performed directly on equations (4.23). Therefore the Fourier coefficients are given by,

$$a_k = \frac{2}{T} \cos \Delta\phi \int_{-T/2}^0 \sin \omega_c t \cos k \omega t dt + \frac{2}{T} \sin \Delta\phi \int_{-T/2}^0 \cos \omega_c t \sin k \omega t dt + \frac{2}{T} \int_0^{T/2} \sin \omega_c t \cos k \omega t dt \quad (4.24)$$

$$b_k = \frac{2}{T} \cos \Delta\phi \int_{-T/2}^0 \sin \omega_c t \sin k \omega t dt + \frac{2}{T} \sin \Delta\phi \int_{-T/2}^0 \cos \omega_c t \sin k \omega t dt + \frac{2}{T} \int_0^{T/2} \sin \omega_c t \sin k \omega t dt \quad (4.25)$$

Solutions to these integrals can be found in mathematical tables<sup>11</sup> such that if  $m^2 \neq n^2$  then,

$$\int \sin mx \sin nx dx = \frac{\sin(m-n)x}{2(m-n)} - \frac{\sin(m+n)x}{2(m+n)}$$

$$\int \cos mx \cos nx dx = \frac{\sin(m-n)x}{2(m-n)} + \frac{\sin(m+n)x}{2(m+n)}$$

$$\int \sin mx \cos nx dx = -\frac{\cos(m-n)x}{2(m-n)} - \frac{\cos(m+n)x}{2(m+n)}$$

If (4.24) and (4.25) are evaluated then the coefficients are,

$$a_k = \frac{(1 - \cos \Delta\phi)}{T} \left[ \frac{1}{D} + \frac{1}{S} - \frac{\cos(DT/2)}{D} - \frac{\cos(ST/2)}{S} \right] + \frac{\sin \Delta\phi}{T} \left[ \frac{\sin(DT/2)}{D} + \frac{\sin(ST/2)}{S} \right] \quad (4.26)$$

$$b_k = \frac{(1 + \cos \Delta\phi)}{T} \left[ \frac{\sin(DT/2)}{D} - \frac{\sin(ST/2)}{S} \right] - \frac{\sin \Delta\phi}{T} \left[ \frac{1}{D} + \frac{1}{S} - \frac{\cos(DT/2)}{D} - \frac{\cos(ST/2)}{S} \right] \quad (4.27)$$

where  $D = \omega_c - k\omega$  and  $S = \omega_c + k\omega$  for  $k = 1, 2, 3$ , etc. The magnitudes of the spectra are given by,

$$C_k = (a_k - j b_k)/2 \quad (4.28)$$

It must be noted that the carrier magnitude is given by the coefficient  $C_\ell$  where  $\ell = Tf_c$ ,  $C_1$  being that of the fundamental modulation frequency  $\omega/2\pi$  (or  $1/T$ ). The ratio between  $C_\ell$  and  $C_{\ell+1}$  or  $C_{\ell-1}$ , the largest of the modulation spectra is the carrier rejection. This has been calculated for various angles of  $\Delta\phi$  near 180 degrees and is shown in Figure 4.9. The two curves of Figure 4.9 are in agreement with data given by Tsai et al.<sup>12</sup> However, the curves are more general in that any value of carrier rejection can be related to phase error or amplitude imbalance whereas those of Tsai are for specified values of rejection.

It is not possible by observation of the spectrum to distinguish between the presence of carrier caused by phase error or amplitude imbalance. However, with the MESFET phase shifter described in this work the gains (and hence amplitudes) can easily be balanced by observing a dip in the carrier level, leaving only that caused by phase error. To obtain the combined effect of phase error and amplitude imbalances and rise time equations (4.23) must be multiplied by the modulation equations (4.17) or (4.21). The overall spectrum may then be obtained by convolution of each individual spectrum.

A considerable amount of information can therefore be obtained by

observing the spectrum of the modulated output from the phase shifter. The measurement technique requires a spectrum analyser and a square wave generator capable of switching the phase shifter near its limit. The slotline type phase shifter is thought to have an advantage during switching because of the balanced nature of the phase splitting divider.

#### 4.8 CONCLUSION

This chapter has brought together the various components discussed and developed in the previous two chapters. A constraint of  $0/180$  degrees was shown to exist for optimum phase shifter performance. This constraint and the bandwidth reduction caused by the long reference lines of the dispersive phase shift circuits lead to the conclusion that the slotline type divider is the best choice for a MESFET phase shifter. The  $0/180$  degree constraint was circumvented by developing the parallel type structure. This was seen to require excessive devices and circuitry as the numbers of bits rises so a circuit consisting of only two  $0/180$  degree phase shifters and two switched amplifiers was investigated. The circuit was made to exhibit four bits of phase shift and has an overall gain increase. When switching effects are considered the slotline type phase shifter again offers an advantage due to its balanced nature. Finally, the use of spectrum analysis has been discussed as a means of measuring the switching times, phase error and amplitude imbalance of the phase shifter's output.

4.9 REFERENCES

- 1 Tri T. Ha, Solid-State Microwave Amplifier Design, Wiley, 1981, p. 36 and p. 215.
- 2 V.J. Albanese and W.P. Peyser, An Analysis of a Broad-Band Coaxial Hybrid Ring, IRE Trans. MTT6, October 1958, pp. 369-373.
- 3 H. Yamamoto, K. Morita and S. Komaki, QPSK System Error Rate Performance, Review of the Electrical Communication Laboratories, Vol. 25, No. 5-6, May-June 1977, pp. 515-526.
- 4 C.W. Craig and H.K. Craig, A Low-Loss Microstrip X-Band Diode Phase Shifter, 5th European Microwave Conference, 1975, pp. 518-521.
- 5 W.R. Bennett and J.R. Davey, Data Transmission, McGraw-Hill, 1965, pp. 202.
- 6 M.J. Fithian, Two Microwave Complex Weighting Circuits, IEEE MTT Symposium 1980, pp. 126-128.
- 7 B. Glance and N. Amitay, A Fast-Switching Low-Loss 12 GHz Microstrip 4-PSK Path Length Modulator, IEEE Trans. COM-28, October 1980, pp. 1824-1828.
- 8 C. Louis Cuccia and E. Wesley Matthews, PSK and QPSK Modulators for Gigabit Data Rates, IEEE MTT Symposium 1977, pp. 208-211.
- 9 H. Ogawa, M. Aikawa and M. Akaike, Integrated Balanced BPSK and QPSK Modulators for the Ka-Band, IEEE Trans. MTT30, March 1982, pp. 227-234.
- 10 K.F. Riley, Mathematical Methods for the Physical Sciences, Cambridge University Press, 1974.
- 11 H.B. Dwight, Tables of Integrals and Other Mathematical Data, MacMillan, 1961, pp. 98, 105 and 115.

- 12 W.C. Tsai, T.L. Tsai, S.F. Paik and I.S. Carnes, PSK Modulator using Dual-Gate FETs, IEEE International Solid-State Circuits Conference, 1979, pp. 164-165.

CHAPTER 5MEASUREMENTS AND RESULTS OF PHASE SHIFTER COMPONENTS5.1 INTRODUCTION

This chapter will present the results of various measurements done on the components used in the construction of the phase shifters. Results will be given for the substrate loss and dispersion associated with a 50 ohm microstrip line. The coaxial to microstrip transitions are known to cause a discontinuity effect and some evidence will be given for this.

The device's measured scattering parameters will be presented with specific emphasis on comparing the predicted off-biased parameters with those actually measured. The performance of the narrow band amplifier will be assessed and its viability as a microwave switch with an on state gain demonstrated.

Various aspects of the passive components (Chapter 3) used in the phase shifter's construction will be shown. The bandwidth of the input divider when one of its outputs is mismatched is measured and compared with the theory developed in Chapter 4. The phase and magnitude behaviour of the two dispersive phase shift networks will be briefly discussed and the advantages of the slotline type divider displayed.

The following chapter will present the measured performance of the complete (integrated) phase shifter circuits. One will use the Schiffman, one the band pass stub network and two others the slotline type divider.

As mentioned previously, network measurements have been performed using a Hewlett Packard 8410S manual network analyser. Gain (or loss) measurements are performed by first calibrating the analyser for a 0 dB reference with either a short circuit termination or a through connection (SMA to SMA). Calibrating scales are obtained by use of the test channel gain control on the 8410B unit. This is thought<sup>1</sup> to have a setting accuracy of better than  $\pm 0.2$  dB. The circuit to be measured is then substituted for the short or through connection. The same technique is used for transmission (and differential) phase except that the calibration scale is produced by the phase offset control on the 8412A phase-magnitude display unit. This is thought<sup>1</sup> to have an accuracy of better than 2 degrees for a 180 degree offset. Results are obtained via a 8750A storage normaliser onto an XY plotter.

## 5.2 SUBSTRATE AND TRANSITIONS

Of specific interest is the transmission loss that the substrate causes a length of microstrip to exhibit. Coupled with this is the effect introduced by the coaxial to microstrip transition which is known to exhibit reactive effects and contribute a loss. At the frequencies used for this work (about 10 GHz) it is possible that dispersion may be a significant factor.

The loss measurements are performed using a 2 inch length of 50 ohm microstrip line at either end of which is an Omni Spectra type OSM 244-4A transition. The Epsilam 10 substrate is 0.635 mm thick ( $h$ ) and is clad with 1 oz copper (approximately 0.038 mm thickness). The required microstrip width ( $w$ ) and associated guide wavelength ( $\lambda_g$ ) (or effective dielectric constant) for a specified line impedance are obtained from curves<sup>2</sup> and listings<sup>3</sup>. For 50 ohms,  $w$  is taken as 0.65 mm.

The effect of finite metallisation is not taken into account though it is known<sup>4</sup> that this effectively widens the microstrip hence lowering  $Z_0$ . Its effect is greatest on narrow lines,  $W/h \rightarrow 0.1$ .

Shown in Figure 5.1 is the measured insertion loss of this line. Also shown is the line's insertion loss as given<sup>5</sup> by the substrate's manufacturer. It will be noticed that the measured line exhibits an excess insertion loss. There are several possible causes for this. Firstly, the presence of transition insertion loss<sup>6</sup> possibly caused by radiation at the transition point. If a straight line least squares fit is performed on the data points then the excess loss ranges from 0.03 dB per transition at 6 GHz to 0.038 dB at 12 GHz. Two further causes of loss are line mismatch (ie.  $Z_0 \neq 50$  ohms) and the reactive elements that appear to be associated with the transition<sup>7</sup>. Both of these give rise to insertion loss ripple. For the line mismatch the ripple's magnitude is independent of frequency. The reactive elements that can be used to model the transition<sup>7</sup> consist of a shunting capacitance at the coaxial side plus a series inductance. One transition on its own would behave as a low pass network but two when spaced by a length of line gives rise to periodic ripples of increasing magnitude with frequency. The line mismatch causes insertion loss dips when the line's length is an odd multiple of a quarter-wave length whereas that caused by the transitions occurs at half-wavelength frequencies.

It will be noticed that the measured loss has a distinct periodic ripple. Also, its magnitude increases with frequency indicating that the transitions are behaving as reactive discontinuities. Without performing measurements below 6 GHz it is difficult to deduce whether there is any contribution from line mismatch. The measured ripple is about 0.15 dB at 10 GHz and modelling of the line and transitions (element values as given by Wight et. al.<sup>7</sup>) predicts 0.06 dB ripple for 50 ohms line impedance. The transition plus a 45 ohm line causes 0.11 dB

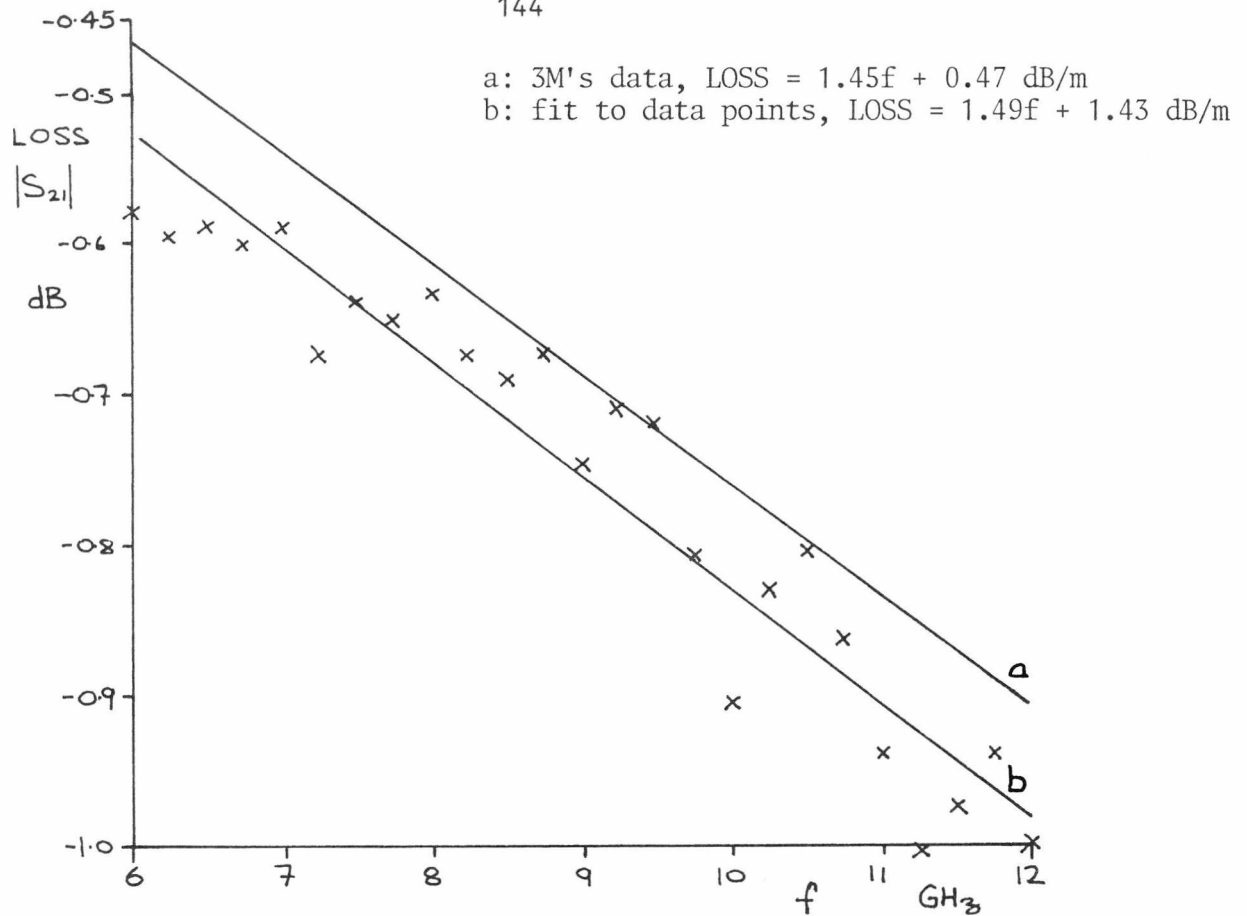


Figure 5.1 : Insertion loss of a 50.8 mm length of 50 ohm microstrip line on Epsilam 10 substrate plus that of two SMA transitions.

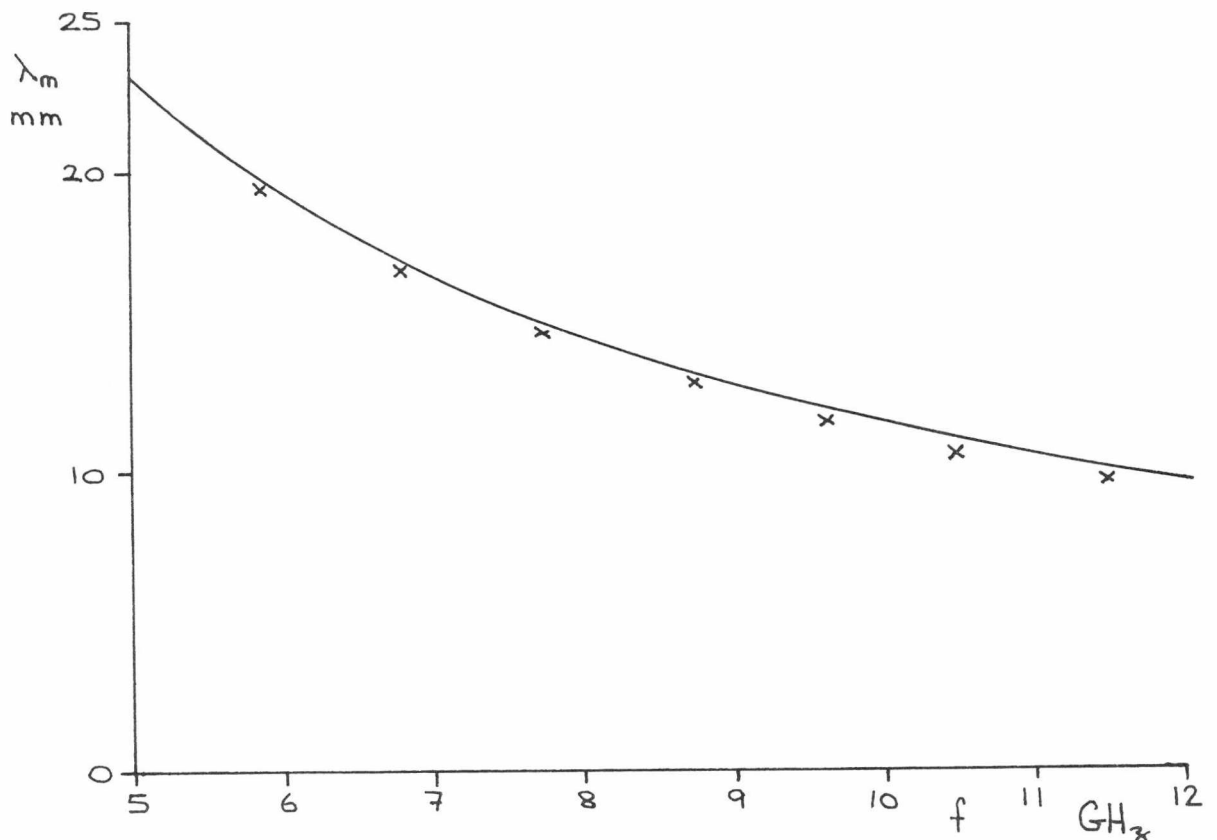


Figure 5.2 : Microstrip wavelength derived from the resonances of a 50 ohm ring. Error in measured wavelength is approximately 3%. Continuous curve is for  $\lambda_0/\lambda_m = 2.6$

peak-to-peak ripple. Hence, the transition definitely does give rise to a discontinuity though no satisfactory measure of line impedance accuracy has been obtained. Taking into account these effects, the Epsilam 10's measured loss is in agreement with the manufacturers (see Figure 5.1).

A measure of line dispersion (or actual microstrip wavelength) can be obtained by using Troughton's resonant ring technique<sup>8</sup>. A closed ring of microstrip does not suffer end effects and by making it large, mutual inductance effects are avoided. Loose coupling to the ring is used so that the unloaded Q factor can be measured. The ring used here consists of a 50 ohm line having a mean circumference of 116.6 mm (measured at centre of line), this being approximately ten wavelengths at 10 GHz. The microstrip wavelength  $\lambda_m$  is given by  $\bar{c}/n$  where  $\bar{c}$  is the mean ring circumference and n is the harmonic number of the resonance. This number is established by noting the frequency of the resonance and hence  $\lambda_m$  can be plotted against frequency.

These measured resonances and associated microstrip wavelengths are shown in Figure 5.2 along with the non-dispersive wavelength from curves<sup>2</sup> ( $\lambda_o/\lambda_m = 2.6$  where  $\lambda_o$  is the free space wavelength). An increasing deviation from this curve is noted at higher frequencies being approximately 2.5% different at 10 GHz. This compares with 4% dispersion normally quoted<sup>7</sup> for a 50 ohm line on identical thickness alumina. The conclusion drawn from this measurement is that the Epsilam 10 material is no worse than alumina in this respect.

The measurement of the ring's Q factor allows a further estimate of the line's loss to be obtained. The Q factor of a length of lossy line is given by<sup>2</sup>,

$$Q = \frac{\beta l}{2 \tanh \alpha l} \quad (5.1)$$

Since  $\tanh \alpha l \sim \alpha l$  for  $\alpha l \ll 1$  then this equation can be reduced and rearranged to give  $\alpha = \pi/\lambda_m Q$  nepers/m. For the 6.79 GHz resonance a  $Q$  of  $136 \pm 14$  is observed resulting in loss of 1.36 nepers/m or  $11.8 \pm 1.2$  dB/m. This is virtually identical to the least squares fit value from Figure 5.1 and compares to a manufacturers value of 10.2 dB/m at 6.8 GHz. It is suspected though, that this value of loss is subject to further uncertainty since  $Q$  values of between 100 and 196 were observed at other resonant frequencies with no trend of a decrease with increasing frequency.

### 5.3 DEVICE SCATTERING PARAMETER AND GAIN COMPRESSION MEASUREMENTS

The jig used for device scattering parameter measurement and device mounting was discussed in Chapter 2. Figures 2.1 and 2.2 show the device mounting and microstrip layout respectively. Briefly, recalling the design of this jig, near identical mounting to that used by the device's manufacturer is employed, the lengths of microstrip between the device and transitions are kept to a minimum to reduce loss and the bias networks and d.c. breaks are included since device bias cannot be applied via the H.P. 8743A S parameter test unit used in this work.

In view of the narrow band nature of the amplifier design (*viz.*: Chapter 2, section 2.6, 10 to 20%) 8 to 12 GHz measurements are satisfactory. This is fortunate since outside of this band the presence of the bias network may be significant. The physical dimensions of the microstrip used for the bias network are as given in Table 5.1 below. Its topology is shown in Figures 2.2 and 2.20.

$Z_o$	100 $\Omega$	25 $\Omega$
$\omega$	0.15 mm	2.00 mm
$\ell(\lambda/4)$	3.00 mm	2.70 mm

Table 5.1 : Dimensions of the device's bias network for a 10 GHz centre frequency using 0.635 mm thickness Epsilam 10.

The results of two measured devices are given, both being from the same manufacturer's batch, Plessey number F1286 I/6. As discussed in Chapter 2, de-embedding has not been used because of the uncertainty of the calibrating terminations. The parameters are therefore as seen at the transitions with phase reference planes established at the end of the microstrip near the device. Though it is the off-biased device's parameters that are of most interest since they are unknown for an actual device, the on-biased device parameters as measured, are also given for comparison with the Plessey data<sup>9</sup>. These results are shown in Figures 5.3 to 5.6.

Consider first the off biased device's parameters ( $V_{GS} = -3v$ ). Of most importance is the device's transmission loss as given by  $|S_{21}|$  in Figure 5.5. This is at worst greater than -8 dB at 10 GHz. Comparing this with the measured gain when biased on ( $V_{GS} = 0v$ ) of 5 dB, an unmatched device on to off ratio of better than 13 dB is observed. Both devices seem to exhibit decreasing attenuation with rising frequency. Recall from Chapter 2, Figure 2.7, that the proposed pinched off model predicted a peak from 10 to 12 GHz. It is possible though, that if the measurement were extended to 14 GHz a peak would be visible. Considering further this model then the measurements indicate that  $C_f$  whose value strongly determines  $|S_{21}|$ , does in fact increase when  $V_{GS}$  is made

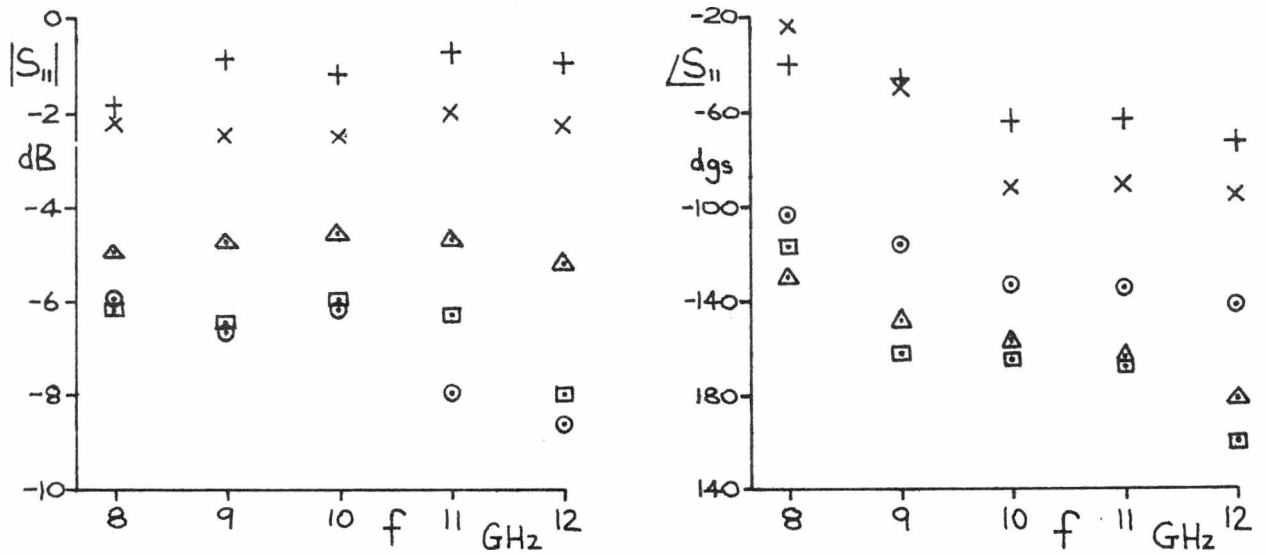


Figure 5.3 : The measured  $S_{11}$  of two devices.  $\square$ , device A biased on and  $\times$ , biased off.  $\circ$ , device B biased on and  $+$ , biased off.  $\Delta$ , Plessey data,  $I_{DS} = I_{DSS}$ .

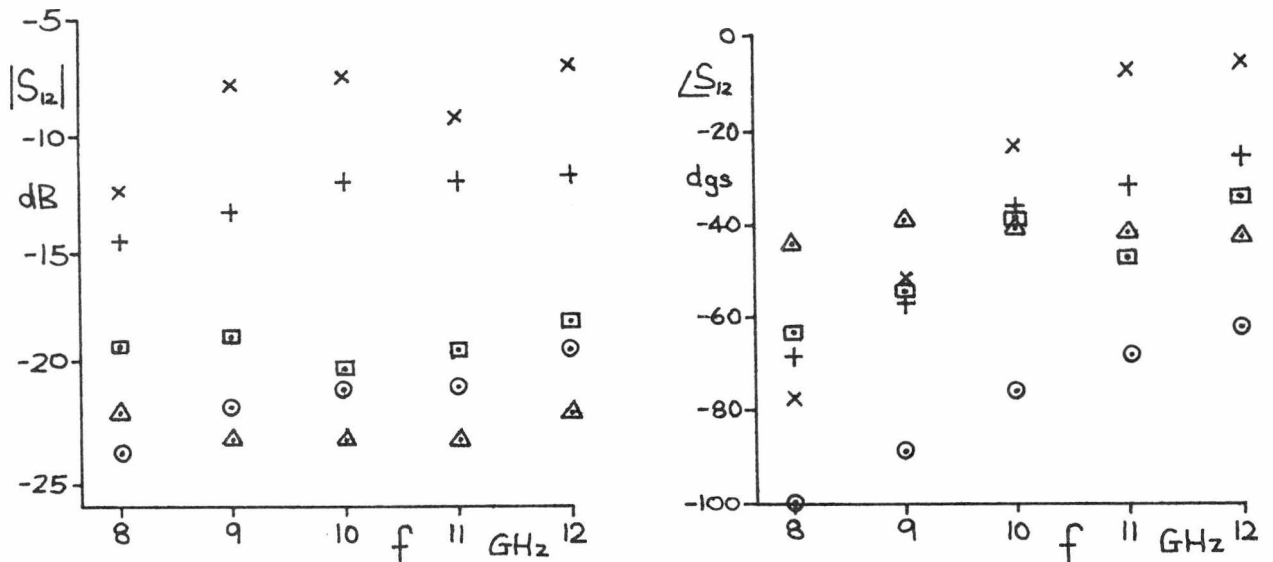


Figure 5.4 : The measured  $S_{12}$  of two devices.  $\square$ , device A biased on and  $\times$ , biased off.  $\circ$ , devices B biased on and  $+$ , biased off.  $\Delta$ , Plessey data,  $I_{DS} = I_{DSS}$ .

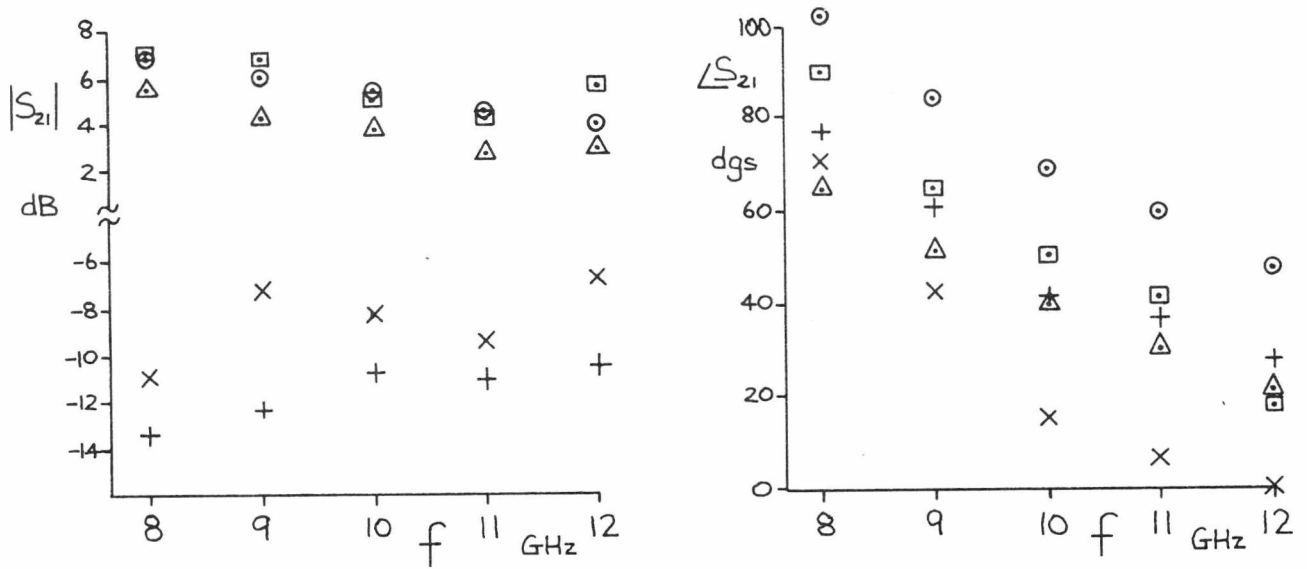


Figure 5.5 : The measured  $S_{21}$  of two devices.  $\square$ , device A biased on and  $\times$ , biased off.  $\circ$ , device B biased on and  $+$ , biased off.  $\Delta$ , Plessey data,  $I_{DS}=I_{DSS}$ .

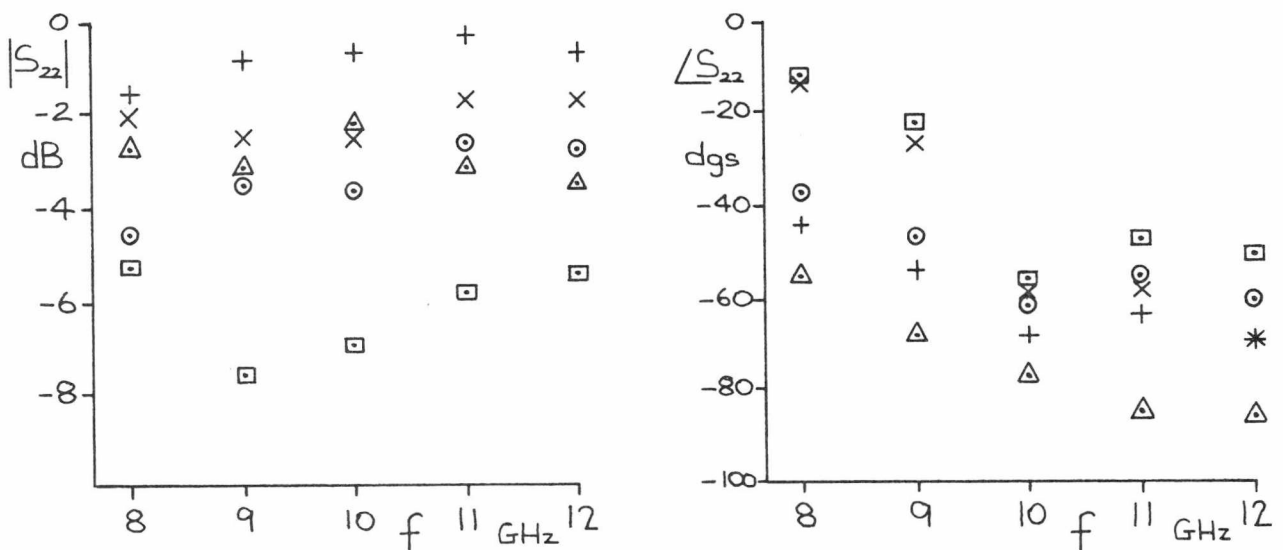


Figure 5.6 : The measured  $S_{22}$  of two devices.  $\square$ , device A biased on and  $\times$ , biased off.  $\circ$ , device B biased on and  $+$ , biased off.  $\Delta$ , Plessey data,  $I_{DS}=I_{DSS}$ .

negative. Doubling the on-biased model value to 0.056 pF has given a reasonable estimate of  $|S_{21}|$ . The argument of  $S_{21}$  shows some agreement, the model predicts a decrease of phase from about 35 degrees at 8 GHz to about 5 degrees at 12 GHz whereas the measurements show a greater variation of approximately 70 down to 10 degrees. The predicted reciprocal nature of the off biased device can be seen by the similarity between  $|S_{21}|$  and  $\angle S_{21}$  with  $|S_{12}|$  and  $\angle S_{12}$  as shown in Figures 5.5 and 5.4 respectively.

As expected, the device's off-biased reflection coefficients increase in magnitude compared to its on-biased values.  $|S_{11}|$  shown in Figure 5.3 displays a return loss of typical -1.5 to 2.0 dB, the on-biased being better than -4.5 dB. Similarly,  $|S_{22}|$  exhibits a return loss of typically -1.0 to -2.0 dB compared to an on-bias average value of about -3.0 dB. The argument of  $S_{11}$  changes by a considerable amount as would be expected by the large change in  $C_g$  effected by  $V_{GS}$  decreasing from 0 to -3v. An approximate change of 80 degrees is seen in Figure 5.3. A small change in the argument of  $S_{22}$  is displayed of less than 10 degrees. Hence,  $S_{11}$  changes by a large amount, 3 dB and 80 degrees from its on to off biased values whereas  $S_{22}$  change is small, 1.5 dB and 10 degrees.

If again, a comparison is made to the lumped element model, a similar change in  $\angle S_{11}$  and  $\angle S_{22}$  is seen with frequency through a 20 to 30 degree offset occurs between the measured and predicted parameters. For the magnitude of these two scattering parameters some disagreement is seen, more so with  $|S_{11}|$ , the model predicting a drop from -1.1 dB to -2.7 dB from 8 to 12 GHz whereas the measured devices are reasonably constant with frequency. One possible explanation for the decrease in the model's  $|S_{11}|$  is that just above 14 GHz the gate and source inductance ( $L_g$  and  $L_s$ ) and the gate capacitance ( $C_g$ ) plus possibly the feedback capacitance ( $C_f$ ) experiences a series resonance. This would

seem to be confirmed by the phase of  $S_{11}$  as it rises to 180 degrees somewhere above 14 GHz and the magnitude of  $S_{11}$  which will drop to an approximate value limited by the intrinsic gate resistance,  $R_i$  of  $S_{11} \approx 0.6$ . Why such an effect is not seen in the actual device is not fully understood at present, suffice to say, that measurements outside 8 to 12 GHz may reveal this effect or else the model is deficient in some way.

The differences in the measured and predicted values of  $|S_{22}|$  are more in terms of actual magnitude rather than change with frequency, though again, like  $|S_{11}|$  this discrepancy occurs. The model's value for the output return loss is -0.5 to -1.0 dB whereas -2.0 to -1.0 dB has been measured. Such differences are not serious and may be caused by substrate loss and transition mismatch.

The off biased device measurements can be briefly summarised as follows. A potential useful on to off ratio has been observed which will improve when the device is matched. The lumped element model's prediction of the important  $|S_{21}|$  parameter was reasonable and the measurements appear to confirm that the feedback capacitance is bias ( $V_{GS}$ ) dependent. The device reciprocity has been confirmed and near symmetry observed in an actual device.

Moving the discussion to the on-biased device measurements, then some general trends have been observed in these results. These trends are frequency independent, effects seen at 8 GHz are the same at 12 GHz, and are the same for both devices. Firstly, the measured  $S_{11}$  and  $S_{22}$  have smaller magnitudes than as given by the device manufacturer<sup>8</sup>. Secondly, the measured magnitudes of  $S_{21}$  and  $S_{12}$  are greater than as given by the manufacturer. Lastly, the measured and given scattering parameter arguments are comparable apart from slight phase offsets in some cases.

The drop in reflection coefficient could to some extent be explained

by the effect of microstrip losses. However, the increase in  $|S_{21}|$  and  $|S_{12}|$  is contrary to what would be expected if this were the cause. It appears that some unintentional device matching is occurring, reducing  $|S_{11}|$  and  $|S_{22}|$  and increasing  $|S_{21}|$ . It is possible that this might be happening since the lumped element model of the transition (see previous section 5.2) has an electrical structure that could effectively match the device noting also that the length of microstrip between these is about a half wavelength at 10 GHz. Hence, both the microstrip loss and the presence of the SMA transition may be introducing measurement errors especially in parameter magnitudes.

It is further suspected that the device's scattering parameters could be subject to a spread in values though these two devices from the same batch are similar to each other. These measured values are at the edge of the 20% tolerance quoted by the manufacturer and it is further suspected that the published data may be subject to a degree of manufacturer's conservatism in that they have described their device as being worse than it actually is. These effects could be resolved by performing some kind of de-embedding or measuring many devices from several batches to obtain some statistical confidence about their spread of parameters.

Shown in Figure 5.7 is the variation of  $|S_{21}|$  with gate to source voltage at the specific frequency of interest, 10 GHz. It can be seen that the greatest change occurs for  $V_{GS}$  between -1.0v and 2.4v. The same has been observed with the other three scattering parameters, both their magnitudes and angle. The slight variation from 0v to -1.0v indicates that the gain of a switch (amplifier) can be adjusted by about a dB for say phase shifter balance without a significant change in the device's match.

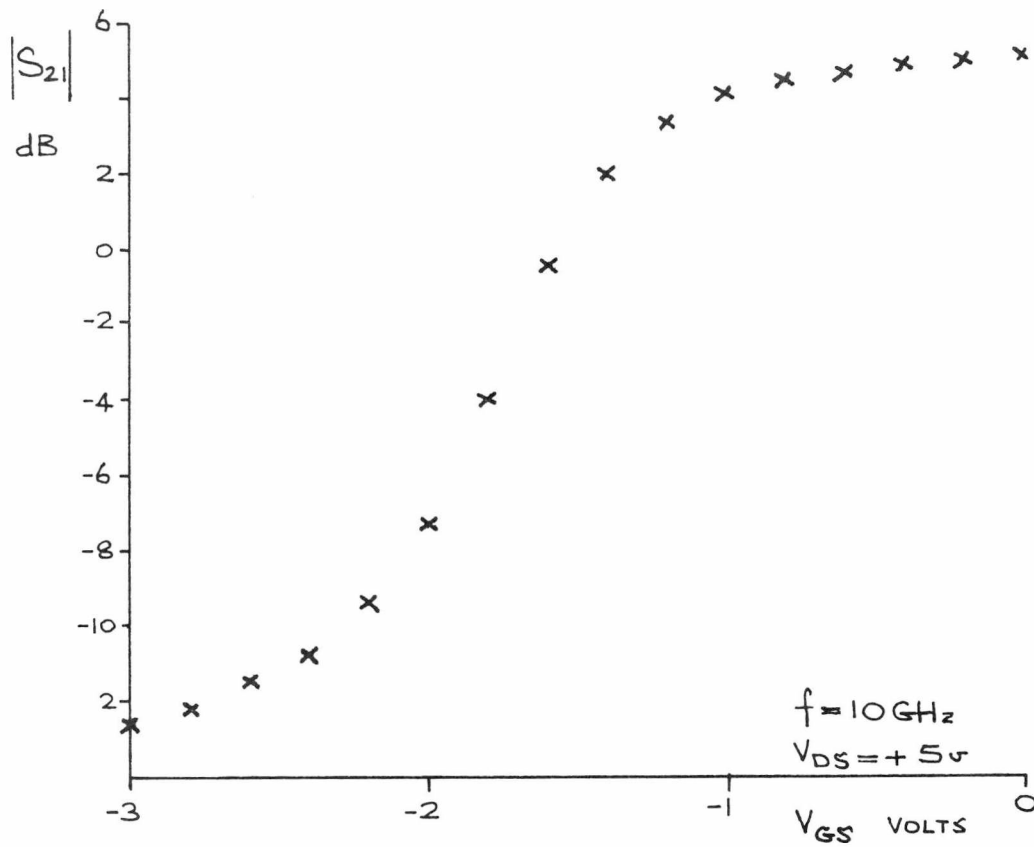


Figure 5.7 : Variation of device  $|S_{21}|$  with gate to source voltage. Output power is less than 0 dBm when  $V_{GS}=0\text{v}$ .

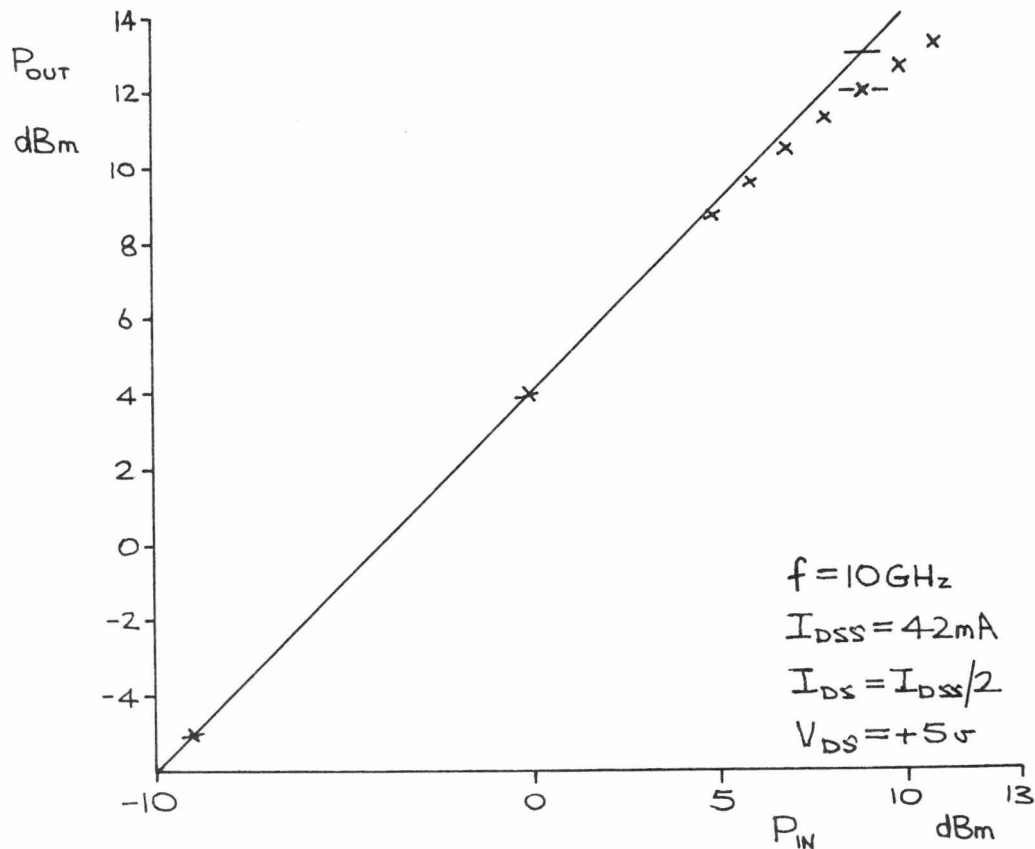


Figure 5.8 : Gain compression of unmatched device.

Figure 5.8 shows that the unmatched device has a 1 dB gain compression of 12 dBm output power at the maximum signal handling bias of  $I_{DS} = I_{DSS}/2$ . This is 1 dB less than the typical value quoted<sup>9</sup> by the manufacturer though they give no indication as to what device  $I_{DSS}$  this applies.

#### 5.4 AMPLIFIER PERFORMANCE (MESFET SWITCH)

The design of the MESFET amplifier that was used as the basis for a switch was discussed in Chapter 2, its electrical structure being shown in Figure 2.10. The actual width of the microstrip used for the quarter-wave transformers was made narrower than required (higher  $Z_q$ ) in case the actual device parameters are like those measured. If the parameters are in keeping with the Plessey data then the line width can easily be increased by use of conductive paint, which is shown in Figure 5.9.

Observation of this circuit's input and output return losses indicated that the addition of conductive paint was required to increase the line width to that of the original design. The added conductive paint gave widths that were comparable to that needed for the Plessey data and this leads to the conclusion that the device's parameters are in keeping with this data. The final responses were also achieved by adjusting the device's bias to obtain good gain and return losses. Note that two identical amplifiers were constructed side-by-side on the substrates. This allowed the testing of phase shifter ideas without the need to construct a complete circuit, dividers and phase shift networks being added on separate substrates. The amplifier responses presented here are for the best circuit of the pair.

Figure 5.10 shows the forward gain of the amplifier. A satisfactory

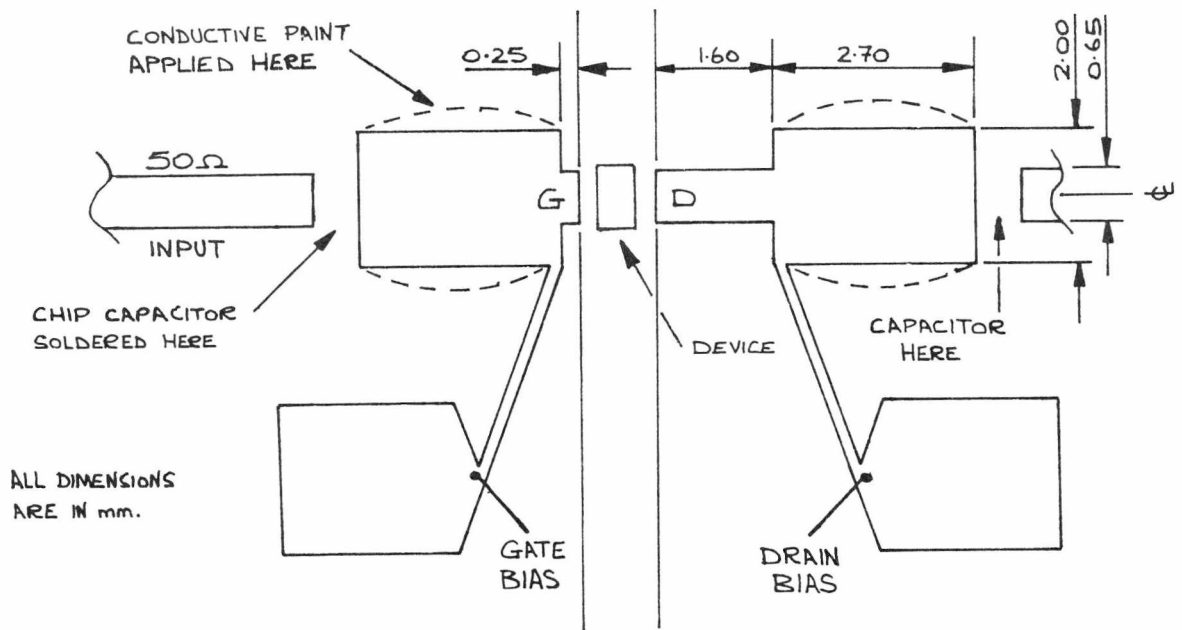


Figure 5.9 : Microstrip layout of MESFET amplifier that is used as a switch.

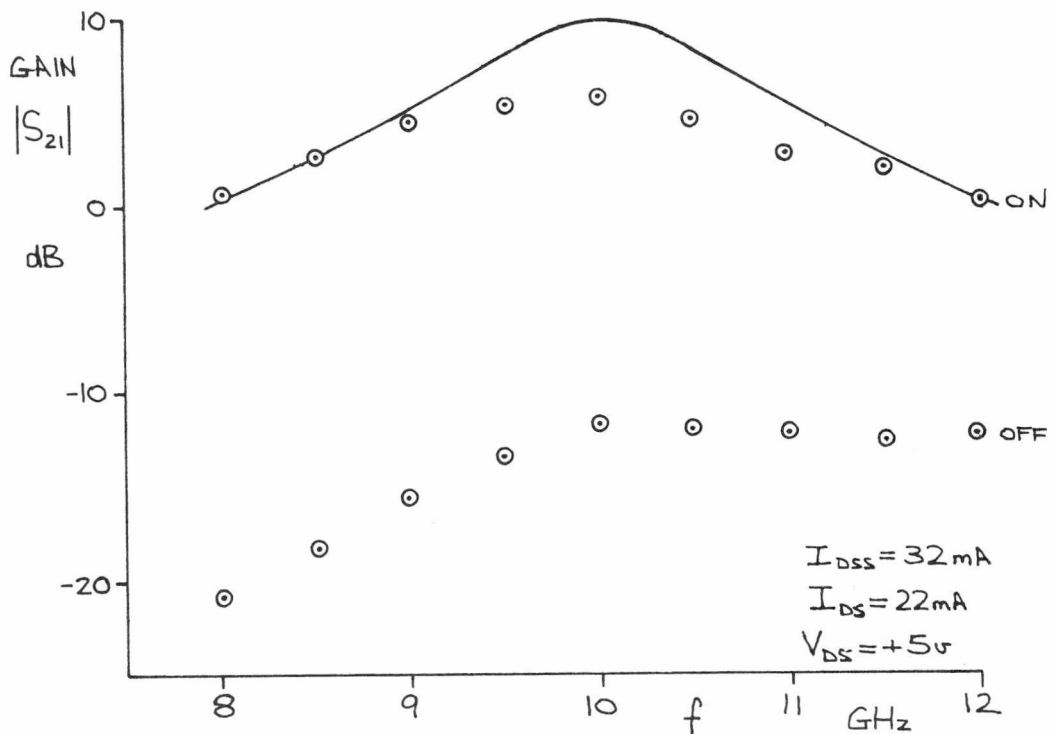


Figure 5.10 : Forward gain/loss of MESFET amplifier/switch. Continuous curve is for the predicted on biased state.

gain of 5.5 dB is observed at centre frequency of 10 GHz. This is less than the theoretical gain of 9.8 dB possibly because of losses in the microstrip and conductive paint and further loss caused by radiation at the wide microstrip discontinuities<sup>10</sup>. Radiation is known to be taking place since the presence of objects a few centimetres above the circuit disturbed it electrically. Also, adjusting the device's bias to a negative value would cause a slight reduction in gain (Figure 5.7). If the device is switched off an on to off ratio of 17 dB is measured. This is in agreement with that predicted by the Plessey data and device lumped element off biased model. Most useful is the increase in 3 dB bandwidth to 2.6 GHz. This is possibly caused by the damping effect of the losses.

The input and output return losses are shown in Figures 5.11 and 5.12. Both of these are satisfactory, the input being better <sup>than</sup> 9 dB over a 2 GHz band and the output, as expected is narrower. They are both broader than predicted, again probably because of damping effect of the matching circuit's losses. The switched-off amplifier's return losses are as expected, the input being highly reflective because of the large change in the MESFET device's  $S_{11}$  and the output return loss less so since there is only a small change in  $S_{22}$ .

Figure 5.13 shows that the matched device has an improved output power level for 1 dB gain compression. This is seen to occur at about 14.5 dBm, 2.5 dB improvement over the device itself. It appears from Figure 5.13 that the amplifier is tending to a saturated output power limit of just above 15 dBm.

In view of the satisfactory performance of this amplifier in terms of confirming the device's biased on parameters, measured gain, switch on to off ratio and bandwidth it was deemed not necessary to construct a discrete two-way MESFET switch. The theoretical designs for these circuits should give reasonably predictable behaviour when integrated

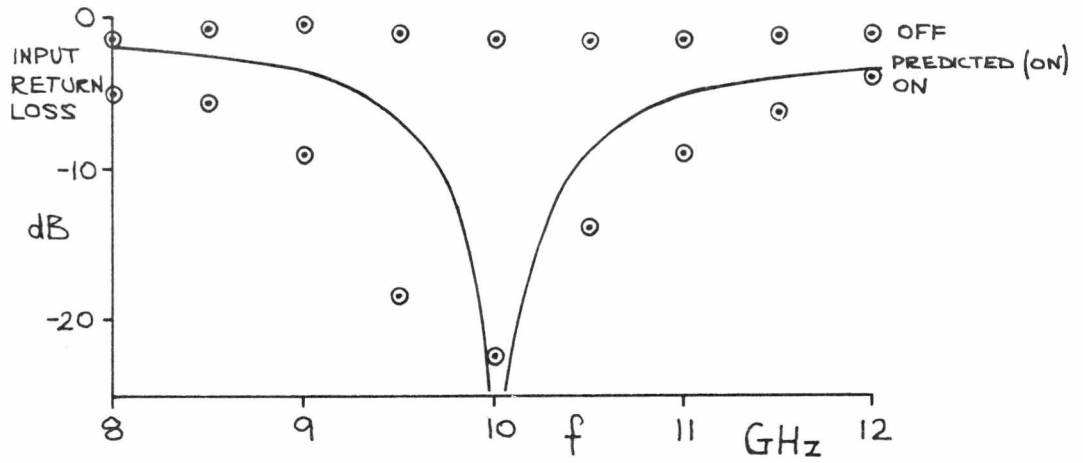


Figure 5.11 : Input return loss of MESFET amplifier/switch.

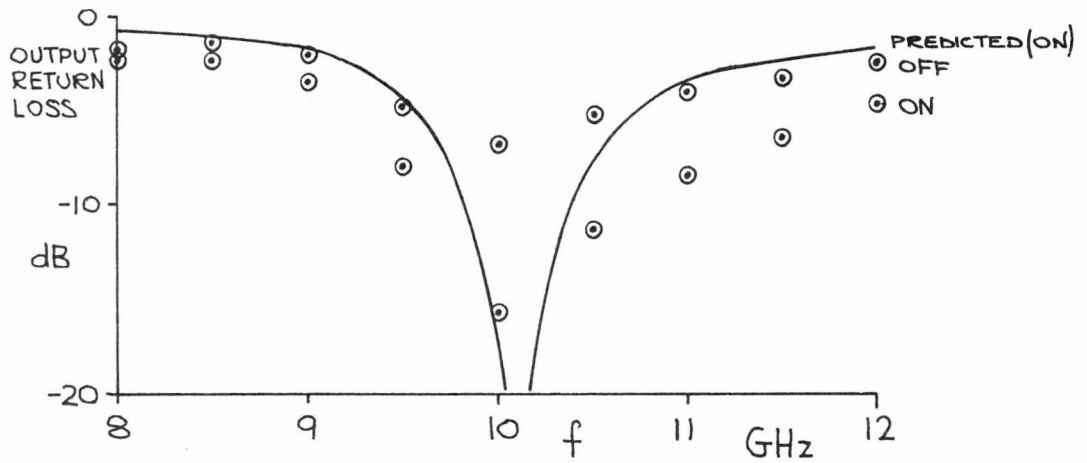


Figure 5.12 : Output return loss of MESFET amplifier/switch.

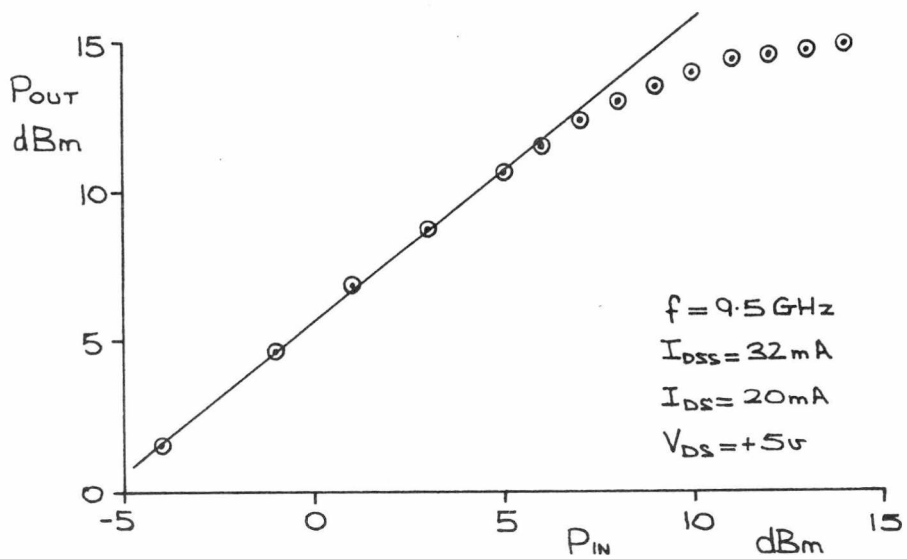


Figure 5.13 : Gain compression of MESFET amplifier/switch.

into complete phase shifter circuits.

### 5.5 TRANSMISSION BANDWIDTH OF POWER DIVIDERS WITH A MISMATCHED OUTPUT

In section 4.3 of Chapter 4 it was shown that the mismatch from the off biased device will impose a bandwidth constraint on a phase shifter circuit. This is dependent on the length of line between the device and the input divider's junction. Also it was indicated that the uncompensated Wilkinson divider may have a slight bandwidth advantage over the tee in this respect. To test this each of these dividers was constructed on microstrip, the Wilkinson's 70.7 ohm lines being a quarter-wave at 10 GHz. One output port of each divider was terminated with a SMA short circuit at its transition.

The transmission  $|T|$  to the second output and the input return loss  $|R|$  were measured with the network analyser and are shown in Figures 5.14 and 5.15 for the tee and Wilkinson respectively. For a short circuit termination ( $|\rho| = 1$ ) the maxima of Figure 5.14 should be at 0 dB but these are observed to be less because of line loss and transition effects, the maxima of  $|R|$  being slightly less than  $|T|$  since the reflection has to travel further. The same applies to the Wilkinson noting that its maxima for  $|T|$  have a theoretical value of -0.5 dB for  $|\rho| = 1$ .

The length of line between the short circuit and the divider's junction can be determined from the frequency spacing of the transmission minima. This for the tee (Figure 5.14) is 3.26 wavelengths at 10 GHz. Evaluating the bandwidth with this value using equation (4.5) gives 1.08 GHz. The observed 3 dB bandwidth of the four transmission maxima in Figure 5.14 are 1.15, 1.15, 0.98 and 0.95 GHz giving an average value of 1.06 GHz, a very reasonable agreement with the theory. This spread of values is thought to be possibly caused by the transitions and their

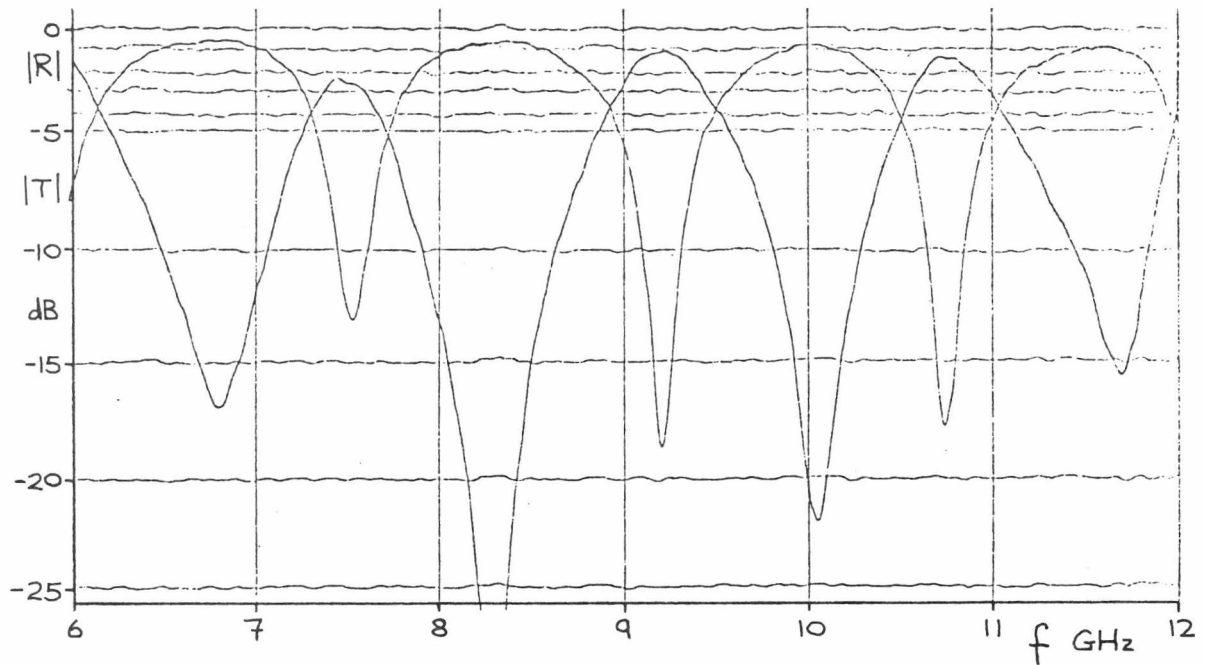


Figure 5.14 : Transmission  $|T|$  (insertion loss) and input return loss  $|R|$  of a tee divider with its second output mismatched with a termination having  $|\rho|=1$ .

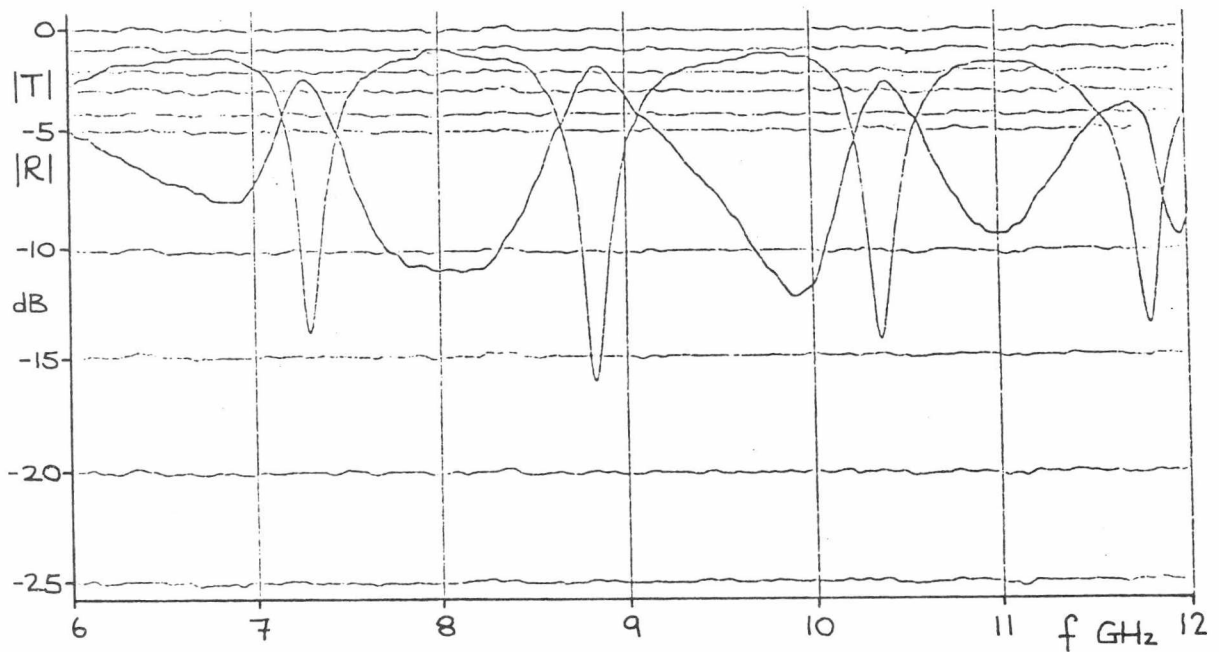


Figure 5.15 : Transmission  $|T|$  (insertion loss) and input return loss  $|R|$  of an uncompensated Wilkinson divider with its second output mismatched with a termination having  $|\rho|=1$ .

equivalent model. The mismatch reflection has to traverse one of these twice before returning to the junction. This is thought to result in slight shifts in the position of the various minima. The above value of wavelength is also subject to this uncertainty since it is calculated from the frequency of one minimum only (9.2 GHz).

Considering Figure 5.15 and the behaviour of the uncompensated Wilkinson, it can be seen that the transmission maxima are slightly broader. These have values of 3 dB bandwidth 1.15, 1.14 and 1.025 GHz giving an average of 1.105 GHz. This value should not be compared directly with the tee's average bandwidth since the length of line associated with the Wilkinson is longer, 3.4 wavelengths. However, one or other bandwidth can be adjusted by the ratio of these lengths so that a direct comparison can be made. Adjusting the Wilkinson gives 1.15 GHz and this compares with a value of 1.06 GHz for the tee, an 8.5% improvement. A figure of 13% was suggested in Chapter 4 though this was not definite since the frequency dependent behaviour of the Wilkinson had not been taken into account when arriving at this value. If the bandwidth is defined at either the -1 or -0.5 dB points the advantage of the Wilkinson would become more apparent because of the flat topped nature of its transmission maxima.

#### 5.6 THE DISPERSIVE PHASE SHIFT NETWORKS

Two types of dispersive phase shift network have been used to give a differential phase shift that is more constant with frequency than that of a half wavelength line. These were discussed in Chapter 3 and are the Schiffman coupled lines and a bandpass circuit consisting of shunt stubs. Prior to the construction of a complete phase shifter circuit each of these networks was fabricated to demonstrate their phase

shifting ability.

Consider first the Schiffman network. As discussed in Chapter 3, section 3.8, two cascade networks having a stepped design are about optimum for this application. Fortunately, a design that can be used here has been given by Schiek and Köhler<sup>11</sup>. Their design was on 0.51 mm thick alumina for a 6 GHz centre frequency. Line width and spacing need to be scaled for the Epsilam 10's thickness of 0.635 mm and likewise line lengths reduced for the increase in frequency. The change in dielectric constant from 9.7 (alumina) to 10.2 (Epsilam 10) is small and is hence neglected.

The topology of this cascade pair is shown in Figure 5.16. Also shown is the one and a half wavelength reference line and a tee divider. This circuit will form the input side of a phase shifter (discussed in Chapter 6) up to the two-way MESFET switches input matching circuitry and includes the length of mismatch phase compensating line. The dimensions given in Figure 5.16 are for the microstrip photographic mask. Etching undercut is known to take place at each conductor edge up to about half the copper metallisation thickness. For 1 ounce copper clad substrate the metallisation thickness is about 0.04 mm. An allowance has been made for this in the given dimensions.

The required gap width is 0.069 mm in the narrow region of the coupled lines and 0.062 mm in the wide. The photographic process used for this work sets a limit to the minimum mask line width of 0.05 mm. If the undercutting is added to this, a width in excess of the desired is obtained. However, observation of the etching in a narrow gap between microstrip has shown that the undercutting is very much reduced. A final width of between 0.06 and 0.07 mm is therefore expected.

The circuit's behaviour that is of most interest is the transmission to one or other outputs whilst the second is terminated in a mismatch.

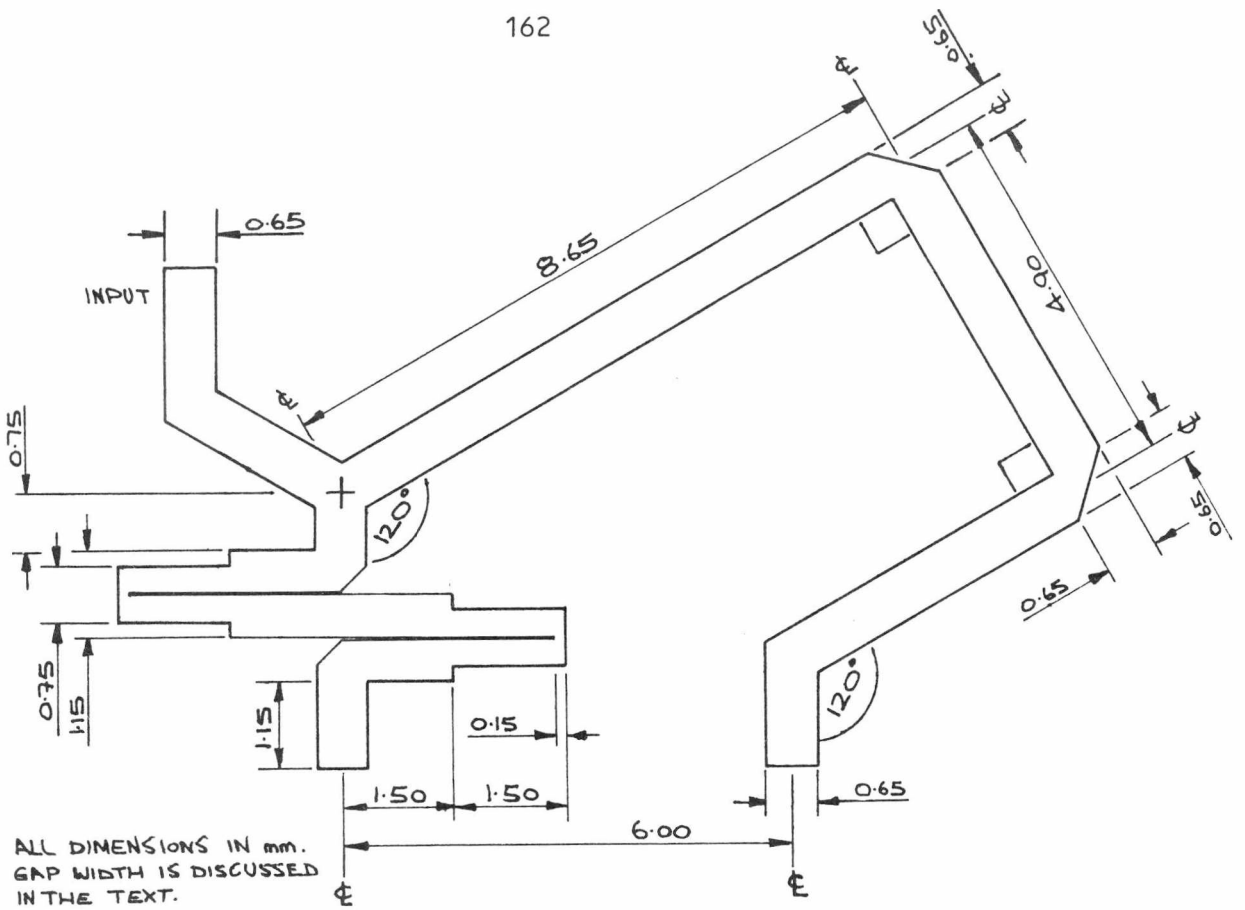


Figure 5.16 : Microstrip layout of a 180 degree differential phase shift network using a cascaded pair of Schiffman coupled lines.

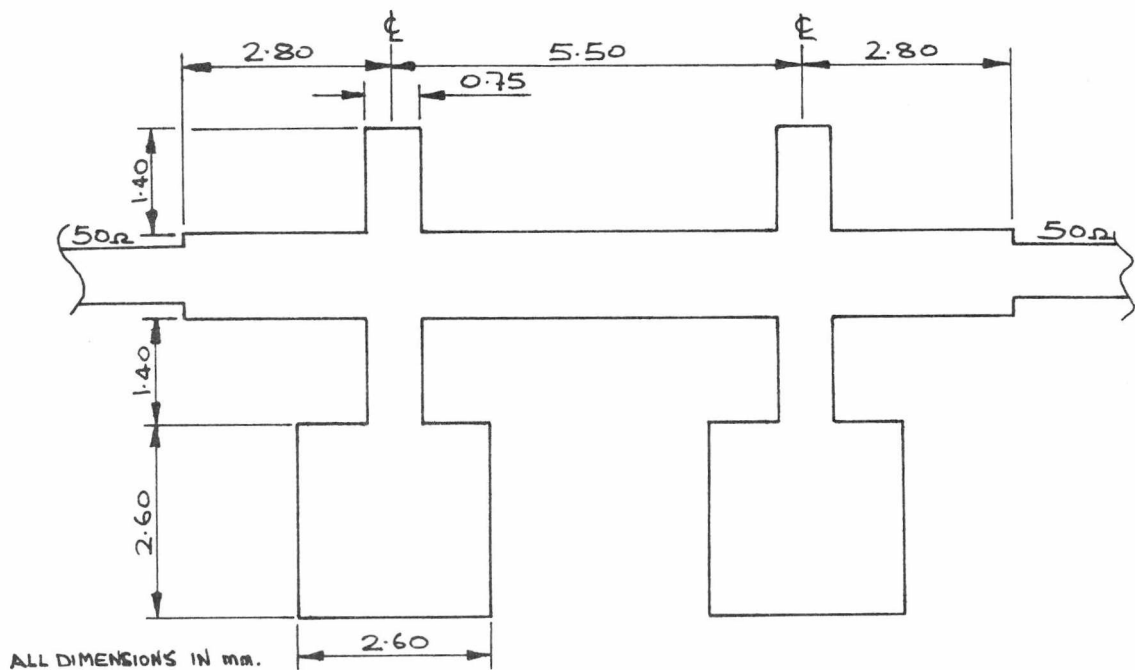


Figure 5.17 : Microstrip layout of a cascaded pair of stub type phase shift networks.

These magnitudes and arguments are shown in Figures 5.18 and 5.19. The dips in the transmission magnitude are caused by the mismatch returning with a phase equal to that of a short circuit (argument of 180 degrees). The observed 3 dB bandwidth of the reference line's transmission magnitude response is 1.99 GHz and from equation (4.5) gives a line length of 20.5 mm between the mismatch and divider's junction. Physically, this length is 22.5 mm when a path is taken at the centre of the microstrip width. The transmission along the reference line appears to be taking the shortest possible path at the corners caused by the equivalent capacitive discontinuity<sup>12</sup> at these points. This line shortening or phase advance effect can also be seen from the phase error in Figure 5.19. This is between 9 and 25 degrees from 9 to 10.5 GHz, the 2 mm length difference gives 16 degrees error at 10 GHz.

The response of the Schiffman network's transmission magnitude though adequate over 1 GHz is poorer than expected, its 3 dB bandwidth being only 75% of that of the reference line. In view of its shorter electrical (and physical) length a broader bandwidth would be expected. A possible explanation can be found by observing this network's three input return losses as shown in Figure 5.20. This is measured with 50 ohm terminations on both outputs and with the tee divider should result in a steady return loss of -9.5 dB. As can be seen this is far from the case. Though it is difficult to conclude anything definite from this it is suspected that the Schiffman behaviour in respect of return loss is far from good. The tee and reference line are known to be well behaved and hence the Schiffman pair, because of their complex structure, are at fault.

The poor performance of the Schiffman's is thought to be a result of the difficulty in being able to control accurately the gap between the pair of lines. Further, the finite metallisation thickness has not

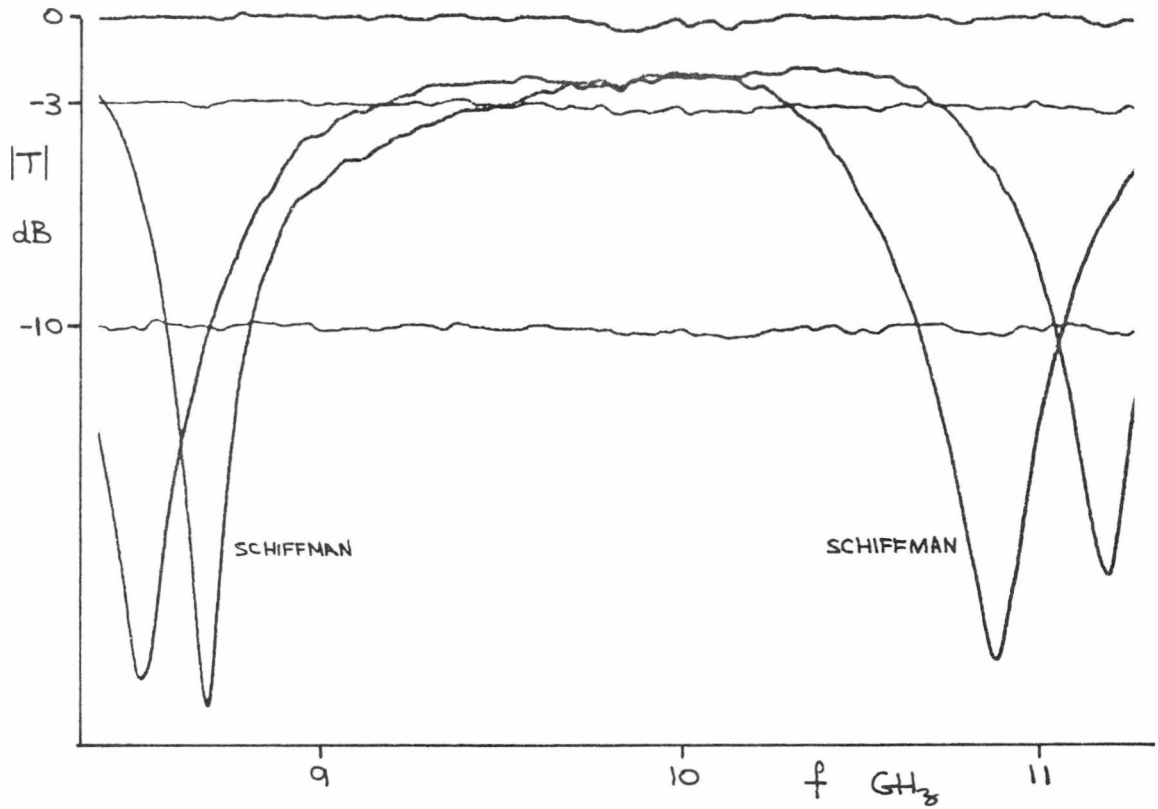


Figure 5.18 : Transmission  $|T|$  (insertion loss) from tee input to Schiffman and reference line outputs. Second output is match terminated ( $|\rho|=1$ ) during measurement.

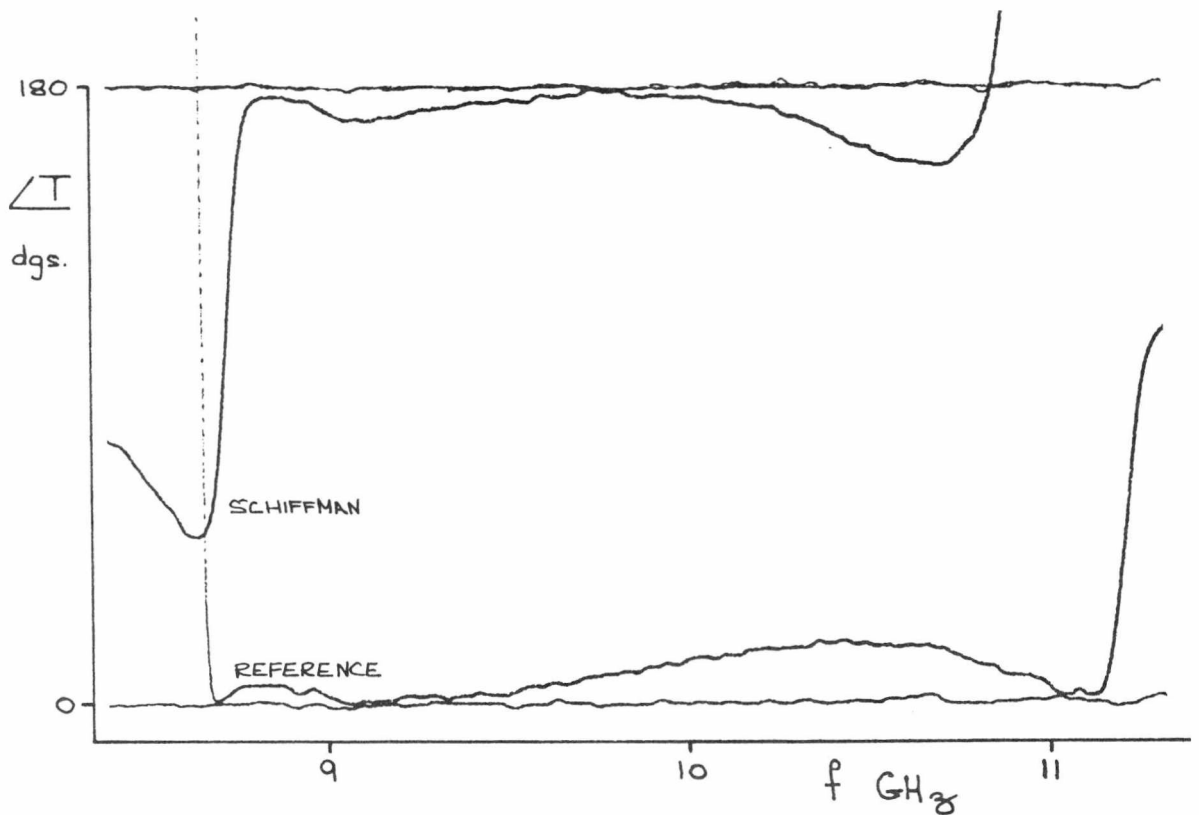


Figure 5.19 : Transmission phases associated with the outputs shown in Figure 5.18 above.

been taken into account and possibly causes a lowering of the odd mode impedance. Solutions to this are to use a better photographic process (greater original mask enlargement, present process uses a 10 times reduction) and a substrate with thin metallisation such as alumina. This though would incur the complex processing requirements of alumina. An alternative solution is to use a circuit that does not require accurately fabricated narrow gaps between microstrip.

One possible alternative is the band pass circuit consisting of shunt stubs that was discussed in Chapter 3, section 3.9. Though this circuit avoids the gap difficulty it is not without an attendant problem. At the frequencies used in this work the 30.7 ohm lines required for optimum performance need a width that is becoming a significant fraction of a wavelength and would give rise to microstrip tee junction discontinuity effects. To avoid this, section 3.9 demonstrated that the line impedances could be raised and also that the stub and main line impedances need not be equal. The consequences of changing these two impedances is shown in Figures 3.12 to 3.15.

The topology of a cascade pair of stub networks is shown in Figure 5.17. The main line impedance  $Z_0$  is 35 ohms and the stub impedances  $Z_s$  are 45 ohm. The short circuit stub termination is formed by a low impedance (15 ohm) open circuit quarter-wave stub as seen in Figure 5.17. This gives adequate performance about the centre frequency, causing a serious degradation at only the octave band edges.

After adjusting the reference lines length to give 180 degrees phase difference at the 10 GHz centre frequency, the network and reference line exhibited a differential phase of -172 and 170 degrees at 9 and 11 GHz respectively. This is slightly in excess of the predicted phase error of 6 degrees at these frequencies. The network's input return loss is better than -9.5 dB and its insertion loss (transmission) is approxi-

mately -1 dB from 9 to 11 GHz.

This network though being an improvement over the Schiffman is far from good. Despite its complexity, the phase error displayed is only half that of a half wavelength delay line. It is thought that discontinuity effects at the junction of the stubs and main line are still significant. This effect could be reduced by use of a substrate with a lower dielectric constant so causing a lengthening of the microstrip's wavelength. This would result in a greater area of circuit which at present is spread due to the stubs and reference lines length. The deficiency of both the stub and the Schiffman networks for the application in this work lead to the pursuit of the third method investigated as a means of producing a phase difference, the slotline-type power divider. Both networks have, however, been used to develop the single gate MESFET phase shifter concept, the performance of these will be discussed in the following chapter.

#### 5.7 PERFORMANCE OF SLOTLINE-TYPE POWER DIVIDER

The phase splitting slotline to microstrip coupling and the electrical structure of this power divider were introduced in Chapter 3, section 3.11; its circuit being shown in Figure 3.18. Its physical structure and performance will now be discussed.

The divider's microstrip and slotline topology is shown in Figure 5.21. The dimensions for the slotline were obtained from the curves of Mariani et. al.<sup>13</sup>. The slotline coupling line is made a quarter wavelength long between the microstrip centre lines at the 10 GHz centre frequency. No reference is known at present for the exact phase reference planes of the microstrip to slotline coupling. This is, therefore, assumed to be at the centre of both the slot and microstrip.

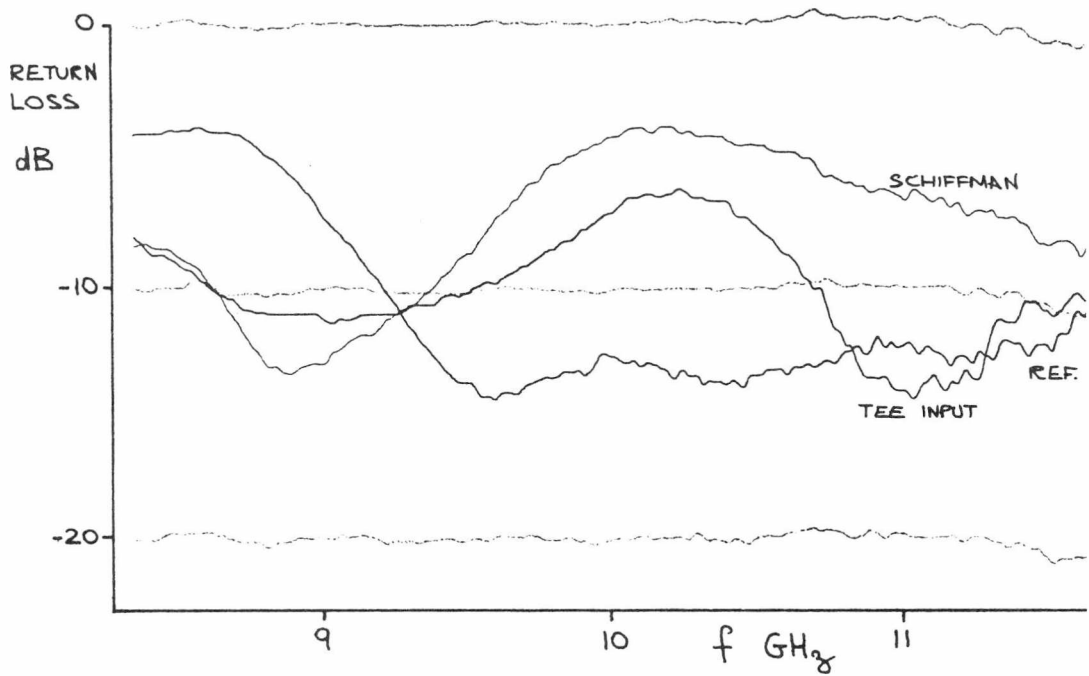


Figure 5.20 : Input return losses of Schiffman phase shift network (with tee divider and reference line). All outputs are matched during measurement.

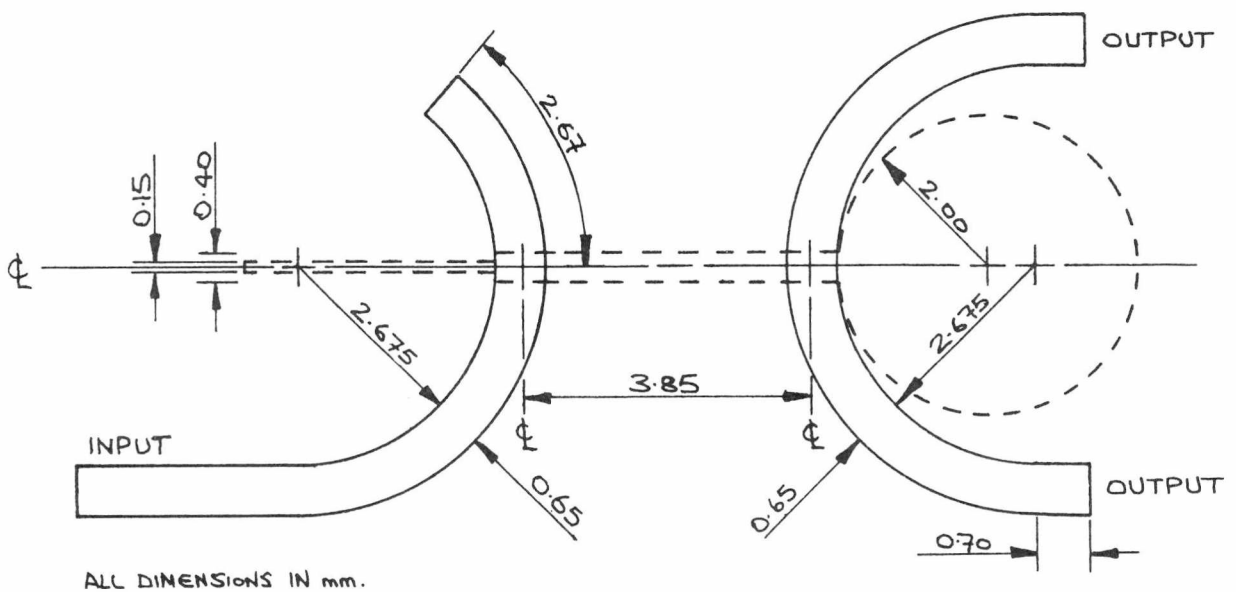


Figure 5.21 : Microstrip and slotline (broken lines) geometry of the slotline type power divider.

The two stubs, the microstrip open circuited and the slotline short circuited, have been corrected for their respective end effects by shortening their lengths. Their lengths are given by<sup>14</sup>:

$$\left. \begin{aligned} \ell_{SL} &= \frac{\lambda_{SL}}{2\pi} \tan^{-1} \left( \frac{Z_{SL}}{2\pi f L_{SC}} \right) \\ \ell_{MS} &= \frac{\lambda_{MS}}{2\pi} \tan^{-1} \left( \frac{1}{2\pi f Z_{MS} C_{OC}} \right) \end{aligned} \right\} \quad (5.2)$$

where  $f$  is the 10 GHz centre frequency,  $\lambda_{SL}$  the slotline wavelength with associated impedance  $Z_{SL}$  and inductive end effect  $L_{SC}$  and  $\lambda_{MS}$  is the microstrip's wavelength with associated impedance  $Z_{MS}$  and capacitive end effect  $C_{OC}$ .  $L_{SC}$  is obtained from the curves of Knorr and Saenz<sup>15</sup> and is about 0.05 nH for the 50 ohm slotline stub and  $C_{OC}$  according to Silvester and Benedek<sup>16</sup> is 0.034 pF. The circular structure is a slotline open circuit.

It will be noted that the metallisation thickness ( $t = 0.038$  mm) is significant when compared to the slot's width ( $\omega$ ). For the 96 ohm line the  $t/\omega$  ratio is 0.1 and that for the 50 ohm line is 0.25. Data given by Kitasawa et. al.<sup>17</sup> indicates that for  $t/\omega = 0.1$  a 6.7% reduction in the slotline's impedance and a 3.4% decrease in its  $\sqrt{\epsilon_{eff}}$  is obtained. The 96 ohm line's impedance ( $Z_{SL}$ ) should therefore be increased to 103 ohms. If the line's width is increased from 0.4 to 0.48 mm to give this impedance the slot's  $\sqrt{\epsilon_{eff}}$  decreases from 1.953 to 1.923 (1.5%). This combined decrease in  $\sqrt{\epsilon_{eff}}$  gives rise to an increase in the value of  $N$ , the effective coupling transformer's ratio from 0.86 to 0.873 (from Knorr's equations<sup>18</sup>). This increase in  $N$  requires a reduction in  $Z_{SL}$  which, using equation (3.48), is now 92.7 ohms lower than the original impedance. It is, therefore, concluded that the

effects of the finite metallisation for this section of slotline will probably cancel and hence the slot's width is not changed from its original design value of 0.4 mm for a 96 ohm line with  $t/w = 0$ .

The required slot width according to Mariani's curves is 0.035 mm for the 50 ohm stub. This is very impractical when using the Epsilam 10 material. Keeping in mind the problems experienced when trying to construct narrow gaps for the Schiffmans, an actual slot width of 0.15 mm is used. This has an impedance of 70 ohms and a  $t/w$  ratio of 0.25. The exact reduction in this impedance is not known since Kitasawa's data ranges only from  $t/w = 0$  to 0.1. However, it appears that the relationship is nearly linear and hence a reduction in impedance of 17% can be inferred giving 58 ohms. The final etched slot width is observed to be about 0.12 mm and so it is suspected that the stub's impedance is near the required 50 ohms. It is worth noting that an increase in impedance here causes a broadening of the divider's bandwidth with the consequent degradation of in-band return loss.

Figure 5.22 shows the measured input return loss of this circuit. This, though worse than the model predicts, is typically -20 dB in the 9 to 11 GHz band of interest and is satisfactory for this work. There are many elements in this circuit that could cause this discrepancy. Those so far discussed are the uncertainty in the coupling phase reference planes and the slot's impedance and line wavelength. Also the step between the two slot widths may be causing discontinuity effects and similarly the slotline open circuit may have an associated capacitance.

The power division and phase split error are shown in Figures 5.23 and 5.24 respectively. The amplitude imbalance is less than 0.4 dB from 6 to 11.3 GHz. This is thought to be caused by the effect of the transition discontinuity. Direct coupling between the micro-

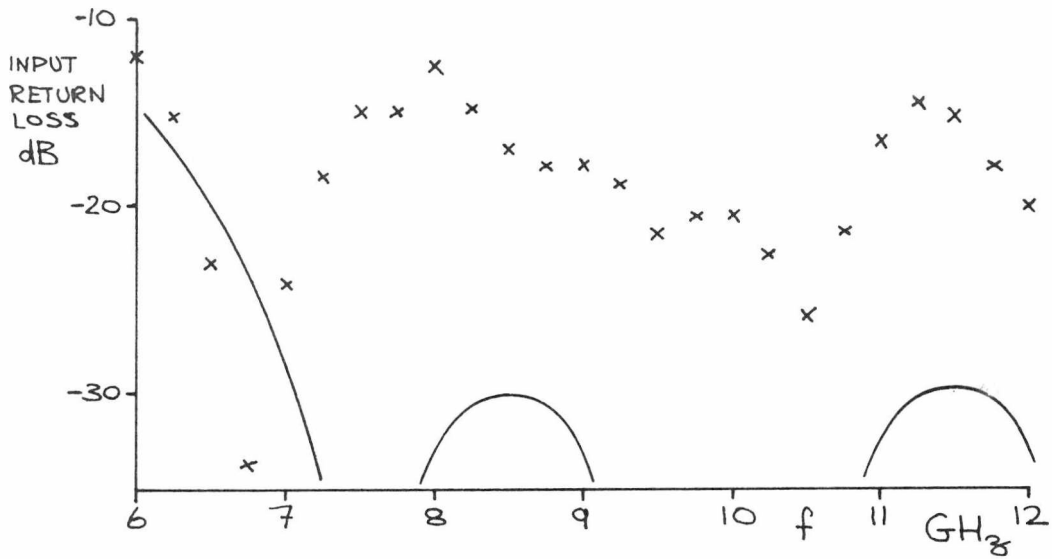


Figure 5.22 : Input return loss of slotline type power divider.  
Both outputs are matched during measurement.  
Continuous curves are the predicted response.

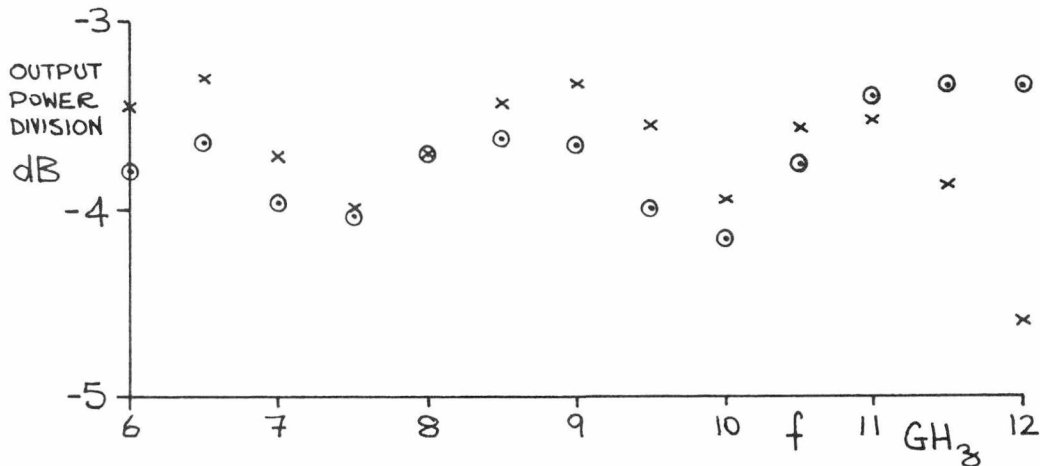


Figure 5.23 : Output power division (both outputs) of slotline type power divider.

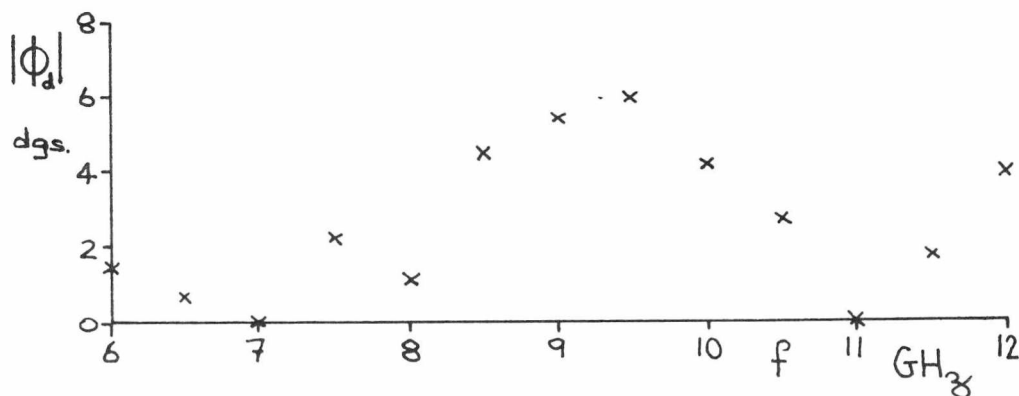


Figure 5.24 : Phase deviation from 180 degrees split observed at the outputs of the slotline type power divider.

strips has been measured as being below -26 dB and can be accounted for by coupled line theory. This contributes only a small amount to the 0.4 dB amplitude imbalance.

These measurements were performed on a circuit centred in a **25.4mm** square substrate. The total length of microstrip between the input and an output port is about 2.5 cms and causes most of the 0.5 dB excess insertion loss that is observed. The peak in the phase error (deviation from 180 degrees phase split) at 9.5 GHz corresponds to a peak in the amplitude imbalance and is most likely caused by the transition problem also. In an integrated phase shifter circuit the output transitions would not be present and hence the divider's performance may be better in this situation. Further device bias adjustment would allow for the amplitude error to be balanced out. These imperfections apart, the broad band nature of this divider can be seen. It displays less than 6 degrees phase error over the observed octave and a satisfactory return loss and power split also.

Since the output dividing junction is also the physical output of the divider, only lengths of switch mismatch phase compensating lines are required between it and the switch's inputs. This implies a broader bandwidth for a slotline type phase shifter than one using the dispersive type phase shift networks with their long reference lines.

### 5.8 Conclusion

The ability of the single gate MESFET device to perform microwave switching as a matched amplifier has been demonstrated. A gain of about 5.5 dB has been observed with an on to off ratio of 17 dB. The highly mismatched off biased state was confirmed. Though narrow band matching has been used for the amplifier's design, a 3 dB bandwidth of

2.6 GHz centred about 10 GHz is seen. Despite obtaining this performance by circuit trimming, the adjustment necessary gave weight to the idea that the device's parameters are similar to the manufacturer's data.

Problems in the construction of narrow gaps between microstrip lines was displayed in the poor performance measured of the Schiffman phase shift network. The move to using the stub network was an improvement though its performance was not good. The design and understanding of slotline and its coupling nature with microstrip was rewarded by the good performance of a constructed phase splitting divider. This is satisfactory over an octave which is more than adequate for this work.

5.9 REFERENCES

- 1 Hewlett Packard Measurement/Computation Instrument Catalogue, 1983, pp. 450-453.
- 2 R.J. Collier, Lecture Notes on Microstrip Circuits, University of Kent, October 1981.
- 3 COMPACT CAD Program, Compact Engineering Inc., USA, Routine TRLINES.
- 4 I.J. Bahl and D.K. Trivedi, A Designer's Guide to Microstrip Design, Microwaves, May 1977, pp. 174-182.
- 5 Epsilam 10 Data Sheet, 3M Company.
- 6 V. Buontempo, Equivalent Circuit of Coaxial (APC-7) to Microstrip Transition, Electronics Letters, Vol. 11, 15 May 1975, pp. 220-222.
- 7 J.S. Wight, O.P. Jain, W.J. Chudobiak and V. Makios, Equivalent Circuits of Microstrip Impedance Discontinuities and Launchers, IEEE Trans. MTT22, January 1974, pp. 48-52.
- 8 P. Troughton, Measurement Techniques in Microstrip, Electronics Letters, Vol. 5, 23 January 1969, pp. 25-26.
- 9 Plessey GAT4 Data Sheet, Publication No. P51872, Issue 2-1177.
- 10 A.G. Derneryd, Linearly Polarized Microstrip Antennas, IEEE Trans. MTT24, November 1976, pp. 846-851.
- 11 B. Schiek and J. Köhler, A Method for Broad Band Matching of Microstrip Differential Phase Shifters, IEEE Trans. MTT25, August 1977, pp. 666-671.
- 12 H.M. Altschuler and A.A. Oliner, Discontinuities in the Centre Conductor of Symmetric Strip Transmission Line, IRE Trans. MTT8, May 1960, pp. 328-339.

- 13 E.A. Mariani, C.P. Heinzman, J.P. Agrios and S.B. Cohn, Slotline Characteristics, IEEE Trans. MTT17, December 1969, pp. 1091-1096.
- 14 A. Podcameni and M.L. Coimbra, Slotline Microstrip Transition on Iso/Anisotropic Substrate: A More Accurate Design, Electronics Letters, Vol. 16, 25 September 1980, pp. 780-781.
- 15 J.B. Knorr and J. Saenz, End Effect in a Shorted Slot, IEEE Trans. MTT21, September 1973, pp. 579-580.
- 16 P. Silvester and P. Benedek, Equivalent Capacitance of Microstrip Open Circuits, IEEE Trans. MTT20, August 1972, pp. 511-516.
- 17 T. Kitasawa, Y. Hayashi and M. Suzuki, Analysis of the Dispersion Characteristic of Slotline with Thick Metal Coating, IEEE Trans. MTT28, April 1980, pp. 387-392.
- 18 J.B. Knorr, Slotline Transitions, IEEE Trans. MTT22, May 1974, pp. 548-553.

CHAPTER 6RESULTS OF THE COMPLETE PHASE SHIFTER MEASUREMENTS6.1 INTRODUCTION

So far it has been demonstrated that the single-gate MESFET device is capable of performing microwave switching whilst giving an insertion gain when it is in its on state. The object of this research is also to develop a digital phase shifter that utilises these devices and possesses an overall insertion gain itself. In Chapter 4 it was demonstrated, in theory, that provided the switch's off state mismatch was taken into consideration, a 0/180 degree phase shifter could be constructed that required only two MESFET devices.

The necessary 180 degree phase shift circuits for use with the switches have been investigated and one in particular, the slotline-type power divider promised a very good phase shifter performance. The network measurements on this type of phase shifter and those using the Schiffman and stub network will now be presented. The results of switching speed measurement, and power handling performed on the former circuit, will also be given.

6.2 A PHASE SHIFTER USING THE SCHIFFMAN NETWORK

This phase shifter consists of the 180 degree differential phase shift network shown in Figure 5.16 and the two-way MESFET switch of Figure 6.1. The design of this switch was given in Chapter 2, section 2.7.2. The inputs to the two-way switch are separated from the phase

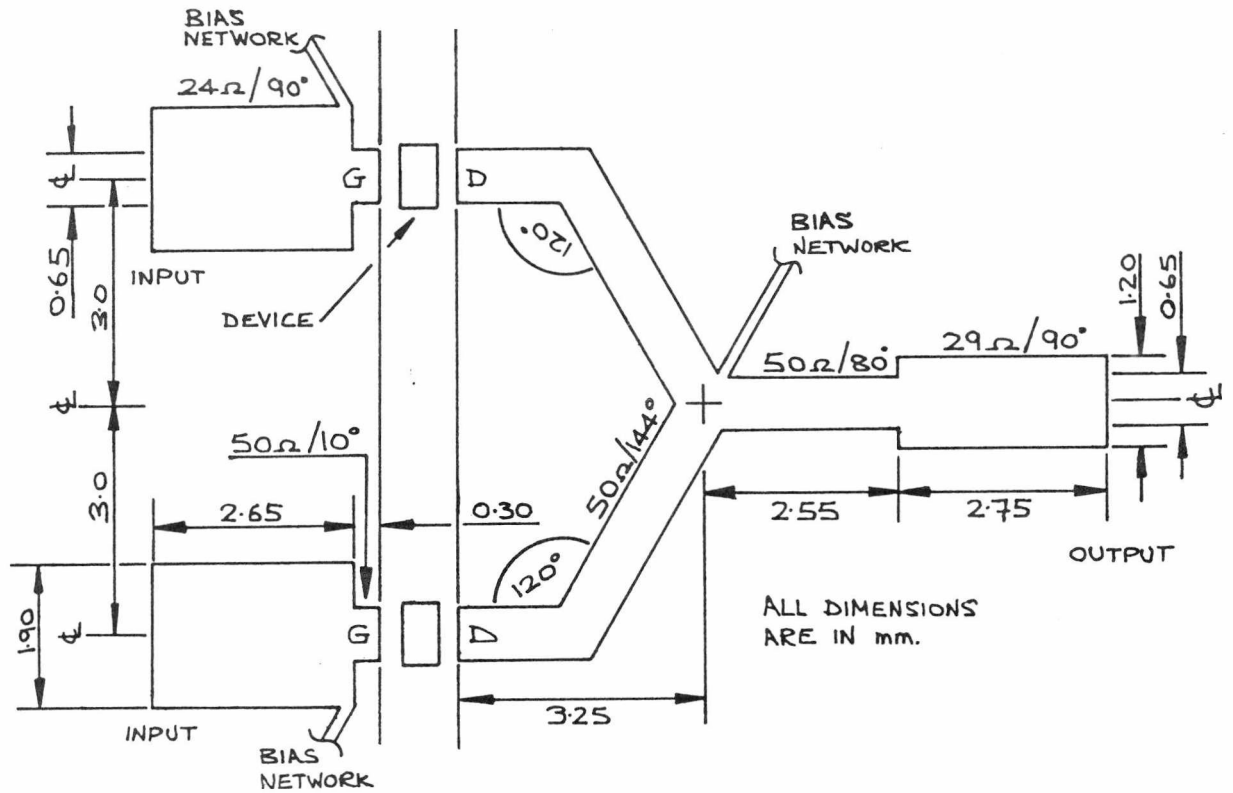


Figure 6.1 : Microstrip topology of the two-way switch used in the construction of the phase shifter with the Schiffman network.

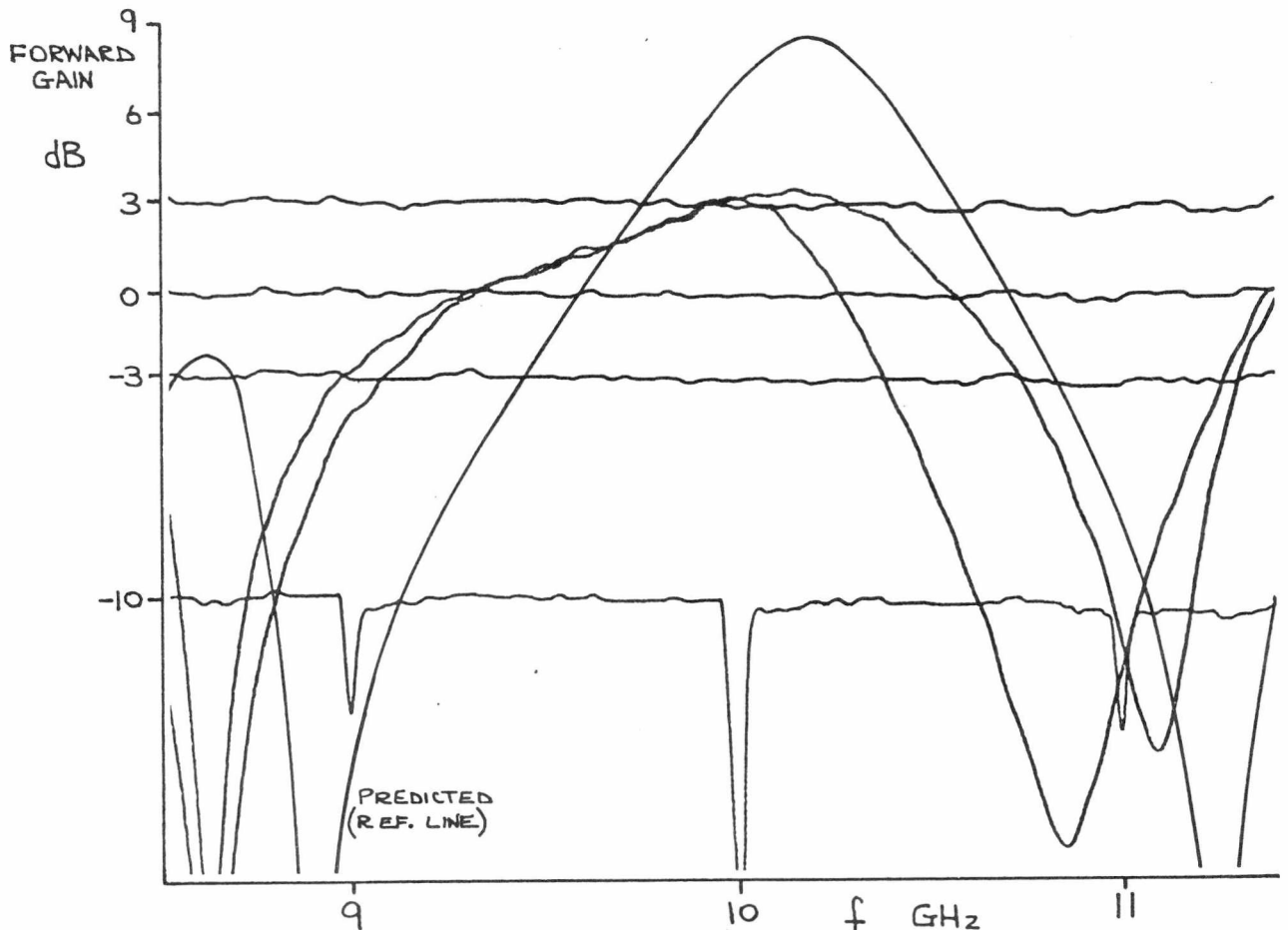


Figure 6.2 : Forward gain response of the 0/180° phase shifter using the Schiffman network. The two response curves are for each phase state.

shift network by chip capacitors to serve as d.c. breaks. The capacitors used are American Technical Ceramics type 100A. These are treated as being comparable to a length of transmission line. When a length of 50 ohm microstrip line was cut and a 10 or 100 pF chip inserted there was no observable change in the line's insertion loss or transmission phase. The chip capacitor's electrical length on the microstrip is, therefore, taken as if it was continuous microstrip and here it is part of the mismatch phase compensating line. The complete phase shifter circuit is mounted on a 2.5 cm square supporting block.

The phase shifter's forward gain response curve is shown in Figure 6.2. Over 3 dB of gain has been obtained at a frequency of 10 GHz. Like the response of the MESFET amplifier, the measured gain is about 4 dB less than predicted at 10 GHz. This gain decrease is a trend that has been observed in all the circuits constructed in this work as will be seen later in this chapter. It is probably caused by the several effects discussed in Chapter 5, section 5.4, in connection with the MESFET amplifier/switch. Recalling that a 4.3 dB gain loss was observed there, a gain loss of about 5 dB occurs at the 10.2 GHz peak of the theoretical response, the slight excess caused by the longer lengths of line used in the phase shifter.

The frequency response of the phase shifter's gain follows the general behaviour of the differential phase shift network (see Figure 5.18). The rising gain between 9.5 and 10 GHz is caused by the superposition of the phase shift network's response with that of the two-way switch (this is similar to that shown in Figure 2.18). The downward shift in the measured response's dips is thought to be caused by microstrip discontinuity effects<sup>1,2</sup>. These can be modelled as shunting capacitances and added lengths of line at the discontinuity. Their effect when included in the computer model is to produce a downwards

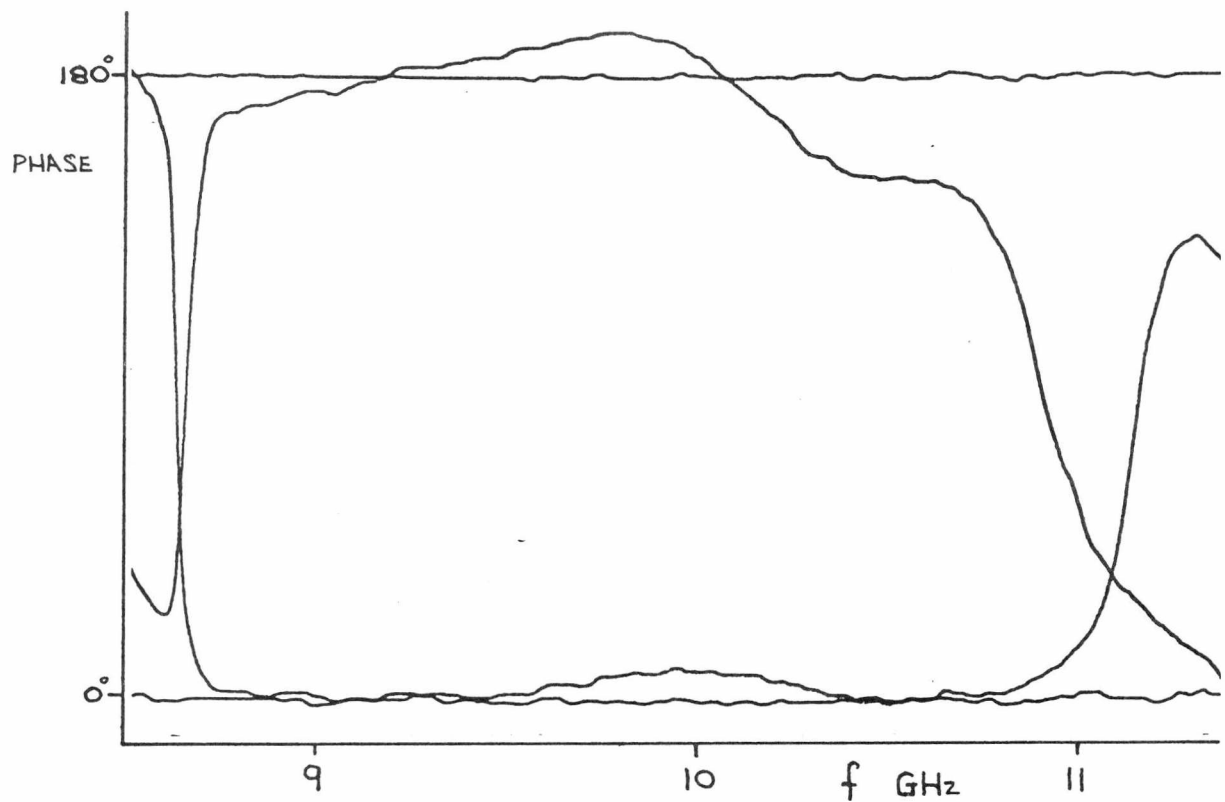


Figure 6.3 : Forward transmission phases of the phase shifter using the Schiffman network.

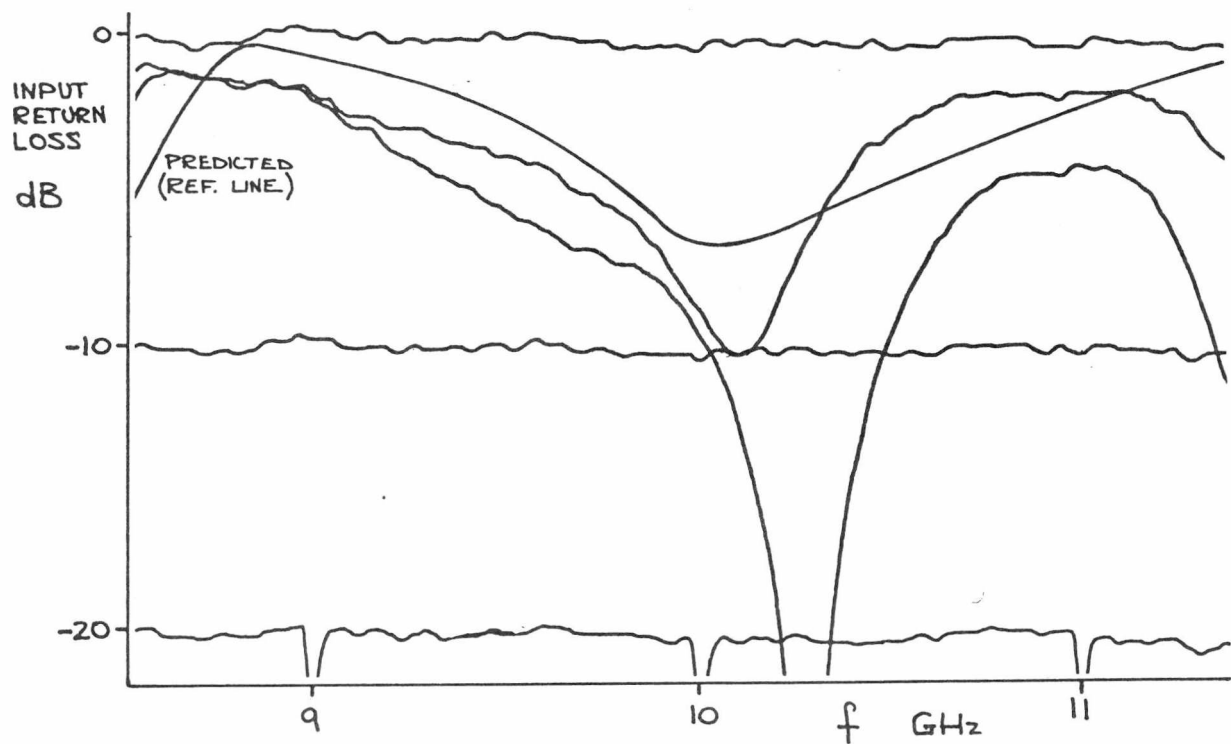


Figure 6.4 : Input return loss of the phase shifter using the Schiffman network. The two measured response curves are for each phase state.

shift in the response. The circuit's phase shift, shown in Figure 6.3, is within 5.5 degrees of 180 degrees in the 9 to 10 GHz region. Outside this region it is seriously degraded by the mismatch from the off-biased device.

The phase shifter's input return loss is shown in Figure 6.4. Though poor, it is comparable to the predicted response. The phase of each return loss (for each phase state) is different by only a small amount (typically less than 20 degrees) and so tuning discs could be placed at the shifter's input to improve the return loss. The output return loss (not shown) is worse, being less than -3 dB from 9 to 10 GHz though dips below -10 dB were observed at 11 GHz. The computer model gives a return loss figure of less than -3.2 dB from 9 to 11 GHz. These poor return losses, both measured and predicted were found to be caused by the presence of the  $S_{21}$  scattering parameter of the two-way switch. This has a magnitude and phase that causes it to add to the mismatch parameter  $S_{22}$  at the phase shifter's input divider. The consequence of this, as discussed in Chapter 4, section 4.4, is the observed poor return losses. This, therefore, lead to the development of the two-way MESFET switch with the cascaded pair of quarter-wave output matching transformers and is used in the remaining phase shifters discussed in this chapter.

It is difficult to define the bandwidth of this phase shifter exactly because of the difference in amplitudes above 10 GHz. If, however, the mean of these is taken, a 3 dB bandwidth of about 1 GHz is seen though at the band edges, the return losses are very poor. Despite this circuit's deficiencies the principle of being able to use two single gate MESFET devices as switches in a phase shifter that exhibits a gain has been demonstrated. Improvements in this phase shifter circuit will now be discussed.

### 6.3 A PHASE SHIFTER USING THE STUB TYPE NETWORK

The second experimental phase shifter that was constructed used the stub type 180 degree differential phase shifter network as shown in Figure 5.17. (The required 1.5 wavelength reference line is not shown). The two-way MESFET switch used is shown in Figure 6.5. (This has the cascaded pair of output matching quarter-wave transformers). Again, chip capacitors are placed at the switches inputs for d.c. breaks. An uncompensated Wilkinson divider is now used at the shifter's input to take advantage of this divider's slightly broader bandwidth when operated with a mismatch termination. Since the required lengths of mismatch phase compensating lines are 171.5 degrees, nearly a half wavelength, they are not used, the slight error being trivial. This angle is obtained from equation (3.19), this switch has an argument of  $S_{22} = 163$  degrees.

In view of the large impedance steps present in this circuit, large changes in microstrip width are necessary. These have an associated discontinuity effect and compensation<sup>3</sup> has been applied to the microstrip by rounding the corners of the lines at these width changes. The same has been applied to the corners of quarter-wave lines and open circuit stubs of the phase shifting network to reduce the fringing capacitances at these points. Right angled bends of the microstrip (reference line) are mitred as before.

The measured gain response of this phase shifter is shown in Figure 6.6. Two pairs of results are shown to demonstrate the effect of device bias adjustment. Reducing the device's gate bias from zero to a value of about -0.6v has improved the phase shifter's gain in the 9 to 10 GHz frequency range. Device parameter change with bias is thought to have improved device matching and hence overall phase shifter gain. Again, the drop in peak gain is observed when compared to the predicted



and also the downwards shift in frequency of the response dips. The measured dips at 10.2 GHz are caused by effects in the output circuitry of the two-way switch (since for each phase state they occur at the same frequency) and correspond to the predicted dip, 10.6 GHz. The measured dips are more severe because the off-biased device returns a mismatch to the output combining junction more like a short circuit in magnitude than the model's scattering parameters do. The 10.6 GHz measured dip is caused by the switch's input mismatch returning to the input divider via the reference line.

Because of this poor response it was decided that an attempt would be made to try and improve the shifter's performance over a narrow bandwidth centre at 9.45 GHz. By adjusting device biases, gain (amplitude) balance was obtained near this centre frequency as can be seen in Figure 6.7. Unfortunately the asymmetry introduced into this phase shifter circuit by the phase shift network causes large amplitude imbalances at everything but one frequency. Taking the mean value of the two gain responses, a 3 dB bandwidth of about 650 MHz has been obtained.

The associated phase of the output signals required trimming of the reference line to achieve the 180 degree shift. This resulted in a phase error of less than 7.5 degrees over the band of interest as is shown in Figure 6.8. The original input return loss was observed to vary from -3.3 dB at 9 GHz to 7 dB at 10 GHz. This was improved by placing a metal rectangle on the microstrip input. The length of this rectangle approximates to a microstrip quarter wavelength and its inward facing edge is about a quarter of a wavelength from the input divider's junction. The width of the rectangle is obviously greater than the 50 ohm microstrip's width and is adjusted to obtain the best match.

The topology of this matching circuit is consistent with what is

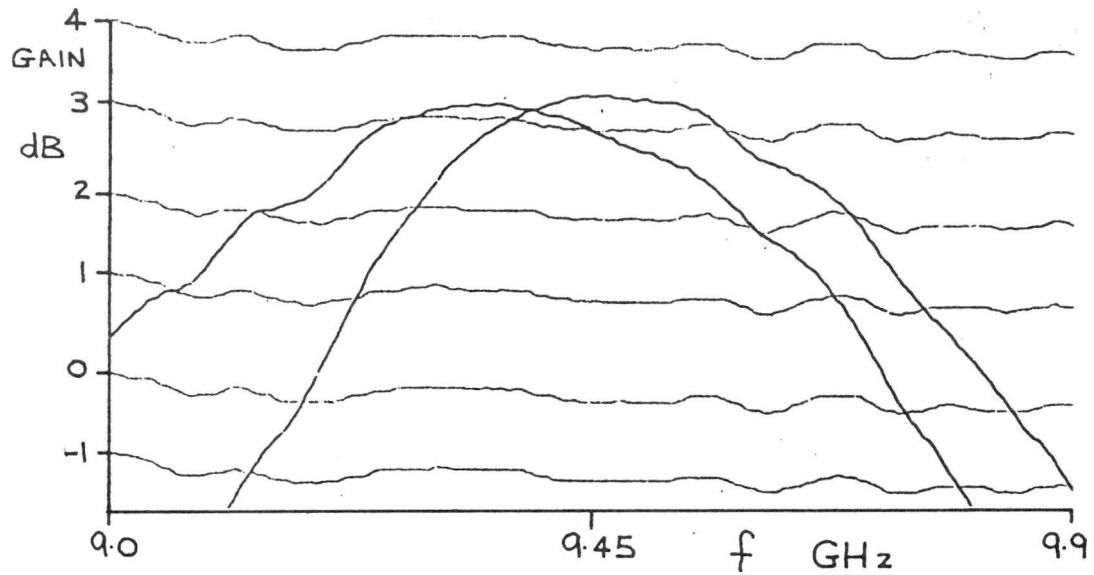


Figure 6.7 : Improved gain responses of stub type phase shifter for each phase state.

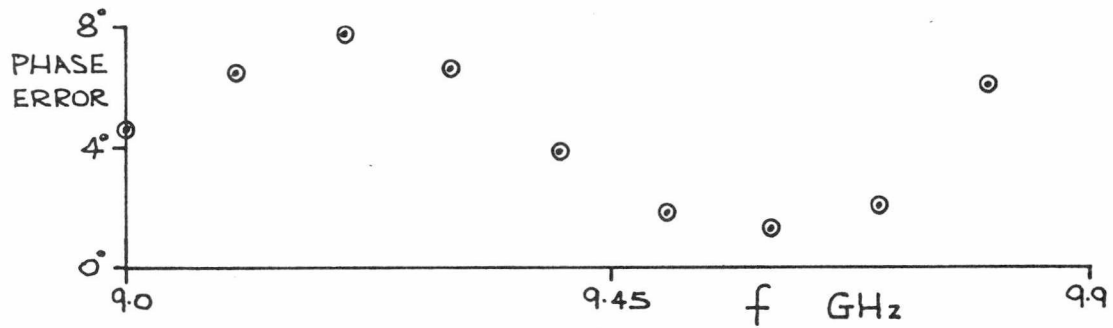


Figure 6.8 : Phase deviation from  $180^\circ$  shift observed in forward transmission of the stub type phase shifter.

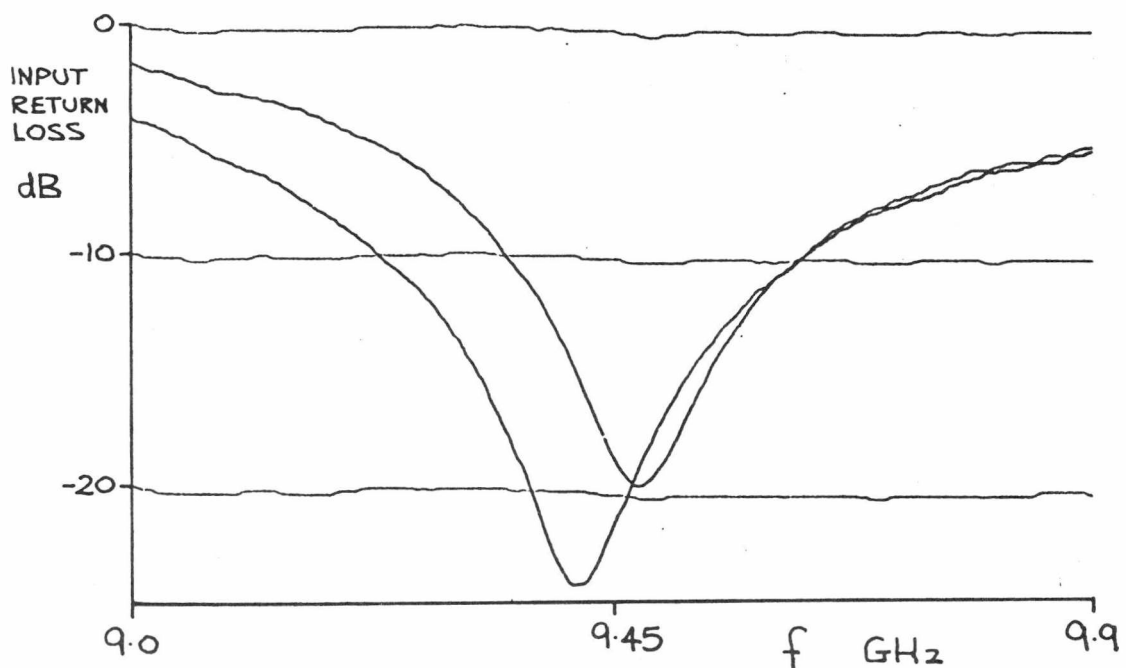


Figure 6.9 : Improved input return losses of the stub type phase shifter.

required to match the shifter's input. The 50 ohm match from the two-way switch's on-biased input is transformed to 100 ohms at the Wilkinson's input junction. The mismatch from the off-biased device has a reflection coefficient magnitude approaching unity and since its phase is adjusted to be zero at the divider's junction is consequently very much greater than 100 ohms at this point. The common input impedance is therefore greater than 50 ohms necessitating a matching transformer with an impedance greater than  $Z_0$  (50 ohms) when placed at the divider or one less than  $Z_0$  a quarter of a wavelength away like the metal rectangle. The adjusted return losses are shown in Figure 6.9. The output return loss which has not been adjusted is about -5.6 dB at 9.45 GHz with a dip below -10 dB at 9.8 GHz.

It would appear that there has been very little advantage in using either the stub-type phase shift network or this two-way MESFET switch. However, the more compact nature of this switch will be noted when compared to the previously used switch. Also, use of this switch has resulted in slightly improved return losses, especially at the output which is in keeping with the predictions produced by the computer models of these circuits. Some bandwidth has been lost by the sharp gain roll-off of the two-way switch above 10 GHz but this has probably been accentuated by the switch's input mismatch effect. The asymmetry and resultant amplitude imbalance of the phase states is a consequence of using a differential phase shift network whose halves are inherently dissimilar. Further improvement in this phase shifter must take the form of using a phase shift network that is symmetrical and has less length between the switch's inputs and the shifter's input junction. The slotline-type power divider has the potential of achieving this required improvement and its application in a phase shifter will now be discussed.

#### 6.4 PHASE SHIFTERS USING THE SLOTLINE-TYPE POWER DIVIDER

Two identical experimental phase shifters have been constructed that use the slotline type split phase power divider. It was hoped that the parallel phase shifter technique (Chapter 4, section 4.7) could be investigated using these two circuits though unfortunately this work was not completed. The pair do, however, demonstrate the reproducibility of this circuit design.

The two-way MESFET switch used in this phase shifter is virtually identical to the circuit shown in Figure 6.5. It was found that the impedance of the input matching quarter-wave transformers could be increased slightly without seriously degrading the switches input match. By raising the line's impedance from 16 to 18 ohms the microstrip width can be reduced from 3.3 to 2.9 mm and this helps to reduce discontinuity effects<sup>2</sup>.

The slotline-type power divider is shown in Figure 5.21. The output lines are composed entirely of mismatch phase compensating line lengths. Their lengths are given by equation (3.19) and since  $\arg(S_{22})$  is 163 degrees their electrical lengths is 0.476 wavelength or 5.45 mm using 50 ohm microstrip at 10 GHz. The last 0.7 mm of both of the divider's outputs is removed and chip capacitors substituted as d.c. breaks. Though only one is required here for this purpose, two are used to preserve the phase shifter's symmetry; 8.2 pF capacitors are used to allow fast switching.

The slotline circuit in the microstrip's ground plane is situated over a milled recess 5 mm deep in the substrate's supporting block. Its area is kept small so as to avoid it being a resonant cavity within the 9 to 11 GHz band. Having near rectangular dimensions of 13 by 5 mm, it should exhibit a waveguide cut-off of 11.5 GHz and so resonant effects are above the band of interest in this work. The complete phase

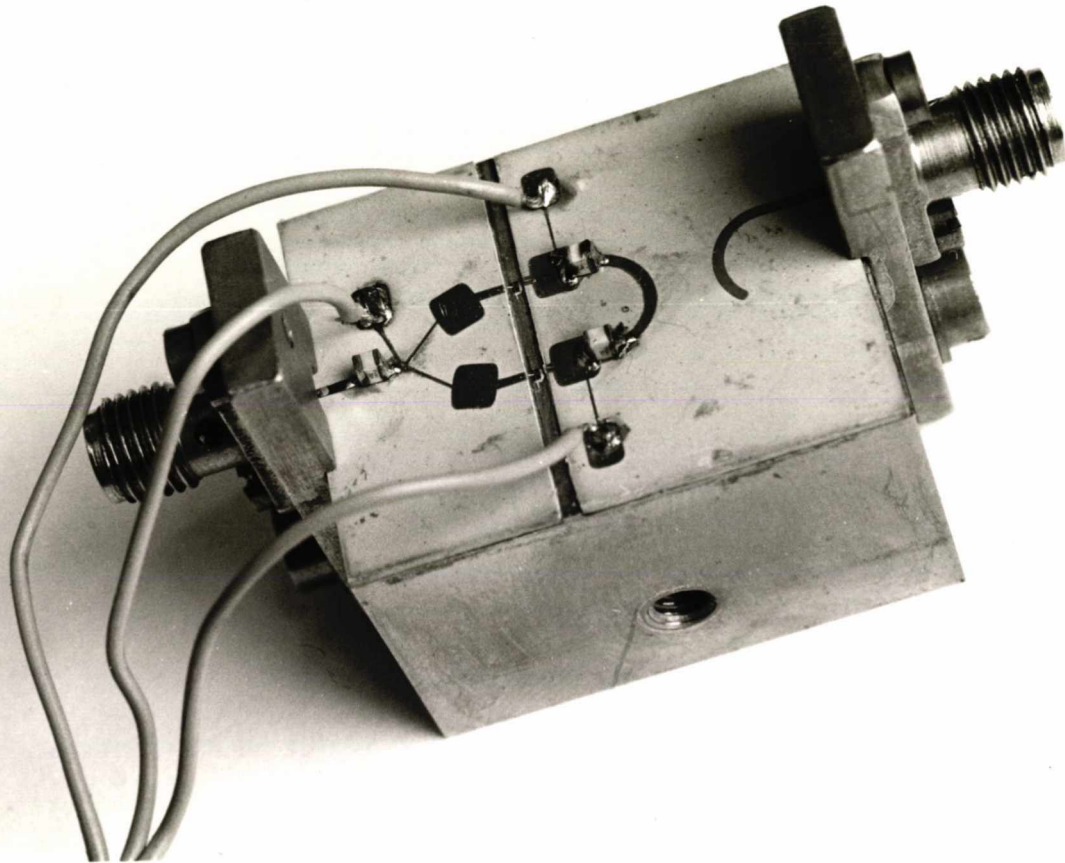


Figure 6.10 : The slot-line type phase shifter. (Approximately 2.5 times full size).  
The microwave input is on the right-hand side.

shifter has a substrate area of 30 by 24 mm, the substrate pair being spaced by the 1 mm width ridge upon which the devices are mounted. The assembled circuit plus device bias control circuitry is shown in Figure 6.10.

The first phase shifter's gain versus frequency response is shown in Figure 6.11. This response is as observed before the device's biases have been adjusted to obtain a good gain and an amplitude balance. As can be seen, a very good agreement occurs between each phase state over the 6 to 12 GHz frequency, better than either previous phase shifter. The dips at 11 GHz are caused by the two-way switch's output circuitry and those at 6.1 GHz by the input mismatch effect at the divider's junction. If the measurement could be extended above 12.4 GHz a corresponding dip would probably be seen at about 13 GHz. The broader nature of this phase shifter is clearly obvious.

Of most interest is the phase shifter's behaviour in the 8.0 to 10.5 GHz region where its peak gain occurs. The device's biases have been adjusted (from 0v to a slightly negative value) to achieve an amplitude balance at and about the 9.5 GHz centre frequency. The improved gain response is shown in Figure 6.12. The peak gain is now 2.8 dB and the response displays a -3 dB bandwidth of 1.42 GHz. The maximum amplitude imbalance is 0.4 dB but this occurs only at the upper bandwidth edge. Similarly, the maximum phase error is 6 degrees but this only occurs at the lower bandwidth edge.

The second slotline-type phase shifter displayed a slightly poorer gain response (not shown). The peak gain was 2.7 dB with a -3 dB bandwidth of 1.18 GHz. The bandwidth reduction cannot be completely explained by the slight narrowing of the spacing of the response's gain dips since the 3 dB bandwidth of the circuits with zero device bias is 1.69 GHz for the first and 1.62 GHz for the second. The second

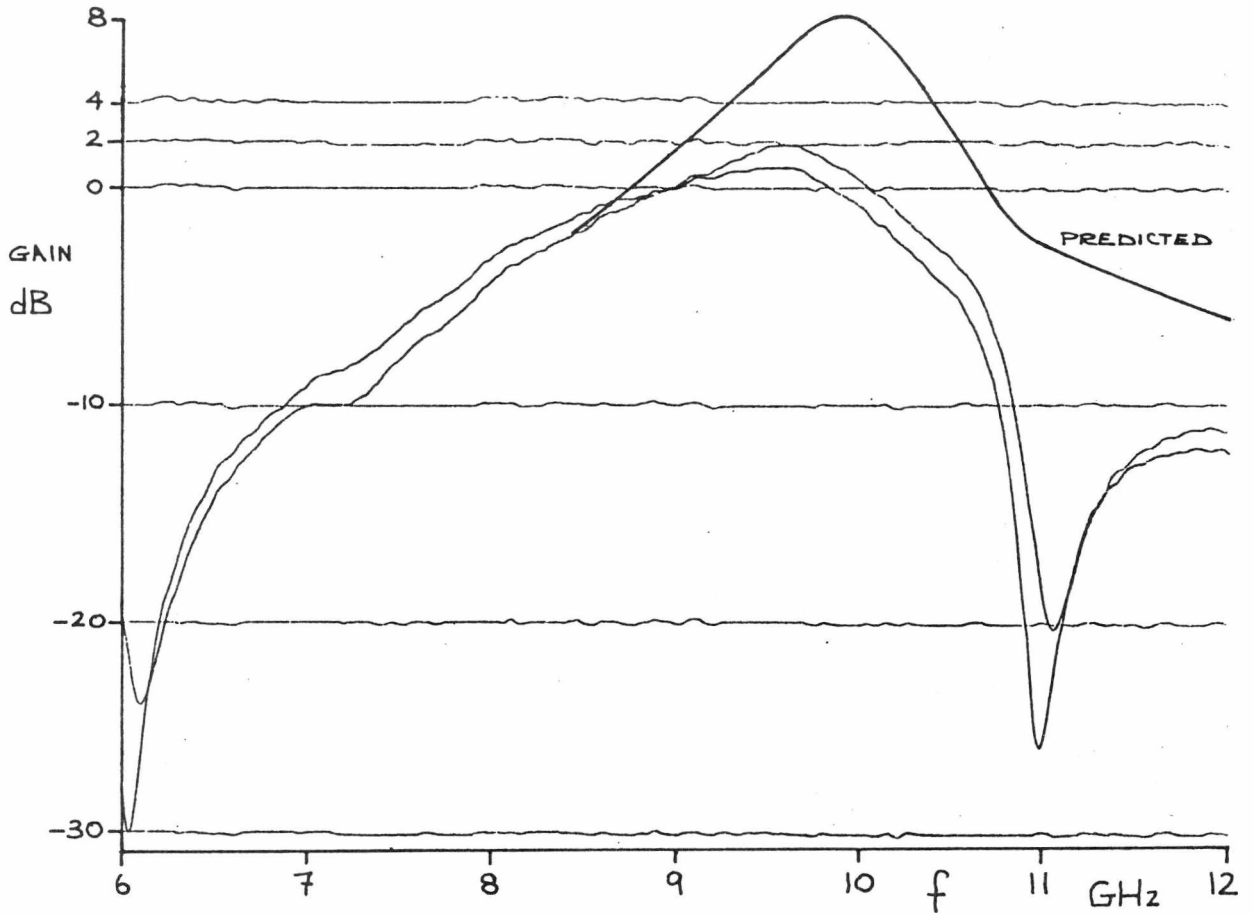


Figure 6.11 : Forward gain for each phase state of  $0/180^\circ$  phase shifter using the slotline-type phase splitting power divider. Both device gate biases are at 0v.

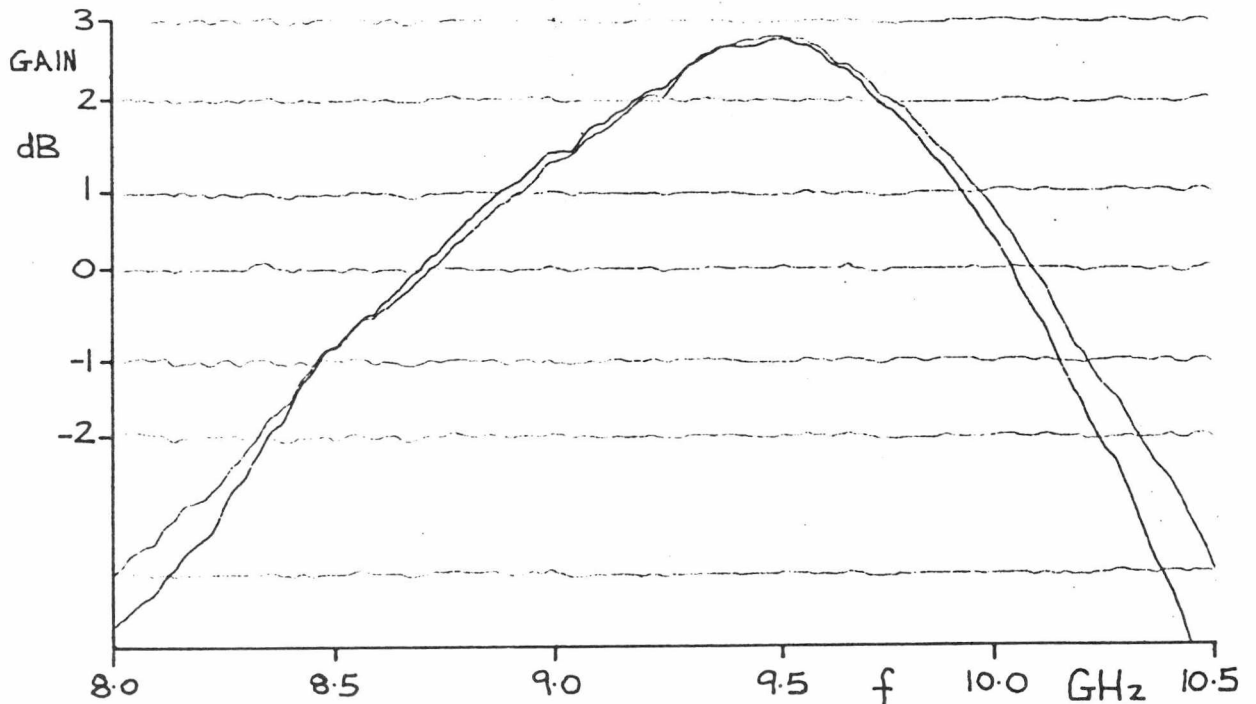


Figure 6.12 : Forward gain of slotline-type phase shifter after adjustment of the device biased to maximise gain and reduce amplitude imbalance.

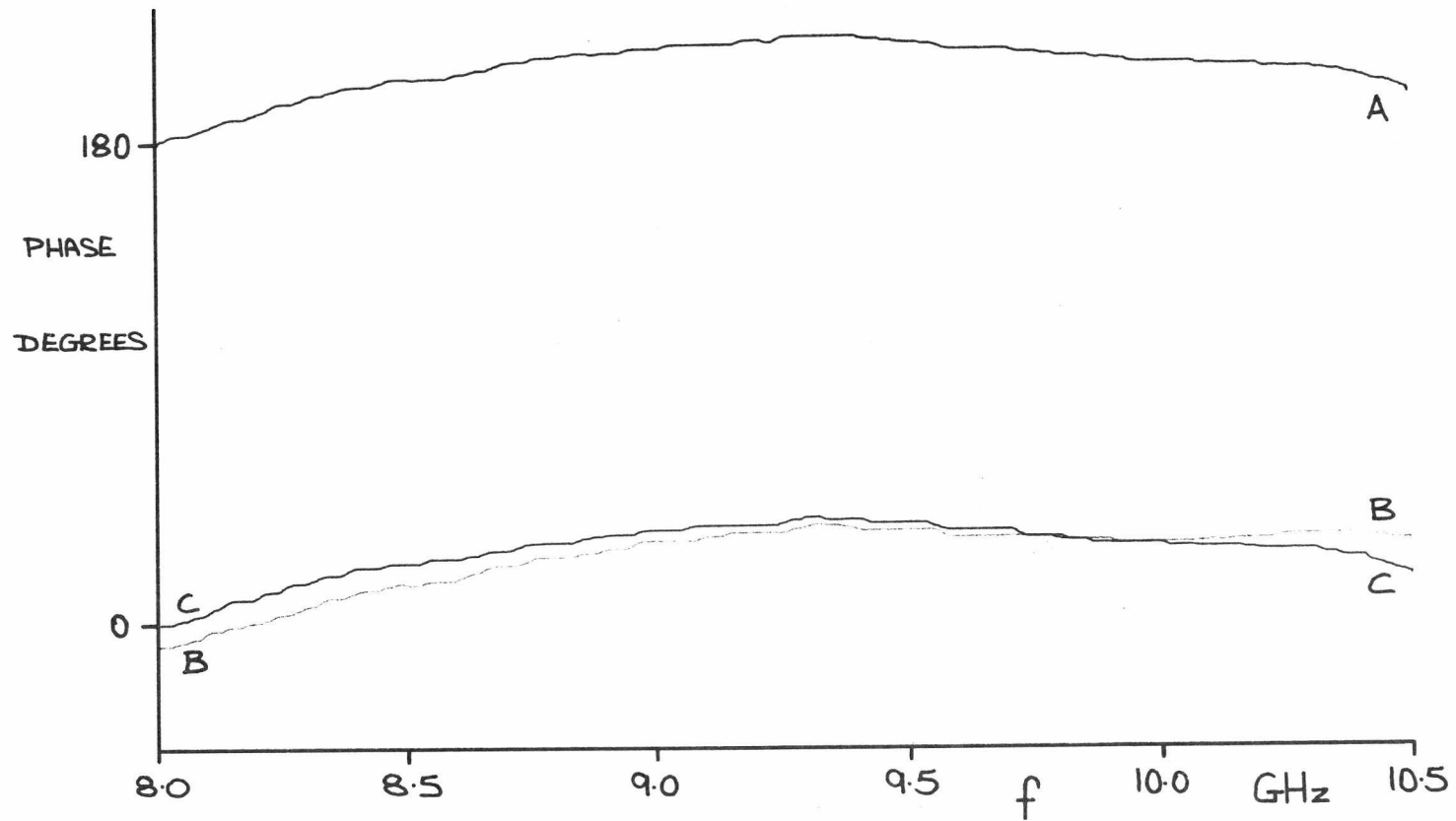


FIGURE 6.12B: FORWARD TRANSMISSION PHASE OF THE SLOT-LINE TYPE PHASE SHIFTER. A, PHASE 1. B, PHASE 2. C, PHASE 1 PLUS 180 DEGREES OFFSET.

circuit did, however, require more negative device voltages to obtain the peak gain and balance. It is, therefore, thought that the consequent device parameter changes are the cause of the narrower bandwidth. It should be noted that both pairs of devices are from the same batch number F1435/4. The second phase shifter exhibits a slightly poorer input return loss though in all other respects the two phase shifters are comparable.

The first phase shifter's input return loss is shown in Figure 6.13. The downwards frequency shift of the dip from the predicted value is thought to be caused by an incorrect phase compensating line length, ie. line spacing between the divider's output junction and the two-way MESFET switch's input. Despite this, a return loss of better than -5 dB is seen within the -3 dB bandwidth. The output return loss is in better agreement but unfortunately the 0.5 GHz downwards shift in the peak of the gain response means that this now corresponds to a poorer portion of the output return loss curve. Both of these return losses are as observed for the phase shifter without any additional tuning elements at either the input or output.

It is worth noting that the phases associated with these return losses display a difference of at most 14 degrees between phase states for the input return loss and 30 degrees for the output (across all of the 6 to 12 GHz band). Considerable scope therefore exists for the application of further matching here in view of the good amplitude similarities also. Since the off-biased device's mismatch should be returned to the divider's output junction with a phase of 180 degrees if the compensating lines lengths are correct, the mismatch impedance seen here is real only. The quarter-wavelength of slotline could hence have its impedance changed to effect a better match at the phase shifter's input.

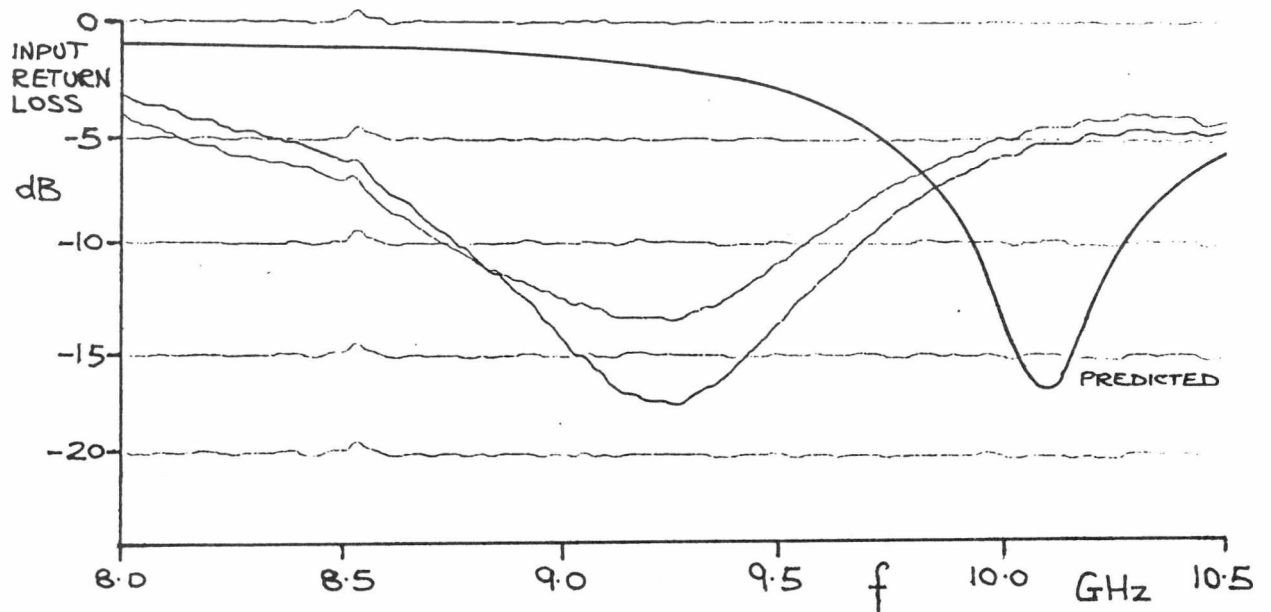


Figure 6.13 : Input return losses of the slotline-type phase shifter for each phase state.

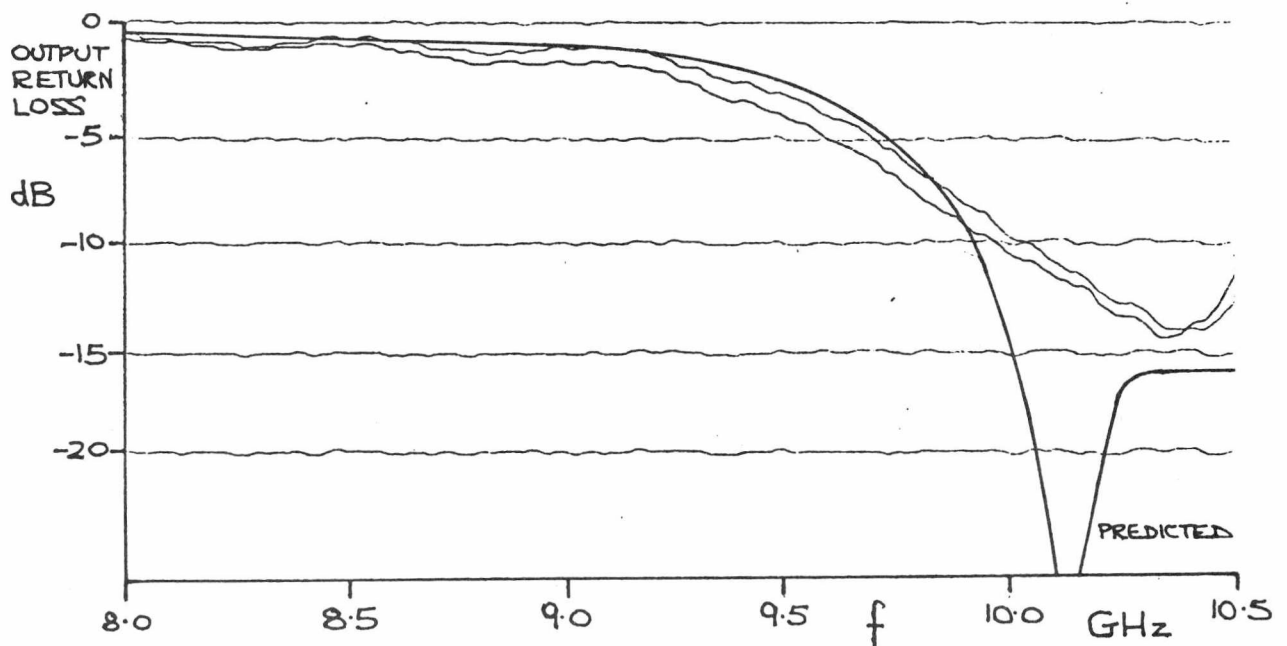


Figure 6.14 : Output return losses of the slotline-type phase shifter for each phase state.

### 6.5 SWITCHING SPEED AND SPECTRUM OBSERVATIONS

In Chapter 4, section 4.8, the use of frequency domain measurements were discussed as a means of determining the switching time of a digitally phase modulated signal. The technique relies upon knowing how finite rise and fall times affect the spectral components of a square-wave modulated signal. A measured spectrum is then inspected and compared to a set of curves showing the spectral variation of total rise and fall times as a percentage of switching period and an estimate of switching time obtained.

To obtain the maximum speed from the phase shifter the output of a pulse generator is applied direct to the gates of the MESFET device pair. A fast pulse generator (Hewlett Packard 8080 system consisting of 8081A+8083A+8084A) was available that possessed complementary outputs with negative going pulses of 2v amplitude into 50 ohms that could be given a d.c. offset. The 2v peak-to-peak amplitude is sufficient to take the devices into pinch-off and the d.c. offset allows the shifters gain to be peaked. 50 ohm non-inductive resistors are placed at the phase shifter's device gate bias networks to provide terminations for the generator and equal lengths of coaxial lines are used to minimise differential switching delays and hence jitter. For a square-wave output a maximum frequency of 150 MHz is obtainable which is adequate for the measurement of switching times of about 1 nS, the pulse generator itself having a transition time of less than 800 pS. The spectrum was observed with a Hewlett Packard 8559A/853A spectrum analyser.

First a check is performed on the spectrum of the pulse generator. Its measured spectral component magnitudes at 150 MHz are given in Table 6.1.

Component	Relative Magnitude (dB)
1st (150 MHz)	0
2nd (300 MHz)	-15
3rd ( etc )	-11.5
4th	-18
5th	-21.5
6th	-22
7th	-34
8th	-35
9th	-42

Table 6.1 : Measured spectrum of 8080A  
pulse generator.

The even harmonic spectra are thought to be caused by differences in the mark to space ratio which cannot be adjusted to reduce these. Fitting the odd harmonic spectrum magnitudes to the curves of Figure 4.9 gives a total transition time of approximately 25%. The generator's transition time is therefore 12.5% of the 150 MHz period or 833 pS. This is in good agreement with the equipment manufacturer noting that there is about a  $\pm 5\%$  fitting accuracy to the curves.

For the second slotline phase shifter modulated at a 5 MHz rate the classic square-wave odd harmonic spectrum is seen in both upper and lower side bands (USB and LSB) of the shifters output. All even harmonic spectra are -41 dB down relative to the first harmonic amplitudes. The carrier rejection is -36 dB relative to these also and referring to Figure 4.8 arises due to either 0.2 dB amplitude imbalance or less than 0.1 degrees phase error or a combination of these. This is consistent with the network analysis measurements at 9.5 GHz.

The observed spectral components of the phase modulated signal from the output of the second slotline-type phase shifter is given in Table 6.2 below for 150 MHz modulation rate.

Modulation Component	100 MHz		150 MHz	
	LSB (dB)	USB (dB)	LSB (dB)	USB (dB)
Carrier	-18	-	-12	-
1st	-0.5	0	-0.5	-0.5
2nd	-18	-17	-12.5	-13
3rd	-12	-10.5	-14	-13
4th	-19.5	-18.5	-14.5	-14.5
5th	-19	-16	-36	-16.5
6th	-22	-18.5	-22.5	-15
7th	-26	-20	-31	-27
8th	-26	-18	-34	-20.5
9th	-32	-26	-30	-36

Table 6.2 : Measured spectrum of phase modulated signal from slotline-type phase shifter for 150 MHz and 100 MHz modulation rates.

The carrier is -12 dB down on the fundamental components indicating a degradation of the phase accuracy and amplitude balance at the data rate is increased. A deviation from one-to-one mark to space ratio may be the cause of this as indicated by the presence of the even harmonic components.

It will be noticed that there is considerable difference between the spectral components of each side band for the fifth harmonic and above for a 150 MHz rate. It is not fully understood at present as to why such a sharp drop should occur since at a modulation rate of 100 MHz, though a difference in the side bands is still observed, the

difference is less severe. The band pass nature of the output matching circuitry is likely to reduce the magnitudes of the higher order spectra though probably not to the extent seen at 150 MHz.

Fitting the 100 MHz spectra to the curves of Figure 4.9 then a transition time of  $700 \pm 50$  pS is obtained from the USB and  $970 \pm 130$  pS from the LSB. Taking the average of these a transition time of  $840 \pm 220$  pS is estimated for the slotline-type phase shifter; hence, sub-nanosecond switching has been achieved.

#### 6.6 SIGNAL HANDLING

The 1 dB gain compression point for the second slotline-type phase shifter has been measured at an output power level of 9.9 dBm. This is for the circuit's 9.5 GHz centre frequency with the device biases adjusted to -0.7v to maximise the shifter's gain. At this voltage the devices are operating near 50% of  $I_{DSS}$ . The poorer signal handling when compared to either the matched amplifier or the device itself is probably caused by the phase shifter's poor output return loss of -4 dB at 9.5 GHz. Recall from Chapter 5 that device matching was thought to cause the 2.5 dB gain compression improvement seen there. The lower than predicted phase shifter gain and also losses in the shifter's output circuitry may be responsible for a further power handling reduction also.

The phase shifter's intermodulation distortion is characterised by the 3rd order intercept point. This has been measured by the two-tone method. Two 9.5 GHz signals of equal amplitude with a 25 MHz frequency difference are applied to the phase shifter's input. As their amplitude is changed the variation in the amplitude of these

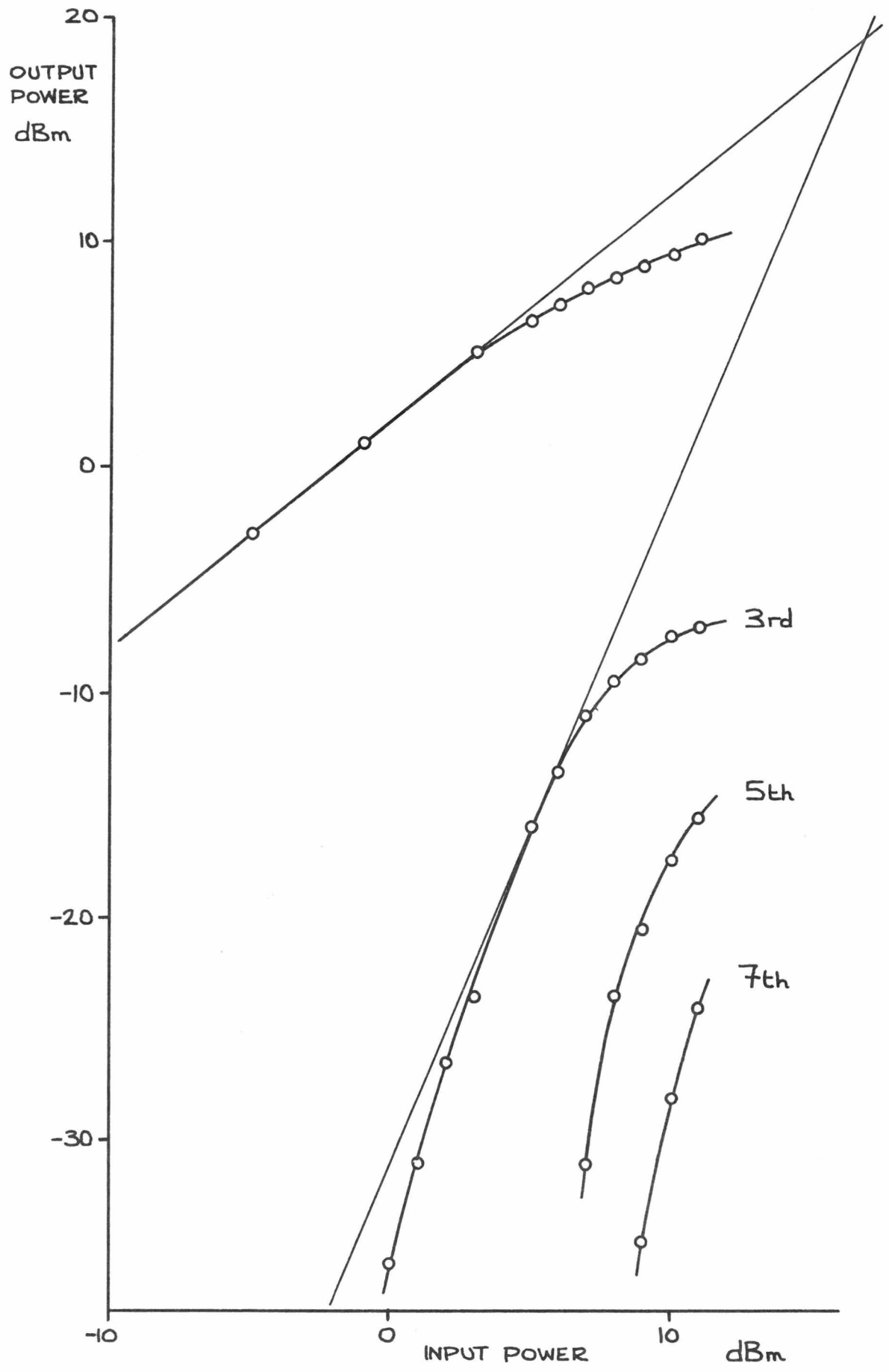


FIGURE 6.15: THIRD ORDER INTERCEPT POINT AND HIGHER ORDER INTERMODULATION COMPONENTS FOR THE SECOND SLOT-LINE TYPE PHASE SHIFTER.

signals is noted and also the amplitudes of the third order products which lie adjacent to these.

A plot of these measured output signals as the input pair are varied is shown in Figure 6.15. The input, output and third order signals are taken as the sum of their respective pairs. If a linear third order gradient is fitted tangentially to the measured data an intercept point of  $+19 \pm 1$  dBm is observed. The reason for the increased gradient of the third order response below the tangential point is not known though it has been observed by others<sup>5</sup>. There is no known data available to the author for the GAT4's intermodulation performance. However, Minasian<sup>6</sup> gives data for a 4 GHz amplifier using a  $1 \times 300$   $\mu\text{m}$  NEC device operated with a 3v drain supply and -0.6v gate bias. This displays a 1 dB gain compression at under +10 dBm output power and a third order intercept of about +22 dBm.

### 6.7 CONCLUSION

It has, therefore, been demonstrated that two single-gate MESFET devices in combination with a suitable phase shift network can be made to cause a digital phase shift whilst also providing an insertion gain of a few dBs. The phase shifter circuit that offered the best performance was, as expected, the one using the slotline-type power divider. Though its gain is similar to the others, its bandwidth is wider and displays good phase accuracy and amplitude balance. A switching speed of less than 1 nS has been estimated for the transition between phase states.

6.8 REFERENCES

- 1 R. Horton, Equivalent Representation of an Abrupt Impedance Step in Microstrip Line, IEEE Trans. MIT21, August 1973, pp. 562-564.
- 2 P. Benedek and P. Silvester, Equivalent Capacitances for Microstrip Gaps and Steps, IEEE Trans. MIT20, November 1972, pp. 729-733.
- 3 J.A.G. Malherbe and A.F. Steyn, The Compensation of Step Discontinuities in TEM-Mode Transmission Lines, IEEE Trans. MIT26, November 1978, pp. 883-885.
- 4 H. Jasik, Antenna Engineering Handbook, McGraw-Hill, 1961, pp. 30-21.
- 5 H.A. Willing, C. Rauscher and P. de Santis, A Technique for Predicting Large-Signal Performance of a GaAs MESFET, IEEE Trans. MIT26, December 1978, pp. 1017-1023.
- 6 R.A. Minasian, Intermodulation Distortion Analysis of MESFET Amplifiers Using the Volterra Series Representation, IEEE Trans. MIT28, January 1980, pp. 1-8.

CHAPTER 7CONCLUSION7.1 SUMMARY OF RESULTS

A method of using a single-gate MESFET device as a microwave switch that exhibits an on-state insertion gain has been investigated and demonstrated. This premise was based on the idea that a device operating normally in a circuit as an amplifier gives an insertion gain and should exhibit less gain or even an insertion loss if its supply voltages are changed by suitable amounts. This has been substantiated by noting that as the device's gate voltage is taken negative towards the pinch-off voltage the drain current reduces to zero and the device's amplifying mechanism ceases to function causing it to be lossy. Further confirmation of this was obtained from the device's lumped element equivalent model. The component values of this were fitted to known scattering parameters. The device's off biased parameters could then be inferred from the pinched-off model developed from this by noting the voltage dependent components and modifying them suitably.

Device measurements have indicated that the forward gain term  $|S_{21}|$  can be made to change by about 17 dB when the gate bias is taken from 0 to -3v (pinch-off voltage). A similar change (the switch's on to off ratio) was observed from a matched device operating as a 10 GHz amplifier with 7 dB gain and a 3 dB bandwidth of 1.4 GHz. An important feature of this switch is the large terminal mismatches it displays when off. This is expected since the device's reflection parameters also change appreciably from fully on to pinch-off. Both increase in

magnitude and the input reflection coefficient is accompanied by a large change of phase also.

The lumped element model proved of further use since the device's off biased performance could be connected to specific components and their values within the model. These, in turn, could be related to the device's physical structure. This allowed proposals to be made to improve device parameters for specific application as amplifying switches. Fortunately, physical changes required to improve  $S_{21}$  also result in improved values for  $S_{11}$  and  $S_{22}$ .

A two-way switch for use in phase shifter construction has been developed. It was noted that an advantage in terms of d.c. biasing and switch control exists if a common drain combining configuration with separate gates and grounded sources is used. Practical constraints necessitate bringing the drains together with microstrip circuitry and this can also serve as the two-way switch's output matching network. Relevant three port theory, useful in the design of this two-way switch has been given and also a method for designing a switch. Though a discrete two-way switch was not constructed its predicted performance in terms of gain, on to off ratio and bandwidth is like that of the basic MESFET switch just discussed. The input to the off biased device is again highly mismatched and by design the on biased device input and common output are matched.

Chapter 3 introduced the proposed form of the phase shifter. Its simple structure consists of the two-way switch preceded by either a phase splitting power divider at the input or an "in phase" divider and differential phase shift network. Recalling that the off biased device will present a mismatched termination ( $S_{22}$ ) to one of the divider's outputs, an analysis was performed to assess the effect of this on the behaviour of various power dividers. The conclusions

drawn from this are that the compensated Wilkinson power divider suffers an inherent 3 dB power division loss (T) and improves the consequent mismatch at its input (R) (caused by  $S_{22}$ ) by -6 dB, both of which are independent of  $S_{22}$ 's phase. For the uncompensated Wilkinson and tee a different situation exists. It was shown that if a mismatch is present, this can be used to recover part of the 3 dB power division loss by suitably adjusting the phase of the mismatch as it returns to the dividers junction. This also minimises the input mismatch. If possible, the mismatch's magnitude should approach or equal unity since then the input return losses are minimised and the transmission (or recovered divider power) are maximised. The tee offers better performance in this respect when compared to the uncompensated Wilkinson.

The differential phase shift networks require long reference lines. Though the mismatch's phase could be corrected at one frequency, the phase/frequency response of these networks causes shifts in  $S_{22}$  phase off the centre frequency. A theory has been developed to relate the line's length to the transmission bandwidth of the divider. Measurements on a tee divider have been performed and the results obtained support the theory. Further measurements on an uncompensated Wilkinson indicate that this has a slight bandwidth advantage if this is defined at either the -0.5 or -1 dB points as opposed to the -3 dB points where they are similar.

Further to this, the necessity to return the mismatch with the correct phase to the divider's junction for optimum performance was shown to impose a phase shift angle constraint of 0/180 degrees on the overall phase shifter. This is not as restrictive as it seemed since a parallel structure was discussed whereby two 0/180 degree phase shifter plus a 90 degree delay and two switchable amplifiers (MESFET

switch) could be used to cause four bits of digital phase shifts.

Two dispersive type differential phase shift networks have been investigated and employed in phase shifters with a degree of success. These were the Schiffman coupled lines and a band pass circuit consisting of shunt stubs. Both phase shifters exhibited insertion gains of approximately 3 dB at about 10 GHz and served to prove phase shifter and two-way switch design. In other respects they were deficient, the problems of which were thought to be caused by construction difficulties experienced with the microstrip and phase shift networks and the inherent asymmetry of their structure.

Noting these problems, a phase splitting power divider was developed. This utilised the coupling properties of slotline to microstrip to effect a broad band split phase power division. It was designed to operate over an octave and results show that this is so in terms of phase and amplitude split being limited only by its input return loss. Two novel experimental phase shifters were constructed using this divider. Again, insertion gains of about 3 dB (at 9.5 GHz) were observed though now this is accompanied by good amplitude balance, a consequence of the dividers symmetry. Since this form of phase shifter does not possess the long reference lines of previous circuits, its bandwidth is determined by the device matching of the two-way switch rather than divider/mismatch effects. Hence, a 3 dB bandwidth of 1.4 GHz has been measured which is 40% wider than either previous dispersive phase shifters. The amplitude imbalance is less than 0.4 dB in this bandwidth and the phase accuracy of the 0/180 shift better than 6 degrees.

Spectrum analysis of the phase modulated signal has allowed an estimate of the phase shifters transition time to be obtained. For the slotline type phase shifter this is less than 1 nS and is thought to be

limited more by device drive circuits and the necessary d.c. breaks than the device itself. The phase shifter's 1 dB gain compression point is 10 dBm and for the basic MESFET switch (matched amplifier) is 14.5 dBm.

### 7.2 COMPARISON WITH OTHER PHASE SHIFTERS

A comparison with a recently reported<sup>1</sup> MESFET phase shifter and a PIN diode type<sup>2</sup> is shown in Table 7.1. The MESFET circuit referred to, though of a monolithic construction and using dual-gate devices with the same gate dimensions as the Plessey GAT4 used in this work, has a similarity in its circuit topology. It used two devices with a common input gate connection (c.f. common drain connection used in this work) and is a switched path type shifter with an overall insertion gain. The PIN circuit is a fast low loss phase shifter.

### 7.3 FUTURE WORK

It has been mentioned on several occasions and in one instance with the stub type phase shifter circuit demonstrated that further matching components can be added to the input and output to improve the return losses. Use could be made of this to obtain a more level gain response across a frequency band of interest. A broader response may be achievable with these added components and also by use of more sophisticated device matching. Use could be made of Bode's integral to ascertain the limits of this.

Whilst on the subject of device matching it is worth noting that the distributed components used in this work could be replaced by lumped elements. By choosing a high pass type matching network for one

	This work Slotline type	MESFET	PIN diode
Centre frequency	9.5 GHz	9.8 GHz	12 GHz
Insertion gain	+2.8 dB	+3 dB	-1 dB
Bandwidth	1.4 GHz	2.2 GHz	0.5 GHz
Phase error	< 6°	< 10°	< 4°
Amplitude modulation	<0.4 dB	<1.0 dB	<0.2 dB
Switching speed	<1 nS	Not known	<0.4 nS
Power handling	10 mW	Not known	Not known
Device bias, ON	$V_{GS} = 0v$ $I_{DS} = 50 \text{ mA}$ $V_{DS} = 5v$	Not known	$V_{DF} < 1.0v$ $I_{DF} = 20 \text{ mA}$
Device bias, OFF	$V_{GS} = -3v$ $I_{DS} = 0 \text{ mA}$ $V_{DS} = 5v$	Not known	$V_{DR} = -7.5v$ $I_{DR} = 0 \text{ mA}$

Table 7.1 : 0/180 degree phase shifters.

Notes on Table 7.1 : The bandwidth of both MESFET phase shifters is defined as the -3 dB gain points. The PIN circuit has its bandwidth defined by the points where its insertion loss differs by  $\pm 0.1$  dB from the nominal 1 dB value. The phase errors and amplitude modulations given are the maximum observed in the whole of these bandwidths.

device and low pass for the other the phase shifting and device matching can be performed with the same components. Taking this a stage further, the associated power dividers could be replaced by lumped components or even incorporated into the matching/phase shift networks themselves. This structure is now eminently suitable for fabrication as a monolithic GaAs integrated circuit. Such techniques have been presented before by Pengelly<sup>3</sup> though in this case dual-gate devices have been employed and provide gain in the form of an active combiner.

Continuing on the theme of device fabrication, single-gate device pairs could be made that have a common drain and source in parallel with separate gates. If their physical structure was optimised for microwave switching applications, a useful discrete MESFET device would be available noting that most commercial devices are either low noise single and dual-gate types or power devices, monolithic microwave integrated circuits excepted.

There appears to be no reason why the single-gate MESFET phase shifter could not be redesigned at higher frequencies such as in the millimetre-wave bands (Q-band particularly). All that is required of the device is a few dBs gain at the required operating frequency with a reasonable off biased insertion loss. A gain of over 6 dB has been reported<sup>4</sup> at 27.5 GHz for a 0.3  $\mu\text{m}$  device. Inspection of this device's lumped element model indicates that a satisfactory on to off ratio might be observed. To reduce substrate losses at these frequencies quartz or sapphire dielectrics could be used. Alternatively the phase shifter could be assembled in a waveguide structure. The phase splitting slotline to microstrip transition could become a fin-line to microstrip transition. The devices would remain embedded in microstrip circuitry and after combining their outputs the phase shifter's output could be returned to fin-line.

A final area where the phase shifter and MESFET switch may be considered in future work is for fast digital applications. The two device pair with the common source and drains that have previously been discussed is a logic NOR gate. The phase shifter is itself behaving as an exclusive-OR gate. If the control voltages to each device gate are different in a binary logic sense, the phase shifter gives a microwave output with an inversion (180 degrees phase shift) if these are interchanged. If these are made equal, either with both devices on or off, no microwave output appears. Hence, the microwaves can be gated according to the logical combination of its control signals.

Also, an exclusive-OR relationship exists between the phase shifter's output and the combination of its microwave and common control input. The 9.5 GHz microwaves could be a clocking signal and the control a data stream. Exclusive-OR gates are the basic components of binary comparators and adders, a vital part of any computer.

This work forms a useful part of the growing research into gigabit logic, phased arrays and advanced communications and the novel application of devices in these fields. It is interesting to note that the solution to many microwave problems often requires adopting a hybrid approach to circuit construction (c.f. microstrip and slotline used here). Lastly, only by collaboration between the device manufacturers and circuit designers can major improvements in microwave components be achieved with the resultant benefits for the systems engineers.

7.4 REFERENCES

- 1 J.L. Vorhaus, R.A. Pucel and Y. Tajima, Monolithic Dual-Gate GaAs FET Digital Phase Shifter, IEEE Trans. MTT30, July 1982, pp. 982-991.
- 2 B. Glance and N. Amitay, A Fast-Switching Low-Loss 12 GHz Microstrip 4-PSK Path Length Modulator, IEEE Trans. COM28, October 1980, pp. 1824-1828.
- 3 R.S. Pengelly, GaAs Monolithic Microwave Circuits for Phased-Array Applications, IEE Proc., Vol. 127, Part F, No. 4, August 1980, pp. 301-311.
- 4 P. Forrest, D. Daniel, R. Bennett, C. Oxley and J. Arnold, H.F. Gallium Arsenide FET Amplifiers, IEE Colloquium, GaAs FET Microwave Devices and Applications, December 1982, paper 7.

